# DIFFERENTIAL EFFECTS OF SEROTONIN AND NITRIC OXIDE ON THE INTRINSIC PROPERTIES AND NETWORK ACTIVITY OF CORTICAL NEURONS

Thesis submitted for the degree of

Doctor of Philosophy

at the University of Leicester

by

Rodrigo Roberto Bammann MSc

Department of Cell Physiology and Pharmacology

University of Leicester

2015

Rodrigo R. Bammann

# Differential effects of serotonin and nitric oxide on the intrinsic properties and network activity of cortical neurons

## Abstract

Serotonin (5HT) and nitric oxide (NO) are important signalling molecules with roles in behavioural control and various psychological conditions. Various lines of evidence suggest interactions between 5HT and NO signalling, however little is known about their interaction in modulating intrinsic properties of cortical neurons and the effects on the neuronal network activity in the cortex.

This project studied the effects of 5HT and NO on cultured neurons isolated from Wistar rat cortices. 5HT and NO produced diverse responses in cortical neurons, reflecting the heterogeneity of cortical neuron types. Neither 5HT nor NO appeared to significantly modulate glutamate induced depolarisations. However, they affected the number of APs elicited by the glutamate response, hinting at the possible modulation of intrinsic membrane properties.

Subsequently, $k$-Means clustering based on 10 electrophysiological parameters was used to divide cultured cortical neurons into 10 different cell types with consistent firing properties. 5HT and NO had diverse, cell-type specific effects on neuronal excitability and cellular parameters in these cell types. Furthermore, 5HT and NO showed complex interactions between each other, suggesting modulatory cross-talk. Using ODQ to block soluble guanylate cyclase activity suggests that NO effects are mediated not only by sGC/cGMP signalling, but also S-nitrosylation.

Comparing results obtained in cell culture to data from acute cortical slices showed similarities in basic cellular properties. However, 5HT and NO effects on pyramidal cell properties differed markedly between slices and cultures. At the network level, 5HT increased the spontaneous EPSC frequency in pyramidal neurons through $5HT_2$ receptors, whereas NO had no effect. Interestingly, NO was able to reduce the 5HT induced increase in EPSC frequency when inhibitory synaptic interactions were blocked, possibly by modulating $5HT_1$ receptor function. The results obtained demonstrate the interaction between 5HT and NO in modulating both intrinsic membrane properties and neocortical network activity.

## Acknowledgements

First and foremost I would like to thank my supervisor, Volko Straub, for all the patience, guidance and knowledge he has applied to this project, along with so many other situations in the last four years, and for showing me so many aspects of science. My gratitude also extends to my co-supervisor Nick Hartell for providing the set-up and technical expertise and to Jonathan McDearmid for his help and advice on many occasions. Moreover, I would like to thank the support staff within the Central Research Facility at University of Leicester, and the Department of Cell Physiology and Pharmacology for their support and encouragement, in particular Ian Forsythe and Blair Grubb.

I deeply appreciate the financial support provided by the College of Medicine, Biological Sciences and Psychology at University of Leicester, without which I would not have been able to complete this project.

Finally, many thanks to my family – my parents Roberto and Adriane Bammann, as well as my brothers and sister – for so many things. Many friends also helped me throughout this project but special thanks to Jim Sinclair, for the encouragement and help in seeing the lighter side, and Tom and Dan, for keeping me on track. A special note of thanks also goes to Silvia Ponzoni for starting my career in neuroscience. And last, but not least, I am forever in debt for all the support and help in many aspects given by my wife Sarah (as well as the sanity points) and my daughter Inara, who reminded me of what is important.

There is just not enough space here to demonstrate my appreciation for all your help during these last years.

**Table of contents**

**Abstract**

**Acknowledgements**

## List of tables

## List of figures

## List of abbreviations

| | |
|---|---|
| 5HT | serotonin hydrochloride/5-hydroxytryptamine |
| 7-NI | 7-nitroindazole |
| 8-OH-DPAT | ($R$)-(+)-8-hydroxy-DPAT hydrobromide |
| aCSF | artificial cerebrospinal fluid |
| αMe5HT | α-methylserotonin maleate salt |
| AP | action potential |
| ara-C | cytosine β-D-arabinofuranoside |
| ATD | acute tryptophan depletion |
| ATP | adenosine triphosphate |
| BC | basket cell |
| BIC | Bayesian information criterion |
| cAMP | 3',5'-cyclic adenosine monophosphate |
| cGMP | cyclic guanosine monophosphate |
| ChC | chandelier cell |
| CNS | central nervous system |
| CRC | Cajal–Retzius cells |
| DAG | diacyl glycerol |
| DEA | diethylamine NONOate sodium salt hydrate |
| DMC | Dunn's multiple-comparison test |
| DMSO | dimethyl sulfoxide |
| DNAse | deoxyribonuclease I |
| EM | expectation-maximisation algorithm |
| EPSC | excitatory post-synaptic current |
| EPSP | excitatory post-synaptic potential |
| FBS | foetal bovine serum |
| FS | fast spiking interneuron |

| | |
|---|---|
| GABA | γ-aminobutyric acid |
| GPCR | G protein-coupled receptor |
| GTP | guanosine triphosphate |
| HBSS | Hank's balanced salt solution |
| HCN | hyperpolarisation-activated channel |
| $I_h$ | hyperpolarisation-activated currents |
| IMS | industrial methylated spirit |
| $IP_3$ | inositol 1,4,5-trisphosphate |
| IPSC | inhibitory post-synaptic current |
| $I_r$ | input resistance |
| ISI | inter-spike interval |
| IV | current-voltage relationship |
| KS | Kolmogorov-Smirnov test |
| MC | Martinotti cell |
| MLM | multi-level modelling |
| NADPH | nicotinamide adenine dinucleotide phosphate |
| NC | nutrient cocktail |
| NgC | neurogliaform cell |
| NMDA | N-methyl-D-aspartate |
| NO | nitric oxide |
| (e,n,i)NOS | (endothelial, neuronal, inducible) nitric oxide synthase |
| ODQ | 1H-[1,2,4]oxadiazolo[4,3-a]quinoxalin-1-one |
| PBM | Pakhira, Bandyopadhyay and Maulik index |
| PCA | principal component analysis |
| PDE2/3/5 | phosphodiesterase 2/3/5 |
| PDL | poly-D-lysine hydrobromide |
| $PIP_2$ | phosphatidylinositol 4,5-bisphosphate |

PKA/C/G      protein kinase A/C/G

PLC          phospholipase C

PN           principal neuron

PS           parameter set

SC           supervised clustering

SD           standard deviation

SEM          standard error of the means

SERT         serotonin transporter

sGC          soluble guanylyl cyclase

SN           stellate neuron

SS           slow spiking interneuron

VIP          vasoactive intestinal peptide

W-S t test   Welch's refinement of Student's two-tailed $t$ test

## 1 General introduction

1.1  Discovery of serotonin and nitric oxide as neurotransmitters

In 1935 enteramine was isolated and described as a substance responsible for intestinal tissue contractions by Vittorio Erspamer (Vialli & Erspamer 1937). Subsequently, a substance named serotonin was obtained from blood serum, purified and described as a vasoconstrictor (Rapport et al. 1948). With the chemical structure resolved (Rapport 1949), enteramine and serotonin were found to be the same compound, which based on its chemical structure was named 5-hydroxytryptamine (5HT). This monoamine is found primarily in the gastrointestinal tract, platelets, and in the central nervous system (CNS), in which 5HT acts as a neuromodulatory signalling molecule. 5HT is derived biochemically from tryptophan, through ring hydroxylation of tryptophan by tryptophan hydroxylase and side chain decarboxylation by aromatic amino acid decarboxylase. Tryptophan hydroxylase 2 is also found in the central nervous system (CNS), and it is the rate-limiting step of this reaction (Fitzpatrick 1999; Walther et al. 2003).

Another transmitter responsible for modulating synaptic function is nitric oxide (NO). This free radical was identified as a signalling molecule in the CNS in 1987, when it was discovered that the activation of N-methyl-D-aspartate (NMDA) receptors would generate NO and cause cyclic guanosine monophosphate (cGMP) generation in adjacent cells (Garthwaite & Garthwaite 1987). This gas is biosynthesised endogenously in mammals from L-arginine by three forms of nitric oxide synthase (NOS) enzymes: neuronal (nNOS), endothelial (eNOS) and inducible (iNOS). The activity of the first two (nNOS, eNOS) is mainly regulated by intracellular calcium levels, while the third enzyme (iNOS) is controlled at the level of gene expression. nNOS is present in the CNS, and eNOS seems also to be relevant in the regulation of brain function (Haul et al. 1999; Garthwaite et al. 2006).

## 1.2 The role of serotonin and nitric oxide in behavioural control

Following the discovery of serotonin in the brain, 5HT has been shown to influence many different behaviours and mental conditions. 5HT is involved in the modulation of practically all behavioural processes, such as aggression (Kumar et al. 2014), memory (López-Vázquez et al. 2014), learning (Stolyarova et al. 2014), feeding (Otlivanchik et al. 2014), sleeping (Tabuchi et al. 2013), and reproductive behaviour (Jiménez-Trejo et al. 2007), as well as in sensory function such as pain (Heddini et al. 2014) and motor function (Leech et al. 2014). Disturbances in serotonergic signalling have been linked to depression (Angoa-Pérez et al. 2014), schizophrenia (Selvaraj et al. 2014), anxiety-disorders (Kronenberg et al. 2008), autism (Cook & Leventhal 1996), and obsessive compulsive disorder (Soomro et al. 2008).

Similarly, it has been reported that the gasotransmitter NO is also associated with the control of a wide range of behaviours and many of the same functions (Saleh et al. 2014; Rodriguez-Gomez et al. 2014; Pitsikas 2014; S. Wang et al. 2014; Kentish et al. 2014; Dittrich et al. 2014; Nutsch et al. 2014). Efforts have previously been made to understand the overlapping effects of 5HT and NO on aggression (Chiavegatto et al. 2001), in which nNOS knockout mice were significantly more aggressive than wild type animals. This aggression could be reversed by the application of $5HT_1$ receptor agonists, but in knockout mice the concentration of the agonists needed to be higher to revert to normal behaviour levels. Furthermore, studies of acute tryptophan depletion (ATD), in which subjects are fed with orally administered tryptophan-free protein-carbohydrate mixture to study serotonergic function in the control of behaviour, show that this depletion impairs object recognition. The application of BAY 60-7550, a highly selective inhibitor of phosphodiesterase 2 (PDE2) that enhances the concentration of both 3',5'-cyclic adenosine monophosphate (cAMP) and cGMP, and vardenafil, an inhibitor of the enzymatic activity of PDE5 leading to the intracellular increase of concentration of cGMP, normalised the ATD-induced short-term memory deficit in object recognition tasks (van Donkelaar et al. 2008). Further evidence for the interaction between the two neuromodulators comes from the application of tryptophan hydroxylase inhibitors, which leads to serotonin depletion in subjects, resulting in cortical hyperexcitability, i.e. increased generation of cortical spreading

depression events, and facilitation of trigeminal nociception (Supornsilpchai et al. 2006), an effect that could be counteracted by inhibiting NO production (le Grand et al. 2011).

## 1.3 Anatomical organisation of the cortex

The cortex is the largest part of the CNS in mammals, with primarily two divisions. The phylogenetically older area of the cortex, located in the medial temporal lobe, is termed the allocortex. This region is involved with olfaction and survival functions and contains the olfactory system and the hippocampus. The allocortex can be divided into two components, the paleocortex and the archicortex. The former includes the piriform lobe and the entorhinal cortex, whereas the latter consists of the hippocampus, a three-layered cortex that deals with encoding declarative memory and spatial functions. The other, largest division of the cortex is the neocortex, which is involved in many higher functions such as sensory perception, spatial reasoning, motor commands, language and conscious thought (Lui et al. 2011), and is therefore responsible, directly or indirectly, for the control of many of the aforementioned behaviours. The prefrontal cortex in particular is responsible for different aspects of executive functions and goal-directed behaviour, and for regulation of hierarchical social status (for review, see Szczepanski & Knight 2014; F. Wang et al. 2014).

In addition to being the largest cerebral tissue, the neocortex is also the most developed brain structure, with a horizontal as well as a vertical structure. Cranial structures help divide the neocortex into four regions, the frontal, parietal, occipital and temporal lobes. Each region is responsible for performing different functions, such as vision in the primary visual cortex in the occipital lobe, hearing in the primary auditory cortex in the temporal lobe, language processing in the frontal lobe and social and emotional processing in the orbitofrontal lobe.

The regional heterogeneity is widely recognised in this arealisation of cortex into functional domains, which were initially defined based on functional studies. There is also evidence for the role of various transcription factors in the determination of this arealisation (O'Leary & Sahara 2008). This heterogeneity also extends to the properties

of the cortical neurons and their position in the cortical structure. At the most basic level, it is possible to group the various neurons into two types, glutamatergic excitatory neurons, mostly but not exclusively pyramidal cell type, and γ-aminobutyric acid (GABA)-secreting inhibitory interneurons. Interneurons constitute around 20% of the cells in the cortex (Hendry et al. 1987), whereas pyramidal neurons are the most abundant cell type (around 80% of the cells; Peters & Kara 1987). The density of pyramidal neurons across the cortex varies and is used to define the division into horizontal cortical layers.

This division into laminar regions was first used by Brodmann to describe the neocortical subtypes, together with their morphology (Brodmann 1909). In more recent years, this division was also refined by the use of molecular methods, which in some cases would reveal further heterogeneity even within the anatomically defined layers (Arlotta et al. 2005; Molyneaux et al. 2009). Nevertheless, it is commonly accepted that the neocortex presents six layers, based on morphological appearance. This is due to the different soma densities in the individual layers of the cortex, as well as the densities of both pyramidal neurons and interneurons. These two neuron types can be differentiated based on their axonal projections and dendritic branches, their connectivity pattern and differences in their electrophysiological properties (Chen et al. 1996). However, the six layers are not present in all regions of the cortex. For example, the primary motor cortex lacks layer IV. Similarly, layer IV also appears to be absent in the prefrontal cortex of non-primate mammals (Van Eden & Uylings 1985).

The division of cortical layers starts with layer I, the most external one, to deeper levels in the neocortex ending up at layer VI. Layer I, the molecular layer, contains relatively sparse cells, and consists of mainly apical dendritic tufts of pyramidal neurons, horizontal oriented axons, stellate cells and glial cells (Shipp 2007). However, it also contains a unique neuron type called Cajal–Retzius cells (CRC), which are present during early development and appear to decline in numbers during post-natal development (Soda et al. 2003; del Río et al. 1995). The CRCs express and release reelin, an important factor in the control of radial migration of projection neurons. They also form synaptic contacts with dendrites of pyramidal neurons (Meyer et al. 1999).

Layers II/III contain densely packed small and medium sized pyramidal neurons, as well as non-pyramidal neurons with vertically oriented axons that project to the other layers (Gilbert & Wiesel 1979). Neurons from these regions send axons to ipsilateral and contralateral neocortical areas, establishing interhemispheric synaptic connections (Fame et al. 2011).

The internal granular layer IV contains spiny stellate, star pyramidal neurons and pyramidal cells, and is the main target of thalamocortical afferents. This layer receives input from peripheral sensory organs, and together with the columnar axonal arborisation of the spiny stellate cells, supplemented by the oblique to horizontal projection pattern in pyramidal neurons, this layer distributes sensory information to the other layers for further processing (Staiger et al. 2004).

The deep layers V and VI consist of large pyramidal neurons, with layer VI having a sparser density of neurons than layer V and many small spindle-like pyramidal and multiform neurons. Afferents from layer V project to the brainstem and spinal cord, whereas layer VI sends efferent fibres to the thalamus (Zhang & Deschênes 1998). Layer VI pyramidal neurons form a precise, highly organised communication system between the cortex and the thalamus: neurons from layer VI that send axons to the thalamus will be in the same cortical column as neurons that receive synaptic input from the same thalamic neurons.

Although the neocortex is divided into distinct layers, there is extensive communication between the various layers. The functional unit of the cortex is referred to as a minicolumn, which comprises around 80 to 120 neurons, that are coordinated by radial glia (Noctor et al. 2001). This minicolumn is a vertical group of neurons through the cortical layers of the brain, and consists of the major cortical cell types (Figure 1-1). This column receives inputs from the thalamus, which seems to connect mainly to layer IV, and to a lesser extent to layers III, V and VI (Thomson & Lamy 2007; Petreanu et al. 2009). Layers II/III, in turn, send projections to higher order integrative cortical areas (i.e. association areas) and the contralateral cortex, as well as to principal neurons (PNs) from layer V. The pyramidal and stellate neurons (SNs) from layer IV send connections to all the other layers, mainly to layers II/III, but receive little

input from the other neurons (Thomson & Lamy 2007; Lefort et al. 2009). Layer V PNs also send projections to higher order layers and the contralateral cortex, as well as to subcerebral targets, ipsilateral striatum and higher order thalamus. These cells, differently from layer IV PNs, receive inputs from multiple cortical neurons, but send little output to local neurons (Brown & Hestrin 2009). Corticothalamic cells from layer VI not only send projections to the thalamus, but also to cortical layer IV, targeting interneurons and some PNs (Thomson 2010; Lee & Sherman 2009). In addition to the PNs, responsible for maintaining the connectivity in the columnar unit, there are three major classes of interneurons, parvalbumin-, somatostatin-, and $5HT_3$ receptor-expressing types. Basket cells (BC) that target the soma and proximal dendrites, and chandelier cells (ChC) that target the axon initial segment of principal cells are parvalbumin-expressing fast-spiking interneurons. These cells also receive inputs from the thalamus, and from other inhibitory cells (Cruikshank et al. 2007; Pfeffer et al. 2013). Somatostatin-expressing interneurons inhibit other interneurons and target the dendritic tufts of the pyramidal neurons (Pfeffer et al. 2013; Xu et al. 2013). This group consists mainly of Martinotti cells (MC) that receive their input from local pyramidal neurons (Adesnik et al. 2012; Pfeffer et al. 2013; Xu et al. 2013). The final group of interneurons are $5HT_3$ receptor-expressing neurons. There are two types of these interneurons, neurogliaform cells (NgC), releasing GABA as a volume transmitter (Oláh et al. 2009), and vasoactive intestinal peptide (VIP)-expressing cells. VIP cells target somatostatin-expressing interneurons (Lee et al. 2013; Pfeffer et al. 2013). Within the neocortical network, the interneurons have a more local function, whereas the pyramidal neurons can both interact locally with other neurons in the neocortex, or communicate extrinsically via axons projecting to other brain regions (Figure 1-1).

While it is possible to divide cortical cells into two major groups, high-throughput transcriptome-profiling in mice demonstrated diverse gene expression patterns within and across neocortical layers suggesting a much wider diversity among cortical neurons (Belgard et al. 2011). Furthermore, the various interneurons possess quite distinct morphologies in the neocortex, while the basic shape of pyramidal neurons is considerably more conserved. However, dendritic morphology is not a reliable method for identifying the different interneurons. Axonal arborisation is a more useful
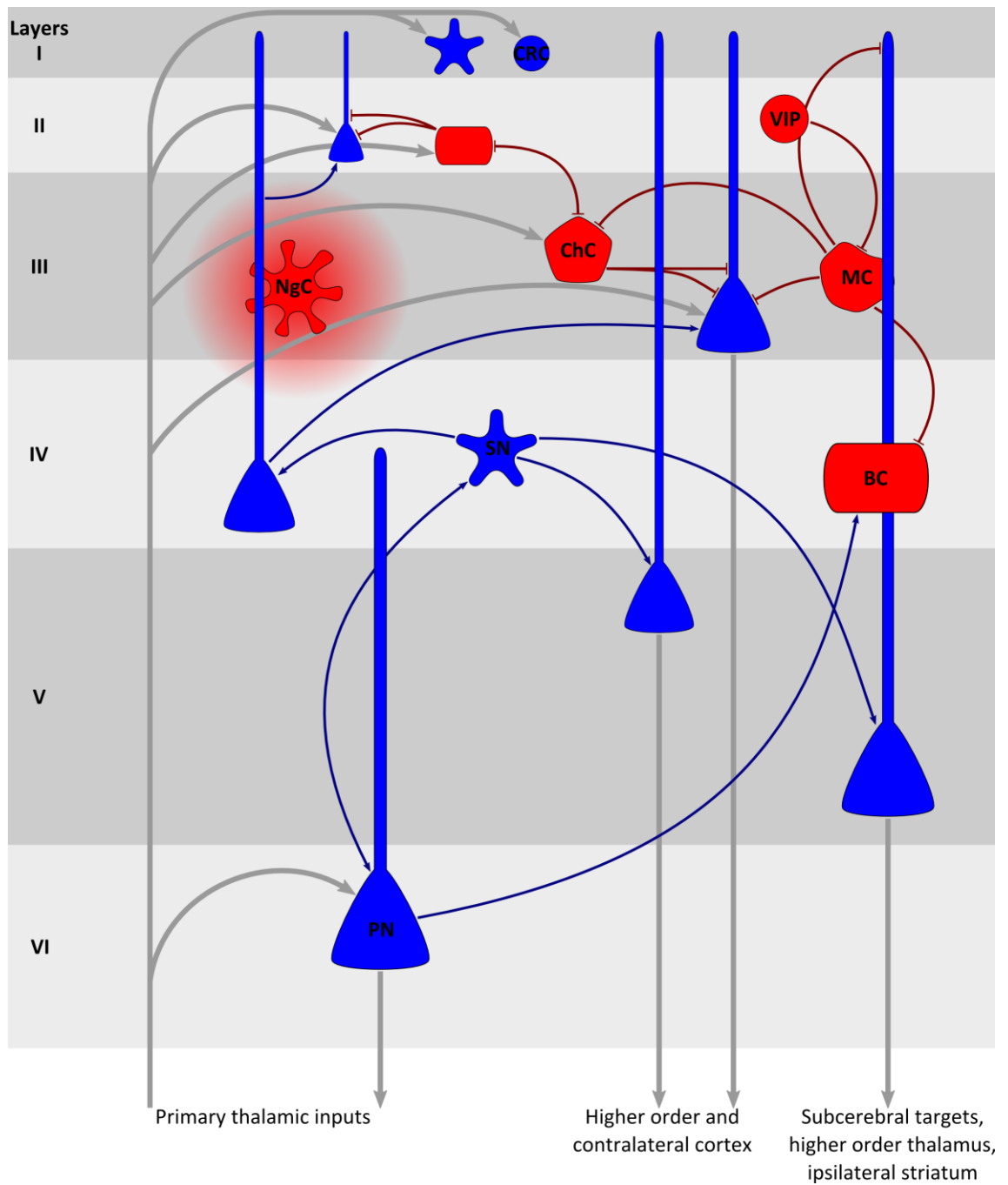
Figure 1-1: Connectivity between the neocortical layers as well as inputs to and outputs from the cortex (gray). PN principal neurons; BC basket cells; SN stellate neurons; NgC neurogliaform cells; MC Martinotti cells; ChC chandelier cells; VIP $5HT_3$ expressing interneurons; CRC Cajal-Retzius cells.

parameter for this, since the interneurons are specialised to target different parts of other neurons, different layers and different regions (Somogyi et al. 1998; DeFelipe 1997). At an electrophysiological level, there are different types of cells demonstrating varied action potential (AP) responses to injected currents, e.g. variation in sustained number of APs elicited, bursts of APs elicited at the beginning of the pulse, inter-spike intervals (ISI), among other properties. Pyramidal neurons from layer V, for example, have at least three different types of responses, including regular spiking, intrinsic bursting and non-inactivating bursting (Dégenètais et al. 2002). Interneurons, on the other hand, have been divided into five types based on their electrophysiological properties (non-accommodating, accommodating, stuttering, irregular spiking and bursting; Markram et al. 2004). Some of these types have been further divided into burst, delayed, classical, repetitive, initial and transient subtypes (Markram et al. 2004). This classification was based on the steady-state response to a sustained current injection for interneurons from all six cortical layers.

## 1.4 Clustering approaches for the division of cortical neuron types

To properly understand the electrophysiological properties of the various types of neurons in the neocortex and their modulation by neuromodulators, it is important to characterise and distinguish the neurons. This can best be achieved through the use of cluster analysis, a technique that has been applied to cortical neurons to identify the various types of pyramidal and interneurons. Clustering algorithms have been used to show, for example, that a subpopulation of glutamatergic non-pyramidal neurons from layer VI has similar electrophysiological properties to spiny stellate and layer II/III pyramidal neurons, whereas another group of layer VI cells was singular in presenting tonic firing (Andjelic et al. 2009), and that in the mouse somatosensory barrel cortex there are four types of interneurons, considering electrophysiology, molecular parameters and morphology of the cells (Perrenoud et al. 2012).

Various algorithms have been developed for the purpose of grouping different data points into distinct clusters that share similar properties. One algorithm that has been used quite extensively is Ward's method. This method has been used, for example, to

divide types of somatostatin-expressing interneurons, to classify neuropeptide Y expressing interneurons, and to identify fusiform neurons with distinctive features (McGarry et al. 2010; Karagiannis et al. 2009; Halabisky et al. 2006; Cauli et al. 2000). Ward's method is a hierarchical agglomerative clustering technique that groups data points adjacent to each other using a bottom-up approach. This method works by joining two data points that are closest in Euclidian distance (the distance between two points in a metric space), then by joining the next set of data points, and continues in this way until all points correspond to specific groups. One flaw of this technique is that once a data point is assigned to a cluster, it is inflexible in changing that point's classification. Another is that new points can only be assigned to existing clusters, rather than being assigned to new clusters where appropriate. A benefit of the technique is that it is an unsupervised method, reducing the risk of human error and bias in the definition of individual cell clusters, although it has been suggested that *a priori* knowledge of the data points in a supervised clustering may result in a better definition of the cells (Guerra et al. 2011).

An alternative unsupervised clustering method is the *k*-Means algorithm, which partitions the data into k clusters based on the distance of the data points to the nearest mean Euclidian distance of k centroids, or prototypes. This algorithm has been used to identify four different parvalbumin-expressing interneurons in layers II/III of the visual cortex in mice based on the cells' intrinsic membrane properties (Helm et al. 2013). A more in-depth discussion of clustering algorithms will be presented in Chapter 3.


## 1.5 Cellular signalling pathways for serotonin and nitric oxide

The defined and reliable classification of individual cells into distinct clusters will make it easier to identify 5HT and/or NO modulation of the various electrophysiological properties of neocortical neurons. Without classification, effects by either neuromodulator could be missed in the population average of all un-classified neurons as individual cell types might show different types of responses.

At least fourteen distinct 5HT receptors that mediate the effects of 5HT on cell physiology have been identified in mammals. These receptors are divided into seven main families, $5HT_1$ to $5HT_7$; some of these families have distinct subtypes (i.e. $5HT_{1A}$, $5HT_{1B}$, $5HT_{1D}$, $5HT_{1E}$, $5HT_{1F}$, $5HT_{2A}$, $5HT_{2B}$, $5HT_{2C}$, $5HT_{5A}$, $5HT_{5B}$; Hoyer et al. 1994). With the exception of $5HT_3$, which is a ligand-gated ion channel (Derkach et al. 1989), all of the others are part of the major G protein-coupled receptor (GPCR) family. The 5HT receptor families can be grouped into $G_i/G_o$-protein coupled receptors ($5HT_1$ and $5HT_5$) that have a predominantly inhibitory effect on neuronal activity (Araneda & Andrade 1991; Puig et al. 2010), $G_q/G_{11}$-protein coupled receptors ($5HT_2$) and the $G_s$-protein coupled receptors ($5HT_4$, $5HT_6$ and $5HT_7$; Figure 1-2A). $5HT_2$ as well as $5HT_4$, $5HT_6$ and $5HT_7$ receptors have predominantly excitatory effects on neuronal activity (Béïque et al. 2007; Bonsi et al. 2007; Goaillard & Vincent 2002; Chen et al. 2008).

The $G_i/G_o$- and $G_s$-protein coupled receptors modulate the activity of adenylate cyclase, with the former inhibiting and the latter stimulating enzyme activity (Sunahara et al. 1996). This enzyme catalyses the conversion of adenosine triphosphate (ATP) to cAMP and pyrophosphate. cAMP has multiple functions including the activation of cAMP-dependent protein kinase, or protein kinase A (PKA), which can modulate ion channel function by phosphorylation (reviewed in Bers 2002). $G_q/G_{11}$-protein coupled receptors, on the other hand, activate phospholipase C (PLC; Tanaka et al. 2000), cleaving the phosphatidylinositol 4,5-bisphosphate ($PIP_2$) into diacyl glycerol (DAG) and inositol 1,4,5-trisphosphate ($IP_3$). $IP_3$ binds to $IP_3$ receptors in the endoplasmatic reticulum, opening calcium channels and increasing the cytosolic calcium concentration in the process (Nishizuka 1988; Berridge 1993). DAG activates protein kinase C (PKC) and facilitates the translocation of PKC from the cytosol to the plasma membrane (Figure 1-2A; Berridge 1993).

NO production in the CNS occurs mainly via the calcium-calmodulin controlled enzyme nNOS. With the rise of intracellular calcium ions, calmodulin is activated, which then binds and activates nNOS. nNOS is a homodimer with each subunit containing two functional domains, a carboxyl terminal reductase and an amino terminal oxygenase domain (Figure 1-2B). The first domain binds two flavins as well as nicotinamide adenine dinucleotide phosphate (NADPH); in the second domain, the cofactor

tetrahydrobiopterin and L-arginine can be bound (Schild et al. 2006). The result of this catalysed reaction is NO, citrulline and $NADP^+$. With NO being an amphiphilic radical gas, it is highly water and lipid soluble and mobile, passing through cellular membranes with little resistance. Because of this locomotion ability, it is also considered a volume transmitter as it is not confined to a conventional synapse (Steinert et al. 2008).

NO has two known pathways to modulate cellular properties (Figure 1-2B). One of these occurs by the direct reaction of NO with thiol groups in proteins, the so-called S-nitrosylation. Interestingly, this mechanism can be controlled by enzymes responsible for reversing S-nitrosylation, the denitrosylases, making this mechanism analogous to phosphorylation (Benhar et al. 2009). S-nitrosylation has a ubiquitous influence on signal transduction and the regulation of diverse cellular responses. For example, the stimulation of N-methyl-D-aspartate (NMDA) receptors leads to the activation of $p21^{Ras}$ through the generation of NO via NOS. This activation is caused by S-nitrosylation (Yun et al. 1998) and may result in neuronal differentiation, plasticity, and long-lasting neuronal responses (Macara et al. 1996). Moreover, nitrosylated $p21^{Ras}$ can also stimulate ATP-sensitive potassium channels (Lin et al. 2004). Direct S-nitrosylation can also occur in calcium-dependent potassium channels in vascular smooth muscle cells (Bolotina et al. 1994). There is evidence that S-nitrosylation can affect serotonergic pathways, as is the case in pulmonary vasoconstriction, caused by $5HT_2$ receptor activation. This 5HT effect could be inhibited, in a reversible manner, by the NO-donor S-nitrosoglutathione and it has been suggested that this is due to direct nitrosylation of the $5HT_2$ receptor (Nozik-Grayck et al. 2002).

The other pathway that mediates NO effects on cellular properties is by binding to the NO receptor soluble guanylyl cyclase (sGC). This receptor is then activated and catalyses the conversion of guanosine triphosphate (GTP) to cGMP (Kimura et al. 1975). This binding domain is a haem group with a high affinity for NO (Martin et al. 2006), and there is a near instantaneous increase in the activity of sGC in neurons after being switched on by NO (Bellamy & Garthwaite 2001). The activation of sGC has a half-maximal activity value of around 10 nM NO in cells (Mo et al. 2004).

The increase in cGMP has many different actions in neurons. It can directly modulate hyperpolarisation-activated cyclic nucleotide-gated ion channels (Fesenko et al. 1985; Moosmang et al. 2001). It can also bind directly to PDE enzymes, such as PDE2, PDE3, and PDE5 (Bender & Beavo 2006). Another function of cGMP is to activate cGMP-dependent protein kinase, or protein kinase G (PKG), which can modulate vesicle trafficking (Wang et al. 2005), ion channel function, and acts on several other substrates, mostly by modulating the activity of various phosphatases (Bender & Beavo 2006), which can increase or decrease the levels of phosphorylation of proteins.

Possible interactions between 5HT and NO have been reported. For example, the application of tryptophan hydroxylase inhibitors, which leads to serotonin depletion in subjects, has been discovered to increase the level of nNOS immunoreactivity and NADPH diaphorase reactivity in the CNS (Tagliaferro et al. 2003; Ramos et al. 2002), the latter being an index of enzymatic NOS activity. However, it has also been shown that acute tryptophan depletion reduces the expression nNOS synthase in the rat hippocampus (Liu et al. 2013).

In addition to the fact that both 5HT and NO can modulate ion channel activity via phosphorylation caused by either PKA or PKG, PKG can also decrease intracellular calcium release by the phosphorylation of $IP_3$-receptor-associated cGMP kinase substrate, which then inhibits $IP_3$ receptor function (Schlossmann et al. 2000). This could affect 5HT responses that are mediated by $5HT_2$ receptors. Interactions between 5HT and NO signalling could also occur at the level of phosphodiesterases. For example, PDE2 activity is stimulated by cGMP, but hydrolyses both cAMP and cGMP, and has been suggested to mediate cross-talk between cGMP and cAMP signalling. Another interaction could be with PDE3, which can be activated by PKA phosphorylation (Bender & Beavo 2006).
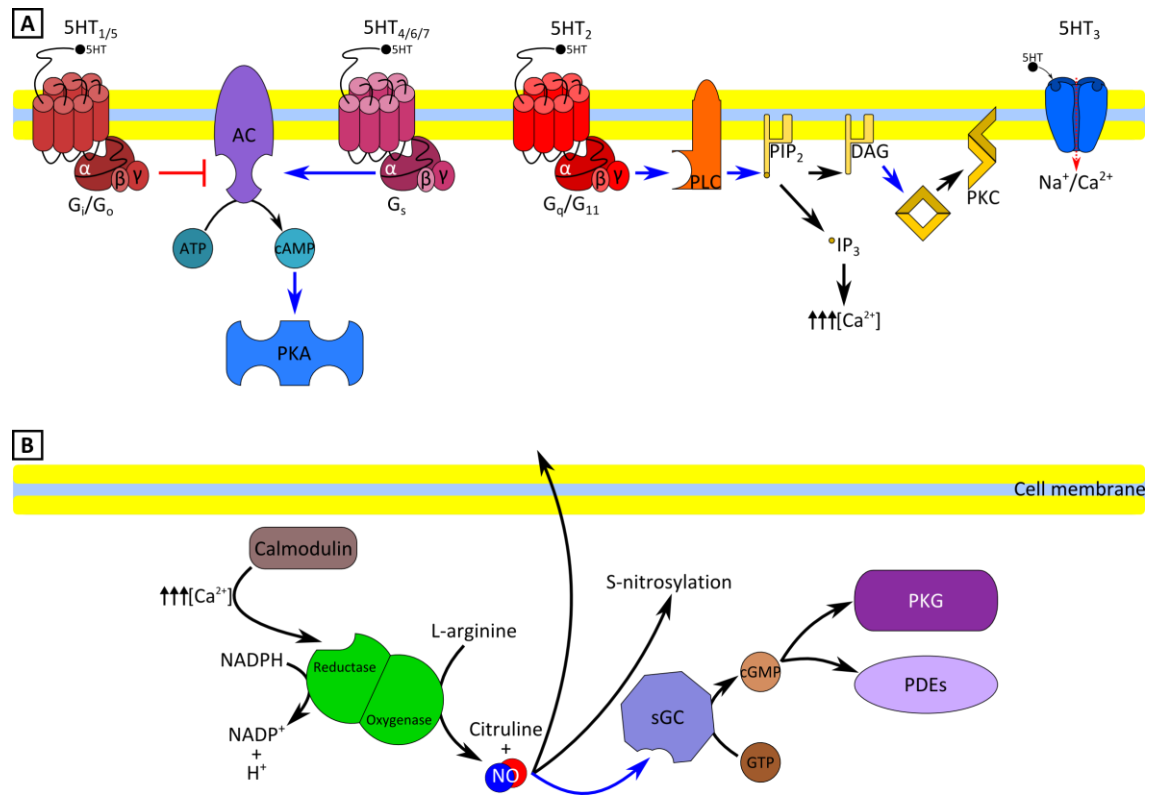
Figure 1-2: (A) 5HT receptor families and their signalling pathways, showing activation (blue arrows) and deactivation (red stops) of the various downstream pathways. (B) Enzymatic production of NO and its various signalling pathways. Bottom part of the cell membrane represents intracellular region. Blue arrows show excitation/activation, red stops show inhibition/inactivation.

## 1.6 Localisation of serotonin receptors and nitric oxide synthase expression in the cortex

The serotonergic system originating from neurons in the dorsal and ventral raphe nuclei extends to almost every region of the brain. The cortex in particular has a substantial widespread serotonergic innervation (Wilson & Molliver 1991a; Wilson & Molliver 1991b; Hoover & Vertes 2007; Weissbourd et al. 2014; Pollak Dorocic et al. 2014; Ogawa et al. 2014). Consistent with this extensive serotonergic innervation, there is widespread expression of 5HT receptors throughout the cortex. The distribution of the various serotonergic receptors is heterogeneous between the cortical areas (Mengod et al. 2006). $5HT_{1A}$ and $5HT_{1B}$ are expressed widely in the cortex, with the neocortex expressing the receptors mainly in the deeper layers, with two dense bands at layers V and VI. Staining suggests localisation of these receptors on the basal dendrites and cell bodies of pyramidal neurons in these layers and also in layers II/III, as well as on the somata and dendrites of stellate cells (Pompeiano et al. 1992). $5HT_{2A}$ shows an anteroposterior expression gradient in the cortex, with pyramidal cells in layer V expressing a high density of $5HT_2$ receptors, as well as non-pyramidal neurons in layer VI and GABAergic interneurons in the middle layers of the cortex (Andrade & Weber 2010). Although both $5HT_{1A}$ and $5HT_{2A}$ receptors are coexpressed in the medial prefrontal cortex, they are not necessarily present in the same layers.

$5HT_3$ receptors are expressed in interneurons throughout the cortical layers (Puig et al. 2004; Férézou et al. 2002; Vucurovic et al. 2010; Lee et al. 2010), whereas pyramidal neurons from the somatosensory cortex and especially the motor cortex from juvenile rats showed a high density of neurons stained for $5HT_4$ receptors. Other areas, such as the visual or the orbital cortex showed a low density of pyramidal neurons stained for $5HT_4$ receptors (Suwa et al. 2014). $5HT_5$ is expressed mildly in the neocortex of wild type mice (Waeber et al. 1998), but intense hybridisation has been found in the entorhinal and piriform cortical areas in rats (Kinsey et al. 2001). The localisation of $5HT_6$ receptors have been described as being expressed generally in the cortex, most notably in the piriform cortex (Ward et al. 1995; Kinsey et al. 2001). $5HT_7$ receptors, on the other hand, are located in layers I to III of the rat's cortex, both in pyramidal

neurons and GABAergic interneurons (Thomas & Hagan 2004; Bonaventure et al. 2004).

Neurons expressing NOS are randomly distributed in the various layers of the cerebral cortex. Pyramidal neurons from all layers except layer I presented immunoreaction to NOS during the early stages of adulthood as well as in aged rats, either in the cell soma only or in the whole neurons (Chung et al. 2004; Cha et al. 1998). Some GABAergic interneurons also expressed NOS (Kubota et al. 2011), and in the rat primary somatosensory cortex layers I-III presented the highest density of neurons expressing NADPH, which coincides with neurons that express NOS (Bredt et al. 1991).  The dendritic arbours of NADPH-positive neurons from layers IV-VI are predominantly vertically oriented (Nogueira-Campos et al. 2012). This widespread expression of NOS may be responsible for the maintenance of the homeostatic plasticity process and control of the excitation-inhibition balance in the cerebral cortex (Le Roux et al. 2009).

There is evidence to suggest that 5HT-containing neurons are morphologically and functionally related to NOS-positive neurons. For example, a subset of serotonergic neurons in the dorsal raphe nuclei also express NOS (Simpson et al. 2003). Other monoaminergic neurons in the brain have also been shown to possess NADPH diaphorase activity (Johnson & Ma 1993) or nNOS immunoreactivity (Wang et al. 1995). At the functional level, it has been reported that application of NO donors can enhance 5HT release in the medial preoptic area and in the striatum (Lorrain & Hull 1993; Guevara-Guzman et al. 1994). There are also reports of direct interaction between NO and the serotonin transporter (SERT), a member of the $Na^+/Cl^-$-dependent transporter family responsible for the reuptake of serotonin after its release from neurons (Torres et al. 2003). NO donors inhibited the reuptake of serotonin by SERT (Bryan-Lluka et al. 2004) presumably through the cGMP pathway, although not directly by the phosphorilation of SERT by PKG (Wong et al. 2012). Another possible interaction is between SERT and nNOS, which occurs through direct binding of the enzyme to SERT (Chanrion et al. 2007). This connection not only modulates the reuptake of 5HT, but also regulates the production of NO.

## 1.7 Project aims

Although there is extensive literature showing evidence for morphological overlap between 5HT and NO signalling pathways, the interaction between the release of 5HT and NO, and a range of potential mechanisms that could mediate cross-talk between both neuromodulators' signalling pathways, very few studies have directly investigated possible interactions at the cellular and synaptic levels. One recent study in the pond snail showed that NO can increase the postsynaptic effect of 5HT in an identified neuron (Straub et al. 2007). Despite the fact that serotonergic and nitrergic signalling pathways overlap, to date no studies have been conducted on mammalian cortical neurons to investigate this potential cross-talk at the cellular level.

In the current study, cell cultures prepared from Wistar rat cortices were used to address this question. In particular, the study will focus on the hypothesis that 5HT and NO signalling pathways interact in the modulation of the intrinsic properties of mammalian cortical neurons. Initial experiments focused on the effects of 5HT and NO on spontaneous activity and glutamate-evoked responses in cultured neurons. The results of these experiments hinted at the possible modulation of intrinsic membrane properties of the neurons by both 5HT and NO.

It also became apparent that the responses are very heterogeneous, possibly reflecting the heterogeneity of cell types present in the cortex. Therefore, it was necessary to devise a procedure to effectively group neurons with similar electrophysiological properties. With this identification it was possible to characterise the modulatory effects of 5HT and NO on different electrophysiological parameters. Furthermore, the results provided evidence for non-linear interactions between 5HT and NO signalling pathways. Interactions between the two neuromodulators appeared to involve both sGC/cGMP signalling and S-nitrosylation.

The experiments in cortical cultures were complemented by studies in acute cortical slices to assess the similarity between neurons in cultures and intact tissue. Finally, the effects of 5HT and NO on spontaneous activity in acute cortical slices were assessed. The results obtained show an interaction between 5HT and NO in the modulation of

both intrinsic membrane properties of cortical neurons and neocortical network activity.

## 2 Materials and Methods

## 2.1 Animals

All experiments were carried out on cortical neurons from Wistar rats, aged 0-2 days after birth for cell culture and 12-17 days after birth for tissue preparations. All procedures were conducted in strict accordance with the Home Office Code of Practice for the Humane Killing of Animals under Schedule 1 of the Animals (Scientific Procedures) Act 1986.

Gibco® foetal bovine serum (FBS), Neurobasal® Medium (1x), B-27® Serum Free Supplement (50x), Gibco® L-glutamine, penicillin/streptomycin (5k u/ml: 5k µg/ml) and Hank's Balanced Salt Solution (HBSS) were obtained from Life Technologies™; KCl, $CaCl_2$ and glucose were obtained from Fisher Scientific; $MgCl_2$ and NaOH were obtained from VWR; kynurenic acid was obtained from Tocris Bioscience; 1H-[1,2, 4]oxadiazolo[4,3-a]quinoxalin-1-one (ODQ) was obtained from Cayman Chemical. All remaining chemicals were obtained from Sigma-Aldrich®.

## 2.2 Cell Culture

The cell culture procedure used was adapted from a previously published protocol (Young et al. 2005) and is described in detail below.

### 2.2.1 Media and solutions for cell culture

Unless otherwise stated, the solutions were prepared in cell culture-grade water (Sigma, W3500). Percentage values always relate to the final volume. The solutions were prepared as follows:

**Cell culture medium:** Neurobasal (basal medium, Life Technologies, 21103-049) + 2% B-27 Supplement (serum-free supplement, Life Technologies, 17504-044) + 1% penicillin/streptomycin (antibiotic, Life Technologies, 15070-063).

**Nutrient Cocktail** (NC; in mM): 50 L-glutamine (Life Technologies, 25030-024), 100 sodium pyruvate (Life Technologies, P5280-25G), 100 L-serine (Life Technologies, S4311-25G).

**Plating medium:** Cell culture medium + 10% heat inactivated FBS (10270) + 1% NC.

**Maintenance medium:** Cell culture medium + 1% NC.

**Dissection solution** (in mM): 130 NaCl, 5.4 KCl, 0.4 $MgCl_2$, 9.6 HEPES, 1.8 $CaCl_2$, 25 glucose, pH 7.4 adjusted with NaOH.

**Digestion mixture:** 5 mg of protease from *Streptomyces griseus* type XIV (Sigma, P5147) and 5 mg thermolysin from *Geobacillus stearothermophilus* type X (Sigma, P1512) in 10 ml sterile-filtered, cell culture-grade water.

**Deoxyribonuclease I** (DNAse, 4000 units/ml): 7.03 mg of DNAse per 1 ml of cell culture-grade water.

**Preparation of cover slips for cell culture:** The preparation of cover slips was carried out under sterile conditions in a laminar flow hood. Circular glass cover slips (13 mm diameter; Agar Scientific, L4097-1) were flame sterilised and two cover slips were placed into each well of a 6-well Nunc™ cell culture plate (VWR International, 734-0991). Each cover slip was covered with 0.2 ml 0.01% Poly-D-lysine hydrobromide (PDL, average mol weight 30k-70k; Sigma, P7280) and the 6-well plate covered with its lid. After 1 hour, the PDL was removed and the cover slips were washed three times with cell culture grade-water. The cover slips were left overnight in the laminar flow hood to air-dry and stored afterwards in an incubator until the day of use.

2.2.2 Dissociated cell preparation

All steps of this procedure were carried out in a laminar flow cabinet to reduce the risk of contamination of the culture dishes. Any solution that came into contact with non-sterile components was filter sterilised prior to use. Tools were sprayed with 70% industrial methylated spirit (IMS) before use and forceps were flame sterilised. Newborn Wistar rats (P0-P2) were culled by cervical dislocation, according to the Home Office Code of Practice for the Humane Killing of Animals under Schedule 1 of the Animals (Scientific Procedures) Act 1986, followed by decapitation, in the designated procedure room within the University of Leicester. The severed head was immediately placed in ice cold dissection solution. The scalp was removed by scalpel cutting rostral-caudally from forehead to spinal cord; the exposed skull was then opened using scissors to carry out a continuous lateral cut from the spinal cord to the forehead, above the ear and eye line. The skull was folded out revealing the cortex; the brain was carefully removed from the rest of the encasing skull using spatulas and placed with the dorsal side up on an ice cold dissecting pad that was humidified with dissection solution. The brain hemispheres were divided with a scalpel and each hemisphere was processed separately. If present, the olfactory bulb was removed. By holding the brainstem lightly with forceps it was possible to flip the cortex over, exposing the hippocampus. The cortex was separated by cutting with a scalpel between the hippocampus and cortex at a $30^o$ angle towards the cerebellum, separating those regions and the ventral part of the hemisphere from the cortex. Meninges were carefully removed using forceps and the cortex was left in ice cold sterile dissection solution.

Cortices were then cut into ~1 $mm^2$ pieces and transferred to a 30 ml tube. Excess buffer was removed, and filter sterilised digestion mixture was added directly to the pieces, in order to reduce/break down connective tissue and facilitate tissue dissociation. The mixture was gently homogenised and left at room temperature for 30 minutes.

Next, digestion solution was removed and 3 ml HBSS (14170) with 30 µl DNase (Sigma, DN25) was added. The mixture was gently triturated with a previously fire polished

glass Pasteur pipette, by pipetting up and down against the bottom of the tube. This was followed by 3 minutes of centrifugation at 250 G. The solution was discarded and the pellet was re-suspended in 3 ml plating medium. Centrifugation at 250 G was repeated for 3 minutes. After this, the plating medium was discarded and 1 ml of fresh plating medium was added to the tube, followed by homogenisation of the mixture. The cell density was then counted using a haemocytometer and adjusted with plating medium to achieve a final cell density of ~1.10 x $10^6$ cells/ml.

The dissociated cells were then plated onto cover slips by placing a drop of 50-100 μl of the cell suspension into the centre of each cover slip. The plates and plating medium were left in an incubator (37°C, 95% $O_2$/5% $CO_2$) for 1 hour, after which each well was topped up by carefully adding 2 ml of plating medium. Finally, a check was made to ensure that the cover slips were positioned securely at the bottom of the well.

48 hours after cell plating, media from each well was exchanged for fresh plating medium containing 5 μM cytosine β-D-arabinofuranoside (ara-C; Sigma, C6645) to stop proliferation of glial cells. After 24 hours, the ara-C containing plating medium was replaced with 2 ml of maintenance medium in each well. Subsequently, half the media per well (1 ml) was changed for fresh maintenance medium once per week. Experiments were carried out on 14 – 20 day old cultures.

## 2.3 Tissue preparation

The tissue preparation procedure for the recording of cortical neurons in acute brain slices was adapted from a previously published protocol (Barnes-Davies & Forsythe 1995) and is described in detail below.

### 2.3.1 Solutions

**Dissection solution** (in mM): 2.5 KCl, 4 $MgCl_2$, 0.1 $CaCl_2$, 10 glucose, 1.2 $NaH_2PO_4$, 25 sucrose, 22.5 $NaHCO_3$, 1 kynurenic acid (0223) and 0.01 7-nitroindazole (7-NI; Sigma,

N7778; 7-NI was first dissolved in dimethyl sulfoxide (DMSO) to prepare 100 mM stock solution; the final DMSO concentration in the dissection solution was 0.01%).

**Artificial Cerebrospinal Fluid** (aCSF; in mM): 124.9 NaCl, 2.5 KCl, 1 MgCl$_2$, 2 CaCl$_2$, 10 glucose, 1.2 NaH$_2$PO$_4$, 22.5 NaHCO$_3$, and 0.01 7-NI (final DMSO concentration 0.01%).

### 2.3.2 Dissection and slicing procedure

All solutions were oxygenated with 95% O$_2$/5% CO$_2$ gas at least 1 hour prior to the procedures and continued to be oxygenated during the procedures and experiments. The dissection solution was partially frozen until a slushy consistency was obtained. Juvenile Wistar rats (P12-P17) were culled by cervical dislocation, according to Home Office Code of Practice for the Humane Killing of Animals under Schedule 1 of the Animals (Scientific Procedures) Act 1986, followed by decapitation using a scalpel, in the designated procedure room within the University of Leicester. The severed head was immediately placed in a container with ice. The scalp was removed by cutting with a scalpel rostral-caudally from forehead to spinal cord. The exposed skull was then opened using scissors to cut caudal-rostrally from spinal cord to forehead, on the dorsal part of the head. Additional cuts were made perpendicularly from this initial cut in the centre of the skull. The skull quadrants were folded out revealing the cortex; the brain was carefully removed from the rest of the encasing skull using a spatula and immediately placed in ice cold slicing solution for transport.

The brain was then placed on an ice cold dissecting pad, humidified with dissection solution, with the dorsal side facing upwards. The brain was divided with a coronal cut around the proximodistal axis of the hippocampal CA1 region and the frontal part was fixed with the cut-surface first to a 752/M Vibroslice Tissue Cutter (Campden Instruments, UK) fixed tissue holder using a small quantity of cyanoacrylate adhesive. The tissue holder was moved to the temperature controlled vibroslice tissue bath with the dorsal side of the brain facing the blade and the chamber was filled with dissection solution. The blade was set to oscillate in the horizontal plane at 3k RPM and advanced at ~0.62 mm/s. 250 μm slices were cut starting at bregma+3.0 going to bregma+2.2,

according to rostral-caudal coordinates depicted in the rat brain atlas (Paxinos & Watson 2007). Slices were placed directly into an incubation chamber containing normal aCSF and 1 mM kynurenic acid for incubation for 1 hour, after which the slices were moved via transfer pipette to a stage chamber mounted on a Burleigh® Gibraltar® fixed stage for electrophysiology.

## 2.4 Electrophysiology

### 2.4.1 Extracellular solutions

Cover slips with neuronal cell cultures were placed in the microscope chamber and held in place by application of a small amount of silicon grease to the bottom of the chamber. A Sylgard® (Dow Corning) mould was made and placed over the cover slips to reduce the volume of the bath. For recordings from neuronal cultures the composition of the basic extracellular solution was as follows (in mM): 135 NaCl, 5 KCl, 1.5 $MgCl_2$, 25 HEPES, 2 $CaCl_2$, 10 glucose, pH 7.4 adjusted with NaOH.

For the recording of neuronal cells in slices, prefrontal cortical slices were placed in the microscope chamber and held in place by a U-shape harp with a flattened platinum frame and nylon strings. For brain slices the basic extracellular solution used was aCSF with the following composition (in mM): 124.9 NaCl, 2.5 KCl, 1 $MgCl_2$, 2 $CaCl_2$, 10 glucose, 1.2 $NaH_2PO_4$, 22.5 $NaHCO_3$, and 0.01 7-NI (final DMSO concentration 0.01%). The solution was constantly bubbled with 95% $O_2$/5% $CO_2$ to ensure oxygen saturation and maintain the pH.

The recording chamber was constantly perfused at a rate of 1 ml/s using a MINIPULS Evolution® peristaltic pump (Gilson®). All electrophysiological recordings were carried out at room temperature (20-22°C). Any additional chemicals for pharmacological studies were added to the appropriate basic extracellular solution. Their final concentration is as follows (in μM): 50 Serotonin hydrochloride (5HT, Sigma, H9523), 100 diethylamine NONOate sodium salt hydrate (DEA; Sigma, D5431), $10^3$ kynurenic

acid, 50 (for cell culture)/100 (for brain slices) picrotoxin (Sigma, P1675), 1 ODQ (Cambridge Bioscience, CAY81410), 1 MDL 72222 (Sigma, T102), 1 ketanserin (+)-tartrate salt (Sigma, S006), 50 α-methylserotonin maleate salt (αMe5HT; Sigma, M110), 25 (R)-(+)-8-Hydroxy-DPAT hydrobromide (8-OH-DPAT; Tocris, 0529).

### 2.4.1.1 Measuring nitric oxide release

DEA is a nitric oxide (NO) donor, which spontaneously dissociates into diethylamine and NO in a pH-dependent, first-order process with a half-life of 16 minutes at room temperature and pH 7.4. In order to quantify the actual NO concentration in the bath, NO release from DEA was measured directly using an amperometric sensor (ISO-NO Mark II NO meter, WPI, USA). This sensor has a selective membrane which allows NO to diffuse, but excludes other molecules that could interfere with NO detection. Detection is based on the oxidisation of NO at the electrode, resulting in an electrical current proportional to the concentration of NO in the sample. This current was recorded with a MiniDigi 1A A/D converter (Axon Instruments, Foster City, CA) and calibrated using the decomposition of S-nitroso-N-acetyl-D,L-penicillamine (SNAP) in the presence of cupric (II) sulphate ($CuSO_4$) as a catalyst (both provided with the kit). This method generates a fixed quantity of NO in solution that is proportional to the known SNAP concentration enabling the construction of a calibration curve (Figure 2-1A). Quantification of NO released by DEA under experimental conditions was obtained immediately after the calibration by placing the sensor in the perfusion system just before it entered the bath. A sample of the calibration is shown in Figure 2-1A, together with the amount of NO released by the donor.

Independent measurements were carried out at four different time points during the project. A concentration of 0.1 mM of DEA was used, the same concentration used during experiments. The average final concentration of NO released by DEA, measured with the ISO-NO Mark II sensor, was 6.35 ± 0.28 µM (n=4). NO concentrations were also measured during co-application of DEA and 5HT to determine whether the presence of 5HT affects the release of NO (Figure 2-1B). However, the resulting NO concentration was similar to the one previously obtained (n=2). Depleted DEA (left for

more than 2 days in solution at room temperature) was also measured (Figure 2-1B). As expected, the sensor did not respond during application of the depleted donor (n=2) confirming that the sensor response to fresh DEA is indeed due to NO and not some other component in the solution.

## 2.4.2 Intracellular recording of neurons

Standard whole cell patch clamp techniques were used to record electrical activity of 726 cortical neurons in cultures and brain slices. Recordings were carried out in either current clamp or voltage clamp mode. Recordings that showed changes of more than 25% in resting membrane potential (current clamp) or holding current (voltage clamp) were discarded and not included in the total number of recorded cells and the analysis. Recordings that fulfilled these criteria showed stable input and serial resistance as well as electrophysiological parameters for periods of over ten minutes (Figure 2-2). The membrane potential or whole-cell current was recorded using a Multiclamp 700A amplifier (Axon Instruments, Foster City, CA). The signals were filtered at 6 kHz before being sampled at 12.5 kHz using a Digidata 1322A A/D converter (Axon Instruments, Foster City, CA) and pCLAMP software. The data were stored on a PC (AMD processor 2.49 GHz and 896 Mb of RAM memory) running Microsoft Windows XP Service Pack 3 as the operating system. Microelectrodes for intracellular recording were manufactured from 1.5-mm borosilicate capillary glass (World Precision Instruments, Sarasota, FL) using a Sutter P-97 flaming/brown micropipette puller (Sutter Instrument, Novato, CA). Tip resistance was 3–9 MΩ for recordings when filled with pipette solution containing (in mM) 10 NaCl, 140 K-gluconate, 1 $MgCl_2$, 10 HEPES, 0.2 EGTA, 4 $Na_2ATP$ and 0.3 GTP at pH 7.3. Care was taken to adjust the osmolarity of the intracellular solution to ~10 mOsm less than the extracellular solutions with the addition of double distilled water.

For cortical cell cultured experiments, access to the cell was clear; therefore there was no need for strong positive pressure while approaching the cell. A slight positive pressure was applied to avoid debris accumulating at the pipette tip. After initial giga-ohm seal formation, cell membranes were easily ruptured to obtain intracellular
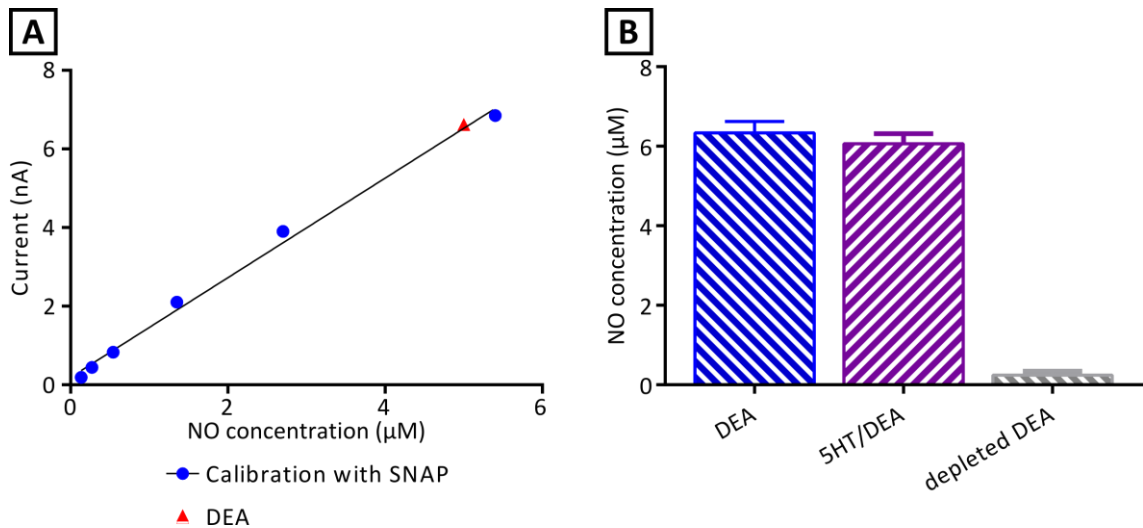
Figure 2-1: (A) Sample of a calibration curve for NO measurement using an amperometric sensor, the ISO-NO Mark II NO meter. The blue circles show measurements for known amount of NO released by SNAP. The triangle indicates the amplitude of the current response caused by 100 µM DEA in the extracellular solution and the corresponding NO concentration. (B) Graphs showing the average amount of NO released by freshly made 100 µM DEA (n=4), 100 µM DEA with 50 µM 5HT (n=2) and 100 µM depleted DEA (n=2).
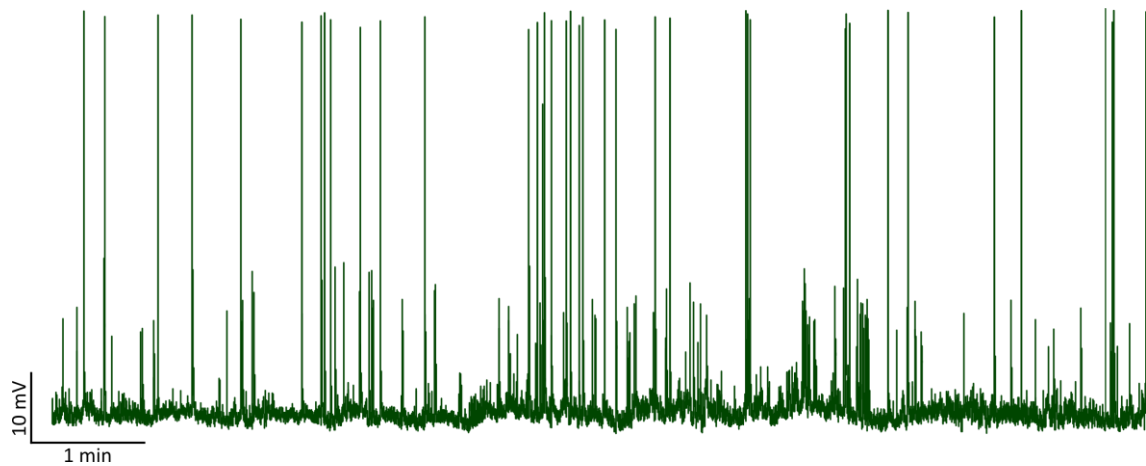


Figure 2-2: Example trace of a long stable recording, demonstrating that the passive membrane potential didn't change over a period of more than ten minutes.

access. In brain slice experiments, strong positive pressure inside the micropipette was required in order to clear the target cell from connective tissue.

A liquid junction potential value of -11 mV was measured before experiments, allowing the correction of membrane potential recordings accordingly in all experimental protocols.

2.4.3 Electrophysiological analysis

Electrophysiological properties of cortical neurons were recorded in either current or voltage clamp mode. In both modes, spontaneous activity of the cells was recorded continuously. Excitability of cells was analysed in current-clamp mode using a protocol that consisted of the application of 400 or 500 millisecond (ms) current pulses ranging from -140 picoAmps (pA) to +200 pA (step increment: 20 pA). All electrophysiological recordings were analysed using Spike2 version 6.15 (Cambridge Electronic Design) with custom-written scripts. The steady-state change in membrane potential as the result of current injection was measured at 10 ms before the end of the pulse. The effects of hyperpolarisation-activated currents ($I_h$) and membrane time constant in cortical neurons were measured by the analysis of the membrane potential response to a negative current of -140 pA (Figure 2-3A). $I_h$ was quantified as the ratio of the steady-state response of the membrane, 10 ms before the end of the negative current pulse and the most hyperpolarised membrane potential value within 200 ms of the beginning of the pulse. For manual clustering, a cell was considered to express $I_h$ if the ratio was less than 92.5%. The membrane time constant was calculated by fitting the change in membrane potential beginning from 10% and ending at 90% of the most hyperpolarised point with a single exponential function. The input resistance ($I_r$) was obtained by measuring the steady-state membrane potential response to a -20 pA current step.

Action Potentials (APs) were defined as a rapid increase in membrane potential with a minimum amplitude of +10 mV, resulting in a fast peak that recovers within 10 milliseconds. Rheobase was considered to be the lowest amplitude positive current

injected necessary to trigger at least 1 AP (Figure 2-3A). Spike height adaptation was defined as the ratio between the last and the first AP height amplitude at 200 pA (Figure 2-3B).

The peak of APs was located by fitting a parabola through the highest points after threshold. The start of APs was determined by the first peak of the 3$^{rd}$ derivative of the slope of the membrane potential just before the peak of APs. The slope was calculated using an equal weighting of the points from time t - 0.3 ms to t + 0.3 ms. Trough amplitude of the APs was calculated by subtracting the membrane potential at the start of an AP from the most negative value within the first 20 ms after the AP peak. The width of an AP was determined by finding the point where the membrane potential had risen to 50% of AP's maximum height point, starting from the AP's start point. A horizontal line was applied to this point, and the time (length of line) was measured until the descending membrane potential of the AP crossed this level (Figure 2-3C).

The inter-spike interval (ISI) was defined as the time gap between two successive APs. ISI slope was obtained by plotting the ISIs of all APs elicited in response to a 200 pA current step against the AP number and fitting the data with a linear regression line. The minimum ISI is the shortest ISI between any two APs elicited by a 200 pA pulse. This is a measure of the highest instantaneous firing frequency of a neuron under these conditions. The ratio of the minimum ISI over the maximum ISI was also considered as it provides information about changes in firing frequency during a current pulse (Figure 2-3D). The spike burst pattern was calculated as the quotient of the difference of time between the first and last AP at 200 pA by the total time of the current step (Figure 2-3D). This parameter provides information about the length of AP firing in response to a positive current pulse. A ratio close to 1 indicates that the cell continued to fire APs throughout the current pulse, while ratios significantly lower than 1 indicate more phasic activity.

In some cells 5HT would elicit a transient depolarisation of the membrane potential. Its height was measured as the difference between the average of the membrane potential over a 2-second period, 5 seconds before the start of this response
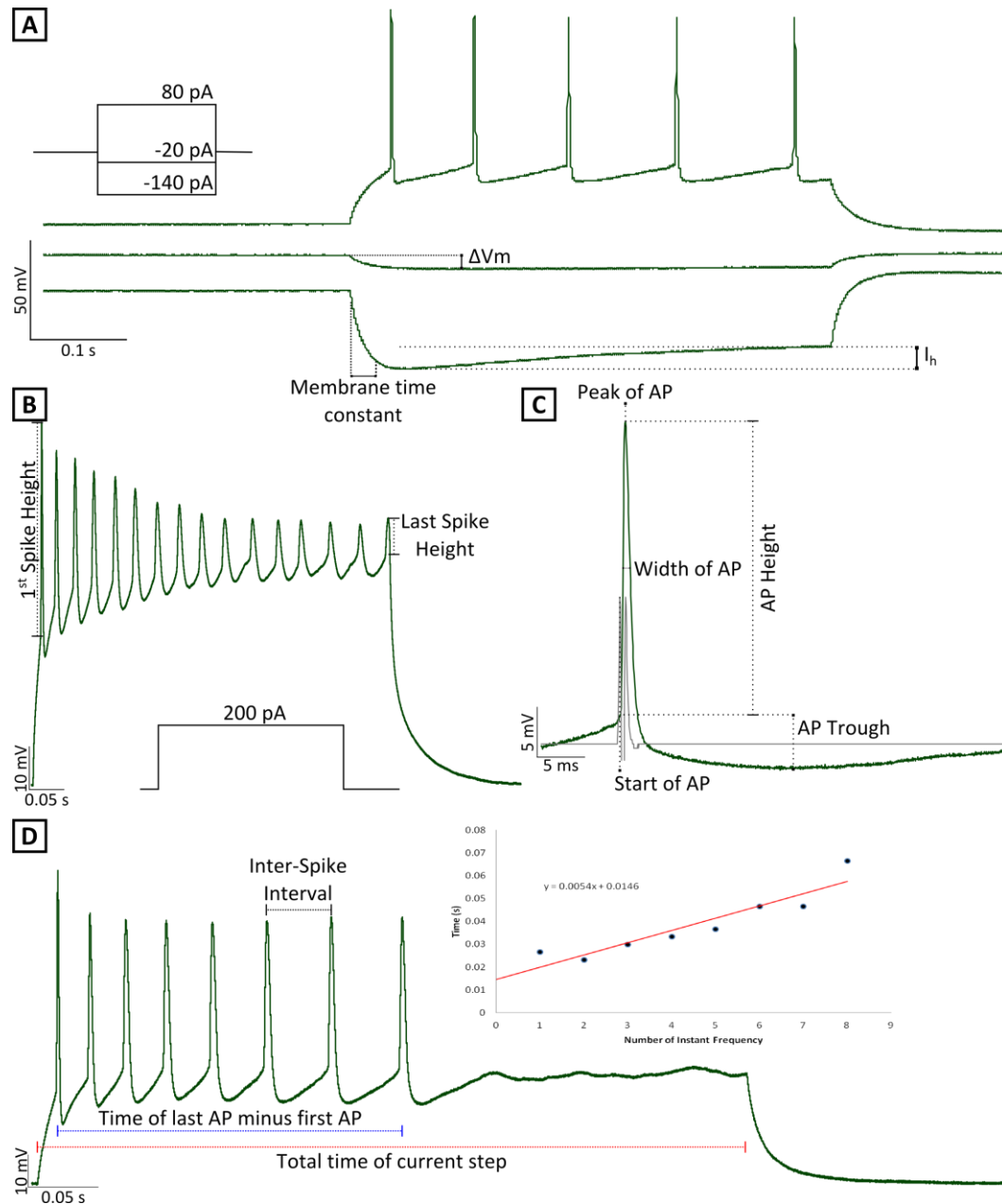
Figure 2-3: (A) Examples of membrane potential responses to three current steps (-140, 20 and 80 pA) recorded in a cortical neuron in cell culture. The lower trace indicates the aspects of the record that were used to measure $I_h$ and membrane time constant. The middle trace shows the measurements that were used for calculating the membrane resistance. The upper trace shows a series of APs in response to an 80 pA current pulse, the rheobase for that cell. (B) Trace showing the amplitude of the first and last AP in a cultured cortical neuron used to calculate spike height adaptation. (C) Record of an AP showing the start of the AP indicated by the positive peak of the third derivative (gray) prior to AP peak, and the amplitude, half-width and trough of the AP. (D) Trace illustrating the measurement of the inter-spike interval, and measurements that were used to calculate the spike burst pattern parameter. The inset graph shows the ISI for that record plotted against the AP number. It also shows the linear regression line fitted to this data that was used to determine the ISI slope at 200 pA.

(baseline), and the positive peak in the membrane potential value during the event. Sometimes this would be followed by a trough, but it always recovered to the baseline value (Figure 2-4A).

Glutamate (60 µM) responses were measured by pressure-application (10 PSI for 50 ms) using a borosilicate capillary glass with a wider tip (1-2 MΩ) directly onto the recorded cells from a distance of approximately 70 µm. The cells' response was a rapid, transient depolarisation, and the area, amplitude and the duration of the response at 50% maximum amplitude were measured as indicated in Figure 2-4B. During the response, the number of APs was also counted.

Spontaneous excitatory synaptic currents were measured using standard voltage-clamp protocols. For spontaneous activity, the recorded traces were filtered post-hoc with the use of an infinite impulse response filter, a filter similar to an analogue filter. In this case, a first order Chebyshev bandpass filter with a ripple factor of 3 and a low-pass cut-off at 1.35 and high-pass cut-off at 1000 Hz was applied. For the detection of excitatory post-synaptic currents (EPSCs), data were further smoothed with a time constant of 0.8 ms. Events with an amplitude larger than 2 pA that were followed by an exponential return to baseline were identified as EPSCs. The amplitude of the EPSC was measured as the difference between the peak current and the average baseline current prior to the EPSC. The EPSC time constant was derived from the exponential fit of the EPSC to baseline (Figure 2-4C).

### 2.4.4 Imaging of cortical cultures and brain slices

Electrophysiological experiments were carried out on an Olympus Binocular BX-50WI microscope with differential interference contrast optics, allowing the visualisation of the neuronal cultures or the brain slices. Images of cortical neurons were recorded using either a COHU Scientific High Performance CCD camera 4900 series and stored on a personal computer with the use of Hauppage!® WinTV-USB, or using a Moticam M1000 camera (Motic®) controlled by the Motic Image Plus 2.0 (Motic®) software.
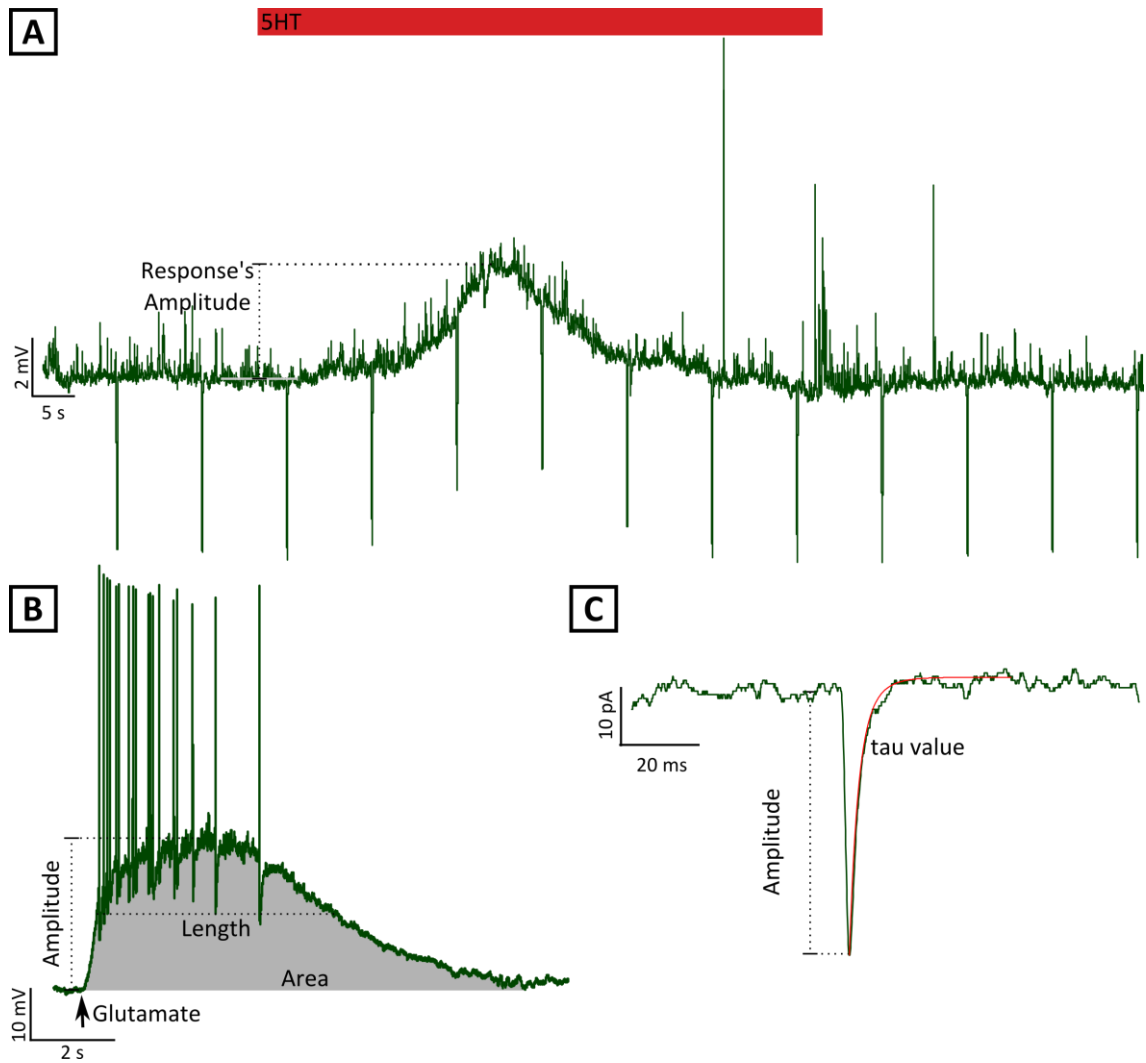
Figure 2-4: (A) Example of depolarisation of membrane potential in response to application of 5HT (in red bar). The figure indicates the measurement of the 5HT response. (B) Example of a response to puff-application of glutamate. Again, the parameters that were used to characterise the response are depicted in the recording, with the area of the response being shown in gray. (C) Sample EPSC recording showing the amplitude and the exponential fit of the current used to determining the decay time constant.

These images were analysed for morphology comparison, in the case of the neuronal cultures, or for position of the recorded cell in brain slices.

Cultured cells were classified as pyramidal-like, bipolar, or multipolar according to the following criteria. A pyramidal-like cell had a triangular perikaryon with three prominent processes (Figure 2-5A$_1$). If the dendritic processes emerged only from opposite poles of the perikaryon, the cell was classified as bipolar (Figure 2-5A$_2$). Cells were classified as multipolar if they had multiple processes of approximately equal lengths and diameter arising from multiple sites around the perikaryon (Figure 2-5A$_3$).

In addition, the area of the perikaryon was measured by outlining the perimeter of the cell's body using Fiji/ImageJ (Figure 2-5B).

## 2.5 Clustering and statistical analysis software

Data obtained was stored in a Microsoft Access 2007 database for further analysis. *k*-Means clustering was carried out using Orange, a data mining toolbox in Python, developed at the Bioinformatics Laboratory, Faculty of Computer and Information Science, University of Ljubljana, Slovenia, together with an open source community (Demšar et al. 2013). Expectation-Maximisation (EM) algorithm was applied using the package mclust for R: A language and Environment for Statistical Computing version 3.0.2 (R Foundation for Statistical Computing, 2013). Clustering validation was obtained using the package clValid for the same software. Principal component analysis (PCA) was run on IBM SPSS Statistics for Windows, version 20.0. (Armonk, NY: IBM Corp).

Statistical analyses were obtained using GraphPad Prism (GraphPad Software), or R version 3.0.2. Nonparametric tests for the comparison of multiple parameters were carried out using the Kruskal-Wallis test, followed by Dunn's multiple comparisons (DMC) test; one-way *t* tests were used to test whether changes in a parameter were significantly different from zero. Kolmogorov-Smirnov (KS) test was used to compare cumulative frequency distributions between before and after treatment application. For the comparison of the parameters between the treatments and control levels, a
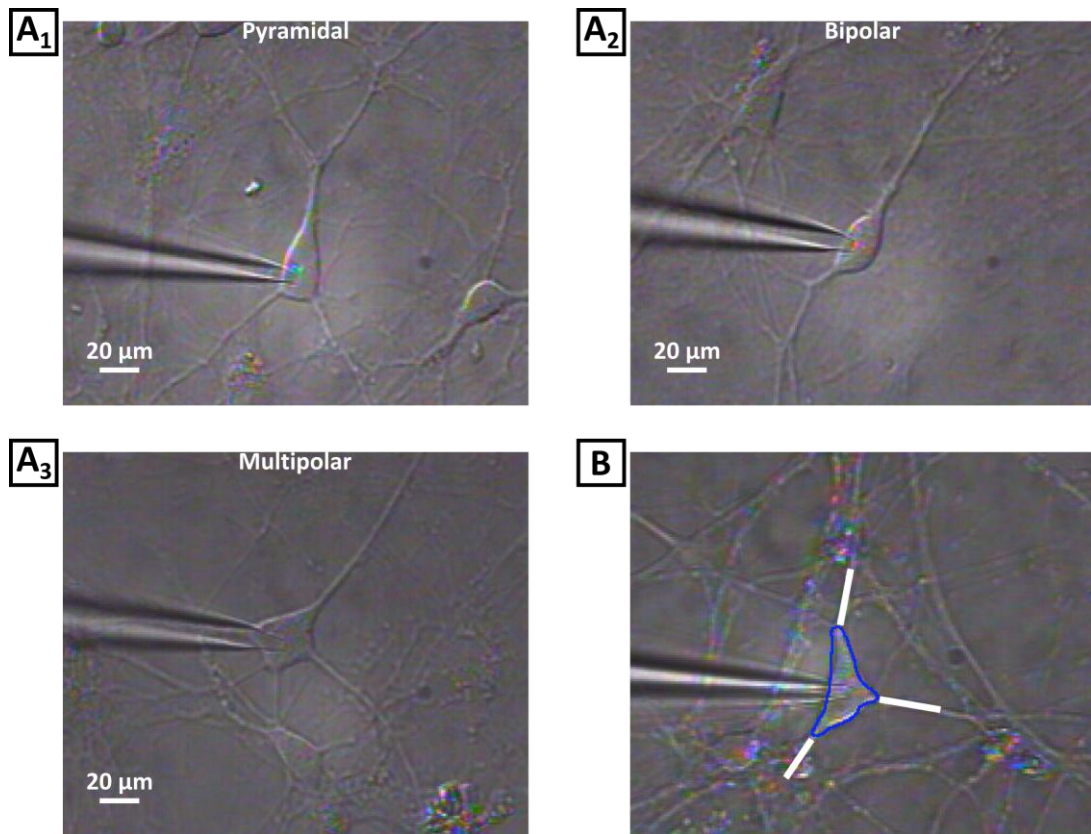
Figure 2-5: (A$_1$ to A$_3$) Examples of the 3 morphologically different types of cultured cortical neurons recorded during the project. (B) Example of a pyramidal neuron with the perimeter (blue) and number of processes (white) highlighted.

non-linear mixed-effect model (MLM) was constructed  using the nlme package for R (Pinheiro et al. 2012). All graphs are showing mean ± standard error of the means (SEM), unless stated otherwise.

Figures were prepared using Inkscape version 0.48.4.

# 3 Clustering cultured cortical neurons - identification of neuron types by electrophysiological properties

In this chapter data will be presented and discussed focusing on the following points:

- The spontaneous activity of cortical neurons within cultured cortical networks, and the modulation of this activity by NO and 5HT;

- The modulation of glutamatergic responses of cultured cortical cells by NO and 5HT;

- Clustering algorithms and parameter sets that were used to classify the recorded neurons into distinct cortical cell types.

## 3.1 Introduction

The use of culturing methods for primary cells has many advantages. It is an accepted model and is widely used for the research of many disorders at various levels, from screening of drugs to studies of their effectiveness, from molecular mechanisms of viral infection and the use of multi-cellular cultures to studying aspects of brain development (Trinchese et al. 2004; Grau & Greene 2012; Kobayashi et al. 2012; Fishbein & Segal 2011). One of the benefits of culturing neurons is that the cells are more accessible to the researcher, especially for electrophysiology: the single layer of cells and lack of connective tissue in cell culture allows quick and easy access to the cell's surface, and the absence of connective tissue also minimises the barriers and diffusion delays to any applied substances (Dichter 1978; Potter & DeMarse 2001). However, one of the disadvantages of cell culture work is the fact that morphological cues to the identity of individual cells based on their position in the intact structure are not available. This is not an issue if the source material for the preparation of the culture consists of a single or very few cell types with clearly distinct morphological and/or physiological properties, but becomes a major issue if the source material consists of diverse and heterogeneous populations of cells as in the case of the neocortex that was studied in this project.

The structure of the neocortex is divided into four different lobes, frontal, parietal, occipital and temporal, each one of them performing various functions. In spite of this division into distinct anatomical areas, all of the cortical areas have a common general structure, a layered division consisting of six layers (layer I to VI). The prefrontal cortex is lacking layer IV. A more detailed description of the cortical connectivity is included in Chapter 1. The neuron types that make up the cortex can be broadly divided into pyramidal neurons and interneurons, with the former being around 80% of the neocortical neurons and the latter being around 20%. Cortical interneurons can be further classified into groups depending on their morphology, biochemical properties and their electrical fingerprint, such as spiny stellate cells, basket cells, excitatory bipolar cells and bitufted cells, among others. The numerous different types of neurons from the various regions can show diversity in their electrophysiological properties (e.g. Takahashi 1965; Calvin & Sypert 1976; McCormick et al. 1985; Povysheva et al. 2013) leading to different firing characteristics such as regular, burst, fast and late spiking (Figure 3-1). Various attempts are being made to provide resources to classify and compare the different neuronal cell types and their electrophysiological properties in the cortex. A freely editable semantic wiki webpage for community-based curation of terms used in neuroscience, NeuroLex (www.neurolex.org) which is a joint project of the Neuroscience Information Network and the International Neuroinformatics Coordinating Facility (Larson & Martone 2013), differentiates between twenty-two different types of neurons in the neocortex (checked in September 2014). Another website, NeuroElectro (www.neuroelectro.org, beta version) maintained at Carnegie Mellon University and the University of British Columbia, demonstrates that within the neocortex there are at least ten groups of neurons with different electrophysiological parameters (checked in September 2014). The physiological properties of these neurons have been extracted from data tables within 36 published articles found primarily in journals such as Journal of Neurophysiology, Epilepsia, European Journal of Neuroscience, Brain Research, Neuron, Neuroscience, Journal of Physiology and Journal of Neuroscience after 1997. While classification in NeuroLex is based on a manual definition of cell types, NeuroElectro uses Principal Component Analysis (PCA) to identify the parameters that vary across different neuron types, making it possible to understand more about
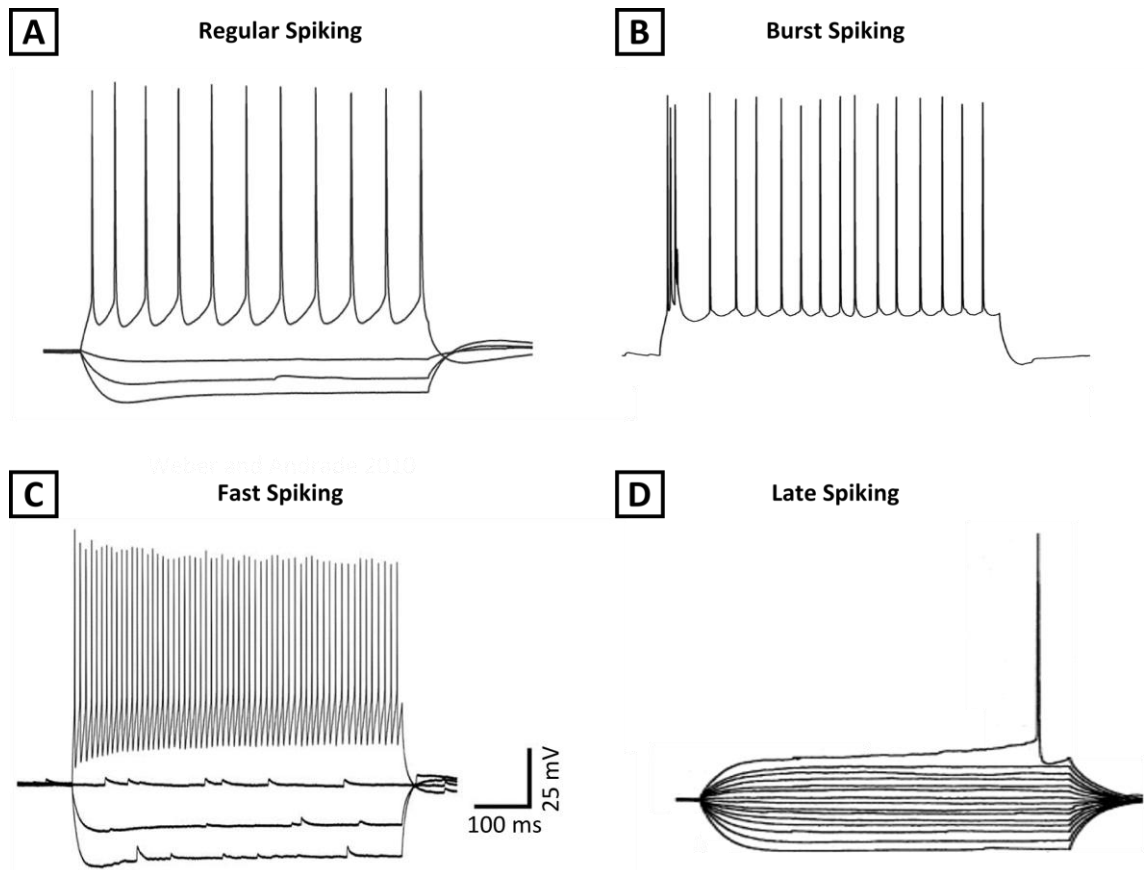
Figure 3-1: Cortical neurons can show differential electrophysiological properties. (A) Example recordings of regular spiking pyramidal neuron and (B) of burst spiking pyramidal neuron from layer V from the prefrontal cortex. (C) Example of fast spiking interneuron from layer V from visual cortex. (D) Example of late spiking interneuron from layer V of perirhinal cortex. Records are adapted from Xiang & Prince (2003), Moyer et al. (2002) and Weber & Andrade (2010).

neuron-to-neuron relationships. This has resulted in strong differentiation of the many clusters of neocortical neurons; however, the website bases its clusters on the previously defined categories, mostly by morphology but also electrophysiology of neurons. When working with cultured cortical neurons from the entirety of the neocortex, there is no spatial information available beyond the gross anatomical area that was used for culture preparation, which makes it more difficult to identify the types of neurons observed.

Without an appropriate method  to classify neurons, especially in cortical cultures, any particular effect on their electrophysiological properties can be diluted by the heterogeneity in the properties of the neurons, or biased by the researcher's knowledge (Kell & Oliver 2004). Thus it is necessary to cluster the cells into groups with defined boundaries. To achieve this, data mining of the recorded electrophysiological properties is required. There are many different types of clustering algorithms that can be used for this, which can be divided into supervised, semi-supervised, weakly-supervised and unsupervised methods. Supervised clustering happens when the researcher uses a more direct approach by explicitly defining the end groups, based on a previously established classification. With unsupervised clustering, the researcher is trying to discover a hidden structure in the available data in an unbiased way, allowing the algorithm to group the data without any previous training (Biemann 2007). Deciding the optimal algorithm for clustering is not a straight-forward task: it requires interactive multi-objective optimisation with trials and failures (Handl et al. 2005).

PCA is one method of unsupervised clustering that has been used for the classification of neurons on the NeuroElectro website, for example. This method reveals the internal structure of the data in a way that best explains the variance of the data; however, it requires that the data has some correlation, since it is based on Pearson correlation coefficients; the data also has to be suitable for data reduction (Field 2009). Another unsupervised method that is frequently used in biological research is *k*-Means clustering (Hartigan & Wong 1979). This technique is a vector quantisation method and consists of an iterative algorithm that minimises the sum of the square of the distances of all objects within a cluster (within-cluster sum of squares) for a given number of clusters. One drawback of this method is that it requires the user to define how many

clusters there are (Pham et al. 2005). The algorithm starts with an initial mean guess for the cluster centres, which can be either random $k$ observations or the mean of random $k$ clusters. Each data point's distance to this initial guess is then analysed and the data point is allocated to the group with the nearest mean. Next, a new centroid value is calculated for each group. The previous two steps are repeated until convergence is reached, which is when the values of the new centroids match the means of the groups.

While $k$-Means clustering relies on the multivariate distance between the data points, other clustering algorithms group data sets by the statistical probability of items being in the same distribution. One such algorithm is Expectation-Maximisation (EM), an iterative method that finds the maximum likelihood estimates of parameters (Dempster et al. 1977; Wu 1983). This algorithm has a 2-step process: in the first step, a function is created for the expectation of the log-likelihood that is evaluated using the current estimate for the parameters; the second step computes parameters by maximising the expected log-likelihood found in the previous step. These parameter estimations are then used to determine the distribution of the variables in the next expectation step.

Other types of clustering analysis are hierarchical clustering, most notably Ward's hierarchical clustering method, which is based on connectivity and results in dendrograms, and density-based clustering, which groups data points into regions of high-density areas. However, it is beyond the scope of this work to describe all the different types and variants of clustering analysis.

This chapter will describe initial observations of the spontaneous activity of cultured cortical neurons and how it is affected by serotonin and nitric oxide. Furthermore, it will present some data on the effects of these neurotransmitters on the response of cortical neurons to focal glutamate application. The main focus of the chapter is the description of the intrinsic electrophysiological properties of cultured cortical neurons and the clustering of neurons into distinct cell types based on these properties. This will be followed by a detailed description of the effects of serotonin and nitric oxide and their interactions on the intrinsic cellular properties in the next chapter.

## 3.2 Spontaneous activity of cultured cortical neurons

In order to obtain an initial overview of the neuronal activity of cortical neurons in cell culture, a total of 48 neurons, aged 12 – 20 days old after plating, were recorded in whole-cell current clamp mode. The cultured cells presented different morphologies including cells with a triangular soma, with processes extending from the three corners; bipolar cells, with an elongated soma and processes emerging from the two corners; or multipolar cells, usually with an approximately square soma shape, but which could also have a more stellate appearance, with four or more processes (Figure 2-4). Although the overall cell density was relatively sparse, the cells' processes formed considerable contacts with neighbouring cells forming extensive networks.

In current clamp mode, the recordings showed frequent excitatory post-synaptic potentials (EPSPs) that occasionally triggered action potentials when the resting membrane potential was adjusted to approximately -70 mV by injection of a small constant holding current. In order to quantify the synaptic activity, EPSPs with an amplitude higher than 5 mV were counted as single events (Figure 3-2A). The frequency of EPSPs was measured over a period of two minutes before drug application and while the neurotransmitters were present in the bath (two to five minutes). The average control frequency of spontaneous EPSPs varied from very low, 0.1 Hz, to high, 9.23 Hz.

From these 48 cells, 32 were bath perfused with 50 µM 5HT and 16 with 100 µM DEA (Figure 3-2A). The application of both drugs changed neither the membrane potential of the cells, nor the input resistance, with the exception of 7 cells, which showed a rapid, transient depolarisation followed by recovery of the membrane potential to the resting value during the application of 5HT. This transient 5HT response will be discussed further in the next chapter (section 4.7). The application of 5HT also produced either an increase or a decrease, or resulted in no change in the EPSP frequency in individual cells (n=32, control: 1.16 ± 0.23 Hz, 5HT: 1.27 ± 0.26 Hz). This variability in the modulation of the spontaneous EPSP frequency was not apparently linked to the resting spontaneous EPSP frequency, with increases and decreases being
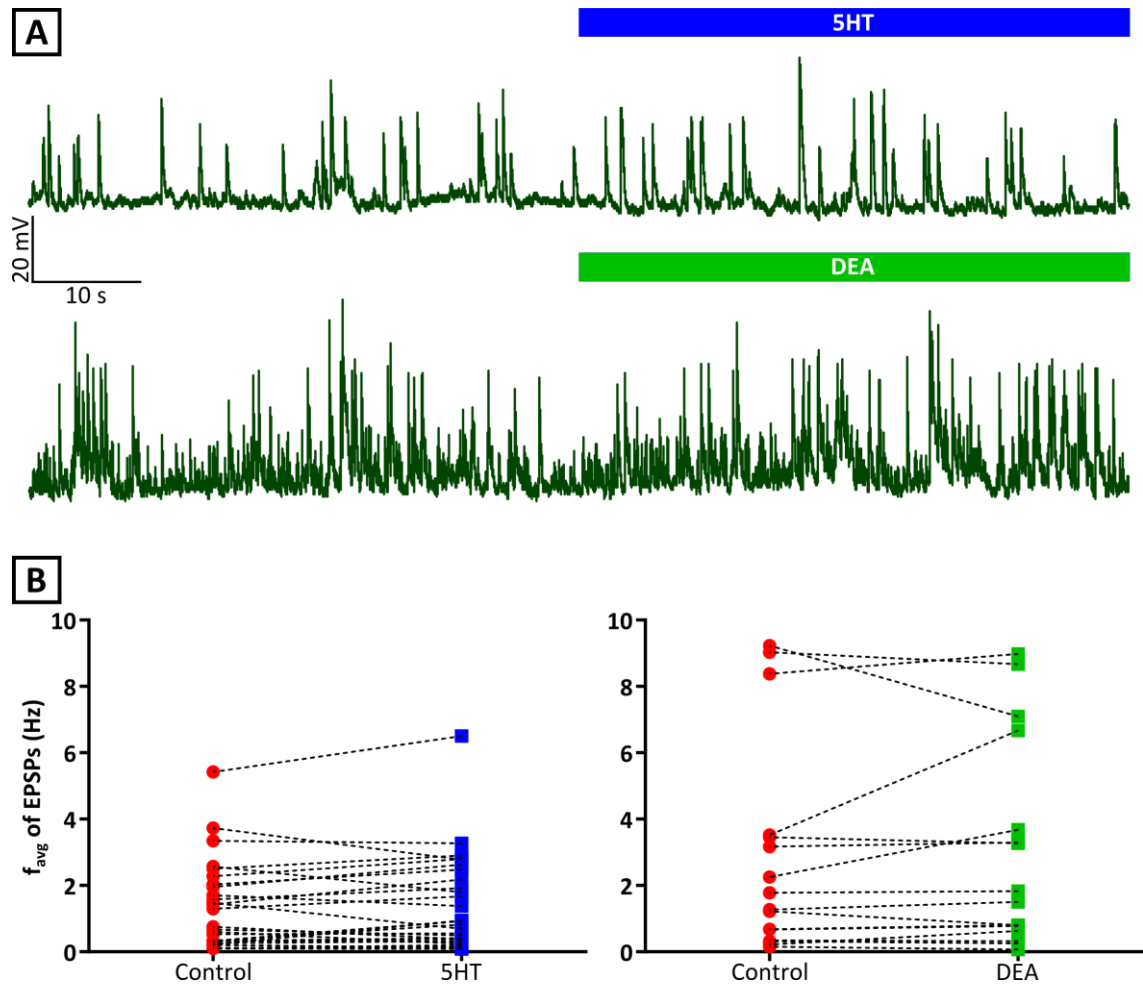
Figure 3-2: 5HT and DEA have no consistent effect on EPSP frequency in cultured cortical neurons. (A) Sample traces showing records of EPSPs before and during drug application in two individual cells. (B) Plots of EPSP frequencies before and during drug application (left: n=32, control: $1.16 \pm 0.23$ Hz, 5HT: $1.27 \pm 0.26$ Hz; right: n=16, control: $2.86 \pm 0.80$, DEA: $3.04 \pm 0.78$). Dotted lines connect data pairs obtained from individual cells.

observed equally in cells that received EPSPs at either low or high frequencies (Figure 3-2B).

Similarly, variable responses were also observed during the application of DEA (n=16, control: 2.86 ± 0.80, DEA: 3.04 ± 0.78). This group of cells contained three cells with the highest spontaneous EPSP frequencies observed, 8.4, 9.0 and 9.2 Hz. But even these three cells presented an example of an increase, a decrease and maintenance of the frequency of EPSPs during the application of the drug (Figure 3-2B).

With this wide range of control values and modulation of the frequency values during the application of drugs, a statistical Wilcoxon matched-pairs signed rank test returned non significant $p$ values ($p$ = 0.1574 for 5HT and $p$ = 0.4943 for DEA).


## 3.3 Modulation of glutamatergic response by serotonin and nitric oxide

Subsequent to the analysis of the effects of 5HT and NO on the overall neuronal activity in sparse cortical cultures, the effect of 5HT and NO on the response of cultured cortical neurons to glutamate was investigated. For this purpose, focal application of glutamate pulses was applied, as described in Chapter 2.

Following the focal application of glutamate, the membrane potential showed a rapid depolarisation. On average, the depolarisation had an area of 199.1 ± 23.5 mV.s, an amplitude of 47.2 ± 1.9 mV, the recovery to 50% of its peak was 3.5 ± 0.3 seconds and the depolarisation elicited 10 ± 4.3 action potentials (APs; n=23; Figure 3-3A). The response in individual cells was very consistent and reproducible for repeated applications of glutamate.

The response of the cell to glutamate was compared between control values and in the presence of both neurotransmitters. The number of spikes elicited by the glutamate response (5HT: 17.6 ± 4.7, DEA: 35.4 ± 10.7; Figure 3-3E), the duration (5HT: 3.3 ± 0.4 s, DEA: 4.0 ± 0.5 s; Figure 3-3C), and the area of the depolarisation (5HT: 183.5 ± 34.9 mV.s, DEA: 208.4  ± 32.3 mV.s; Figure 3-3B) did not change consistently when comparing control values to either 5HT or DEA treatments (Wilcoxon test, p>0.05 for

all comparisons). However, there was a small reduction in the amplitude of the glutamate response in the presence of DEA (n=11, 45.5 ± 2.4 mV, Wilcoxon test, $p$ = 0.0068), but not in the presence of 5HT (n=12, 47.0 ± 2.8 mV, Wilcoxon test, $p$ = 0.3416; Figure 3-3D).

The sample of cortical neurons tested showed that 5HT and NO have very variable effects on the number of APs elicited by glutamate, despite the fact that the underlying glutamate-induced depolarisation remained relatively unaffected. While in some cells the number of APs increased in response to glutamate during either 5HT or NO application, others decreased the number of glutamate-elicited APs. This suggests that 5HT and NO can act on the excitability of individual cortical neurons, affecting neuronal excitability without changing the underlying glutamate-induced depolarisation. A hypothesis for this is that the effects of 5HT and NO on neuronal excitability are cell type-specific.

## 3.4 Clustering by morphology

The initial recordings of neuronal activity of cortical cultures presented above illustrates the considerable heterogeneity in the properties of individual neurons, which was to be expected considering the range of neuronal cell types found in the intact neocortex. Furthermore, the variability of the effects of 5HT and DEA on the number of APs elicited by glutamate suggests that 5HT and NO have differential effects on the intrinsic properties of specific neuronal cell types. Thus, it is important to derive a robust protocol to group neurons, making it possible to compare the effects of 5HT and NO on specific cell types.

The development of cortical neurons in dissociated cell culture results in cells with distinct shapes with similarities to mature neurons *in situ*. It is possible to see, after maturation of the cultured neurons, various neuronal morphologies that appear to resemble neuron types described in the cortex, such as bipolar, pyramidal and multipolar cells (see Figure 2-4). The apparent similarities in appearance between cultured neurons and neurons *in situ* raised the question of whether the cultured cells
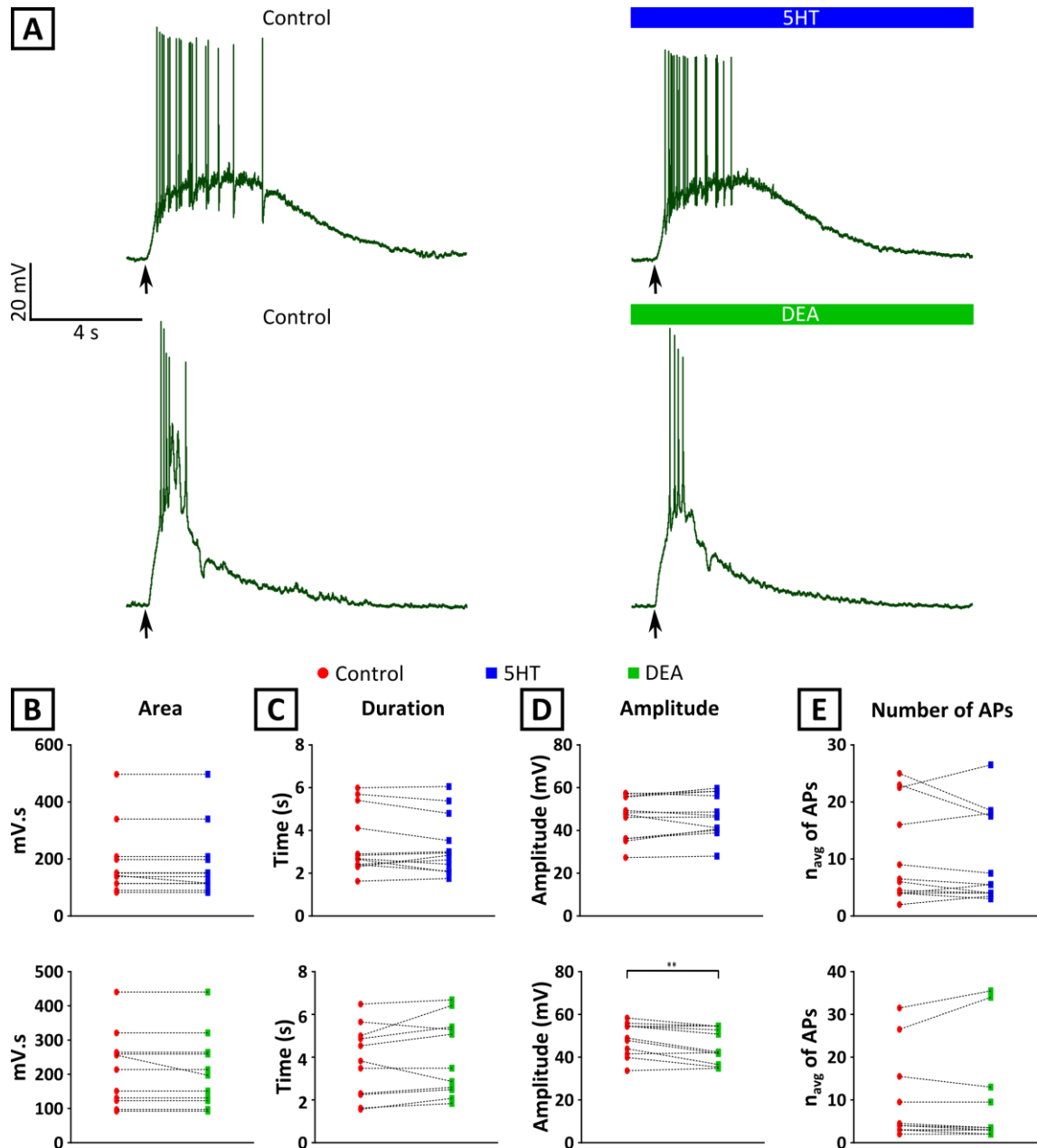
Figure 3-3: 5HT or DEA have little effect on depolarising response elicited by local application of 60 µM glutamate. (A) Focal application of glutamate depolarised the cell's membrane potential, eliciting APs and recovering after a few seconds. (B)-(E) Plots of data pairs obtained from individual cells before and during either 5HT (upper row, n=12) or DEA (lower row, n=11) for the area (B; 5HT: 183.5 ± 34.9 mV.s, DEA: 208.4 ± 32.3 mV.s), duration (C; 5HT: 3.3 ± 0.4 s, DEA: 4.0 ± 0.5 s), amplitude (D; 5HT: 47.0 ± 2.8 mV, DEA: 45.5 ± 2.4 mV) and number of APs (E; 5HT: 17.6 ± 4.7, DEA: 35.4 ± 10.7) of the response to focal glutamate application.

can be divided into groups with similar physiological properties based on their morphological appearance. An attempt of this procedure was made, in which cells were divided into three groups based on the number of processes developed from the soma. This division was done on all 235 cells that were analysed for their excitability.

Of the resulting groups, the group of neurons with two processes, or bipolar cells, contained the lowest number of cells (n=19). Neurons with four or more processes coming from the soma were considered as multipolar cells, and this group contained 58 cells. Having three processes and a pyramidal appearance constituted the largest group, with 158 cells. However, as illustrated by Figure 3-4, it became apparent that the morphologically defined groups were quite heterogeneous in their electrophysiological properties, making it necessary to consider other approaches to classify cells robustly.

## 3.5 Electrophysiological parameters for clustering analysis

As it was not possible to group neurons based on their morphological appearance into distinct groups with specific electrophysiological properties, it became necessary to consider alternative methods to assign neurons to individual types based on their electrophysiological properties. In order to characterise their intrinsic electrophysiological properties, individual neurons were recorded in whole cell current clamp mode and injected with a series of square wave current pulses ranging from -140 to +200 pA at 20 pA increments. A selection of six random samples of these recordings is shown in Figure 3-4 illustrating the wide range of intrinsic properties. These examples include records from neurons with a pyramidal, bipolar and multipolar appearance.

Based on these records, a total of 22 different parameters were considered for clustering the neuronal cells into groups. This parameter set will henceforth be called $PS_{22}$. The parameters, obtained from 235 cultured cortical neurons, were: number of APs at 120 pA current step; number of APs at 200 pA current step; rheobase (i.e. minimum current to trigger APs); amplitude of response to 200 pA pulse; inter-spike
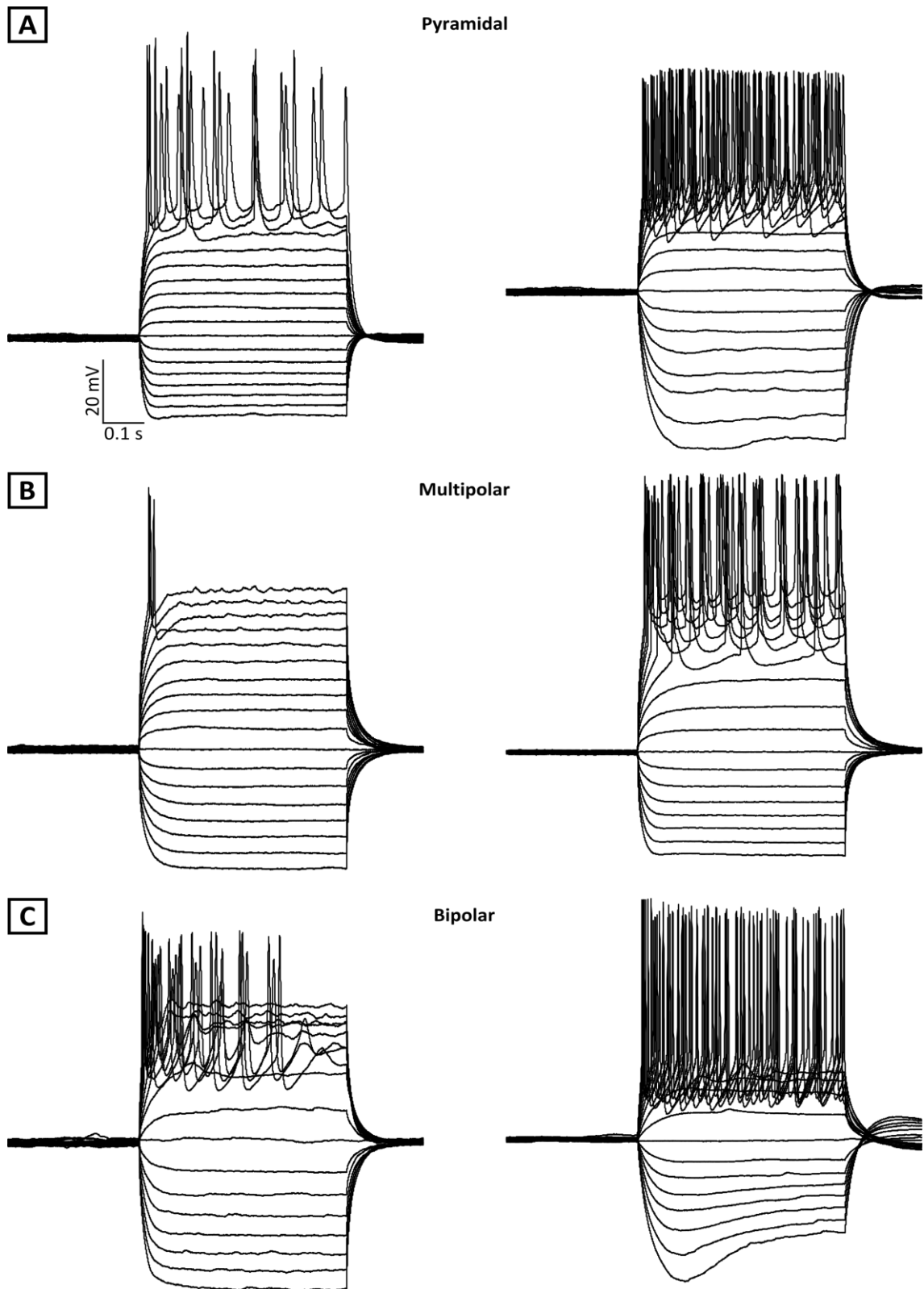
Figure 3-4: Sample traces of recorded cells illustrating the variability of electrophysiological behaviour observed in cell culture. Two sample records each are shown for neurons with a pyramidal (A), multipolar (B) and bipolar appearance (C). The membrane potential responses were elicited by series of 500 ms, square-wave current steps ranging from -140 pA to +200 pA in 20 pA increments.

interval (ISI) slope at 200 pA (i.e. slope of the linear regression line for the plot of the ISI against the AP number); minimum ISI value at 200 pA; the ratio of the minimum to maximum ISI values at 200 pA; spike burst pattern; spike height adaptation; $I_h$ value; input resistance; height of first AP at threshold; trough of first AP at threshold; width of first AP at threshold; height of first AP at 200 pA; trough of first AP at 200 pA; width of first AP at 200 pA; height of last AP at 200 pA; trough of last AP at 200 pA; width of last AP at 200 pA; membrane time constant; area of the cell soma. Spike burst pattern was calculated as the time of last AP minus the time of first AP elicited at 200 pA, divided by the duration of the current injection. Spike height adaptation was then calculated as the amplitude of the last AP over the amplitude of first AP obtained at 200 pA. For the cells that elicited only one AP at 200 pA, all parameters that would consider last AP at 200 pA would be left blank. All parameters from each cell were obtained as the average from multiple measurements. These parameters are further defined in Chapter 2.

The data obtained from the cells was standardised by converting it to a standard score, also called a z-score, which calculates the signed number of standard deviations the data is above or below the mean. The resulting standardisation made it possible to quickly identify outliers in the database. Outliers were defined as any cell that had one of its parameters' z-score lower than -5 or higher than 5. Based on this criterion, thirteen of the recorded cells were considered as outliers and not used for any analysis. Z-score values were used for all unsupervised clustering algorithms.

The mean values ± standard deviations (SD) are listed in Table 3-1. D'Agostino-Pearson's "omnibus K2" normality test was used to test if the data obtained from any of the parameters comes from a Gaussian distribution. The test first computes skewness and kurtosis to quantify the difference in symmetry and shape between the actual distribution and an ideal Gaussian distribution. It then computes a single value from the sum of the discrepancy between these values and the expected ones in a Gaussian distribution. The data obtained shows a non-normal distribution in all parameters, which provides further evidence for the heterogeneity within the cultured cells.

| | Mean   SD | $p$ value |
|---|---|---|
| N of APs at 120 pA | 5.1 ± 4.1 | < 0.0001 |
| N of APs at 200 pA | 7.5 ± 4.7 | 0.0055 |
| Rheobase (pA) | 89.4 ± 41.4 | 0.0022 |
| Vm Amplitude at 200 pA (mV) | 36.1 ± 9.8 | < 0.0001 |
| ISI Slope at 200 pA (ms/n AP) | 7 ± 10 | < 0.0001 |
| Minimum ISI at 200 pA (ms) | 24 ± 13.7 | < 0.0001 |
| Min/Max ISI at 200 pA | 0.43 ± 0.26 | 0.0002 |
| Spike Burst Pattern | 0.56 ± 0.34 | < 0.0001 |
| Spike Height Adaptation | 0.62 ± 0.28 | < 0.0001 |
| $I_h$ | 0.94 ± 0.06 | < 0.0001 |
| $I_r$ (MΩ) | 299.1 ± 135 | < 0.0001 |
| AP Height 1$^{st}$ AP at Threshold (mV) | 65.7 ± 13.6 | 0.0008 |
| AP Trough 1$^{st}$ AP at Threshold (mV) | -10.2 ± 6.2 | < 0.0001 |
| AP Width 1$^{st}$ AP at Threshold (ms) | 2 ± 0.7 | < 0.0001 |
| AP Height 1$^{st}$ AP at 200 pA (mV) | 65.7 ± 12.9 | < 0.0001 |
| AP Trough 1$^{st}$ AP at 200 pA (mV) | -4.0 ± 6.7 | 0.0078 |
| AP Width 1$^{st}$ AP at 200 pA (ms) | 2 ± 0.7 | < 0.0001 |
| AP Height Last AP at 200 pA (mV) | 40.4 ± 19.3 | < 0.0001 |
| AP Trough Last AP at 200 pA (mV) | -8.7 ± 6.2 | 0.0174 |
| AP Width Last AP at 200 pA (ms) | 4 ± 2.6 | < 0.0001 |
| Membrane Time Constant (ms) | 15 ± 8.3 | < 0.0001 |
| Cell's Area (μm$^2$) | 64.6 ± 14.0 | 0.0008 |

Table 3-1: List of the parameters that was used for identification of clusters with their mean values ± SD, from a total of 222 cells. The p values for normality test are also listed.

The data set was further analysed for any correlations using the Kaiser-Meyer-Olkin test, which compares the magnitudes of the observed correlation coefficients to the magnitudes of the partial correlation coefficients. The value obtained for the data (0.678) suggests that these correlations are not particularly strong. In fact, many of the parameters are either weakly or inversely correlated (Pearson correlation).

Clustering techniques rely on the appropriate selection of parameters and the distribution of these parameters. It is therefore important to select the most appropriate parameters that best describe the variation in the observed data. It is likely that there is a certain degree of redundancy in the complete set of $PS_{22}$ that were measured for each cell. This could lead to a subsequent bias in the clustering procedure. In order to identify the minimum parameter set that produces robust clusters of cells with consistent properties, a number of different approaches were compared for the reduction of the overall parameter set.

One of these approaches was PCA, which is a factor reduction analysis that groups the variables instead of the data points, clustering the ones that show some correlation to create a single factor which would allow the description of the process (Field 2009). As a result, a process described by many dependent variables can be depicted in a reduced number of factors that are independent, allowing better understanding of the clustering. It is possible to choose the variable within those factors that best describes each factor process.

Applying PCA to the data set of cellular properties returned nine factor components. The main variable that best describes each factor is listed in Table 3-2, obtained from the pattern matrix of PCA, using Oblimin rotation (direct quartimin rotation) with Kaiser normalisation and converged in eighteen iterations. The nine factors represent 90.47% of the variance of the parameters, and each factor's contribution and initial eigenvalues are shown on Table 3-3. By using direct quartimin rotation, it is ensured that the clusters of variables are intersected by the factors that they relate most, without being highly correlated (Field 2009). The resulting factors were analysed by using the pattern matrix (Table 3-2), which contains the rotated factor loadings of all parameters with a user-defined threshold of 0.4. The best parameters that describe

each factor were then selected and used on some of the clustering algorithms for grouping the data (Table 3-4). This parameter set will be referred to as $PS_9$.

However, the reduction of the parameter set solely on the basis of a mathematical procedure might not be the most appropriate way to select the physiological parameters that best capture the properties of the various types of neurons. The use of different groups of parameters defined by researchers' knowledge might result in a better clustering; this could also prevent strong physiological correlations between parameters. Therefore, two more user-based choices of parameter sets were included in the analysis of unsupervised clustering algorithms. The first of these parameter sets was selected on the basis of a set of criteria that was used for an entirely supervised manual clustering procedure, which consisted of 5 discrete parameters identified as supervised clustering (or SC). For direct comparison, a set of parameters that closely matched the choice of parameters in supervised clustering was also used for unsupervised clustering (without discretisation of parameters) and defined as $PS_5$.

These two parameter sets were chosen on the basis of the parameters that appeared to best describe the firing patterns of the different cell types and consist of the number of APs at 120 and 200 pA, spike burst pattern, spike height adaptation and $I_h$.

The final group of parameters that was used for the analysis of the clustering methods was an extended version of the first user-selected parameter set. This group of parameters consists of ten of the original twenty-two parameters that represent the differences in the overall shape of the electrophysiological behaviour of individual cells. This parameter set will be referred to as $PS_{10}$.

## 3.6 Supervised clustering

Many methods that are used to group the different cortical neurons are based on the "types" of electrophysiological responses to positive current steps. However, individual groups can often not simply be defined on the basis of a single parameter as neurons might differ from each other in different aspects of their electrophysiological behaviour. In this work, it was opted to use 5 parameters, which were discretised into

| | Component | | | | | | | | |
|---|---|---|---|---|---|---|---|---|---|
| | 1 | 2 | 3 | 4 | 5 | 6 | 7 | 8 | 9 |
| ***Spike Height Adaptation*** | ***-0.955*** | | | | | | | | |
| AP Height Last AP at 200 pA | -0.872 | | | | | | | | |
| AP Width Last AP at 200 pA | 0.770 | | | | | | | | |
| ***AP Trough 1<sup>st</sup> AP at 200 pA*** | | ***0.906*** | | | | | | | |
| AP Trough 1<sup>st</sup> AP at Threshold | | 0.901 | | | | | | | |
| AP Trough Last AP at 200 pA | | 0.851 | | | | | | | |
| ***Cell's Area*** | | | ***0.978*** | | | | | | |
| AP Height 1<sup>st</sup> AP at 200 pA | | | 0.975 | | | | | | |
| AP Height 1<sup>st</sup> AP at Threshold | | | 0.975 | | | | | | |
| Vm Amplitude at 200 pA | | | -0.558 | | | | | | |
| ***Spike Burst Pattern*** | | | | ***0.958*** | | | | | |
| N APs at 200 pA | | | | 0.898 | | | | | |
| ***ISI Slope at 200 pA*** | | | | | ***-0.990*** | | | | |
| ***Min/Max ISI at 200 pA*** | | | | | | ***0.880*** | | | |
| Minimum ISI at 200 pA | | | | | | 0.819 | | | |
| ***AP Width 1<sup>st</sup> AP at Threshold*** | | | | | | | ***0.669*** | | |
| AP Width 1<sup>st</sup> AP at 200 pA | | 0.468 | | | | | 0.638 | | |
| ***$I_h$*** | | | | | | | | ***1.005*** | |
| ***Rheobase*** | | | | | | | | | ***-0.843*** |
| $I_r$ | | | | | | | | | 0.814 |
| N APs at 120 pA | | | | 0.533 | | | | | 0.570 |
| Membrane Time Constant | | | | | | | | 0.495 | 0.569 |

Table 3-2: Pattern matrix with the factor loadings. The parameters with higher loading are in bold and italic for differentiation and they are the ones included in the PCA-based parameter sets used for unsupervised clustering.

| Component | Initial Eigenvalues | | |
|---|---|---|---|
| | Total | % of Variance | Cumulative % |
| 1 | 5.078 | 23.083 | 23.083 |
| 2 | 4.032 | 18.327 | 41.410 |
| 3 | 3.168 | 14.401 | 55.811 |
| 4 | 2.104 | 9.564 | 65.375 |
| 5 | 1.575 | 7.158 | 72.533 |
| 6 | 1.392 | 6.329 | 78.863 |
| 7 | 1.164 | 5.291 | 84.154 |
| 8 | 0.849 | 3.857 | 88.011 |
| 9 | 0.540 | 2.454 | 90.465 |

Table 3-3: Initial eigenvalues and percentage of the variance that is accounted for by the first 9 factors identified by PCA. The nine components represent more than 90% of the variance of the data.

Boolean numbers (parameters' states would be 0 or 1): $I_h$, number of APs elicited at 120 pA current step, spike height adaptation, spike burst pattern and maximum number of APs elicited in any current step (Table 3-4). In order to decide the state of each parameter in any one cell, it was necessary to set criteria/thresholds for each of the parameters. These threshold choices were made based on the distribution of all values recorded for each of these parameters (Figure 3-5A to E).

The procedures for measurement of the individual parameters are described in detail in Chapter 2 (section 2.4.3). In brief, $I_h$ was discretised by considering that a cell expresses it if the amplitude of the steady state membrane potential response to a -140 pA current injection was less than 92.5% of the negative peak; this parameter's state would be then represented by 1. Spike height adaptation was calculated as the ratio of the last AP over the first AP height elicited at 200 pA current injection. If the ratio was larger than 50%, the spike height adaptation parameter would be given a value of 1. For the spike burst pattern, defined as the time difference between the first and last AP at 200 pA divided by the current step duration, cells were assigned a value of 1 for values equal to or lower than 80%. This indicates that the cell shows spike frequency accommodation. For the number of APs at 120 pA current step, the neurons were divided into cells that fired more than three APs (state 0), or equal or less than three APs (state 1). And finally, for maximum number of APs, neurons were divided into those that only ever fired a single AP in response to any current step tested (state 1), whereas neurons that fired any more than 1 APs would be assigned to state 0. If this last parameter's state was 1, then the states of spike height adaptation, spike frequency accommodation and number of APs at 120 pA current injected would have also been changed to 1.

This procedure resulted in seventeen distinct cell clusters with unique combinations of these five parameters (out of the thirty-two theoretical possible unique combinations). From those, nine clusters consist of less than ten neurons; together, they represent 17.12% of the total data (Figure 3-6A). Although the cumulative percentage of these groups represented a considerable proportion of the total cells recorded, n numbers in individual clusters were too low for analysis; therefore cells in these clusters were not considered for further analysis.

| | $k$-Means PS$_{22}$ | $k$-Means PS$_{10}$ | $k$-Means PS$_9$ | $k$-Means PS$_5$ | SC | EM PS$_{22}$ | EM PS$_{10}$ | EM PS$_9$ | EM PS$_5$ |
|---|---|---|---|---|---|---|---|---|---|
| N of APs at 120 pA | X | X | | X | X | X | X | | X |
| N of APs at 200 pA | X | X | | X | | X | X | | X |
| Maximum of 1 AP at any current step | | | | | X | | | | |
| Rheobase | X | X | X | | | X | X | X | |
| Vm Amplitude at 200 pA | X | X | | | | X | X | | |
| ISI Slope at 200 | X | X | X | | | X | X | X | |
| Minimum ISI at 200 | X | X | | | | X | X | | |
| Min/Max ISI at 200 | X | X | X | | | X | X | X | |
| Spike Burst Pattern | X | X | X | X | X | X | X | X | X |
| Spike Height Adaptation | X | X | X | X | X | X | X | X | X |
| I$_h$ | X | X | X | X | X | X | X | X | X |
| I$_r$ | X | | | | | X | | | |
| AP Height 1$^{st}$ AP at Threshold | X | | | | | X | | | |
| AP Trough 1$^{st}$ AP at Threshold | X | | | | | X | | | |
| AP Width 1$^{st}$ AP at Threshold | X | | X | | | X | | X | |
| AP Height 1$^{st}$ AP at 200 pA | X | | | | | X | | | |
| AP Trough 1$^{st}$ AP at 200 pA | X | | X | | | X | | X | |
| AP Width 1$^{st}$ AP at 200 pA | X | | | | | X | | | |
| AP Height Last AP at 200 pA | X | | | | | X | | | |
| AP Trough Last AP at 200 pA | X | | | | | X | | | |
| AP Width Last AP at 200 pA | X | | | | | X | | | |
| Membrane Time constant | X | | | | | X | | | |
| Cell's Area | X | | X | | | X | | X | |

Table 3-4: Representation of the parameters chosen for each group of clustering algorithms. The explanation of each parameter and the reason for using them in each clustering algorithm is described in the text.

The largest group contains 21.17% of all the cells (47 out of 222). This group consists of tonic firing neurons that show neither spike height adaptation nor spike frequency accommodation, and fire more than three APs at 120 pA current step. These neurons do not show evidence for the presence of $I_h$. The second largest group, 16.67% of the cells, consists of 37 neurons. In contrast to the largest group, these neurons show more phasic activity as indicated by the presence of spike frequency accommodation and they fire less than three APs at 120 pA, but similar to the largest group they show no spike height adaptation or $I_h$. The third largest group, similar to the largest group, shows no spike frequency adaptation, but differs as it displays strong spike height adaptation; this group contains 15.77% of all the cells (35 out of 222). The other five groups differ to various degrees from each other and consist of between 4.95% (n=11) and 6.76% (n=15) of all the cells analysed.

While the supervised clustering enabled classification of different neuron types, it had some limitations. One of the main limitations is the requirement to set thresholds to define whether or not a certain property is expressed in a particular neuron. Furthermore, decisions are based on a relatively small parameter set. While it would have been possible to include further parameters in these criteria, this would have not

overcome the problem of setting fixed thresholds. Therefore it was decided to explore unsupervised clustering methods which avoided the need to set specific thresholds and compare their performance to the supervised clustering approach.

## 3.7 *k*-Means clustering procedure

For unsupervised clustering, two distinct procedures, *k*-Means clustering and expectation-maximisation (EM) clustering, were compared in order to divide the cultured neuronal cells into distinct groups. This section describes details of the *k*-Means clustering procedure, while the expectation-maximisation clustering will be described in the following section.

*k*-Means clustering requires pre-setting the appropriate number of clusters (*k*). The appropriate value for *k* was obtained by scoring the average distance of data instances
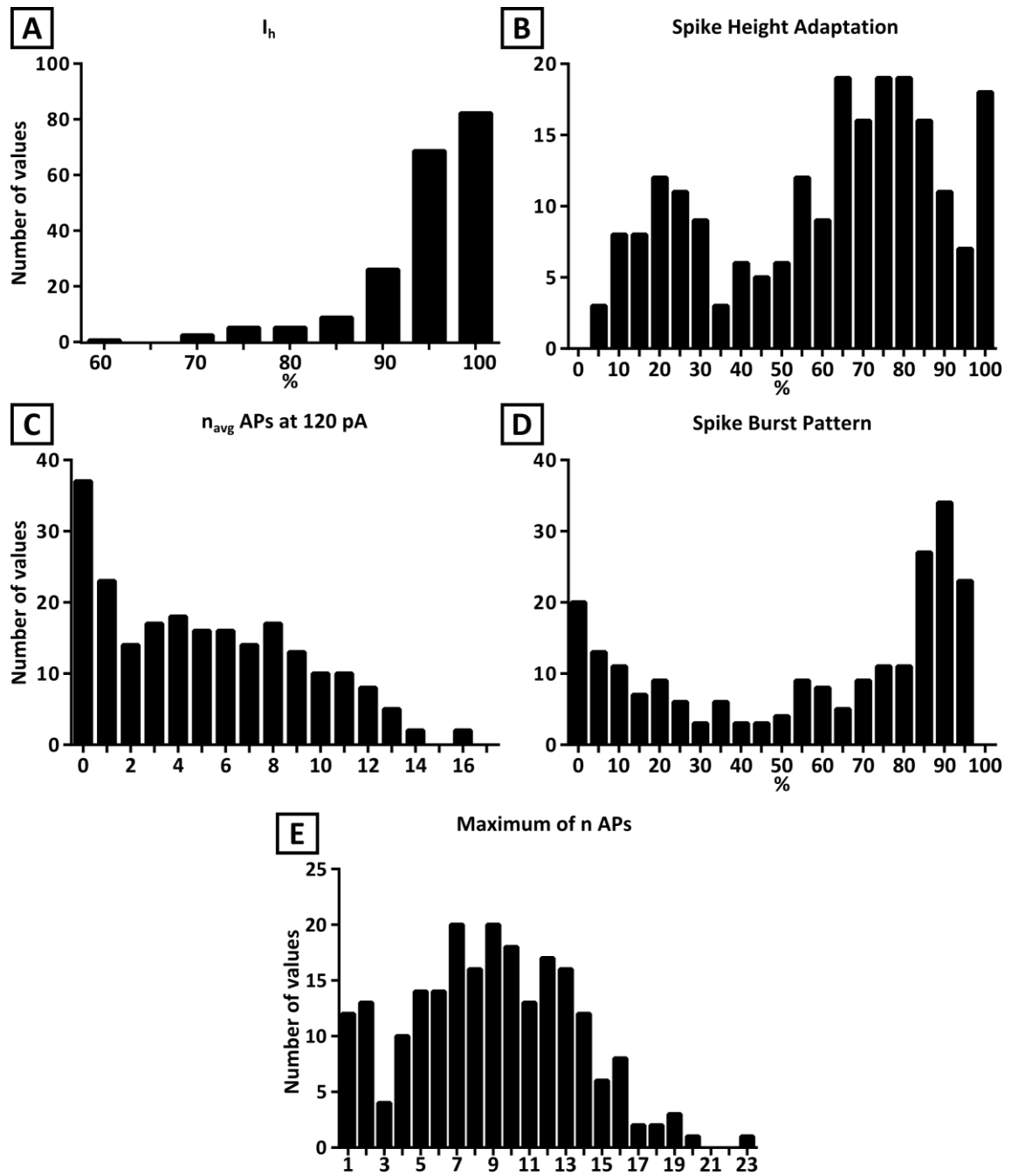
Figure 3-5: Frequency distribution of five parameters used for supervised clustering. (A) Distribution of the values for $I_h$, spike height adaptation (B), number of APs at 120 pA (C), spike burst pattern (D), and maximum number of APs at any current step (E).

to their associated centroids for $k$ values between 2 and 30. The score values were measured from the average distance of data instances to their associated centroid. The lower the value means the better the clusters are defined. The $k$ value was obtained by choosing a value higher than the point of inflection of the scores. For the clustering analysis based on $PS_{22}$, the plotted scores returned for values of $k>8$ show an approximately linear decrease (Figure 3-6B). Therefore, by choosing a $k$ value of 9 it ensures that the clusters are well represented and divided, without creating too many clusters with low $n$ numbers. The distance measured between two data instances was obtained by the square root of the sum of squared per-feature distance (Euclidian distances). The initialisation of the centroids was randomly selected and used as the initial means value (Lloyd-Forgy method). The percentage of cells in each cluster is presented in Figure 3-6B. Clusters 3, 6 and 7 have the highest number of cells (n=33, 43 and 37, respectively), whereas cluster 9 has the lowest (n=12), followed by clusters 1 and 4 (n=14 and 15). The other clusters consist of between 18 and 31 cells per group.

Using parameter set $PS_{10}$ instead of $PS_{22}$ in the clustering algorithm resulted in a similar distribution of cluster sizes with the largest group containing 40 cells, followed by three other groups (n=34, 33 and 31). Five other groups have n between 13 and 18, and one group had n=10 (Figure 3-6B).

When the $k$-Means clustering algorithm was applied to the parameter set obtained through PCA, the ideal number chosen for $k$ was nine. The resulting clusters contained between 13 and 49 cells in each group, with six clusters having n>20, and the other three groups having between 13 and 19 cells.

Finally, for better comparison with the supervised clustering approach, the $k$-Means algorithm was used on a set of parameters that matched the parameter set used in the supervised clustering procedure (section 3.6). The most appropriate $k$ value for this parameter set was nine,  resulting in two clusters with n=39 and 41 cells followed by one cluster with 34 cells, five clusters had cell numbers between 16 and 34, and one cluster contained 10 cells (Figure 3-6B).
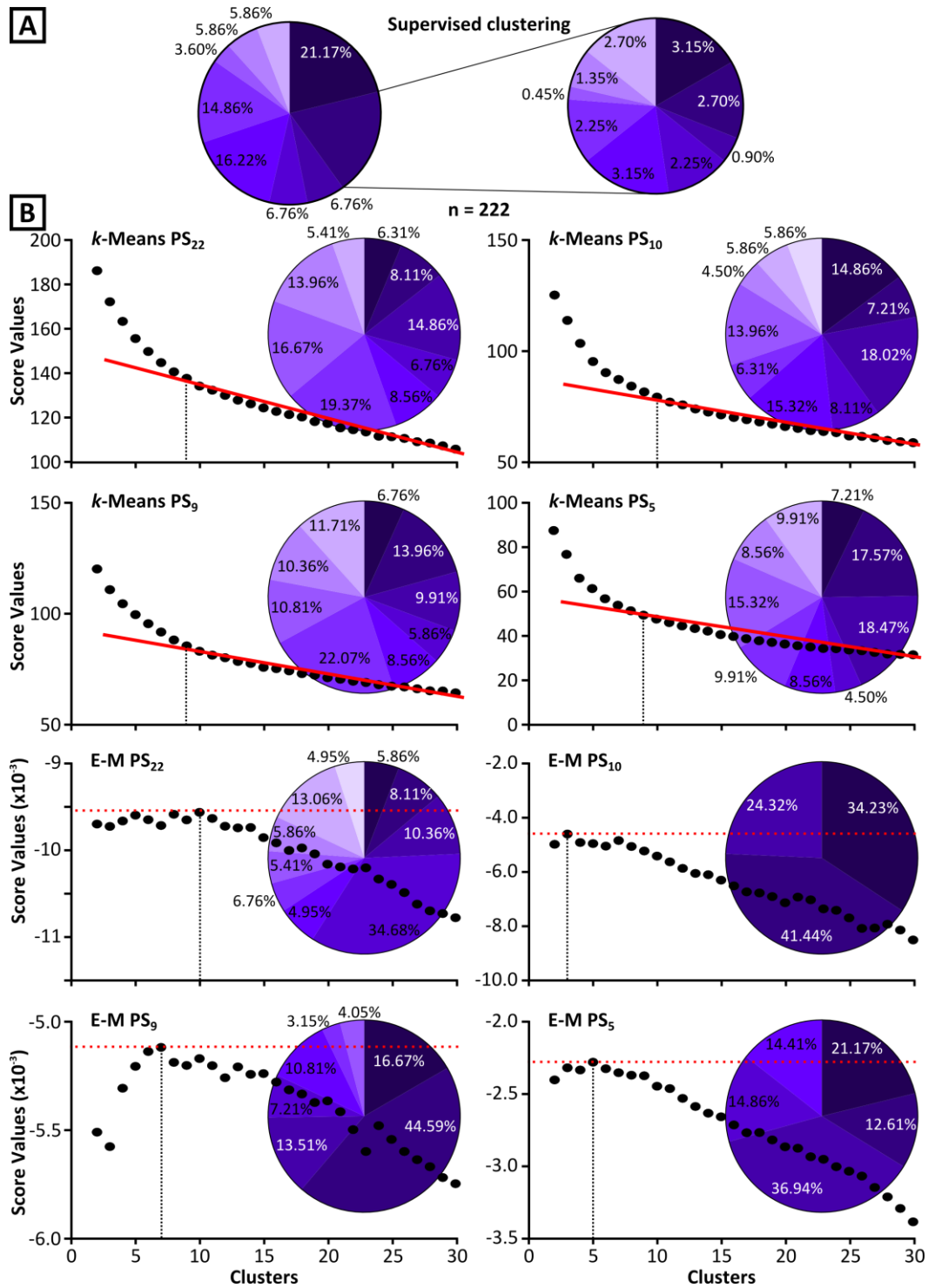
Figure 3-6: Distribution of cluster sizes based on supervised clustering and unsupervised clustering. (A) SC analysis returned 17 groups, 9 of which contained less than 3.2% each of the total cell numbers. (B) Score values plots showing the relationship between score values and pre-set number of clusters for *k*-Means and EM clustering with 22 parameters ($PS_{22}$), 10 parameters ($PS_{10}$) and 5 parameters ($PS_5$). The pie charts to the right show the cluster size distribution for *k* values indicated by the black dashed line on the score values plots. The red solid line presents the score values that decreased linearly in *k*-Means, whereas the dashed red line shows the highest score values for EM.

## 3.8 Expectation-maximisation clustering

Another unsupervised clustering algorithm used was the EM algorithm. The EM algorithm has been applied to a parameterised Gaussian mixture model of the data analysed from all 222 cells. The iterations started with the expectation step, which computes the estimation of the conditional probability that the observations belong to a certain group, followed by the maximisation step, which computes the parameter estimations. The output is the maximum-likelihood estimates of the parameters.

The algorithm was computed for a range of clusters $k$ from 2 to 30, using *a priori* command for multivariate data on the mean and an inverse Wishart distribution prior on the covariance matrix. The Wishart mixture model is the multidimensional version of the chi-square distribution, and this prior command prevents the breakdown of the computations for estimating the model parameters. It can occur when clusters contain only a few observations or if the observations contained in these clusters are very nearly collinear (Fraley & Raftery 2007).

The algorithm computes the Bayesian Information Criterion (BIC, Schwarz 1978) for $k$ values. This BIC is a criterion for model selection based on likelihood function with a penalty term for the number of parameters in the model. It allows the comparison of models with differing parameterisations and/or number of clusters. It is also used to compute the data dimensions and the number of components in the model. Therefore, for each set of parameters where EM was used, selection of the best number of clusters was based on the highest (i.e. least) negative BIC value.

The results were obtained from four different runs of the EM clustering algorithm – one for each of the different parameter sets shown in Table 3-4 and discussed earlier (Section 3.5). The first set of parameters on which EM was used was $PS_{22}$. The clustering algorithm returned a $k$ value of ten groups, with a BIC value of -9649.5.

$PS_{10}$ had a lower $k$ number, three groups, with the BIC value of -4599.6, a better value than the previous set. BIC produced a less optimised value when the EM algorithm was applied to $PS_9$. The $k$ value for this method was seven and the BIC value for seven clusters was -5117.6. However, the best result according to the BIC value was obtained
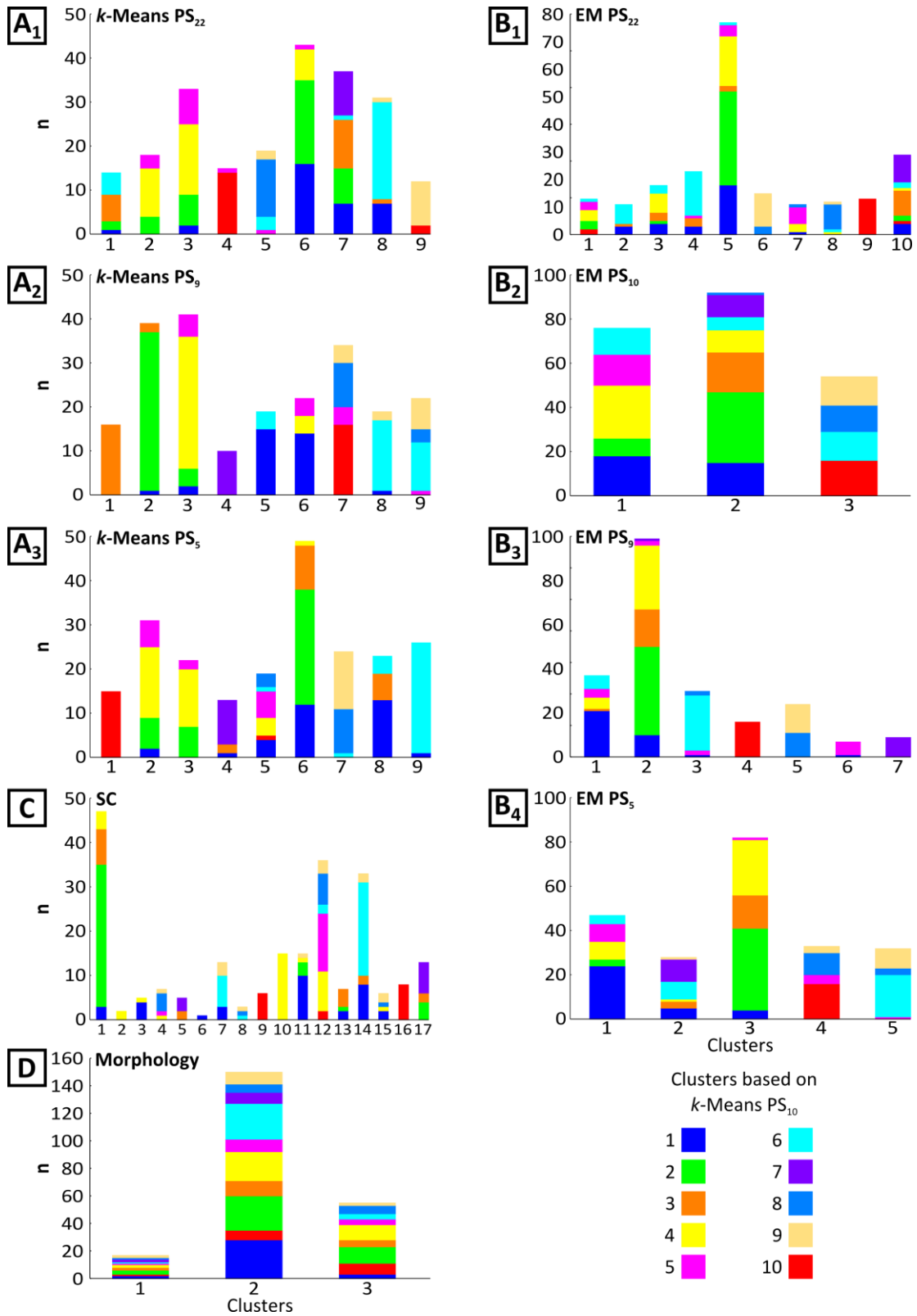
Figure 3-7: Comparison of the grouping of cells based on different clustering algorithms. The individual graphs show stacked bars of the number of cells in each cluster identified by a specific clustering algorithm, *k*-Means clustering (A1-A3), EM (B1-B4), SC (C) and morphology (D). The different colours indicate the assignment of individual cells to the 10 different clusters determined by the *k*-Means algorithm based on $PS_{10}$.

when the $PS_5$ was used in the EM algorithm. This returned a BIC value of -2279.1 for a $k$ value of five. In all the clusters for any of the methods, the lowest n number of data points in any cluster was 7, from the EM algorithm on $PS_9$ (Figure 3-7B). In comparison to $k$-Means clustering, the EM clustering algorithm produced at least one very large group of cells, with more than 33% of all the cells.

## 3.9 Comparison of the clustering methods

As mentioned before, many clustering algorithms have different approaches for the grouping of data. This raises the important question of whether cells that are clustered together by one algorithm would also be grouped together by an alternative algorithm. Furthermore, if cells are grouped distinctly by different clustering approaches, it questions which clustering is 'correct', i.e. most appropriate. In order to assess the distribution of cells to different clusters by the various approaches, cell assignment to clusters based on $k$-Means clustering with $PS_{10}$ was mapped onto the results from the other clustering procedures (Figure 3-8). The figure illustrates a certain degree of consistency between the clustering algorithms, especially the $k$-Means clustering on the basis of distinct parameter sets. For example, most of the cells grouped in cluster 2 by the k-Means $PS_{10}$ procedure are also grouped together by the $k$-Means procedure based on different parameter sets (e.g. cluster 6 for $k$-Means $PS_{22}$, cluster 2 for $k$-Means $PS_9$ and cluster 6 for $k$-Means $PS_5$, Figure 3-7A).  Furthermore, they are also clustered together by most of the EM based algorithms (Figure 3-7B), but spread across the three different morphological groups (Figure 3-7C). Not surprisingly, some of the cells in each cluster are grouped in distinct ways by different algorithms (presumably cells towards the edge of a cluster), and especially the EM-based clustering procedures that resulted in low cluster numbers resulted in the apparent fusion of multiple clusters that were differentiated by other approaches. As a consequence, clusters of cells defined by different algorithms are composed of different individual cells as illustrated in Figure 3-7.

Therefore, several methods were explored to select the most appropriate clustering approach. Various methods have previously been developed to evaluate the
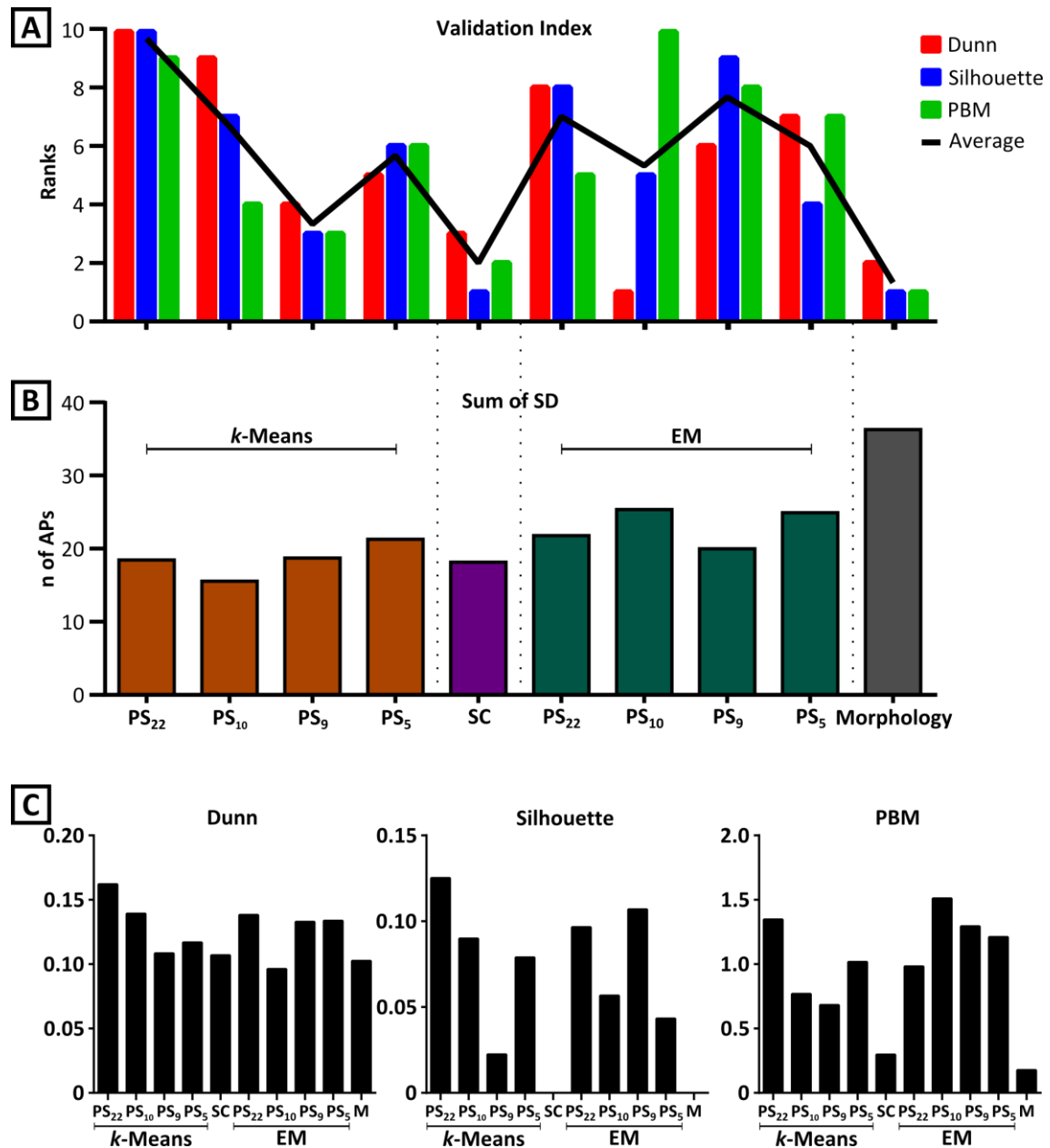
Figure 3-8: The validation indexes show divergence on which clustering method performs best in dividing the recorded cells into distinct groups. (A) Bars show the ranks for each clustering method as judged by three independent internal validation methods. The best performing algorithm was assigned a rank value of 10, while the worst performing algorithm was rated 1. The line shows the average of the ranks for each clustering algorithm.  (B) Bar chart of the average of the sum of the SD for the number of APs at each current step and cell cluster. Lower values indicate less variability in the excitability of cells within a specific cluster. (C) Bar graphs of the values from the three indexes used for ranking in (A).

effectiveness and quality of different clustering algorithms. One such type of evaluation is to assess the division and grouping of each data point without any *a priori* knowledge about the biological functions. These methods are so-called internal validation methods, since the resulting clusters are not compared to previously described data or information and knowledge, but purely judged on the internal data structure.

Three methods were used in this work for internal validations. One is the Dunn index (Dunn 1973), which as with many other internal validation methods, identifies sets of compact clusters with a small variance between the data points in the clusters, and well separated clusters where the centroids of each clusters are far apart. The Dunn index is defined by two parts: it calculates the minimum distance between each cluster, which is obtained from the data points in each cluster that are closest to each other, and divides this value by the diameter of each cluster, which would be the maximum distance separating two points within the clusters.

Another method for validating the clustering algorithms is called Silhouette, a method that provides a succinct graphic representation of the quality of the clustering (Rousseeuw 1987). Again, this method compares the tightness and the separation of the clusters, and by comparing the averaged Silhouette width it is possible to evaluate the effectiveness of the clustering method. In this method larger values also represent a better division of clusters. The closer the index value is to 1, the better the clustering algorithm. The index is derived by calculating the difference between the minimum of the mean distances between all the points in a cluster and the mean distance of one point to the other points inside the same cluster, divided by the higher of those two values. This Silhouette is then averaged for a given cluster, and for the final index value, the mean of the averaged Silhouettes is used.

The last method used to assess the quality of the clustering algorithm is the Pakhira, Bandyopadhyay and Maulik (PBM) index (Pakhira et al. 2005). This validation method uses a fuzzy logic approach to calculate the distances between the data points and their barycentres and the distance between the barycentres themselves. In common with the other two indexes, this method indicates a better clustering algorithm when

the returned index value is larger. For this method, the square of the sum of the distances of all the points to the barycentre of the entire data set divided by the sum of the distances of the points of each cluster to their barycentre is multiplied by the square of the largest distance between two clusters' barycentres.

As the individual validation methods produced distinct results, the validation indexes returned by the three independent methods for each of the clustering methods were rank-ordered in ascending order (i.e. the lowest-scoring clustering algorithm is assigned a value of 1 and the highest scoring clustering algorithm a value of 10). The ranks assigned by the three independent validation procedures to each clustering algorithm were then averaged to enable a comparison of the various clustering approaches based on a combination of all three internal validation methods.

As shown in Figure 3-8A, the various clustering methods returned different internal validation index values. Judged by the average of all ranks for each method, the best clustering method was $k$-Means $PS_{22}$, followed by EM $PS_9$. $k$-Means clustering algorithm with $PS_{10}$ was the third best method for dividing the various cells into groups. When dividing the cells according to their morphology, the internal validation indeces returned a very low average value. The same occurred for the supervised clustering method.

However, when comparing each index separately, the Dunn index ranked the $k$-Means $PS_{22}$ clustering highest, followed by the $k$-Means with $PS_{10}$. In contrast, Silhouette's highest ranks were for $k$-Means with $PS_{22}$ and EM clustering with $PS_9$. SC and grouping by morphology returned the lowest ranks for the Silhouette index, but EM with $PS_{10}$ and morphology returned the lowest Dunn indexes. The PBM index ranked EM clustering with $PS_{10}$ and $k$-Means with $PS_{22}$ as the best performing clustering algorithms. Again, its lowest values were present on the supervised and morphology clustering (Figure 3-8 A).
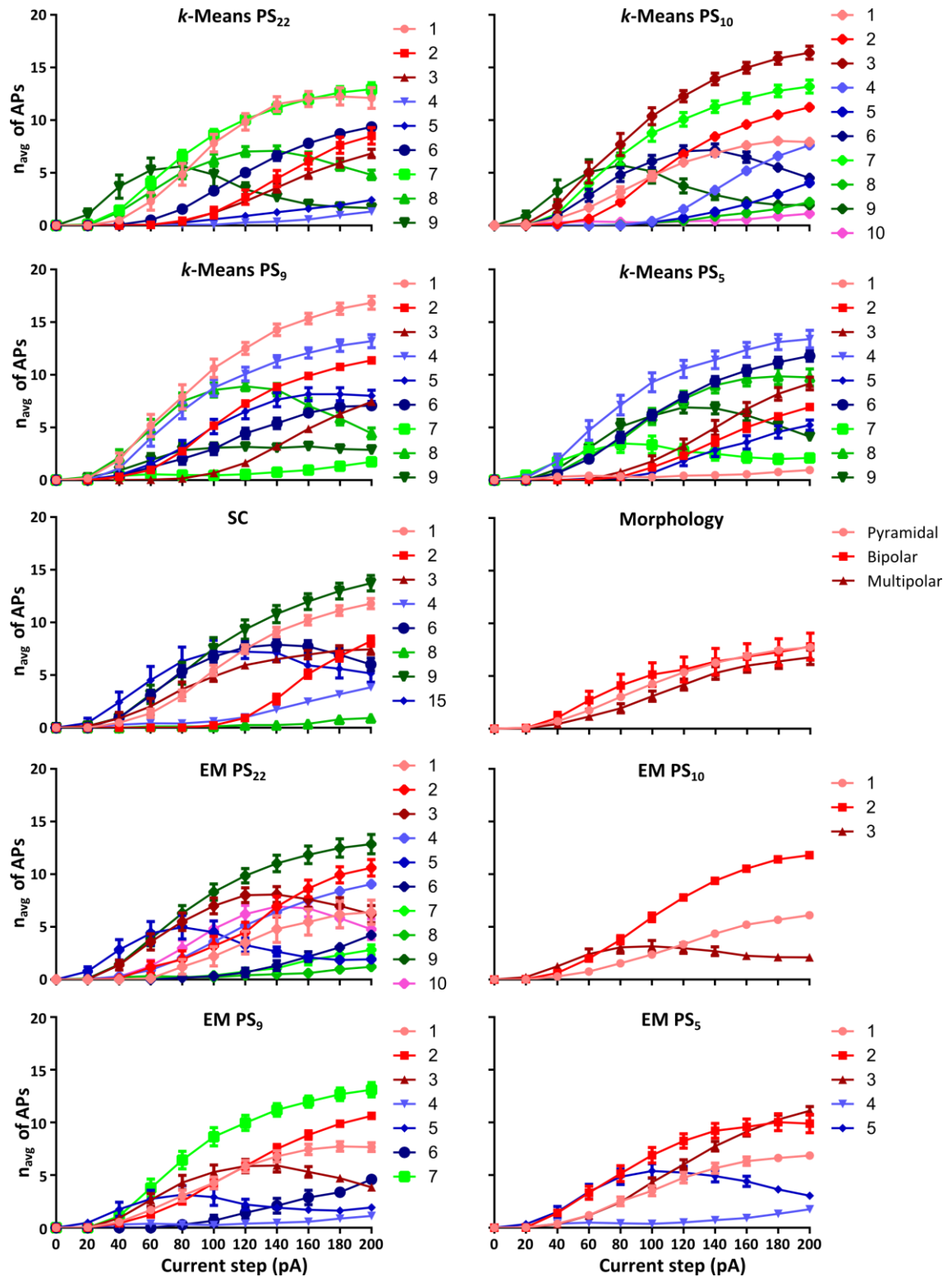
Figure 3-9: Excitability plots obtained after clustering the cells according to ten different types of clustering analysis. The plots show the average number of APs during the first 500 ms of a square-wave current pulse for each group of cells defined by the various clustering algorithms plotted against the amplitude of the current pulse.

3.9.1 Excitability plots of the various clustering techniques

As the internal validation methods described above produced varying results that made it difficult to make a final decision regarding the most appropriate clustering procedure, an alternative approach was considered based on the excitability plots for each group of cells defined by the individual clustering algorithms. This was based on the fact that one of the interests of this work was to study the effects of 5HT and NO on the intrinsic excitability of the membrane of cultured cortical neurons. Therefore it was considered important that the clustering algorithms used divided the cultured neurons into groups with consistent properties as judged by the excitability plots of the various clusters. The excitability plots were obtained by counting the number of APs elicited during the first 500 ms of each positive current step. The injected current values were between 0 and 200 pA increased in 20 pA steps. The cells were divided first into the clusters as described earlier and the mean number of APs elicited by each positive current step was plotted for each cluster as defined by the different clustering methods (Figure 3-9). For the SC method, the clusters with less than 10 cells were not added.

In order to compare the different clustering methods, the SDs of the number of APs elicited by each current step for one cluster were summed and subsequently averaged for all clusters that were defined by one clustering method. The final value was then compared between each method (Figure 3-8B). Judged by this measure, the $k$-Means algorithm performed better than EM and clustering by morphology; the average of the sum of SDs of the number of APs for these clustering algorithms was consistently lower than for the other two algorithms. Furthermore, one of the $k$-Means based clustering procedures performed better than the SC judged by this measure. Overall, the method that used $k$-Means $PS_{10}$ clustering resulted in excitability plots with the lowest level of variability, followed by SC, $k$-Means with $PS_{22}$ and $k$-Means with $PS_9$. When clustering the data points based on $PS_9$, both Euclidian and statistical clustering algorithms showed similar results.

The resulting excitability plots for all $k$-Means algorithms and SC show groups with quite similar properties across the clustering methods.  At least one group had a low

threshold for AP generation and a high number of APs elicited at higher current steps, with average peak number of APs being higher than 10 APs/500 ms. They are groups 7 for $k$-Means with $PS_{22}$, 7 and 3 for $k$-Means with $PS_{10}$, 1 and 4 for $k$-Means with $PS_9$, 4 for $k$-Means with $PS_5$, and 1 and 9 for SC. These groups also do not show a plateau of excitability even at 200 pA current injection, suggesting that these cells could produce even higher firing rates with stronger current injection. For $k$-Means with $PS_{22}$, group 1 presents similar behaviour, the main difference being that their firing rate appears to reach a plateau at higher levels of current.

Groups 4 and 5 for $k$-Means $PS_{22}$, 5, 8 and 10 for $k$-Means with $PS_{10}$, 7 for $k$-Means with $PS_9$, 1 for $k$-Means with $PS_{55}$, and 8 for supervised clustering had high AP firing thresholds and very low numbers of APs elicited at any of level of positive current injected. Group 9 for $k$-Means $PS_{22}$, 9 for $k$-Means with $PS_{10}$, 8 and 9 for $k$-Means with $PS_9$, 7 and 9 for $k$-Means with $PS_5$, and 15 for SC are clusters of cells with low AP firing thresholds and less than 10 APs at any current injected that showed a reduction in the number of APs for currents higher than 100 pA.

Similar behaviours were also observed in groups 8 for $k$-Means $PS_{22}$, 6 for $k$-Means with $PS_{10}$, and 6 for SC. The main difference is that this group of clusters shows a shift of the excitability curve to the right compared to the group of cell clusters described above. Groups 2 and 3 for $k$-Means $PS_{22}$, 4 for $k$-Means with $PS_{10}$, 3 for $k$-Means with $PS_9$, 2, 3 and 5 for $k$-Means with $PS_5$, and 2 for SC consisted of cells with a relatively high firing threshold and a gradual, almost linear increase in number of APs: its highest number of APs did not surpass 7. The rest of the clustered groups in all $k$-Means and SC algorithms showed similar behaviour to these last clustered groups, but with a more sigmoidal than straight excitability line (Figure 3-9).

As most of the EM clustering analyses resulted in lower numbers of cell clusters (3, 5, 7), it is not surprising that they produced excitability plots that could be interpreted as the summation of groups seen in $k$-Means analysis with $PS_{10}$. Only EM $PS_{22}$ resulted in 10 distinct clusters and one can discern types of clusters with similar behaviours compared to the SC and $k$-Means clustering: groups 2, 4 and 9 have a low firing threshold and relatively high number of APs at higher current steps; groups 3, 5 and 10
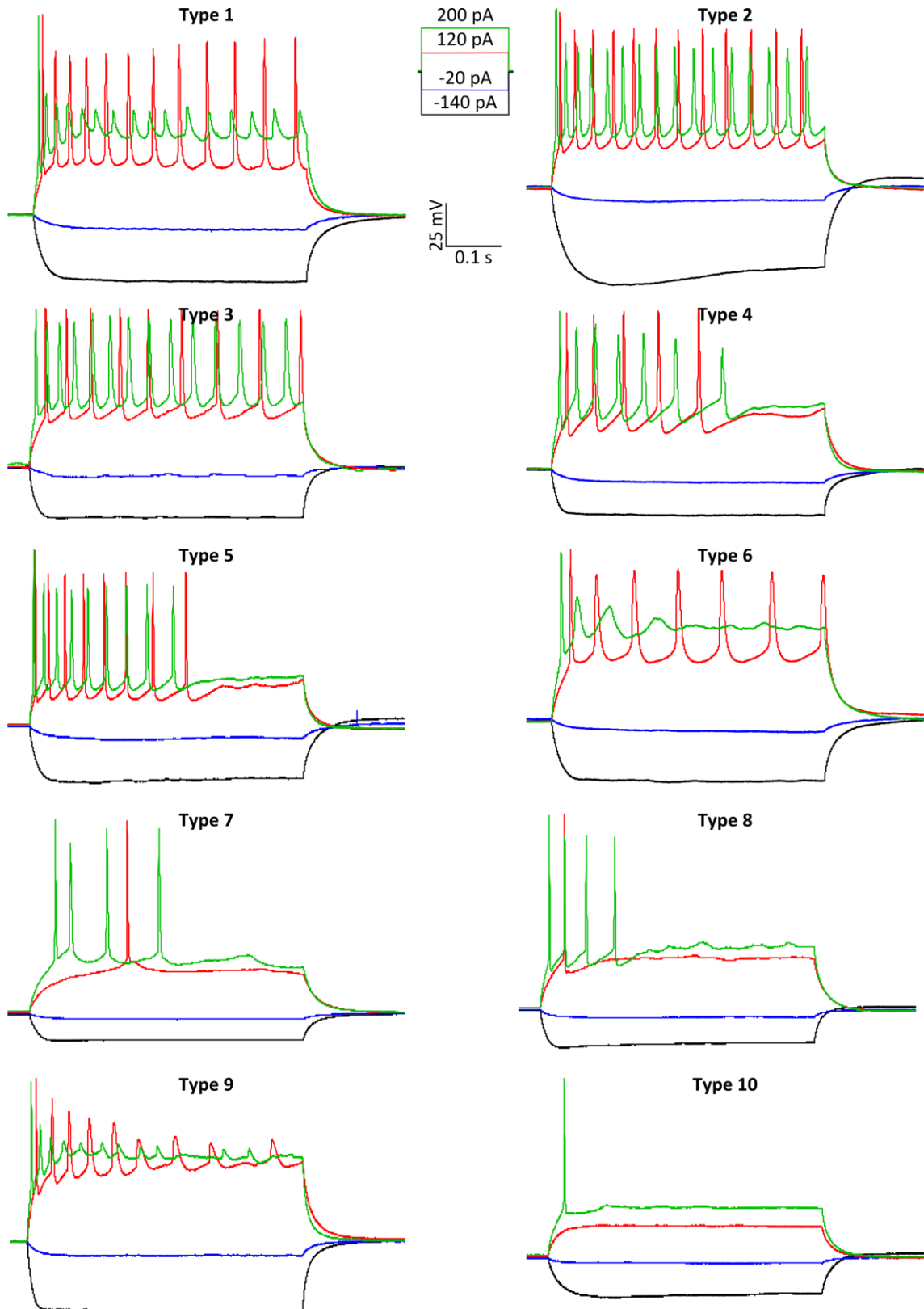
Figure 3-10: Example recordings for the ten different types of cells defined by *k*-Means clustering with $PS_{10}$. Traces are the responses to four different current steps, -140 pA (black), -20 pA (blue), 120 pA (red) and 200 pA (green).

show a reduction in the number of APs at higher current steps. In contrast, groups 7 and 8 have a higher firing threshold and generate few APs at higher current steps, while group 6 also has a relatively high firing threshold, but shows an almost linear and more substantial increase in the number of APs at higher levels of current injection. Group 1, on the other hand, has the same linear increase of excitability, but AP thresholds are low. The EM clustering algorithms with the other parameters sets present groups with similar behaviour but fewer overall groups.

Clustering by morphology resulted in 3 excitability plots with very similar shapes and relatively large variability. This again suggests that morphological information obtained from cultured cortical neurons is not a good predictor of the electrophysiological properties of individual cells.

## 3.10    Description of parameters divided into clusters from $k$-Means $PS_{10}$

Based on the values for the average of the sum of standard deviations for the number of APs at the various positive current steps, it was decided to apply the $k$-Means clustering procedure on $PS_{10}$ to divide the recorded cells into distinct groups. This method resulted in ten types of cells that display quite distinct excitability properties, from low AP firing thresholds with increased number of fast AP at higher current steps, to cells with strong AP height adaptation at higher current steps, and cells with high AP firing thresholds that elicit very few APs at the highest current steps (Figure 3-10). For convenience, groups defined by the clustering technique were re-labelled as cell types 1 to 10 based on the rank order for the average number of APs elicited by a 200 pA current pulse. The excitability plots demonstrating this gradient in number of APs produced is shown in Figure 3-11. The cell clusters were assigned to cell types 1 to 10 in the following order: 3, 7, 2, 1, 4, 6, 5, 8, 9, and 10.

The connection between clusters and cell types can be seen in Table 3-5. The table also shows the mean ± standard error of the means (SEM) values for all 22 parameters measured for each cell type. A Kruskal-Wallis test with post-hoc Dunn's multiple comparison (DMC) test was carried out for each parameter between the various cell
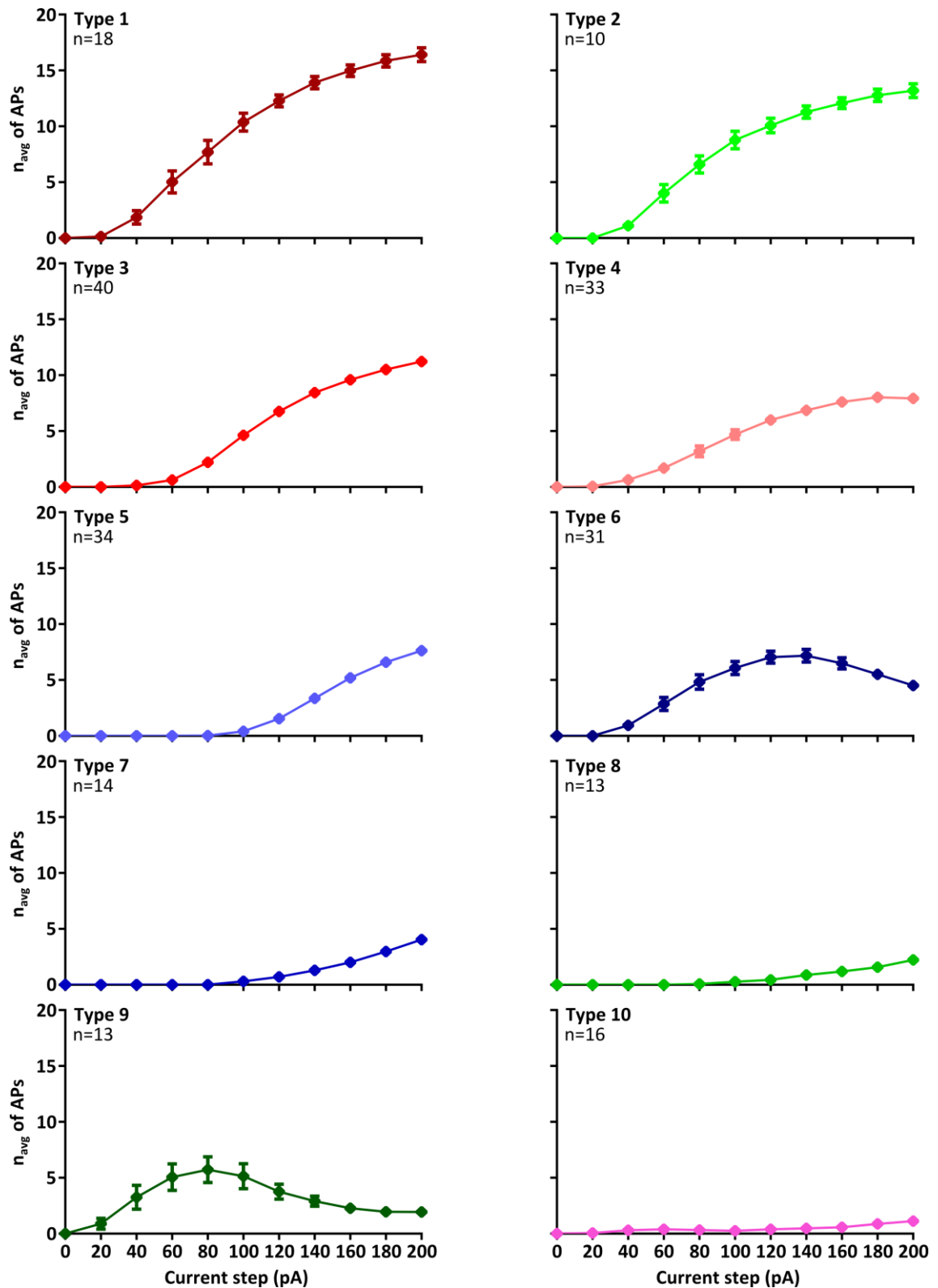
Figure 3-11: Excitability plots obtained from *k*-Means clustering on $PS_{10}$ returned ten different types. This is the same data as presented in Figure 3-9 for *k*-Means clustering based on $PS_{10}$, re-plotted and ordered according to maximum number of APs produced at 200 pA. The individual clusters have been re-labelled as type 1 to type 10.

types. The $p$ values obtained from this multiple comparison test were then plotted in a heat map for easy comparison (Figure 3-12).

As expected from this ordering, type 1 cells presented the highest number of APs at 120 and 200 pA. This group also had one of the highest spike burst pattern values indicating that depolarisation initiates very regular, fast tonic activity in these cells. However, they present strong spike height adaptation. These cells also have one of the highest input resistances, which is probably a contributing factor in producing one of the lowest rheobase values.

When comparing the different types of cells, cell type 2 shares many properties with cell type 1. The most obvious difference is the significantly more pronounced $I_h$ , which sets cell type 2 apart from all the other cell types (DMC: $p < 0.05$). Overall action potentials of cell type 2 have a markedly increased amplitude; there is also a non-significant difference in the input resistance between the two types. In contrast to cell type 1 and 2, cell type 3 does not show any pronounced spike height adaptation and the average input resistance for cell type 3 is significantly lower than in cell type 1 (DMC: $p < 0.05$) resulting in an increase in its rheobase compared to both types 1 and 2, a right shift of the excitability plot and overall lower rates of AP generation. Type 4 cells, as with type 3, have a lower input resistance compared to types 1 and 2, and generate significantly fewer APs in response to a 120 pA and 200 pA current pulses compared to cell type 1 (DMC: $p < 0.01$). This group also has a significantly lower ratio for the spike burst pattern (DMC: $p < 0.01$) when compared to cell types 1 to 3 and shows more pronounced spike height adaptation (DMC: $p < 0.0001$) when compared to cell type 3. Overall, these effects combine to produce a lower threshold excitability plot with a plateau at higher current steps when compared to cell types 1 to 3.

While cell types 1 to 4 show comparatively lower AP thresholds, cell type 5 presents a higher threshold with a linear increase in the number of APs per current step. This cell type also differs significantly from the other types by having a comparatively low input resistance, which is significantly lower than for cell types 1, 2 and 4 (DMC: $p < 0.05$). Consistently, this cell type also has a higher rheobase value (DMC: $p < 0.001$) than cell types 1 to 4, and the minimum ISI at 200 pA increases considerably when compared

| | Type 1 | Type 2 | Type 3 | Type 4 | Type 5 | Type 6 | Type 7 | Type 8 | Type 9 | Type 10 |
|---|---|---|---|---|---|---|---|---|---|---|
| Clusters | C3 | C7 | C2 | C1 | C4 | C6 | C5 | C8 | C9 | C10 |
| N of APs at 120 pA | 12.3±0.5 | 10.1±0.7 | 6.8±0.3 | 6.0±0.4 | 1.5±0.3 | 7.0±0.5 | 0.7±0.2 | 0.4±0.1 | 3.8±0.7 | 0.4±0.2 |
| N of APs at 200 pA | 16.4±0.6 | 13.2±0.6 | 11.8±0.3 | 7.9±0.3 | 7.6±0.3 | 4.5±0.3 | 4.0±0.2 | 2.2±0.3 | 1.9±0.2 | 1.1±0.2 |
| Rheobase (pA) | 57.8±5.2 | 49.3±4.5 | 81.8±2.9 | 70.6±4.3 | 124.5±3.4 | 62.0±3.0 | 135.7±7.8 | 136.4±8.6 | 47.4±5.8 | 141.5±14.1 |
| Vm Amplitude at 200 pA (mV) | 37.8±2.3 | 30.1±1.6 | 33.7±1.4 | 33.6±1.0 | 36.0±1.5 | 45.5±1.9 | 32.0±1.4 | 30.4±1.1 | 46.1±3.0 | 31.1±2.4 |
| ISI Slope at 200 pA | 0.9±0.1 | 1.3±0.3 | 3.7±0.0 | 7.7±0.1 | 9.7±1.3 | 13.6±2.0 | 29.6±3.5 | | | |
| Minimum ISI at 200 pA (ms) | 18±1.3 | 20±1.0 | 24.3±0.8 | 23.3±1.3 | 34±2.6 | 21±1.2 | 32±2.6 | 43±6.9 | 22±2.2 | |
| Min/Max ISI at 200 pA | 0.48±0.03 | 0.45±0.04 | 0.40±0.02 | 0.31±0.02 | 0.38±0.03 | 0.44±0.03 | 0.26±0.03 | | | |
| Spike Burst Pattern | 0.91±0.01 | 0.91±0.01 | 0.88±0.01 | 0.64±0.02 | 0.79±0.02 | 0.23±0.02 | 0.51±0.05 | 0.11±0.02 | 0.04±0.01 | |
| Spike Height Adaptation | 0.50±0.05 | 0.55±0.05 | 0.78±0.02 | 0.46±0.04 | 0.80±0.02 | 0.23±0.02 | 0.83±0.05 | 0.71±0.06 | 0.45±0.06 | 0.98±0.02 |
| $I_h$ | 0.95±0.01 | 0.74±0.02 | 0.97±0.04 | 0.96±0.01 | 0.96±0.00 | 0.94±0.01 | 0.96±0.01 | 0.93±0.02 | 0.94±0.02 | 0.94±0.01 |
| $I_r$ (MΩ) | 407.0±31.0 | 351.9±35.3 | 262.3±10.7 | 317.0±16.9 | 199.6±13.2 | 399.3±24.1 | 197.6±20.3 | 180.8±9.5 | 475.0±31.4 | 259.2±43.1 |
| AP Height 1st AP at Threshold (mV) | 64.5±2.9 | 74.6±2.9 | 64.6±2.0 | 69.0±1.7 | 64.3±2.9 | 63.1±2.9 | 67.4±4.0 | 68.6±2.7 | 65.1±3.3 | 62.5±3.9 |
| AP Trough 1st AP at Threshold (mV) | -12.5±1.7 | -13.2±1.9 | -9.7±0.9 | -11.1±0.89 | -9.3±1.1 | -10.5±0.9 | -9.3±1.9 | -8.2±1.2 | -7.5±1.9 | -11.5±2.0 |
| AP Width 1st AP at Threshold (ms) | 1.9±0.1 | 1.9±0.2 | 2.1±0.1 | 2.2±0.1 | 2.5±0.1 | 2.3±0.1 | 2.2±0.2 | 2.0±0.2 | 2.7±0.2 | 2.1±0.2 |
| AP Height 1st AP at 200 pA (mV) | 62±2.4 | 74.2±2.3 | 62.7±2.0 | 70.2±1.4 | 64.8±2.8 | 62.7±2.7 | 67.7±4.0 | 71.0±2.2 | 65.3±2.6 | 64.7±3.6 |
| AP Trough 1st AP at 200 pA (mV) | -6.9±1.7 | -5.2±1.4 | -3.4±1.0 | -4.8±0.9 | -3.5±1.3 | -2.7±1.0 | -5.5±2.2 | -4.6±1.3 | 2.7±1.8 | -6.5±2.1 |
| AP Width 1st AP at 200 pA (ms) | 1.7±0.1 | 1.8±0.1 | 2.0±0.1 | 1.9±0.1 | 2.3±0.1 | 2.1±0.1 | 2.0±0.2 | 1.9±0.2 | 2.7±0.3 | 2.1±0.2 |
| AP Height Last AP at 200 pA (mV) | 31.5±4.0 | 40.8±3.8 | 47.8±1.7 | 32.6±2.7 | 51.1±2.2 | 14.1±1.7 | 54.9±3.3 | 51.0±4.5 | 29.0±3.9 | 63.4±3.5 |
| AP Trough Last AP at 200 pA (mV) | -8.6±1.6 | -11.4±2.1 | -9.1±0.7 | -10.4±0.8 | -9.7±1.0 | -8.0±1.0 | -11.8±1.7 | -8.5±1.2 | 0.1±1.9 | -6.8±2.2 |
| AP Width Last AP at 200 pA (ms) | 4.7±0.5 | 3.7±0.5 | 3.7±0.2 | 5.2±0.5 | 3.9±0.3 | 6.7±0.7 | 3.0±0.4 | 2.7±0.3 | 5.9±0.7 | 2.1±0.2 |
| Membrane Time Constant (ms) | 18±1.6 | 24±2.2 | 12±0.9 | 15±1.5 | 12±0.8 | 16±1.2 | 10±0.8 | 13±1.2 | 21±3.1 | 17±3.6 |
| Cell's Area (µm²) | 63.8±3.0 | 73.1±3.2 | 62.6±2.0 | 69.0±1.7 | 63.1±2.9 | 62.9±2.9 | 65.1±4.6 | 67.1±2.5 | 64.1±3.1 | 61.4±4.1 |

Table 3-5: Values obtained for all parameters after clustering by using the *k*-Means algorithm on reduced number of parameters. Values are shown as mean ± SEM for each cluster.

especially to type 1 (DMC: $p < 0.0001$). Cell type 7 shares similar properties with cell type 5, the main difference being an increased ISI slope, and decrease in the spike burst pattern ratio and the number of APs at 120 pA and 200 pA. None of the individual differences between cell types 5 and 7 where statistically significant (DMC: $p>0.05$).

Cell types 1 to 5 show broadly tonic activity patterns, while cell types 6 and 9 show distinctly phasic activity with the cessation of spiking activity before the end of the 500 ms current pulse resulting in spike burst pattern values of $0.23 \pm 0.02$ and $0.04 \pm 0.01$, which effectively means that they only fire APs for approximately the first 20% of the current pulse (DMC: $p<0.05$ for cell types 6 and 9 vs cell types 1 to 5, exception: cell type 6 vs cell type 4, $p<0.1$). Also notably, both of these types show very pronounced spike height adaptation. This results in their inability to generate sustained trains of APs in response to larger current injections. This does not appear to be the consequence of a large leak current as cell types 6 and 9 are among the three cell types with the highest input resistances of all cell types. The main difference between cell types 6 and 9 is a lower rheobase and an increase in the input resistance in cell type 9 compared to cell type 6 resulting in fewer APs at 120 and 200 pA.

Cell types 7, 8 and 10 have many features in common; most notably the highest AP firing thresholds of all ten cell types with average values of between $135.7 \pm 7.8$ pA and $141.5 \pm 14.1$ pA. Type 8 cells differ from type 7 by having lower spike burst pattern ratio and cell type 10 mainly differs from type 8 because of its increased input resistance.

It is also worth mentioning that some parameters presented no or almost no statistically significant difference between the various types. They are the height, width and trough of the $1^{st}$ AP at threshold, $I_h$ except for type 2 cells, height, width and trough of the $1^{st}$ AP at 200 pA, the trough of last AP at 200 pA, membrane time constant and cell's area.

The amplitude of the membrane potential as a response to the series of current steps, from -140 to 200 pA, was also analysed. Overall, the current-voltage relationship (IV) plots for all of the different groups of cells have a sigmoidal appearance (Figure 3-13).
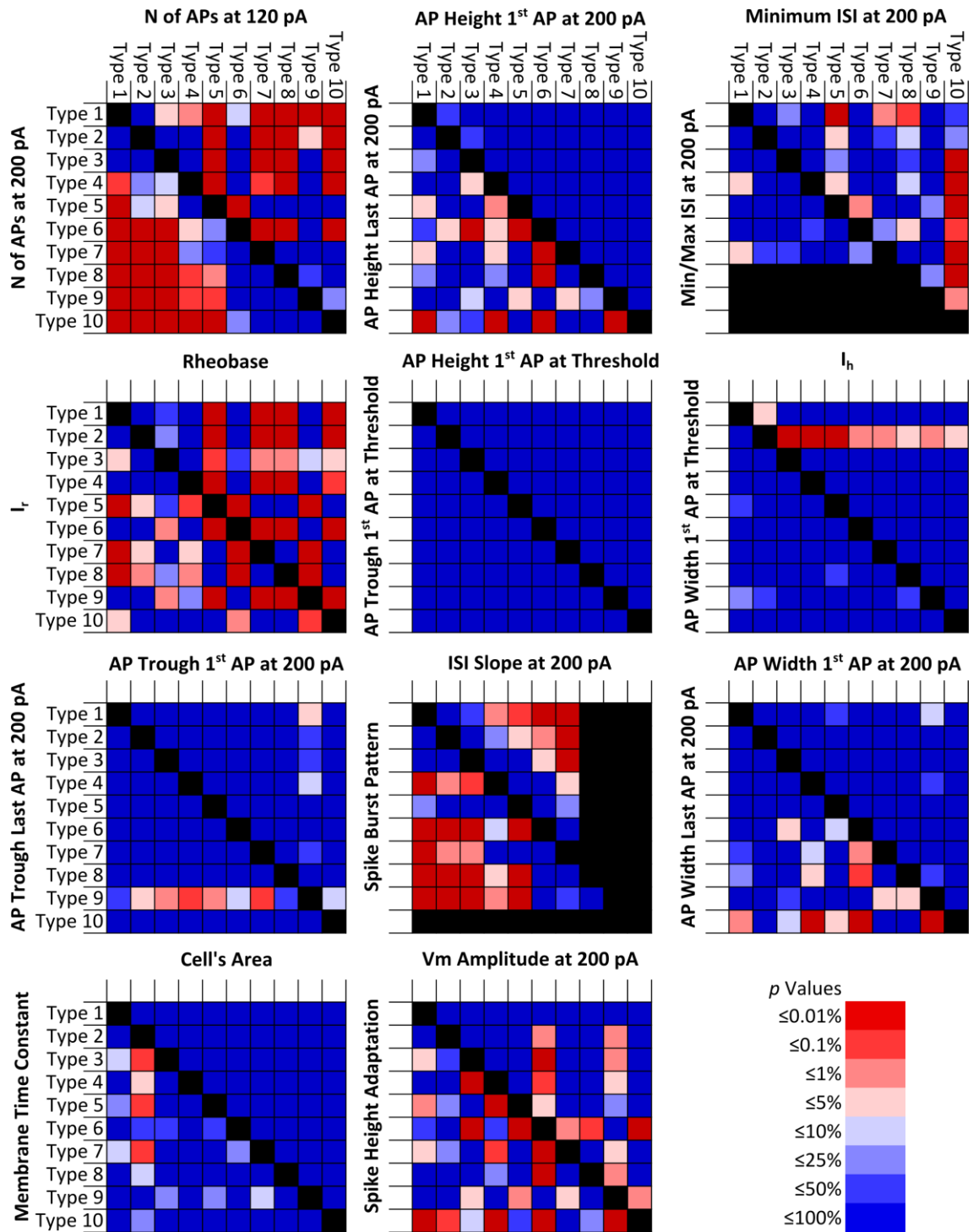
Figure 3-12: Heat maps of the *p* values obtained after using DMCs between the clusters for the parameters. For each side of the heat map, the comparison is for one parameter.

For the positive current steps, the excitability plots became non-linear in all of the different types for larger current injections, which can be attributed to the opening of voltage-gated ion channels. The non-linearity observed throughout the negative current steps suggests that hyperpolarisation-activated ion channels are also expressed in most cell types. This is also visible on some of the sample records shown earlier (Figure 3-10), and this aspect will be discussed further in Chapter 4. In general, cell types 5, 7, 8 and 10 have a shallower curve, compared to the other types. Type 8 has the lowest input resistance of all ten cell types, followed by type 5 and 7. Types 1, 2 and 6 present the least non-linear IV relationships for the negative currents of all the types (Figure 3-13).

## 3.11    Discussion

### 3.11.1  Clustering methods

Data clustering is a data exploration technique that allows the grouping of similar objects into a multidimensional feature space, in this case neurons, in order to facilitate further analysis, processing and understanding of underlying features. There are many different clustering techniques, both supervised and unsupervised. The appropriate clustering technique makes it possible to find hidden characteristics in the data that otherwise would be hard to identify. When dealing with a complex data set such as the many different types of cells with apparently distinct behaviours, it is important to identify the most appropriate parameters to use in the cluster analysis.

Previous attempts to cluster cortical neurons with unsupervised methods have been made mainly for neurons in the intact cortex rather than in cell culture (e.g. Cauli et al. 2000; Andjelic et al. 2009). These were primarily made on interneurons, which are known to be highly diverse in the cortex and present a variety of electrophysiological patterns for excitability. Using unsupervised clustering approaches Cauli et al. (2000) were able to identify three groups of fusiform interneurons in the frontoparietal part of the cortex from Wistar rats by utilising a combination of 48 parameters. Based on
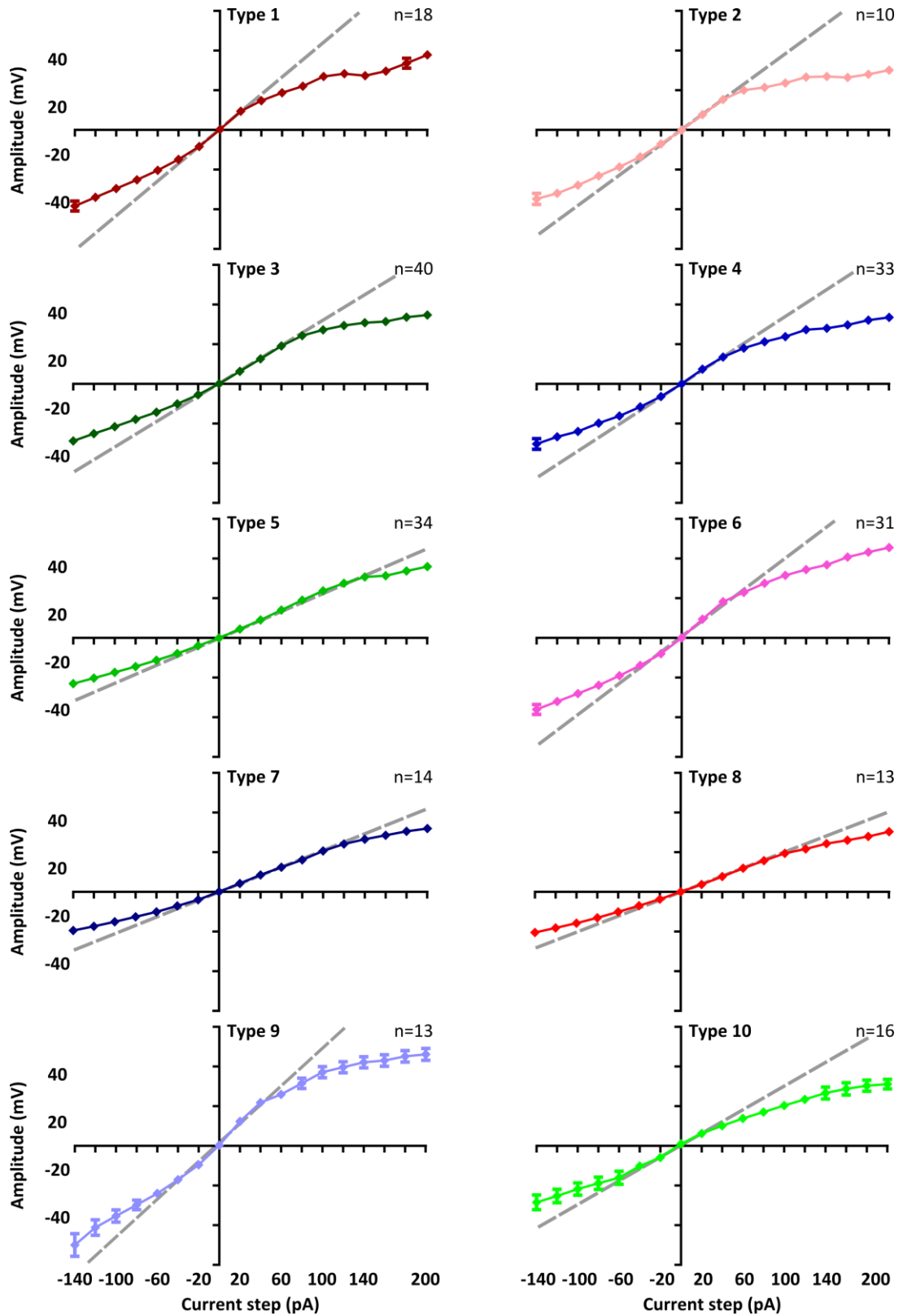
Figure 3-13: IV plots for the ten types of cells. The steady state change in membrane potential from a resting membrane potential of approximately -70 mV is plotted against the amplitude of the current pulse. The dashed lines represent the linear fit through the central data points of the plot where the cells are expected to behave according to Ohm's law.

twelve electrophysiological parameters, Andjelic et al. (2009) could divide recordings from morphologically defined cell types into three groups, one consisting of layer V pyramidal neurons, one that contained a subpopulation of layer VI neurons, and the third group being a heterogeneous assembly of neurons from layers II, III and VI. Both studies used a hierarchical clustering approach, Ward's method (Ward 1963), which is more suitable for parameters described in a discrete, Boolean way.

Another algorithm recently used to classify neocortical interneurons, which uses the affinity propagation method, has the benefit of creating examples for each cluster that help in allocating any new data to a specific cluster (Santana et al. 2013). Its accuracy rate is high when applied to known neurons and reduced numbers of possible groups, but the definition of the best groups is dependable on the group of parameters that is chosen.

The same effect occurs in this work. Since there was a need to observe the effects of specific drugs on the intrinsic membrane properties of the cortical neurons, it is unsurprising that the use of more electrophysiological parameters would result in a better clustering when comparing the standard deviation of the excitability plots of the various types of neurons.

It has been argued that the best method for clustering neurons, especially in a central nervous system region with as many diverse cells such as the neocortex, would be a supervised method (Guerra et al. 2011). In this work, the supervised method proved to be less effective than the *k*-Means algorithm, which had the advantage of speeding up the classification of the various types of cells without *a priori* knowledge of the many cortical neuron types. What is not certain initially is if the cells within clusters would show consistent responses to pharmacological manipulations. Further discussion of this will be in Chapter 4, where changes in electrophysiological properties of the neurons in the presence of 5HT, DEA or both drugs together will be analysed.

Although the final clustering of the records obtained from cultured cortical neurons was based on electrophysiological properties, consideration was also given to the possibility of clustering neurons into distinct groups with specific electrophysiological properties based on their morphological appearance. Previous studies have

demonstrated that the morphology of cortical neurons in cell culture is highly diverse (Kriegstein & Dichter 1983; Dichter 1978). Attempts have been made to classify neurons according to their morphological features in cell culture and it has been suggested that these features are representative of the morphological features in the intact cortex (Kriegstein & Dichter 1983). Even though it has been suggested that cultured cortical neurons can retain morphological, pharmacological and electrical properties of cortical networks *in vivo* (Dichter 1978), few studies have directly reported correlations between the morphological and electrophysiological properties of cortical neurons in cell culture. Furthermore, only a few studies have recorded electrophysiological properties from identified subpopulations of cortical neurons in cell culture. In the past, this was achieved by fluorescent labelling of the neurons while still in the intact tissue prior to cell culture (Huettner & Baughman 1986). The advance of cell-type specific expression of green fluorescent protein (GFP) in recent years has made it possible to apply this approach more widely (Sugino et al. 2006; Feng et al. 2000).

Therefore an initial attempt was made to define types of cortical neurons on the basis of the morphology of the cells in cell culture. This classification considered the number of primary processes of the neurons and the cell soma shape. By only using the number of processes as a definition of morphology of the cells (i.e. bipolar, pyramidal or multipolar), there would be only three types of neurons. Unfortunately this classification does not appear to be sufficient to divide cortical neurons in cell culture into groups with distinct electrophysiological properties. All three groups contained neurons with highly diverse electrophysiological properties. Conversely, all neuron types defined by electrophysiological properties contained examples of each morphologically distinct cell type.

Any unsupervised clustering algorithm used for grouping data points does so without *a priori* biological or physiological knowledge. Instead, clustering is based on index calculations that evaluate how effective the clustering technique is based on the internal cluster structure, i.e. how dense the clusters are and how far apart two clusters are from each other. However, these validating techniques may not always correspond well to the actual physiological information contained within the data. For

example, this could be due to the inclusion of a parameter that is quite variable, but has only a relatively small influence on the overall behaviour of the cells. In this work, out of the ten clustering methods devised and applied to the 222 individual cells, using internal validation methods suggested that the use of all twenty-two parameters in $k$-Means algorithm comes up with the best clustering of the cells. The next two best clustering uses EM. Both methods showed high internal indexes when using the parameter set $PS_{22}$, but also a good combination for clustering is using the statistical algorithm with the parameter set obtained from PCA.

However, visual inspection of the cell clusters produced by the three methods showed a high level of diversity in the firing characteristics of neurons within individual clusters. Furthermore, comparing the averages of the sum of the SD as a measure of the variability in excitability within individual clusters suggests that the algorithms are not the most suitable to divide the cortical neurons into clusters with consistent firing properties, even though it has been suggested to be a better method for clustering biological data (Do & Batzoglou 2008). On the other hand, the EM method with the parameter set that shows the lowest value for the averages of the sum of SD of the number of APs at various current steps (EM with $PS_9$) has a higher value for SD than almost all the $k$-Means methods with different parameter sets.

## 3.11.2 Comparison of cell types

The data obtained shows that a specific cell type's behaviour can be defined by a few specific parameter values. For example, cell type 8 is defined by low number of APs elicited at 120 and 200 pA. These cells show a short burst of phasic activity, but little spike frequency adaptation within the burst of activity. They also have the highest values for the minimum inter-spike intervals. On the other hand, cell type 10 is characterised by production of mainly single APs at the start of the depolarisation. Comparing the parameters that were not used in the final clustering method, it is possible to see significant differences between specific cell types. This supports the conclusion that the clustering procedure accurately divided the cells into specific types with distinct characteristics. For example, the lack of a pronounced trough (after-

hyperpolarisation) after the last AP at 200 pA distinguishes cell type 9 from all the other cell types. However, overall parameters that describe AP shapes appear to be less useful for the definition of the various cell types. For example, the first AP height at threshold and 200 pA current injected is relatively consistent across the different cell types. Similarly, the cell surface area also varies only slightly between the types of cells. Including these parameters in the clustering does not appear to improve the clustering performance as indicated by the comparison of the clustering method based on either $PS_{10}$ or $PS_{22}$.

An interesting point is the similarity in the differences of some of the parameters when they are compared between types of cells. Pairs of parameters such as number of APs elicited by 120 and 200 pA current injection, rheobase and $I_r$, spike burst pattern and ISI slope at 200 pA present similar differences between individual cell types, i.e. if two cell types significantly differ in one of these parameters from each other, these two cells are also more likely to differ significantly in the other parameter. This is not really surprising as it would be expected that e.g. the numbers of APs elicited by 120 and 200 pA, or the threshold current to trigger an AP and the input resistance show some correlation. This suggests that it should be possible to define the types of cells on the basis of fewer parameters. However, this might compromise the distinction of more subtle differences and the clustering performance based on just five parameters ($PS_5$) was judged to be worse than clustering using $PS_{10}$.

Among the ten distinct cell types, five draw attention because they show strong spike height adaptation. When comparing the width of the first AP and the last AP at 200 pA from these cell types, they also show considerable AP broadening. Strong spike height adaptation has been described previously for irregular spiking neurons from layers II-III and V (Cauli et al. 1997), whereas there are cortical interneurons in rats (Quirk 2009) and mice that present spike broadening, which is influenced by Kv3 potassium channels (Erisir et al. 1999).  However, the fact that the APs in cultured cells show both height adaptation and pronounced broadening suggests that the spike height adaptation might be due to different causes.

Although the cell culture system is designed to closely mimic the conditions in the intact brain, the complex network structure of the cortex is not present. Furthermore, cortical neurons in culture lack long-range inputs from other regions of the brain and synaptic activity is also sparser. These factors may contribute to the under-development of ion channels, such as potassium ion channels. Interestingly, the IV plots for the cell types with strong spike height adaptation and spike broadening show a strong rectification in response to larger positive current pulses. This indicates a strong change in input resistance due to the activation of voltage-gated ion channels. Thus, it is less likely that their inability to sustain AP generation for extended periods of time is due to an under-expression of voltage-gated ion channels, but more likely the result of a mismatch between voltage-activated inward and outward currents.

Other cell types are also remarkable due to the fact that they show very phasic activity patterns and only ever generate short AP bursts or a single AP at the start of current pulse. These include cell types 7, 8 and 10 which all generated less than five APs at 200 pA. Another common feature of these cell types is that they have the highest AP thresholds of all cells recorded.

It is possible to find in the literature examples of neuron recordings in acute cortical slices that resemble the behaviour of the various cell types of cultured cortical cells. This suggests that cultured cortical neurons develop in a similar manner compared to their natural environment. However, due to differences in data acquisition and analysis between the published data and the current study, it is difficult to directly relate specific neuron types in intact slices and *in vivo* to the cell types identified in cell culture in this work. For example, not all published studies report the same parameters used in this work, and many studies in acute slices used different types of current clamp protocols, especially with higher values of positive and negative current injected, and/or with larger steps in between. A more detailed discussion of the correlation between the types of neurons identified in this study in cortical cultures and specific neuron types in acute cortical slices will be presented in Chapter 6.

# 4 Modulation of properties of cortical neurons by nitric oxide and serotonin in dissociated neuronal cultures

In this chapter data will be presented and discussed focusing on the following points:

- The modulation of intrinsic electrophysiological parameters by NO and 5HT within defined groups of cultured cortical neurons;

- The signalling pathways that mediate the effects of NO acts on these groups;

- The possible interactions between NO and 5HT signalling pathways that cause the modulation of electrophysiological properties, intrinsic excitability and current-voltage relationship of these neurons;

- The role of $5HT_3$ type receptors in cultured cortical neurons.


## 4.1 Introduction

Transmission of information between neurons through synapses happens with the use of endogenous chemicals called neurotransmitters. Serotonin (5HT) and nitric oxide (NO) can act both as neurotransmitters and as neuromodulators via volume transmission (Bunin & Wightman 1998; Steinert et al. 2008), modulating cellular and synaptic properties. The monoamine neurotransmitter 5HT is produced by neurons located in the raphe nuclei in the brain; the axons of these neurons spread to almost all regions of the brain, with the cortex in particular being densely innervated (Smiley & Goldman-Rakic 1996). The most abundant NO synthase found in the central nervous system, the neuronal nitric oxide synthase (nNOS), is co-expressed in a subpopulation of serotonergic neurons innervating the cortex (Simpson et al. 2003). This enzyme is also present in the layers II to VI of the cortex, whose neurons extend their branches throughout the entire cortical neuropil (Vincent & Kimura 1992; Valtschanoff et al. 1993). Cortical nNOS expressing neurons are mainly a subpopulation of inhibitory interneurons (Gonchar & Burkhalter 1997; Tomioka et al. 2005), but there is also evidence for nNOS expression in pyramidal neurons (Aoki et al. 1998).

The intrinsic membrane properties and excitability of neurons is important for transmission of information. The co-localisation and morphological overlap between 5HT and NOS suggests that there are possible interactions between these two neurotransmitters, such as in the pre-synaptic terminals, where an interaction between the serotonin transporter (SERT) and NO, which decreases SERT cell surface localisation and 5HT re-uptake has been demonstrated (Chanrion et al. 2007). However, despite being expressed extensively in the cortical regions, there are currently no studies reporting the combined effects of 5HT and NO on intrinsic membrane properties and excitability in cortical neurons.

In this work, after clustering the various types of cultured cortical neurons (see Chapter 3), the individual effects of 5HT and NO and the combined effects of 5HT/NO were analysed to discover any significant interactions. The parameters analysed were related to intrinsic membrane properties and excitability of the cells, obtained from records in whole-cell current clamp mode as described previously (Chapters 2 and 3). In total 20 parameters were analysed for the 10 different cell types defined in chapter 3. The data was explored with the aim of identifying consistent changes in parameter values when the cells were bath-perfused with either of the drugs or a combination of both, compared to control levels. The results of the combined application of the drugs were compared to the application of each drug alone to identify whether the co-application of the drugs had a linear, summative effect or resulted in non-linear interactions. Finally an effort was made to clarify the transduction pathways of NO that mediate the effects on the analysed parameters.

## 4.2 Modulation of intrinsic electrophysiological parameters by serotonin and nitric oxide

As described in Chapter 3, by using a *k*-Means clustering algorithm it was possible to define ten different types of cultured cortical neurons based on their electrophysiological properties. Within these ten groups, 197 cells received 5HT, NO (applied as diethylamine NONOate sodium salt hydrate (DEA) which served as an NO donor) or both drugs together, whilst in the presence of picrotoxin and kynurenic acid

to block both excitatory and inhibitory synaptic interactions (see Chapter 2 for details). In some experiments, cells were pre-incubated with 1H-[1,2,4]oxadiazolo[4,3-a]quinoxalin-1-one (ODQ), a highly selective, competitive and irreversible heme-site inhibitor of soluble guanylyl cyclase (sGC), before the application of DEA or 5HT/DEA.

Only data for the four cell types with the largest n numbers (types 3, 4, 5 and 6) were analysed in detail, as these cell types' sample sizes for all treatments were large enough to have sufficient statistical power (i.e. n≥6 for all treatments; Figure 4-1). These four major types of cultured cortical neurons represent 64.4% of all the cells that received any pharmacological treatment.

The effects of 5HT, DEA and both drugs together showed variability in the type of response in the ten different types of cultured cortical neurons. From these types, sample records for cell type 3 are shown in Figure 4-2, and records of the electrophysiological behaviour in the presence of 5HT (red), DEA (green) or 5HT/DEA (blue) are superimposed onto control records (black). In this case, 5HT increased the number of action potentials (APs) elicited at 120 pA, increased the ratio of Min/Max inter-spike interval (ISI) at 200 pA, whereas it decreased spike height adaptation. The membrane potential amplitude at 200 pA was increased. In the presence of DEA, the number of APs at 120 and 200 pA decreased. Spike burst pattern was strongly reduced, i.e. the cell showed a more phasic activity pattern. The width of the first and last AP at 200 pA was increased, but their height was decreased. When both 5HT/DEA were applied, the numbers of APs at 200 pA were decreased, as well as the Min/Max ISI ratio. The amplitudes of the first and last AP at 200 pA were slightly reduced, as was the trough of the first AP at 200 pA.

The effect on all analysed parameters for the ten cell types is summarised in Table 4-1 to Table 4-2. The tables show the average control values for twenty different parameters analysed for each cell type that describe their excitability and firing pattern (Table 4-1) and AP shape (Table 4-2). The change in any value induced by a specific treatment (Δ values) compared to the control of the same cells prior to treatment is listed below each average control value. The first four columns are for cell types 3, 4, 5 and 6, whereas the remaining six columns (in grey) are for the rest of the ten cell

**A** — Cell types

| | 1 | 2 | 3 | 4 | 5 | 6 | 7 | 8 | 9 | 10 |
|---|---|---|---|---|---|---|---|---|---|---|
| Control | 15 | 10 | 40 | 27 | 32 | 28 | 13 | 10 | 11 | 11 |
| 5HT | 4 | 2 | 12 | 7 | 6 | 11 | 2 | 1 | 0 | 4 |
| DEA | 3 | 0 | 22 | 10 | 11 | 12 | 7 | 4 | 3 | 4 |
| 5HT/DEA | 0 | 2 | 15 | 9 | 9 | 11 | 2 | 1 | 2 | 4 |
| (ODQ)DEA | 8 | 6 | 8 | 11 | 9 | 8 | 2 | 4 | 6 | 2 |
| (ODQ)5HT/DEA | 8 | 5 | 8 | 11 | 7 | 7 | 2 | 4 | 5 | 2 |

**B** — Total n = 197 cells

| Cell types | 3 | 4 | 5 | 6 |
|---|---|---|---|---|
| % of total | 20.3 | 13.7 | 16.2 | 14.2 |

| Cell types | 1 | 2 | 7 | 8 | 9 | 10 |
|---|---|---|---|---|---|---|
| % of total | 7.6 | 5.1 | 6.6 | 5.1 | 5.6 | 5.6 |
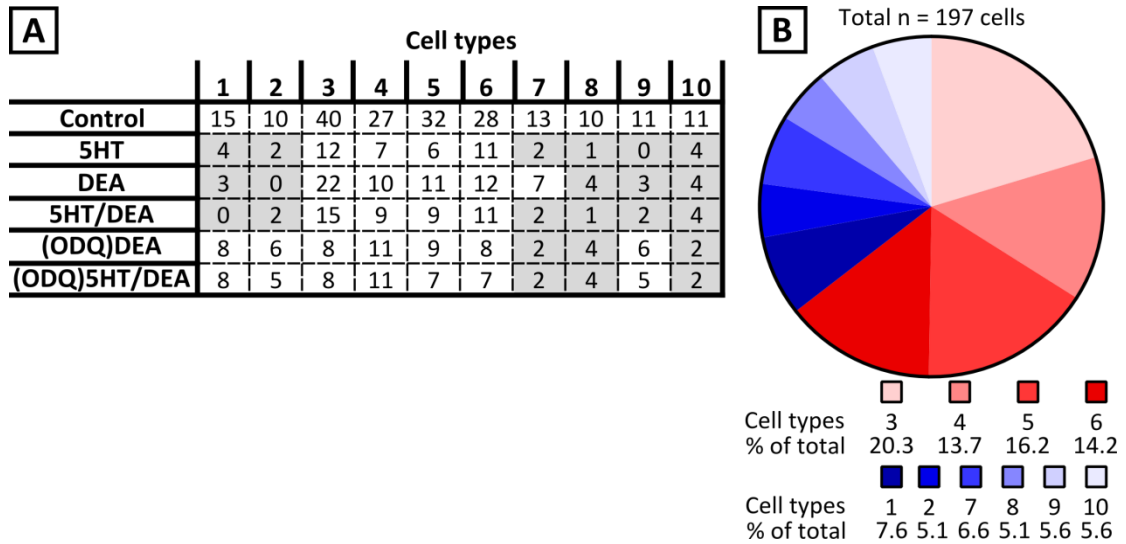
Figure 4-1: Number of cells recorded in the presence of 5HT, DEA, 5HT/DEA, (ODQ)DEA or (ODQ)5HT/DEA. (A) Sample size of the 10 different groups of cultured cortical cells defined by $k$-Means clustering based on $PS_{10}$ (Chapter 3). The numbers in control are for the cells that subsequently received any treatment. Some of the cells received multiple treatments, i.e. 5HT or DEA followed by 5HT/DEA. Grey squares indicate n < 5 experimental trials. (B) Pie-chart showing the percentage of cells in each group. The four cell types that had n≥6 for all treatments (shown in red) represent more than 60% of all the cells recorded.
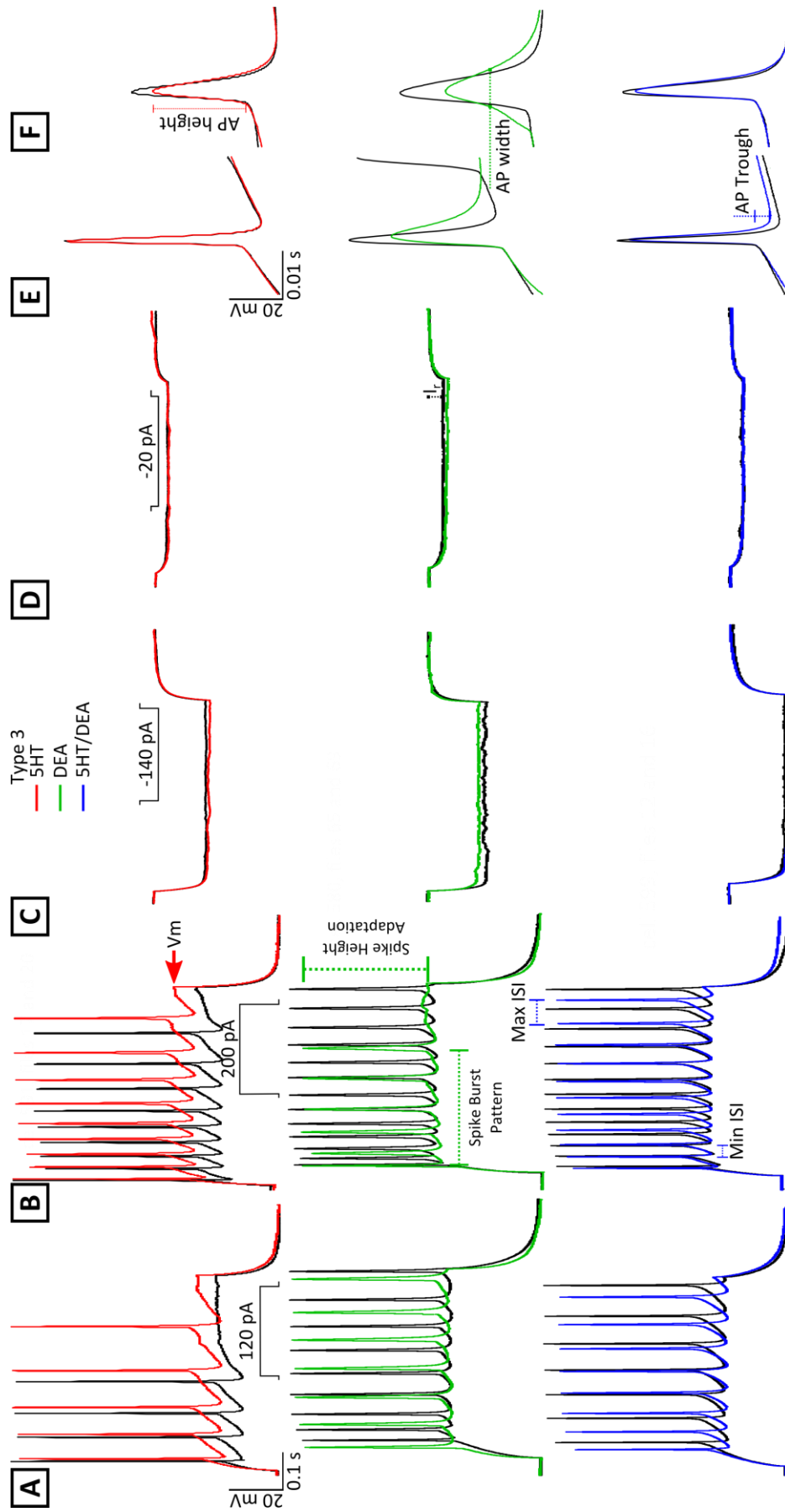
Figure 4-2: Membrane potential responses of three type 3 cells to a series of square current pulses, and the modulation of these responses in the presence of 5HT (red), DEA (green) or 5HT/DEA (blue). (A-B) Depolarisation and AP elicited by a 120 pA (A) and to a 200 pA current step (B). (C-D) Membrane potential response to a -140 pA (C) and to a -20 pA current injection (D). (E-F) Close look at first AP (E) and last AP (F) at 200 pA. Traces show three recorded cells, one for each treatment condition. Control recordings prior to drug application are shown in black, while recordings during drug application are overlapped in different colours.

types. The colour code to the right of each Δ value indicates to what extent a drug treatment affected the control values for the specific parameters in percentage; this was obtained by dividing the difference value by the overall control value.

Of note, drug treatment increased the values observed by more than 100% for the following cell types and parameters: for type 3 cells, ISI slope at 200 pA was increased by 5HT; this parameter also presented an increase of more than 100% for the type 1 cells; for type 4 cells, the ISI slope at 200 pA and the minimum ISI values were increased by DEA.

A multi-level modelling (MLM) approach was used to check whether the effects observed for the various parameters during drug treatment showed significant differences across cell types 3, 4, 5 and 6. This model was developed using the various parameters as outcome, the treatments as fixed effects and the different cells in the experiments as random effects. Simultaneous inference was obtained by using general linear hypothesis for this model, and the $p$ values obtained were stored in a matrix, which was then interpreted as a heat map (Figure 4-3).

This analysis revealed that overall DEA appeared to have more pronounced effects than 5HT on cellular parameters in these four cell types. Compared to control, 5HT caused significant changes in fifteen parameters, while DEA significantly affected thirty-three parameters (Figure 4-3). Furthermore, significant changes induced by 5HT appeared to be more cell type specific as ten of the fifteen were observed in cell type 3 with the other five in cell type 4, but no significant changes were observed in any of the parameters in cell types 5 and 6. In contrast, DEA significantly changes the parameter values in all four cell types, affecting twelve parameters in cell type 5, eleven in cell type 3, five in cell type 4 and five in cell type 6.

For example, DEA significantly reduced the excitability of the cells as indicated by a reduction in APs at 200 pA for cell types 3, 4 and 5 (MLM: $p<0.0001$). A similar group of $p$ values was observed for the minimum ISI at 200 pA, which DEA increased significantly in all but cell type 6 (MLM: $p<0.05$ for cell types 3, 4 and 5). The height of the first AP at 200 pA was significantly reduced by DEA for all but cell type 3 (MLM: $p<0.05$ for cell types 4, 5 and 6), while the width of the first AP at 200 pA was

| | Treatment | Type 3 | Type 4 | Type 5 | Type 6 | Type 1 | Type 2 | Type 7 | Type 8 | Type 9 | Type 10 |
|---|---|---|---|---|---|---|---|---|---|---|---|
| N of APs at 120 pA | Control | 6.8 ± 0.3 | 6.1 ± 0.4 | 1.6 ± 0.3 | 6.8 ± 0.6 | 12.1 ± 0.6 | 10.1 ± 0.7 | 0.8 ± 0.2 | 0.4 ± 0.2 | 3.5 ± 0.5 | 0.3 ± 0.2 |
| | Δ5HT | 1.0 ± 0.6 | 0.6 ± 0.3 | 0.4 ± 0.7 | -0.4 ± 0.5 | 0.2 ± 1.1 | -3.0 ± 2.3 | 0.7 ± 1.0 | 0.0 ± 0.0 | | 0.3 ± 0.2 |
| | ΔDEA | -1.3 ± 0.6 | -0.1 ± 0.3 | 0.2 ± 0.3 | -0.6 ± 0.4 | -1.5 ± 0.2 | | -0.5 ± 0.3 | -0.4 ± 0.3 | -0.9 ± 0.4 | -0.1 ± 0.1 |
| | Δ5HT/DEA | 0.0 ± 0.6 | 0.4 ± 0.5 | 1.5 ± 0.7 | -0.8 ± 0.5 | | 1.2 ± 1.2 | 0.0 ± 0.0 | 0.7 ± 0.0 | -1.3 ± 1.0 | 0.3 ± 0.2 |
| N of APs at 200 pA | Control | 11.2 ± 0.3 | 7.5 ± 0.3 | 7.7 ± 0.4 | 4.5 ± 0.4 | 16.0 ± 0.6 | 13.2 ± 0.6 | 4.0 ± 0.3 | 2.3 ± 0.3 | 1.9 ± 0.2 | 1.2 ± 0.3 |
| | Δ5HT | -1.0 ± 0.9 | -0.2 ± 0.6 | 1.3 ± 0.7 | -0.6 ± 0.3 | -3.3 ± 1.8 | -4.8 ± 3.5 | 1.5 ± 1.2 | 0.3 ± 0.0 | | 0.8 ± 0.8 |
| | ΔDEA | -2.6 ± 0.6 | -1.6 ± 0.5 | -2.1 ± 0.7 | -0.3 ± 0.4 | -2.2 ± 1.0 | | -1.3 ± 0.7 | -1.8 ± 0.6 | -0.5 ± 0.2 | 0.6 ± 0.5 |
| | Δ5HT/DEA | -1.6 ± 0.6 | -0.8 ± 0.6 | -0.5 ± 1.3 | -0.5 ± 0.4 | | 0.2 ± 1.2 | 1.4 ± 1.3 | 0.3 ± 0.0 | -0.8 ± 0.5 | 1.6 ± 0.4 |
| Rheobase (x10 pA) | Control | 8.2 ± 0.3 | 6.6 ± 0.5 | 12.5 ± 0.4 | 6.2 ± 0.3 | 5.9 ± 0.6 | 4.9 ± 0.4 | 13.1 ± 0.7 | 13.7 ± 0.7 | 4.9 ± 0.6 | 15.4 ± 1.5 |
| | Δ5HT | -0.7 ± 0.4 | -0.7 ± 0.4 | 0.3 ± 1.1 | -0.6 ± 0.4 | -1.3 ± 0.6 | 0.3 ± 1.0 | 0.0 ± 0.0 | -2.0 ± 0.0 | | -1.3 ± 1.1 |
| | ΔDEA | 0.3 ± 0.6 | -0.5 ± 0.2 | -0.4 ± 0.5 | -0.1 ± 0.3 | -0.3 ± 0.5 | | 1.5 ± 1.3 | 2.5 ± 1.5 | 0.4 ± 0.4 | -1.2 ± 0.7 |
| | Δ5HT/DEA | -0.6 ± 0.5 | -1.1 ± 0.3 | -1.8 ± 0.6 | -0.5 ± 0.2 | | 0.0 ± 0.0 | 0.0 ± 0.0 | -2.0 ± 0.0 | 0.7 ± 1.3 | -3.0 ± 0.3 |
| Vm Amplitude at 200 pA (x10 mV) | Control | 3.4 ± 0.1 | 3.3 ± 0.1 | 3.6 ± 0.2 | 4.5 ± 0.2 | 3.9 ± 0.2 | 3.0 ± 0.2 | 3.2 ± 0.1 | 3.0 ± 0.1 | 4.8 ± 0.3 | 3.1 ± 0.3 |
| | Δ5HT | 0.4 ± 0.1 | 0.1 ± 0.1 | 0.0 ± 0.2 | 0.1 ± 0.1 | 0.3 ± 0.3 | -1.3 ± 0.5 | 0.1 ± 0.0 | -0.1 ± 0.0 | | 0.3 ± 0.1 |
| | ΔDEA | 0.1 ± 0.1 | 0.0 ± 0.1 | 0.2 ± 0.1 | -0.1 ± 0.1 | -0.1 ± 0.3 | | 0.4 ± 0.3 | -0.1 ± 0.2 | -0.2 ± 0.1 | 0.0 ± 0.1 |
| | Δ5HT/DEA | 0.1 ± 0.1 | 0.0 ± 0.1 | 0.0 ± 0.3 | -0.2 ± 0.0 | | 0.6 ± 0.6 | 0.1 ± 0.1 | -0.1 ± 0.0 | 0.2 ± 0.0 | 0.1 ± 0.1 |
| ISI Slope at 200 pA (x10⁻³) | Control | 4.5 ± 0.5 | 10.6 ± 1.3 | 11.5 ± 1.4 | 11.0 ± 1.1 | 1.3 ± 0.2 | 2.7 ± 0.8 | 42.3 ± 6.6 | | | |
| | Δ5HT | 4.6 ± 5.2 | 0.4 ± 2.5 | -1.8 ± 2.1 | -1.4 ± 2.0 | 2.2 ± 1.8 | 2.5 ± 2.0 | -6.7 ± 5.3 | | | |
| | ΔDEA | 2.9 ± 1.1 | 13.8 ± 4.3 | 2.9 ± 3.2 | 2.4 ± 5.6 | -0.9 ± 0.7 | | -10.9 ± 6.5 | | | |
| | Δ5HT/DEA | 0.4 ± 1.0 | 3.0 ± 1.4 | -2.6 ± 1.6 | -3.3 ± 4.9 | | -0.1 ± 0.4 | -30.3 ± 19.6 | | | |
| Minimum ISI at 200 pA (x10 ms) | Control | 2.4 ± 0.1 | 2.5 ± 0.1 | 3.6 ± 0.2 | 2.1 ± 0.1 | 1.4 ± 0.6 | 2.1 ± 0.1 | 3.4 ± 0.3 | 4.1 ± 0.7 | 1.8 ± 0.3 | |
| | Δ5HT | 0.2 ± 0.2 | 0.3 ± 0.1 | -0.3 ± 0.4 | -0.1 ± 0.1 | 0.1 ± 0.1 | 0.3 ± 0.1 | 0.1 ± 0.3 | 0.7 ± 0.0 | | |
| | ΔDEA | 0.5 ± 0.1 | 4.4 ± 1.2 | 1.7 ± 1.5 | 0.0 ± 0.1 | 0.4 ± 0.2 | | -0.4 ± 1.0 | -0.6 ± 0.4 | -0.2 ± 0.3 | |
| | Δ5HT/DEA | 0.7 ± 0.3 | 0.3 ± 0.1 | 0.0 ± 0.1 | 0.5 ± 0.1 | | 0.1 ± 0.2 | -0.1 ± 0.3 | -0.6 ± 0.0 | -0.3 ± 0.3 | |
| Min/Max ISI at 200 pA (x10⁻¹) | Control | 3.9 ± 0.2 | 3.4 ± 0.2 | 4.1 ± 0.3 | 5.4 ± 0.3 | 3.4 ± 1.6 | 4.3 ± 0.5 | 3.3 ± 0.5 | 7.1 ± 0.8 | 7.6 ± 0.9 | |
| | Δ5HT | 0.7 ± 0.4 | 0.6 ± 0.4 | 0.0 ± 0.1 | 0.3 ± 0.7 | -1.6 ± 1.5 | -5.0 ± 1.3 | 0.0 ± 0.0 | 3.3 ± 0.0 | | |
| | ΔDEA | 0.3 ± 0.3 | 0.7 ± 0.2 | 0.7 ± 0.7 | 0.6 ± 0.8 | -0.1 ± 0.4 | | 0.6 ± 0.8 | -1.5 ± 0.8 | | |
| | Δ5HT/DEA | 1.2 ± 0.5 | 0.6 ± 0.3 | 0.9 ± 0.4 | 1.8 ± 0.7 | | 0.1 ± 0.1 | 0.6 ± 0.6 | -3.0 ± 0.0 | | |
| Spike Burst Pattern (x10 %) | Control | 8.8 ± 0.1 | 6.2 ± 0.3 | 8.0 ± 0.2 | 2.3 ± 0.3 | 9.0 ± 0.2 | 9.2 ± 0.1 | 4.9 ± 0.5 | 1.3 ± 0.3 | 0.4 ± 0.1 | |
| | Δ5HT | -1.3 ± 0.5 | -0.3 ± 0.6 | 0.3 ± 0.1 | -0.4 ± 0.3 | -2.7 ± 1.0 | -4.0 ± 0.8 | 1.8 ± 1.3 | 0.1 ± 0.0 | | |
| | ΔDEA | -1.2 ± 0.4 | -1.4 ± 0.5 | -1.7 ± 0.8 | 0.3 ± 0.6 | -0.2 ± 0.1 | | -2.3 ± 1.1 | -0.7 ± 0.8 | 0.0 ± 0.1 | |
| | Δ5HT/DEA | -1.3 ± 0.8 | -0.4 ± 0.6 | -0.1 ± 0.3 | -0.1 ± 0.4 | | 0.2 ± 0.1 | 0.9 ± 0.5 | 1.8 ± 0.0 | -0.3 ± 0.2 | |
| Spike Height Adaptation (x10 %) | Control | 7.8 ± 0.2 | 4.6 ± 0.4 | 8.1 ± 0.3 | 2.4 ± 0.2 | 5.0 ± 0.5 | 5.5 ± 0.5 | 8.3 ± 0.5 | 7.2 ± 0.7 | 4.5 ± 0.6 | |
| | Δ5HT | -1.6 ± 0.5 | -0.9 ± 0.4 | -1.2 ± 0.8 | -0.1 ± 0.3 | -0.5 ± 0.5 | -0.1 ± 2.1 | -0.4 ± 0.3 | -2.0 ± 0.0 | | |
| | ΔDEA | -0.8 ± 0.3 | -0.1 ± 0.2 | -0.6 ± 0.4 | 0.9 ± 0.4 | 0.5 ± 0.5 | | 0.3 ± 0.4 | 0.7 ± 0.7 | 2.2 ± 1.3 | |
| | Δ5HT/DEA | -1.2 ± 0.4 | -1.4 ± 0.5 | -0.7 ± 0.4 | 0.4 ± 0.2 | | -0.6 ± 0.3 | -0.4 ± 0.1 | 0.0 ± 0.0 | 1.5 ± 0.2 | |
| Ih (x10 %) | Control | 9.7 ± 0.1 | 9.6 ± 0.1 | 9.6 ± 0.1 | 9.2 ± 0.2 | 9.5 ± 0.1 | 7.5 ± 0.2 | 9.6 ± 0.1 | 9.2 ± 0.2 | 9.5 ± 0.2 | 9.9 ± 0.5 |
| | Δ5HT | -0.1 ± 0.1 | -0.1 ± 0.2 | -0.1 ± 0.1 | 0.0 ± 0.1 | 0.0 ± 0.1 | 0.8 ± 0.8 | 0.0 ± 0.1 | -0.5 ± 0.0 | | -0.1 ± 0.2 |
| | ΔDEA | 0.0 ± 0.1 | 0.0 ± 0.0 | 0.0 ± 0.1 | -0.2 ± 0.1 | 0.0 ± 0.0 | | -0.1 ± 0.1 | -0.1 ± 0.1 | -0.2 ± 0.3 | -0.2 ± 0.1 |
| | Δ5HT/DEA | -0.1 ± 0.1 | 0.0 ± 0.1 | 0.0 ± 0.2 | -0.3 ± 0.1 | | 0.9 ± 1.3 | 0.1 ± 0.1 | 0.0 ± 0.0 | -0.6 ± 0.6 | -0.1 ± 0.1 |

Legend: >100% ■ (red) >50% ■ >10% ■ ≤10% and ≥-10% ■ <-10% ■ <-50% ■ <-100% ■ (blue)

Table 4-1: Summary of average values for cellular parameters describing activity pattern. The table shows the average ± standard error of the means (SEM) for control values (dark grey rows), followed by the average difference between treatment and control for 7 parameters in the 10 cell types. Cell types shown with grey background (cell types 1, 2, 7, 8, 9 and 10) are groups with n numbers <6 for individual treatments. The colour coded column to the right of each group represents the percentage of increase or decrease of the values when compared to control.

| Parameter | Treatment | Type 3 | Type 4 | Type 5 | Type 6 | Type 1 | Type 2 | Type 7 | Type 8 | Type 9 | Type 10 |
|---|---|---|---|---|---|---|---|---|---|---|---|
| $I_r$ (x10² MΩ) | Control | 2.6 ± 0.1 | 3.1 ± 0.2 | 1.9 ± 0.1 | 4.1 ± 0.3 | 3.8 ± 0.3 | 3.5 ± 0.4 | 1.8 ± 0.1 | 1.8 ± 0.1 | 4.5 ± 0.3 | 2.2 ± 0.5 |
| | Δ5HT | 0.1 ± 0.1 | 0.2 ± 0.2 | 0.2 ± 0.2 | -0.2 ± 0.3 | 0.6 ± 0.4 | -0.6 ± 0.1 | 0.1 ± 0.0 | -1.1 ± 0.0 | | 0.1 ± 0.2 |
| | ΔDEA | -0.1 ± 0.1 | 0.0 ± 0.2 | 0.3 ± 0.1 | 0.3 ± 0.1 | 0.1 ± 0.4 | | 0.1 ± 0.1 | -0.1 ± 0.1 | 0.2 ± 0.3 | -0.1 ± 0.2 |
| | Δ5HT/DEA | -0.1 ± 0.2 | 0.2 ± 0.2 | 0.1 ± 0.3 | 0.0 ± 0.3 | | -0.1 ± 0.2 | 0.0 ± 0.1 | 0.1 ± 0.0 | 0.7 ± 0.8 | 0.1 ± 0.2 |
| AP Height 1ˢᵗ AP at Threshold (x10 mV) | Control | 6.5 ± 0.2 | 7.1 ± 0.2 | 6.4 ± 0.3 | 6.3 ± 0.3 | 6.2 ± 0.3 | 7.5 ± 0.3 | 6.8 ± 0.4 | 7.0 ± 0.3 | 6.7 ± 0.4 | 6.4 ± 0.4 |
| | Δ5HT | -0.3 ± 0.2 | -0.3 ± 0.1 | 0.0 ± 0.1 | 0.1 ± 0.2 | -0.5 ± 0.3 | -0.7 ± 1.1 | -0.2 ± 0.1 | -0.2 ± 0.0 | | -0.2 ± 0.1 |
| | ΔDEA | -0.2 ± 0.1 | -0.1 ± 0.1 | -0.4 ± 0.1 | -0.1 ± 0.1 | -0.1 ± 0.2 | | -0.5 ± 0.2 | -0.5 ± 0.3 | -0.2 ± 0.2 | -0.1 ± 0.1 |
| | Δ5HT/DEA | -0.2 ± 0.1 | 0.0 ± 0.1 | -0.2 ± 0.1 | -0.2 ± 0.1 | | 0.0 ± 0.0 | 0.0 ± 0.0 | 0.0 ± 0.0 | -0.1 ± 0.2 | -0.3 ± 0.2 |
| AP Trough 1ˢᵗ AP at Threshold (x10 mV) | Control | -1.0 ± 0.1 | -1.1 ± 0.1 | -0.9 ± 0.1 | -1.1 ± 0.1 | -1.0 ± 0.1 | -1.3 ± 0.2 | -0.8 ± 0.1 | -0.8 ± 0.1 | -0.6 ± 0.1 | -0.8 ± 0.1 |
| | Δ5HT | 0.1 ± 0.1 | 0.1 ± 0.1 | 0.1 ± 0.1 | 0.0 ± 0.1 | 0.1 ± 0.1 | 0.5 ± 0.0 | -0.2 ± 0.1 | 0.0 ± 0.0 | | 0.0 ± 0.1 |
| | ΔDEA | 0.1 ± 0.1 | 0.1 ± 0.0 | 0.2 ± 0.1 | 0.0 ± 0.0 | 0.2 ± 0.1 | | 0.2 ± 0.1 | 0.0 ± 0.0 | 0.3 ± 0.1 | 0.2 ± 0.2 |
| | Δ5HT/DEA | 0.1 ± 0.0 | 0.2 ± 0.0 | 0.0 ± 0.1 | 0.0 ± 0.1 | | 0.0 ± 0.0 | 0.1 ± 0.0 | 0.2 ± 0.0 | 0.4 ± 0.0 | 0.0 ± 0.3 |
| AP Width 1ˢᵗ AP at Threshold (ms) | Control | 2.2 ± 0.1 | 2.3 ± 0.1 | 2.6 ± 0.1 | 2.3 ± 0.1 | 2.1 ± 0.1 | 2.0 ± 0.2 | 2.3 ± 0.2 | 2.1 ± 0.2 | 2.8 ± 0.2 | 2.2 ± 0.3 |
| | Δ5HT | 0.1 ± 0.0 | 0.1 ± 0.1 | -0.1 ± 0.2 | 0.0 ± 0.0 | 0.4 ± 0.1 | 0.8 ± 0.8 | 0.0 ± 0.1 | 0.1 ± 0.0 | | 0.0 ± 0.1 |
| | ΔDEA | 0.2 ± 0.1 | 0.0 ± 0.0 | 0.4 ± 0.1 | 0.0 ± 0.1 | 0.3 ± 0.1 | | 0.4 ± 0.3 | 0.1 ± 0.1 | 0.1 ± 0.2 | 0.0 ± 0.0 |
| | Δ5HT/DEA | 0.2 ± 0.1 | 0.1 ± 0.1 | 0.2 ± 0.1 | 0.0 ± 0.0 | | 0.0 ± 0.0 | 0.0 ± 0.0 | 0.2 ± 0.0 | 0.0 ± 0.1 | 0.0 ± 0.1 |
| AP Height 1ˢᵗ AP at 200 pA (x10 mV) | Control | 6.3 ± 0.2 | 7.1 ± 0.1 | 6.4 ± 0.3 | 6.3 ± 0.3 | 6.0 ± 0.2 | 7.4 ± 0.2 | 6.8 ± 0.4 | 7.2 ± 0.3 | 6.6 ± 0.3 | 6.5 ± 0.5 |
| | Δ5HT | -0.3 ± 0.2 | -0.4 ± 0.1 | 0.0 ± 0.2 | 0.1 ± 0.2 | -0.4 ± 0.2 | -1.0 ± 0.8 | -0.1 ± 0.1 | 0.0 ± 0.0 | | -0.1 ± 0.1 |
| | ΔDEA | -0.1 ± 0.1 | -0.2 ± 0.1 | -0.3 ± 0.1 | -0.1 ± 0.1 | -0.5 ± 0.2 | | -0.5 ± 0.3 | -0.6 ± 0.3 | -0.3 ± 0.1 | -0.2 ± 0.1 |
| | Δ5HT/DEA | -0.3 ± 0.1 | -0.2 ± 0.1 | -0.1 ± 0.1 | -0.1 ± 0.0 | | 0.0 ± 0.0 | 0.0 ± 0.0 | 0.0 ± 0.0 | -0.5 ± 0.1 | -0.1 ± 0.1 |
| AP Trough 1ˢᵗ AP at 200 pA (x10 mV) | Control | -0.3 ± 0.1 | -0.4 ± 0.1 | -0.3 ± 0.1 | -0.3 ± 0.1 | -0.5 ± 0.1 | -0.5 ± 0.1 | -0.4 ± 0.2 | -0.5 ± 0.2 | 0.2 ± 0.2 | -0.5 ± 0.1 |
| | Δ5HT | 0.1 ± 0.1 | 0.1 ± 0.1 | 0.1 ± 0.1 | 0.0 ± 0.1 | 0.2 ± 0.1 | 0.3 ± 0.2 | -0.1 ± 0.0 | 0.1 ± 0.0 | | 0.1 ± 0.0 |
| | ΔDEA | 0.1 ± 0.0 | 0.1 ± 0.0 | 0.0 ± 0.0 | 0.0 ± 0.1 | 0.0 ± 0.0 | | 0.0 ± 0.0 | -0.1 ± 0.1 | 0.2 ± 0.0 | 0.1 ± 0.1 |
| | Δ5HT/DEA | 0.1 ± 0.1 | 0.2 ± 0.1 | 0.0 ± 0.0 | 0.0 ± 0.0 | | 0.0 ± 0.1 | 0.0 ± 0.1 | 0.1 ± 0.0 | 0.2 ± 0.3 | 0.2 ± 0.1 |
| AP Width 1ˢᵗ AP at 200 pA (ms) | Control | 2.0 ± 0.1 | 2.1 ± 0.1 | 2.4 ± 0.1 | 2.1 ± 0.1 | 1.9 ± 0.1 | 1.9 ± 0.2 | 2.1 ± 0.2 | 2.0 ± 0.2 | 2.6 ± 0.3 | 2.2 ± 0.3 |
| | Δ5HT | 0.1 ± 0.0 | 0.2 ± 0.1 | -0.1 ± 0.1 | 0.0 ± 0.1 | 0.4 ± 0.1 | 0.8 ± 0.7 | 0.0 ± 0.0 | 0.0 ± 0.0 | | 0.0 ± 0.1 |
| | ΔDEA | 0.4 ± 0.2 | 0.1 ± 0.0 | 0.4 ± 0.2 | 0.1 ± 0.1 | 0.1 ± 0.0 | | 0.5 ± 0.3 | 0.1 ± 0.1 | 0.4 ± 0.1 | 0.0 ± 0.0 |
| | Δ5HT/DEA | 0.3 ± 0.1 | 0.2 ± 0.1 | 0.1 ± 0.1 | 0.0 ± 0.0 | | 0.0 ± 0.1 | 0.0 ± 0.0 | 0.1 ± 0.0 | 0.2 ± 0.1 | 0.0 ± 0.0 |
| AP Height Last AP at 200 pA (x10 mV) | Control | 4.8 ± 0.2 | 3.5 ± 0.3 | 5.0 ± 0.2 | 1.6 ± 0.2 | 2.7 ± 0.4 | 4.1 ± 0.4 | 5.6 ± 0.3 | 5.8 ± 0.3 | 3.0 ± 0.4 | |
| | Δ5HT | -1.2 ± 0.3 | -0.8 ± 0.3 | -0.4 ± 0.1 | 0.0 ± 0.2 | -0.3 ± 0.3 | -0.9 ± 0.8 | -0.4 ± 0.2 | -1.2 ± 0.0 | | |
| | ΔDEA | -0.5 ± 0.1 | -0.2 ± 0.2 | -0.7 ± 0.3 | 0.4 ± 0.2 | 0.1 ± 0.4 | | -0.2 ± 0.5 | 0.0 ± 0.4 | 1.2 ± 0.8 | |
| | Δ5HT/DEA | -1.1 ± 0.3 | -1.1 ± 0.4 | -0.6 ± 0.3 | 0.2 ± 0.2 | | -0.4 ± 0.2 | -0.3 ± 0.1 | 0.0 ± 0.0 | 0.6 ± 0.0 | |
| AP Trough Last AP at 200 pA (x10 mV) | Control | -0.9 ± 0.1 | -1.1 ± 0.1 | -0.9 ± 0.1 | -0.9 ± 0.1 | -0.7 ± 0.1 | -1.1 ± 0.2 | -1.0 ± 0.1 | -0.9 ± 0.1 | 0.1 ± 0.2 | |
| | Δ5HT | 0.1 ± 0.1 | 0.2 ± 0.1 | -0.1 ± 0.2 | 0.1 ± 0.0 | 0.0 ± 0.0 | 0.1 ± 0.5 | 0.0 ± 0.0 | 0.0 ± 0.0 | | |
| | ΔDEA | 0.0 ± 0.1 | 0.0 ± 0.0 | 0.2 ± 0.1 | 0.2 ± 0.1 | 0.0 ± 0.1 | | 0.3 ± 0.2 | -0.1 ± 0.1 | 0.3 ± 0.2 | |
| | Δ5HT/DEA | -0.1 ± 0.1 | 0.2 ± 0.1 | -0.1 ± 0.1 | 0.1 ± 0.0 | | -0.1 ± 0.0 | 0.1 ± 0.1 | 0.2 ± 0.0 | 0.2 ± 0.1 | |
| AP Width Last AP at 200 pA (ms) | Control | 3.7 ± 0.2 | 5.3 ± 0.6 | 4.0 ± 0.3 | 6.3 ± 0.7 | 5.2 ± 0.6 | 3.8 ± 0.5 | 3.0 ± 0.4 | 2.8 ± 0.4 | 6.4 ± 0.8 | |
| | Δ5HT | 0.9 ± 0.3 | 0.8 ± 0.3 | 0.3 ± 0.3 | -0.9 ± 0.5 | 0.2 ± 0.3 | 0.5 ± 0.0 | 0.1 ± 0.0 | 0.3 ± 0.0 | | |
| | ΔDEA | 0.5 ± 0.2 | -0.4 ± 0.4 | 0.5 ± 0.3 | -0.7 ± 0.6 | 0.0 ± 0.3 | | 0.5 ± 0.3 | -0.1 ± 0.2 | -0.7 ± 0.7 | |
| | Δ5HT/DEA | 0.7 ± 0.3 | 0.9 ± 0.3 | 0.3 ± 0.2 | -0.6 ± 0.3 | | 0.1 ± 0.1 | 0.2 ± 0.0 | 0.2 ± 0.0 | -0.3 ± 0.1 | |

Legend: >100%   >50%   >10%   ≤10% and ≥-10%   <-10%   <-50%   <-100%

Table 4-2: Summary of average values for cellular parameters describing AP shape. The table shows the average ± SEM for control values (dark grey rows), followed by the average difference between treatment and control for seven parameters in the ten cell types. Cell types shown with grey background (cell types 1, 2, 7, 8, 9 and 10) are groups with n numbers <6 for individual treatments. The colour coded column to the right of each group represents the percentage of increase or decrease of the values when compared to control.

significantly increased in cell types 3, 5 and 6 by DEA (MLM: $p<0.0001$). In general, almost all of the changes induced by DEA appear to contribute to a reduction in overall neuronal activity in these four cell types.

There are fourteen cases in which the effect of 5HT was significantly different from the effect of DEA, shown in the fourth row in Figure 4-3. In eleven of these fourteen cases, this difference between 5HT and DEA can be account for by either 5HT or DEA having a significant effect, while the other one has no apparent effect. Within these, three parameters are significantly affected by 5HT, but not DEA when compared to control, while eight other parameters are significantly affected by DEA, but not 5HT when compared to control. However, two other parameters are significantly affected by both 5HT and DEA alone, but the effects of 5HT and DEA are also significantly different when compared to control. These are the height of first AP at threshold and last AP at 200 pA in cell type 3 (MLM: $p<0.01$). Furthermore, one parameter, height of first AP at threshold for cell type 6, showed a significant difference between the values in the presence of 5HT and DEA, but neither 5HT nor DEA significantly affected this value compared to control (MLM: $p<0.05$).

Furthermore, the effects observed in the various parameters while in the presence of 5HT/DEA do not necessarily follow the same behaviour when in the presence of either 5HT or DEA alone. For example, there are fourteen parameters across the four cell types 3 to 6 that are significantly affected by either 5HT or DEA alone compared to control (MLM: $p<0.05$). However, these parameters are not significantly changed by 5HT/DEA co-application compared to control levels (MLM: $p>0.05$). Conversely, there are twelve parameters that are only significantly changed in the presence of 5HT/DEA but not in the presence of 5HT or DEA alone (MLM: $p<0.05$). Of these parameters, only the number of APs at 120 pA for cell type 5 shows a statistically significant $p$ value when comparing the effects of 5HT/DEA to either 5HT or DEA alone (MLM: $p<0.05$). Across the other eleven parameters, four parameters (spike height adaptation for cell type 5, the proportion of minimum over maximum ISI at 200 pA and $I_h$ for cell type 6 and the trough of first AP at threshold for cell type 4) presented $p$ values significant in the presence of 5HT/DEA compared to control, but the effects of 5HT/DEA were not significantly different to either 5HT or DEA alone. For the remaining seven parameters
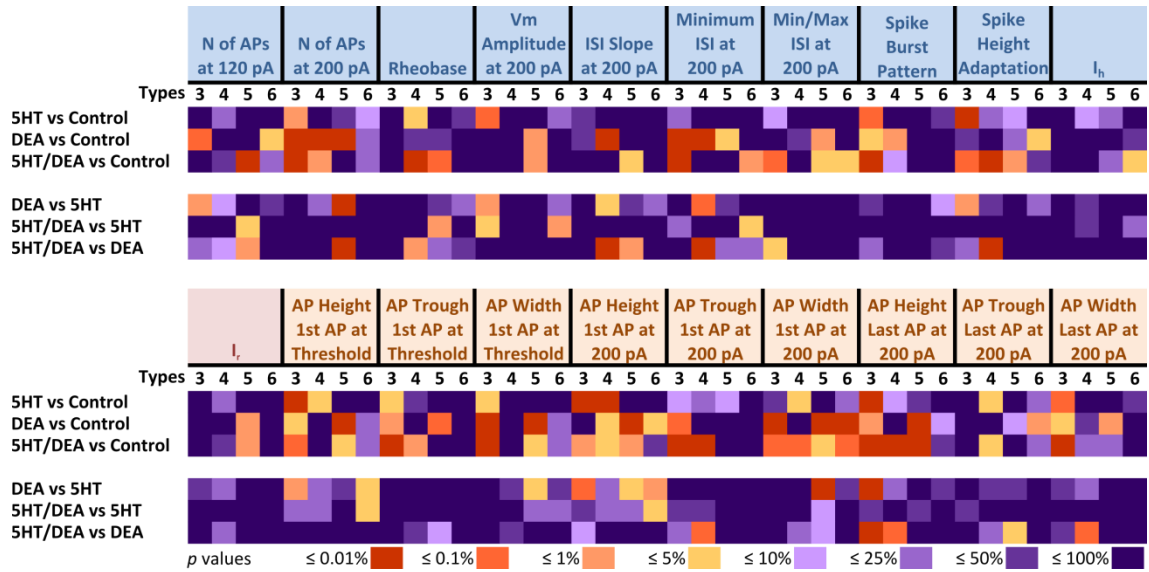
Figure 4-3: Heat map of *p* values obtained from MLM. The four types of cells are in sub columns for each parameter. Each row represents a specific pairwise comparison between two conditions as indicated on the left of the figure. Darker orange colours indicate significant differences amongst treatments, darker purple colours show less significance.

that were only significantly affected by co-application of 5HT/DEA compared to control, the effect of 5HT/DEA was at least significantly different to either 5HT or DEA application alone.

Overall, this analysis provides some indication of an interaction between 5HT and DEA in the modulation of individual cellular parameters. The potential pathways for interaction between 5HT and DEA will be analysed in more detail in section 4.4.

## 4.3 Nitric oxide modulates the response through two different pathways

As described above, NO has quite wide-ranging effects on the electrophysiological parameters analysed. As previously described in Chapter 1, NO can modulate the cellular physiology via different signalling pathways. When DEA is applied it is possible that NO is modulating parameters either through soluble guanylyl cyclase/cyclic guanosine monophosphate (sGC/cGMP) mediated signalling or through S-nitrosylation. In order to have a better understanding of how NO modulates these parameters and at which stage 5HT and NO could interact, ODQ, a highly selective, competitive and irreversible heme-site inhibitor of sGC, was used in some experiments.

In the same way as the tables described above (Table 4-1 and 4-2), Table 4-3 and 4-4 show the average control values (in darker grey) and differences elicited by DEA treatment compared to control, with or without ODQ, for cell types 3 to 6, as well as 5HT/DEA in the presence of ODQ.

The parameter values in the presence of (ODQ)DEA were changed in a similar manner to DEA alone in the majority of the parameters and cell types. However, simply inspecting the direction (sign) of the change showed apparent reversal in five parameters (rheobase, ISI slope at 200 pA, spike burst pattern, $I_r$ for type 6 cells and width of last AP at 200 pA for type 4 cells). The DEA-induced change in these parameters inverted in the presence of (ODQ)DEA, either from negative in the presence of DEA to positive with ODQ, or vice-versa. The direction of change caused by DEA was not changed for the remaining parameters in the presence of (ODQ)DEA, with

| | Treatment | Type 3 | Type 4 | Type 5 | Type 6 |
|---|---|---|---|---|---|
| N of APs at 120 pA | Control | 6.8 ± 0.3 | 6.1 ± 0.4 | 1.6 ± 0.3 | 6.8 ± 0.6 |
| | ΔDEA | -1.3 ± 0.6 | -0.1 ± 0.3 | 0.2 ± 0.3 | -0.6 ± 0.4 |
| | Δ(ODQ)DEA | -1.0 ± 0.7 | -0.5 ± 0.3 | 0.8 ± 0.4 | -1.5 ± 0.9 |
| | Δ(ODQ)5HT/DEA | -0.3 ± 0.8 | -0.7 ± 0.5 | 1.6 ± 0.7 | -1.6 ± 0.6 |
| N of APs at 200 pA | Control | 11.2 ± 0.3 | 7.5 ± 0.3 | 7.7 ± 0.4 | 4.5 ± 0.4 |
| | ΔDEA | -2.6 ± 0.6 | -1.6 ± 0.5 | -2.1 ± 0.7 | -0.3 ± 0.4 |
| | Δ(ODQ)DEA | -1.0 ± 0.6 | -2.6 ± 0.5 | -0.4 ± 0.2 | -0.9 ± 0.3 |
| | Δ(ODQ)5HT/DEA | -1.3 ± 1.2 | -3.4 ± 0.7 | -0.3 ± 0.4 | -1.0 ± 0.3 |
| Rheobase (x10 pA) | Control | 8.2 ± 0.3 | 6.6 ± 0.5 | 12.5 ± 0.4 | 6.2 ± 0.3 |
| | ΔDEA | 0.3 ± 0.6 | -0.5 ± 0.2 | -0.4 ± 0.5 | -0.1 ± 0.3 |
| | Δ(ODQ)DEA | 1.3 ± 0.9 | -0.1 ± 0.4 | -1.0 ± 0.7 | 1.0 ± 0.6 |
| | Δ(ODQ)5HT/DEA | 0.4 ± 1.3 | -0.9 ± 0.4 | -3.0 ± 1.3 | 0.6 ± 0.6 |
| Vm Amplitude at 200 pA (x10 mV) | Control | 3.4 ± 0.1 | 3.3 ± 0.1 | 3.6 ± 0.2 | 4.5 ± 0.2 |
| | ΔDEA | 0.1 ± 0.1 | 0.0 ± 0.1 | 0.2 ± 0.1 | -0.1 ± 0.1 |
| | Δ(ODQ)DEA | 0.2 ± 0.2 | 0.4 ± 0.1 | 0.0 ± 0.1 | 0.0 ± 0.1 |
| | Δ(ODQ)5HT/DEA | 0.3 ± 0.2 | 0.3 ± 0.1 | 0.2 ± 0.1 | 0.0 ± 0.1 |
| ISI Slope at 200 pA (x10$^{-3}$) | Control | 4.5 ± 0.5 | 10.6 ± 1.3 | 11.5 ± 1.4 | 11.0 ± 1.1 |
| | ΔDEA | 2.9 ± 1.1 | 13.8 ± 4.3 | 2.9 ± 3.2 | 2.4 ± 5.6 |
| | Δ(ODQ)DEA | 0.4 ± 1.4 | 17.3 ± 3.7 | 2.2 ± 3.5 | -3.0 ± 2.2 |
| | Δ(ODQ)5HT/DEA | -0.4 ± 1.6 | 0.4 ± 2.9 | 0.2 ± 4.6 | 0.6 ± 2.9 |
| Minimum ISI at 200 pA (x10 ms) | Control | 2.4 ± 0.1 | 2.5 ± 0.1 | 3.6 ± 0.2 | 2.1 ± 0.1 |
| | ΔDEA | 0.5 ± 0.1 | 4.4 ± 1.3 | 1.7 ± 1.5 | 0.0 ± 0.1 |
| | Δ(ODQ)DEA | 0.6 ± 0.2 | 6.6 ± 2.0 | 1.0 ± 0.9 | 0.1 ± 0.2 |
| | Δ(ODQ)5HT/DEA | 0.8 ± 0.4 | 0.4 ± 0.2 | 0.6 ± 0.5 | 0.3 ± 0.2 |
| Min/Max ISI at 200 pA (x10$^{-1}$) | Control | 3.9 ± 0.2 | 3.4 ± 0.2 | 4.1 ± 0.3 | 5.4 ± 0.3 |
| | ΔDEA | 0.3 ± 0.3 | 0.7 ± 0.2 | 0.7 ± 0.7 | 0.6 ± 0.8 |
| | Δ(ODQ)DEA | 0.5 ± 0.3 | 1.5 ± 0.6 | 0.3 ± 0.3 | 0.8 ± 0.4 |
| | Δ(ODQ)5HT/DEA | 1.1 ± 0.6 | 2.8 ± 0.8 | 0.7 ± 0.4 | 1.0 ± 0.4 |
| Spike Burst Pattern (x10 %) | Control | 8.8 ± 0.1 | 6.2 ± 0.3 | 8.0 ± 0.2 | 2.3 ± 0.3 |
| | ΔDEA | -1.2 ± 0.4 | -1.4 ± 0.5 | -1.7 ± 0.8 | 0.3 ± 0.6 |
| | Δ(ODQ)DEA | -0.2 ± 0.2 | -2.0 ± 0.7 | -0.5 ± 0.4 | -0.6 ± 0.2 |
| | Δ(ODQ)5HT/DEA | -0.7 ± 0.6 | -3.1 ± 1.0 | -0.5 ± 0.3 | -0.5 ± 0.3 |
| Spike Height Adaptation (x10 %) | Control | 7.8 ± 0.2 | 4.6 ± 0.4 | 8.1 ± 0.3 | 2.4 ± 0.2 |
| | ΔDEA | -0.8 ± 0.3 | -0.1 ± 0.2 | -0.6 ± 0.4 | 0.9 ± 0.4 |
| | Δ(ODQ)DEA | -0.1 ± 0.2 | -1.0 ± 0.4 | -1.1 ± 0.5 | 1.4 ± 0.6 |
| | Δ(ODQ)5HT/DEA | -1.7 ± 0.7 | -1.6 ± 0.6 | -2.0 ± 0.4 | 1.2 ± 0.3 |
| I$_h$ (x10 %) | Control | 9.7 ± 0.1 | 9.6 ± 0.1 | 9.6 ± 0.1 | 9.2 ± 0.2 |
| | ΔDEA | 0.0 ± 0.1 | 0.0 ± 0.0 | 0.0 ± 0.1 | -0.2 ± 0.1 |
| | Δ(ODQ)DEA | 0.1 ± 0.1 | 0.0 ± 0.1 | -0.1 ± 0.1 | -0.2 ± 0.2 |
| | Δ(ODQ)5HT/DEA | 0.0 ± 0.1 | 0.0 ± 0.0 | -0.1 ± 0.1 | -0.1 ± 0.1 |

>500% ■   >100% ■   >50% ■   >10% ■   ≤10% and ≥-10% ■   <-10% ■   <-50% ■   <-100% ■   <-500% ■

Table 4-3: Summary of average values for cellular parameters describing activity pattern. The table shows the average ± SEM for control values (dark grey rows) and difference between treatment and control, with or without ODQ. The column to the right of each group represents the percentage of increase or decrease in the values when compared to control.

| | Treatment | Type 3 | Type 4 | Type 5 | Type 6 |
|---|---|---|---|---|---|
| $I_r$ (x10² MΩ) | Control | 2.6 ± 0.1 | 3.1 ± 0.2 | 1.9 ± 0.1 | 4.1 ± 0.3 |
| | ΔDEA | -0.1 ± 0.1 | 0.0 ± 0.2 | 0.3 ± 0.1 | 0.3 ± 0.1 |
| | Δ(ODQ)DEA | -0.3 ± 0.1 | -0.1 ± 0.2 | 0.0 ± 0.1 | -0.2 ± 0.3 |
| | Δ(ODQ)5HT/DEA | -0.1 ± 0.2 | 0.2 ± 0.2 | 0.5 ± 0.3 | -0.3 ± 0.3 |
| AP Height 1st AP at Threshold (x10 mV) | Control | 6.5 ± 0.2 | 7.1 ± 0.2 | 6.4 ± 0.3 | 6.3 ± 0.3 |
| | ΔDEA | -0.2 ± 0.1 | -0.1 ± 0.1 | -0.4 ± 0.1 | -0.1 ± 0.1 |
| | Δ(ODQ)DEA | -0.4 ± 0.2 | 0.0 ± 0.1 | 0.0 ± 0.1 | -0.1 ± 0.1 |
| | Δ(ODQ)5HT/DEA | -0.5 ± 0.2 | 0.2 ± 0.1 | 0.0 ± 0.1 | 0.0 ± 0.2 |
| AP Trough 1st AP at Threshold (x10 mV) | Control | -1.0 ± 0.1 | -1.1 ± 0.1 | -0.9 ± 0.1 | -1.1 ± 0.1 |
| | ΔDEA | 0.1 ± 0.1 | 0.1 ± 0.0 | 0.2 ± 0.1 | 0.0 ± 0.0 |
| | Δ(ODQ)DEA | 0.1 ± 0.0 | 0.1 ± 0.1 | 0.0 ± 0.1 | 0.1 ± 0.1 |
| | Δ(ODQ)5HT/DEA | 0.2 ± 0.1 | 0.3 ± 0.1 | 0.0 ± 0.0 | 0.1 ± 0.1 |
| AP Width 1st AP at Threshold (ms) | Control | 2.2 ± 0.1 | 2.3 ± 0.1 | 2.6 ± 0.1 | 2.3 ± 0.1 |
| | ΔDEA | 0.2 ± 0.1 | 0.0 ± 0.0 | 0.4 ± 0.1 | 0.0 ± 0.1 |
| | Δ(ODQ)DEA | 0.2 ± 0.1 | 0.0 ± 0.0 | 0.0 ± 0.1 | 0.0 ± 0.0 |
| | Δ(ODQ)5HT/DEA | 0.3 ± 0.1 | 0.0 ± 0.1 | 0.1 ± 0.1 | 0.0 ± 0.0 |
| AP Height 1st AP at 200 pA (x10 mV) | Control | 6.3 ± 0.2 | 7.1 ± 0.1 | 6.4 ± 0.3 | 6.3 ± 0.3 |
| | ΔDEA | -0.1 ± 0.1 | -0.2 ± 0.1 | -0.3 ± 0.1 | -0.1 ± 0.1 |
| | Δ(ODQ)DEA | -0.3 ± 0.2 | -0.1 ± 0.1 | 0.0 ± 0.1 | -0.2 ± 0.1 |
| | Δ(ODQ)5HT/DEA | -0.4 ± 0.3 | 0.1 ± 0.1 | -0.1 ± 0.1 | -0.1 ± 0.1 |
| AP Trough 1st AP at 200 pA (x10 mV) | Control | -0.3 ± 0.1 | -0.4 ± 0.1 | -0.3 ± 0.1 | -0.3 ± 0.1 |
| | ΔDEA | 0.1 ± 0.0 | 0.1 ± 0.0 | 0.0 ± 0.0 | 0.0 ± 0.1 |
| | Δ(ODQ)DEA | 0.1 ± 0.0 | 0.1 ± 0.0 | 0.0 ± 0.1 | 0.1 ± 0.1 |
| | Δ(ODQ)5HT/DEA | 0.2 ± 0.1 | 0.3 ± 0.1 | 0.1 ± 0.1 | 0.1 ± 0.1 |
| AP Width 1st AP at 200 pA (ms) | Control | 2.0 ± 0.1 | 2.1 ± 0.1 | 2.4 ± 0.1 | 2.1 ± 0.1 |
| | ΔDEA | 0.4 ± 0.2 | 0.1 ± 0.0 | 0.4 ± 0.2 | 0.1 ± 0.1 |
| | Δ(ODQ)DEA | 0.2 ± 0.1 | 0.0 ± 0.1 | 0.0 ± 0.0 | 0.0 ± 0.1 |
| | Δ(ODQ)5HT/DEA | 0.4 ± 0.1 | 0.2 ± 0.1 | 0.1 ± 0.1 | 0.1 ± 0.1 |
| AP Height Last AP at 200 pA (x10 mV) | Control | 4.8 ± 0.2 | 3.5 ± 0.3 | 5.0 ± 0.2 | 1.6 ± 0.2 |
| | ΔDEA | -0.5 ± 0.1 | -0.2 ± 0.2 | -0.7 ± 0.3 | 0.4 ± 0.2 |
| | Δ(ODQ)DEA | -0.3 ± 0.2 | -0.7 ± 0.3 | -0.8 ± 0.3 | 0.9 ± 0.4 |
| | Δ(ODQ)5HT/DEA | -1.4 ± 0.4 | -1.1 ± 0.5 | -1.6 ± 0.2 | 0.8 ± 0.2 |
| AP Trough Last AP at 200 pA (x10 mV) | Control | -0.9 ± 0.1 | -1.1 ± 0.1 | -0.9 ± 0.1 | -0.9 ± 0.1 |
| | ΔDEA | 0.0 ± 0.1 | 0.0 ± 0.0 | 0.2 ± 0.1 | 0.2 ± 0.1 |
| | Δ(ODQ)DEA | 0.0 ± 0.1 | 0.1 ± 0.0 | 0.0 ± 0.1 | 0.2 ± 0.2 |
| | Δ(ODQ)5HT/DEA | 0.2 ± 0.1 | 0.2 ± 0.1 | -0.1 ± 0.1 | 0.3 ± 0.2 |
| AP Width Last AP at 200 pA (ms) | Control | 3.7 ± 0.2 | 5.3 ± 0.6 | 4.0 ± 0.3 | 6.3 ± 0.7 |
| | ΔDEA | 0.5 ± 0.2 | -0.4 ± 0.4 | 0.5 ± 0.3 | -0.7 ± 0.6 |
| | Δ(ODQ)DEA | 0.1 ± 0.2 | 0.4 ± 0.4 | 0.8 ± 0.4 | -0.5 ± 0.7 |
| | Δ(ODQ)5HT/DEA | 1.5 ± 0.7 | 1.0 ± 0.4 | 1.0 ± 0.4 | -0.1 ± 0.5 |

>500%    >100%    >50%    >10%    ≤10% and ≥-10%    <-10%    <-50%    <-100%    <-500%

Table 4-4: Summary of average values for cellular parameters describing AP shape. The table shows the average ± SEM for control values (dark grey rows) and difference between treatment and control, with or without ODQ. The column to the right of each group represents the percentage of increase or decrease in the values when compared to control.

sixteen of them showing a positive change in the parameter value, whereas the value of nineteen parameters were decreased in the presence of DEA or (ODQ)DEA.

In order to further analyse whether the changes in the response caused by ODQ to the effects of DEA were significant, a MLM statistical test was carried out on the values for the various parameters obtained in the (ODQ)DEA and (ODQ)5HT/DEA experiments, comparing them to control and between the different treatments. The result is a heat-map of the *p* values obtained that enables easy visualisation of the statistical significance of changes in each cell type for each parameter (Figure 4-4). With the exception of six parameters, the presence of ODQ alone did not significantly alter the values obtained for the majority of the parameters in the various cell types.

Twenty-three parameters were significantly changed compared to control by DEA in the presence of ODQ. As mentioned above, in a small number of these cases (five of these parameters), ODQ alone has significant effects suggesting non-specific effects of ODQ. However, in the majority of these cases, ODQ alone had no effect implying that DEA can alter cellular parameters in cortical neurons via sGC/cGMP-independent pathways.

Conversely, seven parameters showed no significant difference between (ODQ)DEA and control, but effects on these parameters were significantly different for (ODQ)DEA versus DEA alone (MLM: $p<0.05$). The values of parameters were also significantly affected by the application of DEA alone. This strongly suggests that at least some effects on cellular parameters are mediated by sGC/cGMP-dependent pathways. Thus, the two situations would imply that NO signalling in cortical neurons could be through at least two pathways, the sGC/cGMP pathway, and a cGMP-independent pathway, most probably S-nitrosylation. Furthermore, some of the patterns of effects of DEA on specific parameters in the absence and presence of ODQ suggest that both NO signalling pathways can be active in the same cell and interact, even oppose each other.

Not surprisingly, this also appears to be the case for the interaction between 5HT and NO. It was observed that in thirty-three situations, parameter values in the presence of (ODQ)5HT/DEA were statistically significant from control values. Importantly, in seven
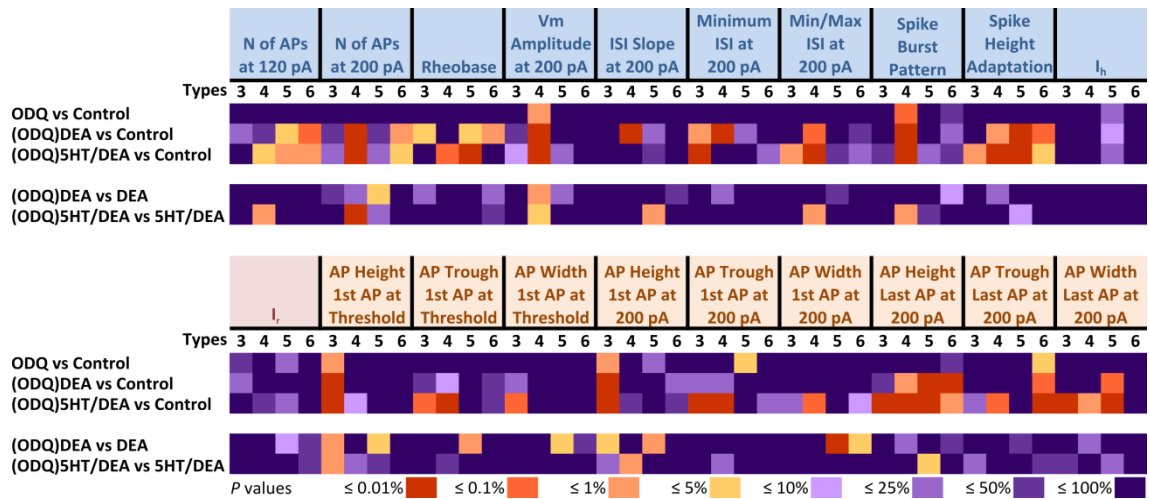
Figure 4-4: Heat map of *p* values obtained from MLM, from experiments in the presence of ODQ. The four types of cells are in sub columns for each parameter. Each row represents a specific pairwise comparison between two conditions as indicated on the left of the figure. Darker orange colour means significant variance in intercepts amongst treatments, darker purple colour shows less significance.

of these thirty-three cases, (ODQ)5HT/DEA effects were significantly different from 5HT/DEA, further supporting the evidence that some of the effects of DEA are mediated via sGC/cGMP-dependent pathways, while others are sGC/cGMP independent.

## 4.4 Interactions between serotonin and nitric oxide pathways

Various analysed parameters changed their values significantly in the presence of either 5HT or DEA, and this change could be either in a positive or negative direction. Sometimes the observed effects in the presence of either drug would be opposite to the other. The effects observed during the co-application of 5HT/DEA, on the other hand, differed in some parameters from the change observed in either 5HT or DEA. There are many possible interactions between them that could explain these values. The simplest interaction could be due to 5HT and DEA acting completely independently, with the individual effects observed presenting a linear summation in the presence of 5HT/DEA. In this case each transmitter would act on electrophysiological properties without modulating the other's activity.

Alternatively, a more complex interaction is also possible, where there is cross-talk between the 5HT and NO signalling pathways, leading to a non-linear summation. In order to distinguish between these two scenarios, the individual effects of 5HT and DEA treatments were summed and compared to the effects of 5HT/DEA co-application, by using a Welch's refinement of Student's two-tailed $t$ test (W-S $t$ test), with Welch-Satterthwaite degrees of freedom.

From the $p$ values obtained for this statistical analysis, it was possible to note (Figure 4-5) that there are only three parameters where the effect of the application of 5HT/DEA is significantly different from the summation of the observed values for 5HT and DEA. They are the ISI slope at 200 pA (W-S $t$ test: $p$ = 0.0427) and minimum ISI at 200 pA (W-S $t$ test: $p$ = 0.0035) for type 4 cells and minimum ISI at 200 pA (W-S $t$ test: $p$ = 0.0081) for type 6 cells. The parameters in type 4 cells present a non-linear interaction, as 5HT does not appear to have a significant effect on its own, but it

reduces the modulation caused by DEA when co-applied (Figure 4-5A). In contrast, in cell type 6, while neither 5HT nor DEA alone produces a significant effect, when co-applied the minimum ISI at 200 pA produces a significantly different value from control (Figure 4-5D). In cell type 4, NO seems to act via a sGC/cGMP-independent pathway, since in the presence of (ODQ)DEA, the parameters' values are qualitatively similar. In contrast, in cell type 6, 5HT/DEA co-application does not significantly change the value for the minimum ISI in the presence of ODQ suggesting that sGC/cGMP signalling is important for this effect.

In addition to these three cases, inspection of the data suggests further examples of non-linear interactions between 5HT and DEA, even though the statistical analysis does not reach significance levels (W-S $t$ test: $p > 0.05$). In fact, only six parameters in three cell types appear to show simple linear summation of the effects of 5HT and DEA when co-applied (Figure 4-5E). It is possible to group the remaining potential non-linear interactions into four patterns: those where 5HT reduces the effects observed in the presence of DEA without having a significant effect on its own (Figure 4-5A), those where DEA reduces the effects observed in the presence of 5HT without having a significant effect on its own (Figure 4-5B), those where 5HT and DEA produce similar changes in the parameters' values but co-application does not result in an additive effect (Figure 4-5C), and finally those that present a significant difference only when both 5HT and DEA are co-applied (Figure 4-5D).

Parameters that showed a reduction of the DEA effect in the presence of 5HT/DEA include the number of APs at 120 pA from type 3 cells, number of APs at 200 pA and spike burst pattern, together with ISI slope and minimum ISI at 200 pA from type 4 cells mentioned above, minimum ISI at 200 pA from type 5 cells and spike height adaptation from type 6 cells. Number of APs at 120 pA for type 3 cells and minimum ISI for type 5 cells seem to be modulated by NO through sGC/cGMP pathway. In type 4 cells, the number of APs at 200 pA and spike burst pattern appeared to be modulated by S-nitrosylation, whereas spike height adaptation in cell type 6 is partially modulated by sGC/cGMP pathway (Figure 4-5A).

The inverse effect, that DEA reduces whichever effect was observed in the presence of 5HT, is observed for the membrane potential amplitude at 200 pA and spike height adaptation of type 3 cells, and spike height adaptation for type 5 cells. Both parameters from type 3 cells are modulated through sGC/cGMP pathway, while spike height adaptation in cell type 6 might be also influenced by S-nitrosylation (Figure 4-5B).

Six other parameters presented a behaviour that could be explained by either drug, 5HT or DEA, modulating the parameters' values to their limits, therefore the co-application of 5HT/DEA will not further increase the change observed in these parameters. Type 3 cells presented this behaviour for spike burst pattern and the height, trough and width of the first AP at threshold through the sGC/cGMP pathway. Type 4 cells presented a similar behaviour for the proportion of minimum over maximum ISI at 200 pA and in the height of first AP at 200 pA. The former seems to be modulated partially through S-nitrosylation and partially through sGC/cGMP, whereas the latter effect is entirely through sGC/cGMP (Figure 4-5C).

Six parameters were only significantly affected, comparing to control levels, when 5HT and DEA were co-applied in type 4, 5 and 6 cells. Type 4 cells presented this change on spike height adaptation, whereas type 5 cells presented this on number of APs at 120 pA and rheobase. Spike height adaptation and number of APs at 120 pA seem to be modulated through both sGC/cGMP-dependent and independent pathways, whereas rheobase could be modulated only by sGC/cGMP-independent mechanism. Minimum ISI, proportion of minimum over maximum ISI at 200pA and $I_h$ from type 6 cells, through sGC/cGMP, had significantly different parameter values from control (Figure 4-5D).

Six other parameters, in cell types 3, 4 and 5, presented a linear summation of the effects observed with 5HT and DEA (Figure 4-5E).

**A — 5HT reduces NO effects**

| | | Percentage difference | | | p values | | | Potential NO signalling mechanisms | p values (W-S t test) |
|---|---|---|---|---|---|---|---|---|---|
| | | 5HT | DEA | 5HT/DEA | 5HT | DEA | 5HT/DEA | | |
| Type 3 | N of APs at 200 pA | | | | | | | cGMP | 0.1054 |
| Type 4 | N of APs at 200 pA | | | | | | | Nitrosylation | 0.3032 |
| Type 4 | ISI slope at 200 pA | | | | | | | cGMP | 0.0427 |
| Type 4 | Minimum ISI at 200 pA | | | | | | | | 0.0035 |
| Type 4 | Spike Burst Pattern | | | | | | | Nitrosylation | 0.2059 |
| Type 5 | Minimum ISI at 200 pA | | | | | | | cGMP | 0.4150 |
| Type 6 | Spike Height Adaptation | | | | | | | cGMP + Nitrosylation | 0.4689 |

**B — NO reduces 5HT effects**

| | | 5HT | DEA | 5HT/DEA | 5HT | DEA | 5HT/DEA | Potential NO signalling mechanisms | p values (W-S t test) |
|---|---|---|---|---|---|---|---|---|---|
| Type 3 | Vm Amplitude at 200 pA | | | | | | | cGMP | 0.1211 |
| Type 3 | Spike Height Adaptation | | | | | | | cGMP | 0.3374 |
| Type 5 | Spike Height Adaptation | | | | | | | cGMP + Nitrosylation | 0.1214 |

**C — 5HT and NO have similar, independent effects**

| | | 5HT | DEA | 5HT/DEA | 5HT | DEA | 5HT/DEA | Potential NO signalling mechanisms | p values (W-S t test) |
|---|---|---|---|---|---|---|---|---|---|
| Type 3 | Spike Burst Pattern | | | | | | | cGMP | 0.2212 |
| Type 3 | Height of 1st AP at Threshold | | | | | | | | 0.2363 |
| Type 3 | Trough of 1st AP at Threshold | | | | | | | | 0.3686 |
| Type 3 | Width of 1st AP at Threshold | | | | | | | | 0.2673 |
| Type 4 | Min/Max ISI at 200 pA | | | | | | | cGMP + Nitrosylation | 0.2275 |
| Type 4 | Height of 1st AP at 200 pA | | | | | | | cGMP | 0.0723 |

**D — 5HT and NO are required to interact to cause effect**

| | | 5HT | DEA | 5HT/DEA | 5HT | DEA | 5HT/DEA | Potential NO signalling mechanisms | p values (W-S t test) |
|---|---|---|---|---|---|---|---|---|---|
| Type 4 | Spike Height Adaptation | | | | | | | cGMP + Nitrosylation | 0.5230 |
| Type 5 | N of APs at 120 pA | | | | | | | cGMP + Nitrosylation | 0.4000 |
| Type 5 | Rheobase | | | | | | | Nitrosylation | 0.2317 |
| Type 6 | Minimum ISI at 200 pA | | | | | | | cGMP | 0.0081 |
| Type 6 | Min/Max ISI at 200 pA | | | | | | | | 0.4595 |
| Type 6 | $I_h$ | | | | | | | | 0.4951 |

**E — 5HT and NO effects have added effects when co-applied**

| | | 5HT | DEA | 5HT/DEA | 5HT | DEA | 5HT/DEA | Potential NO signalling mechanisms | p values (W-S t test) |
|---|---|---|---|---|---|---|---|---|---|
| Type 3 | N of APs at 120 pA | | | | | | | cGMP + Nitrosylation | 0.7197 |
| Type 3 | Minimum ISI at 200 pA | | | | | | | Nitrosylation | 0.9989 |
| Type 3 | Min/Max ISI at 200 pA | | | | | | | cGMP + Nitrosylation | 0.8584 |
| Type 4 | Rheobase | | | | | | | cGMP | 0.8949 |
| Type 4 | Height of last AP at 200 pA | | | | | | | Nitrosylation | 0.8048 |
| Type 5 | N of APs at 200 pA | | | | | | | cGMP | 0.8399 |

Legend:
- $\geq 100\%$ ; $\geq 20\%$ ; $\geq 10\%$
- $\leq -20\%$ ; $\leq -10\%$ ; $0 \pm 10\%$
- $\leq 1$ ; $\leq 0.5$ ; $\leq 0.1$
- $\leq 0.05$ ; $\leq 0.01$ ; $\leq 0.001$ ; $\leq 0.0001$

Figure 4-5: Summary and description of 5HT/DEA effects from the cell types and parameters that 5HT/DEA presents a different effect than the mere summation of 5HT and DEA. The percentage change and the *p* values are the same as previous tables. Potential NO signalling mechanisms presents the possible pathway that NO modulates that specific parameter, either through sGC/cGMP or S-nitrosylation. The last column is for the *p* values obtained from the Welch's refinement of Student's two-tailed *t* test.

## 4.5 Modulation of intrinsic excitability by serotonin and nitric oxide

The previous section demonstrated that 5HT and NO can influence the response of various specific physiological properties. However, a broader view would give insight of the actions of 5HT and NO in the various types of neurons. Neuronal function is controlled to a large extent by intrinsic excitability. 5HT and NO may affect the function of the neurons through their intrinsic excitability, so this was also analysed for the recorded cells. The difference between the averaged numbers of APs under control conditions and in the presence of 5HT, DEA or 5HT/DEA was plotted for all positive current steps. The $p$ values based on MLM were obtained for the differences between the number of APs from treatments and control for each current step, and each data point for the excitability plots was colour coded accordingly. The $p$ values for comparisons between individual treatments were also colour coded, to show significance variation between treatments (Figure 4-6).

It was observed that 5HT had only a weak effect on the overall excitability of the cell types 3, 4, 5 and 6. For types 3 and 4, in the presence of 5HT there was an increase of number of APs in response to current injections between 60 and 160 pA. The 5HT-induced increase in excitability compared to control was significant for current steps at 80 pA in cells type 3 and at 100 pA in cells type 4 (one-way $t$ test: $p<0.05$). Conversely, for type 6 cells, current steps between 120 pA and 180 pA produced a decreased number of APs in the presence of 5HT when compared to control levels, with the differences at 140 and 160 pA being significant (one-way $t$ test: $p<0.05$).

DEA, on the other hand, consistently decreased the excitability of the various cell types. Type 3 cells had this significantly different effect starting at 120 pA current steps, whereas for types 4 and 5 a significant reduction in excitability occurred at current pulses larger than 160 pA for type 4, and 180 pA for type 5 (one-way $t$ test: $p<0.05$). Interestingly, type 6 cells showed a similar decrease, but as with the 5HT effect it was only apparent for a relatively small current range (140-180 pA) and did not occur at 200 pA (one-way $t$ test: $p<0.05$ for 160 pA current step).
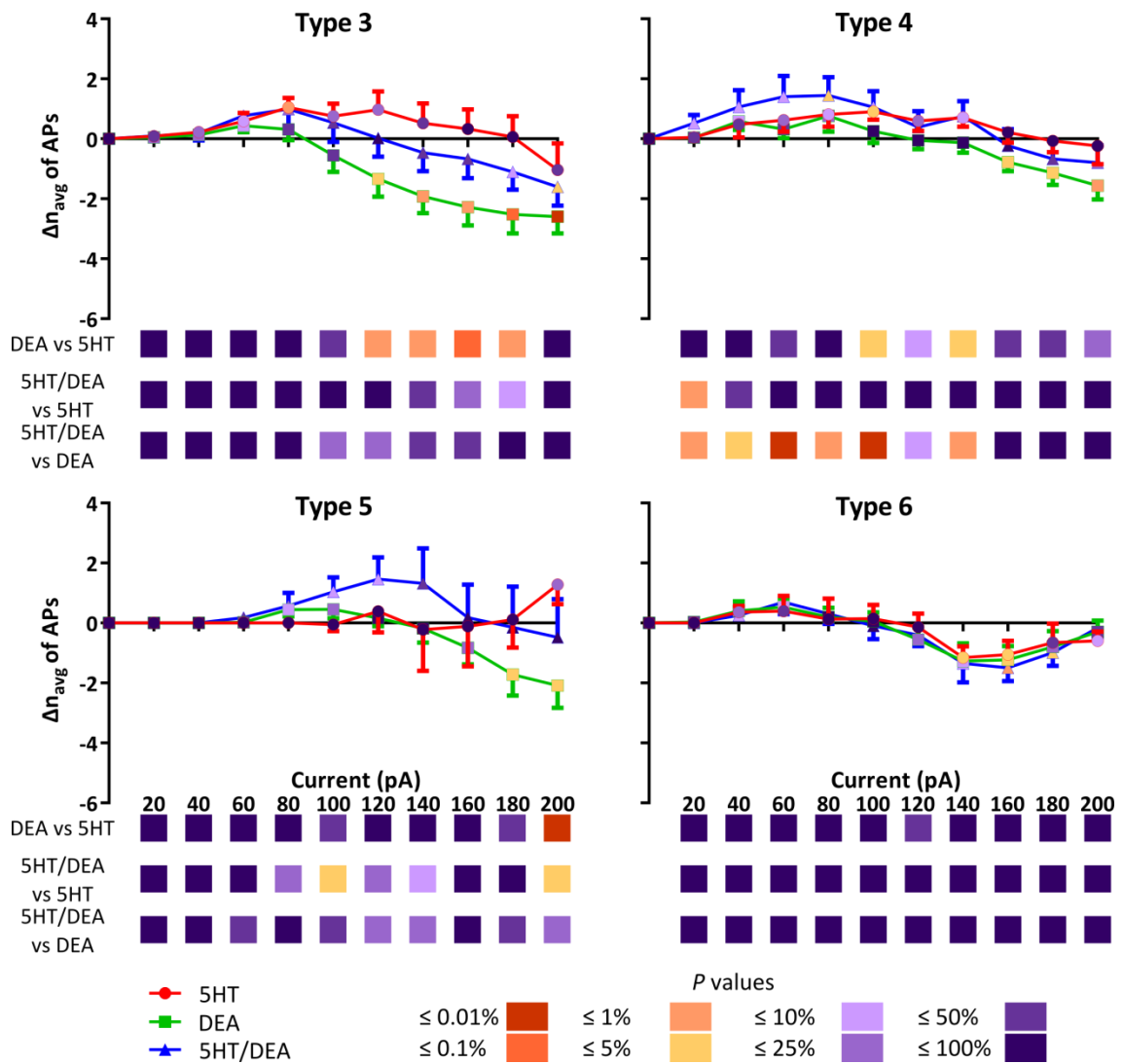
Figure 4-6: Plots of the change in excitability for cell types 3-6 recorded in current clamp mode. The plots show the difference of the average numbers of APs between treatments and control, to highlight changes in the presence of 5HT (red), DEA (green) or 5HT/DEA (blue). For each current step, data points were colour-coded according to the $p$ values obtained from one-way $t$ test to determine whether the value was significantly different from 0. Below each plot is a heat map of the $p$ values for pairwise comparison between individual treatments based on MLM.

There were 3 effect patterns for the combined application of 5HT and DEA. The change in excitability for type 6 cells in the presence of 5HT/DEA was similar to the changes observed with either 5HT or DEA alone, and was statistically significantly different from control at 140 and 160 pA current steps (one-way $t$ test: $p<0.05$). Cell types 3 and 4 changed their excitability in response to co-application of 5HT and DEA in a way that is consistent with a summation of the effects observed for the individual application of 5HT and DEA. Cell type 3 excitability did not significantly differ from the values observed in the presence of 5HT or DEA, and only at 200 pA was the number of APs in response to the current injected significantly different from 0 (one-way $t$ test: $p<0.05$). For cell type 4, the combined effect of 5HT and DEA was significantly different from the one observed for DEA alone at current steps up to 100 pA and at 140 pA and from 5HT at 20 pA (MLM: $p<0.05$). Interestingly, type 5 cells presented an apparent increase in excitability of the cells in the presence of 5HT/DEA between 80 and 140 pA current steps that did not appear to result from the summation of the effects of 5HT and DEA on their own. This variation was significantly different from just 5HT at only 100 pA and at 200 pA (MLM: $p<0.05$).

In order to test whether the effects of DEA are mediated via sGC/cGMP signalling, comparisons were made with treatments in the presence of ODQ. Plots that show changes in excitability and heat maps to visualise statistical comparisons are shown in Figure 4-7. Comparisons between (ODQ)DEA and DEA, and (ODQ)5HT/DEA and 5HT/DEA are shown in the heat maps for each cell type. Compared to control values, the excitability of the cells did not vary significantly when the cells were in the presence of just ODQ for any of the different types, demonstrating that ODQ on its own has no direct effects on cellular excitability. However, cell type 3 in the presence of (ODQ)DEA still shows a reduction in the number of APs elicited at early current steps (80 and 100 pA, one-way $t$ test for 100 pA: $p<0.05$). This reduction appears less pronounced for stronger current pulses compared to DEA on its own (Figure 4-6). In cell type 5, ODQ also reduces the DEA-induced reduction in AP numbers at current pulses larger than 160 pA. This suggests that aspects of the NO-induced reduction in excitability in these cell types are sGC/cGMP-dependent. By contrast, cell type 6 and to a lesser extent cell type 4 show a more striking DEA-induced reduction in AP numbers
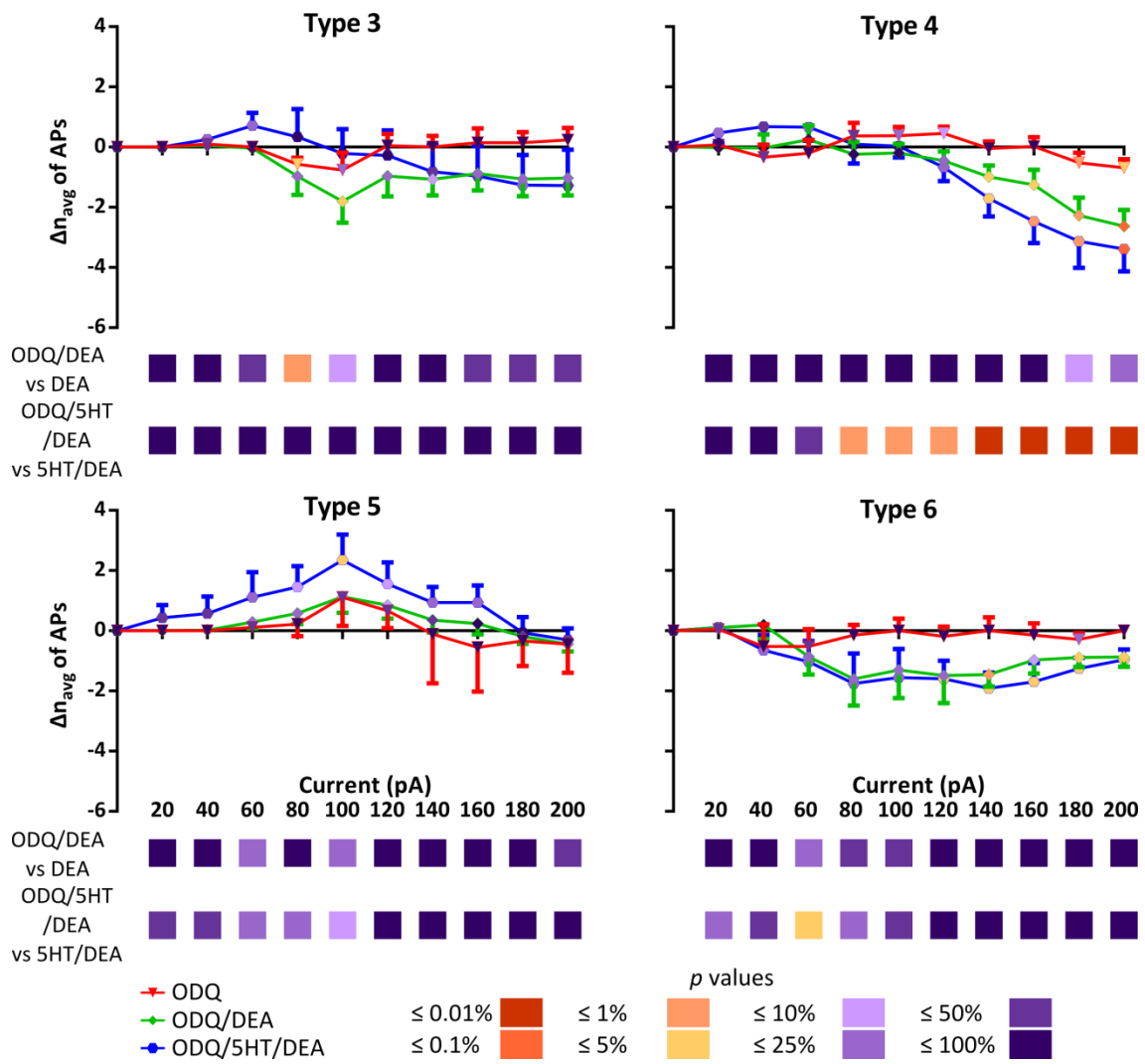
Figure 4-7: Plots of the change in excitability for cell types 3-6 recorded in current clamp mode in the presence of ODQ. The plots show the difference of the average numbers of APs between treatments and control, to highlight changes in the presence of ODQ (red), (ODQ)DEA (green) or (ODQ)5HT/DEA (blue). For each current step, data points were colour-coded according to the $p$ values obtained from one-way $t$ tests to test whether the value was significantly different from 0. Below each plot is a heat map of the $p$ values for pairwise comparison between individual treatments based on MLM.

in the presence of ODQ (Figure 4-7, for comparison see Figure 4-6), which would suggest that sGC/cGMP-dependent signalling in these cell types is responsible for an increase in excitability, while sGC/cGMP-independent mechanisms cause a reduction in excitability. Apart from the difference in the change in excitability in cell type 3 for DEA vs (ODQ)DEA at 80 pA, none of the other comparisons between DEA and (ODQ)DEA show significance.

In the presence of (ODQ)5HT/DEA, cell type 3 displayed a similar effect to 5HT/DEA, with a slight increase of excitability at lower current steps followed by a reduction at later steps. Type 4 showed a different excitability plot when comparing (ODQ)5HT/DEA to 5HT/DEA by having a significant reduction of the excitability, one that seems to be even more than (ODQ)DEA (one-way $t$ test: $p<0.05$ from 140 to 200 pA current step). This cell type also presented a significant difference in the Δ number of APs, in the presence of (ODQ)5HT/DEA, compared to 5HT/DEA for current steps higher than 80 pA (MLM: $p<0.01$). A possible explanation for this behaviour could be that since ODQ was blocking the sGC/cGMP-mediated increase in the excitability, sGC/cGMP-independent mechanisms would be acting to reduce the excitability. A similar behaviour was observed for the lower current steps (from 40 to 120 pA) in cells type 6.

In the case of type 5 cells, the sGC/cGMP-independent effect was to slightly increase the excitability of the cells, while the sGC/cGMP-dependent pathway resulted in a reduction in the excitability of these cells. This increase in excitability effect, in the presence of ODQ, is more pronounced when DEA is co-applied with 5HT, suggesting that there is a possible interaction between 5HT and sGC/cGMP-independent mechanisms.

## 4.6 Modulation of current-voltage relationship by serotonin and nitric oxide

The current-voltage (IV) relationship of the four cell types shows non-linear behaviour in response to negative current steps (Figure 4-8A; see also Figure 3-14) suggesting the presence of hyperpolarisation-activated inward currents. This non-linearity seems to be reduced in some of the treatments: cell types 4 and 6 present a reduction in 5HT,
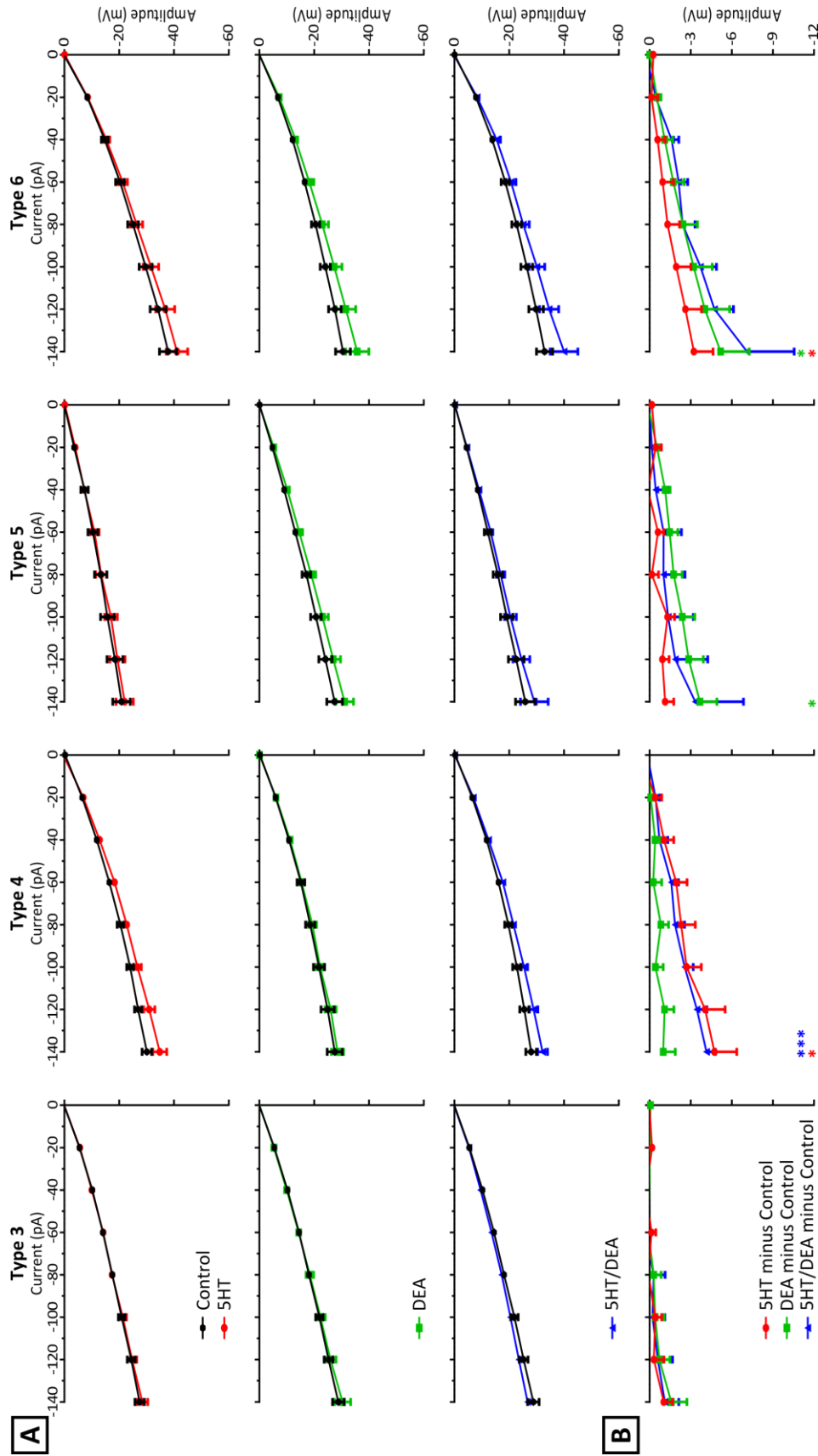
Figure 4-8: Effects of 5HT, DEA and 5HT/DEA on IV relationship for cell types 3-6. (A) The IV plots are shown for current steps from -140 to 0 pA under control conditions (black) and in the presence of 5HT (red), DEA (green) and 5HT/DEA (blue). (B) Plots of differences in amplitudes of voltage-responses during drug treatment minus control for each current step. One-sample t-tests were used to test whether differences at -140 pA were significantly different from 0 (* $p<0.05$, *** $p<0.001$).

types 5 and 6 in DEA, and types 4, 5, and 6 in 5HT/DEA (Figure 4-8A). One-sample $t$-tests revealed that the differences between treatments and control were significant for 5HT treatment in cell types 4 ($p$ = 0.0274) and 6 ($p$ = 0.0448), and DEA treatment in cell types 5 ($p$ = 0.0145) and 6 ($p$ = 0.0309) at -140 pA current step (Figure 4-8B).

Interestingly, the effect of 5HT/DEA application in all cell types appeared to be consistent with a linear summation of the effects of 5HT and DEA on their own. However, the effect of 5HT/DEA was only significant in type 4 cells ($p$ = 0.0002), while in cell types 5 and 6 a rather large variability in the response to 5HT/DEA application prevented the changes from reaching significance (cell type 5: $p$ = 0.3716; cell type 6: $p$ = 0.0661).

Previous experiments have shown that DEA affects the IV relationship for the injection of negative current pulses in cell types 5 and 6, whereas DEA increases the linearity of the IV plots. This effect appears to be mediated mainly through the sGC/cGMP pathway, as this change is not observed when DEA is applied in the presence of ODQ (Figure 4-9A). However, (ODQ)5HT/DEA application still appears to be able to increase the linearity of the IV plots in all cell types.  In cell types 4 and 6 this can be accounted for by the actions of 5HT on its own. On the other hand, in cell types 3 and 5, 5HT alone has rather weak effects and it is not immediately clear how the apparent effect of 5HT/DEA in the presence of ODQ is mediated (Figure 4-9B).

## 4.7 Role of 5HT$_3$ type receptor in cultured cortical neurons

In some cases, when 5HT was bath applied to cortical cells in cell culture, there was a rapid depolarisation, followed by recovery, of the resting membrane potential. The whole event lasted for several tens of seconds and had a median peak amplitude of 10 mV (Figure 4-10A). This type of 5HT response was observed in 19.5% of all the recorded cells that received 5HT (86 out of a total of 441 cells). If just the experiments included in the clustering are considered, 17.37% of the cells showed this depolarisation (Figure 4-10B). Furthermore, the percentage of cells showing this 5HT response remained almost unchanged when only cells defined as types 3 to 6 were
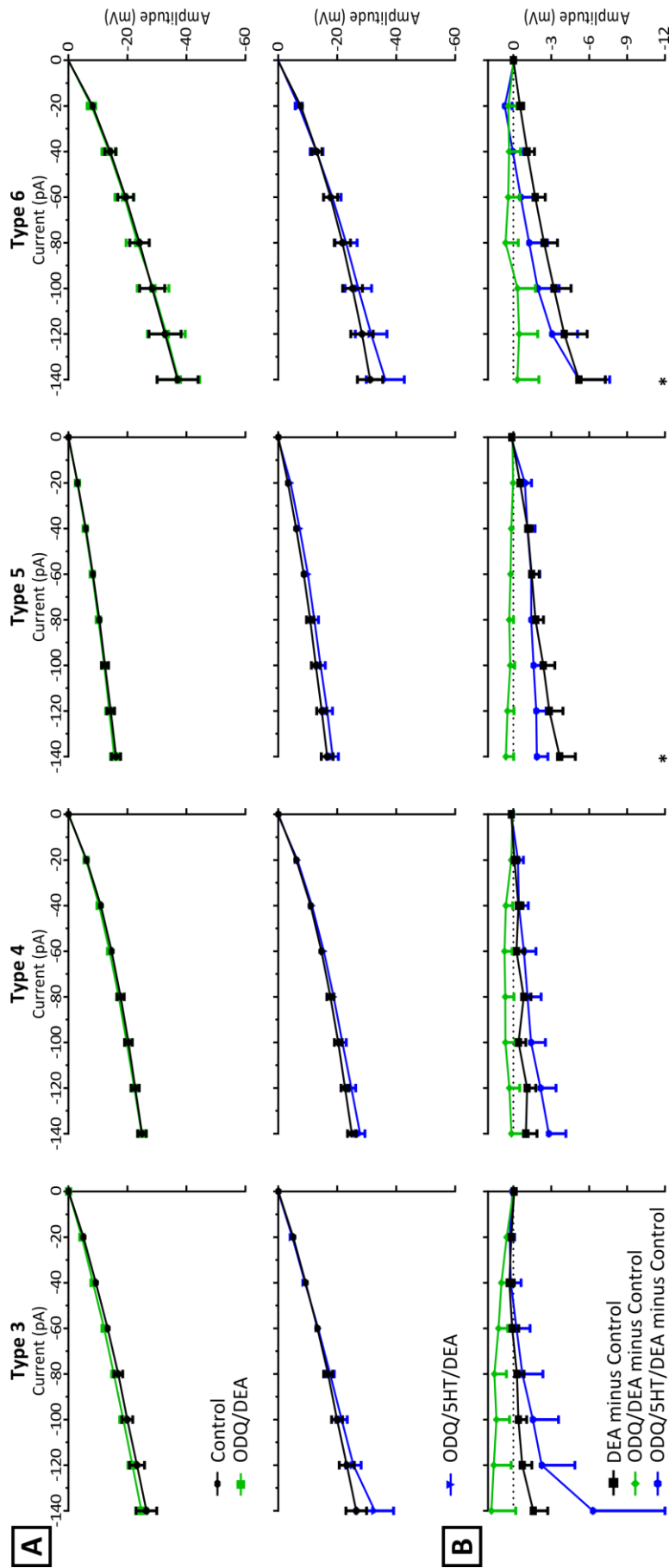
Figure 4-9: Effects of DEA, (ODQ)DEA and (ODQ)5HT/DEA on IV relationship for cell types 3-6. (A) The IV plots are shown for current steps from -140 to 0 pA in the presence of DEA (black), (ODQ)DEA (green) and (ODQ)5HT/DEA (blue). (B) Plots of differences in amplitudes of voltage-responses during drug treatment minus control for each current step. One-sample t-tests were used to test whether differences at -140 pA were significantly different from 0 (* $p<0.05$).

considered (18.87%). Looking at each of the four types of cells analysed, type 3 cells had the highest probability of showing this serotonergic response (40%), followed by type 4 (14.3%). Type 5 and 6 cells each showed an 8.3% chance of having this response (Figure 4-10C).

The amplitude of this response was not modulated when 5HT was co-applied with DEA (Dunn's multiple comparison test, DMC: $p > 0.05$, n=16), and it was also not affected by the $5HT_2$ receptor antagonist ketanserin (1 µM; DMC: $p > 0.05$, n=6).

However, when the cell culture was pre-treated with MDL 72222 (1 µM), a selective $5HT_3$ receptor antagonist, this response completely disappeared (DMC: $p = 0.0132$, n=3), suggesting that this rapid, desensitising depolarisation is mediated by $5HT_3$ receptors (Figure 4-10D).


## 4.8 Discussion

Axons of 5HT neurons are known to innervate almost every structure of the CNS. At the terminals of these neurons, 5HT can act postsynaptically through different signalling mechanisms. The richness of 5HT receptors can be seen in the neocortex, where 5HT receptors are densely localised. Out of all 5HT receptors, $5HT_{1A}$, $5HT_{2A}$ and $5HT_{2C}$ as well as $5HT_7$ are quite abundant in the cortex, especially the prefrontal cortex (Santana et al. 2004; Pompeiano et al. 1992; Clemett et al. 2000). However, the expression of the different receptors seems to be dependent on the development of the cortex (Béïque et al. 2004). $5HT_3$ receptors are present in various parts of the CNS too (Kilpatrick et al. 1987), especially on GABAergic neurons found in the neocortex. Amongst these, it appears particularly prevalent on interneurons that show cholecystokinin immunoreactivity; more than a third of these cells present $5HT_3$ receptors (Morales & Bloom 1997; Puig et al. 2004).

It has previously been reported that 5HT has a dual effect on the membrane potential of neurons from the prefrontal cortex, one phase being a depolarisation and the other a hyperpolarisation of the membrane potential. These two responses are mediated by $5HT_1$ and $5HT_2$ receptors (Araneda & Andrade 1991; Davies et al. 1987). However, in
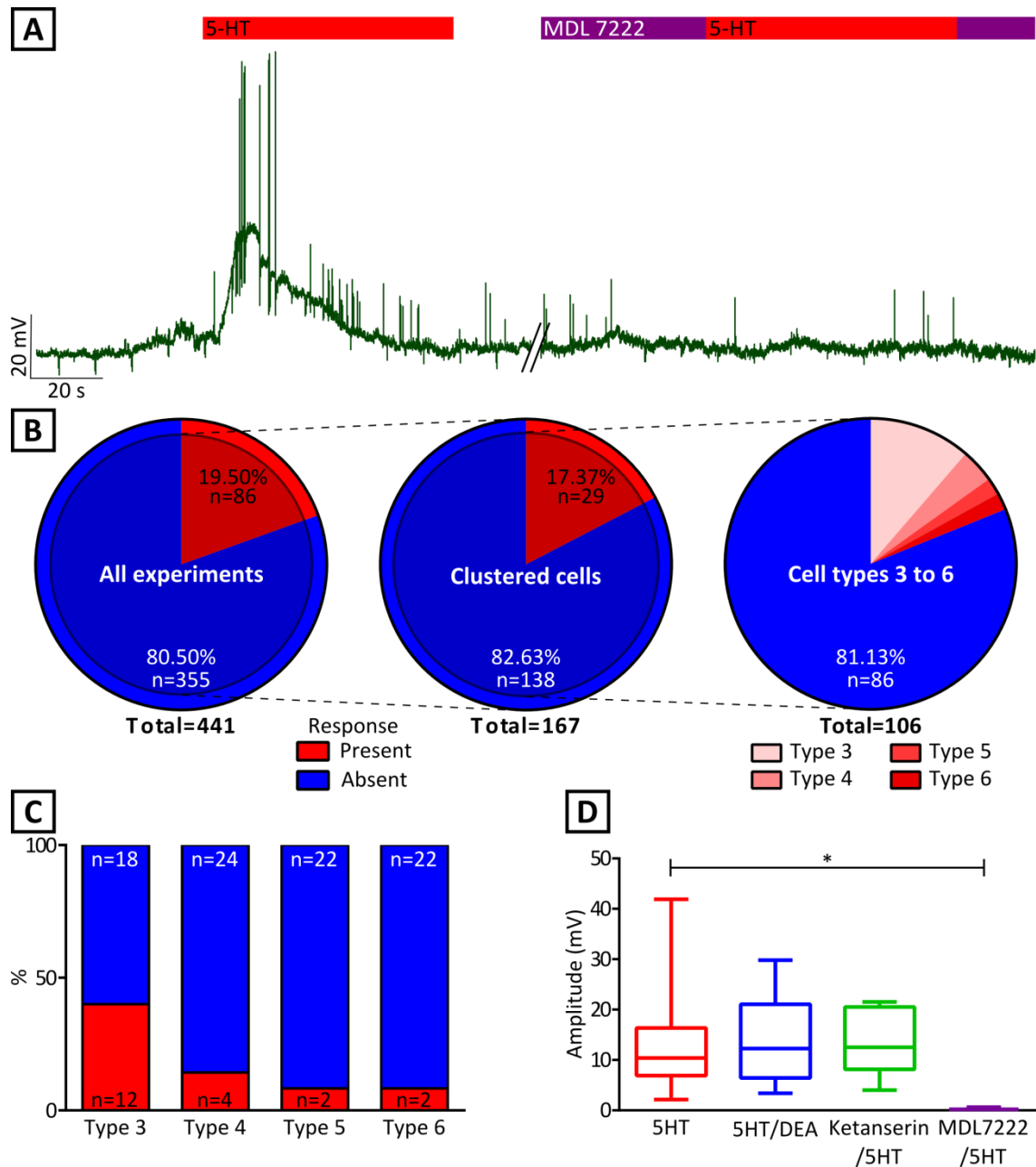
Figure 4-10: Some cells presented a rapid depolarisation in the presence of 5HT. (A) Current clamp record of 5HT-induced depolarisation. Treatment of the same cell with MDL 7222 abolished the response. (B) Pie charts showing the proportion of responsive cells (red) to non-responsive cells (blue) from all experiments, all clustered cells and cell types 3 to 6. (C) Bar graph showing the percentage of cells that presented the 5HT depolarisation (red) compared to those that did not have this response (blue) for cell types 3 to 6. (D) Boxplot showing the interquartile range, median and minimum to maximum range of the amplitude of the 5HT response alone (n=61) and in the presence of DEA (n=16), ketanserin (n=6, $5HT_2$ receptor antagonist), and MDL 7222 (n=3, selective $5HT_3$ antagonist). DMC was used to test whether the amplitudes were different from the ones observed with 5HT alone (* $p<0.05$).

the current study, ketanserin, a $5HT_{2A}$ selective agonist, failed to block this type of response, which occurred in around 18% of the cells treated with 5HT. Thus, the records obtained from cultured cortical neurons provided no evidence for a $5HT_2$ receptor mediated depolarisation. Instead, depolarising responses with rapid desensitisation were blocked by MDL 72222, a $5HT_3$ antagonist. This $5HT_3$-type of response wasn`t modulated by NO.

It has been described that 5HT goes beyond changing the membrane potential of neurons. Modulations of various other parameters have also been reported. For example, in cortical neuron cultures from Sprague-Dawley rats, it has been shown that 5HT can reduce the excitability of the neurons at concentration higher than 30 µM, as well as affecting their spike shapes and the inter-spike interval between the first two spikes elicited by positive current steps (Bianchi et al. 2007). $Na^+$ currents can be modulated by 5HT, which reduces these currents and attenuates the height of backpropagating spikes from the prefrontal cortex (Carr et al. 2002). In lampreys, 5HT has been shown to reduce the amplitude of the AHP and increase the spike frequency of neurons (Wallen et al. 1989). The variety of receptors and cell types in the neocortex results in different modulations of these parameters by 5HT. This is somewhat similar to the results described here that also show a wide range of effects of 5HT on different cellular parameters.

Interestingly, the clustering algorithm used also proved to be efficient in dividing the cells into different cell types that showed specific changes of the various parameters in the presence of 5HT, without even taking into consideration these responses in the algorithm. This is exemplified by the similarity of 5HT-induced changes observed in the excitability plots of cell types 3 and 4 that differ markedly from the changes in cell types 5 and 6.

NO is another neurotransmitter that has been reported to act on various intrinsic membrane properties, and in different animal models. For example, specific motoneurons from the buccal ganglia of snails have been shown to be depolarised by direct application of NO (Park et al. 1998), whereas in the cat's visual cortex NO seems to control spontaneous activity, either by inhibiting or enhancing spontaneous firing

(Cudeiro et al. 1997; Kara & Friedlander 1999). In *in vivo* rat recordings from striatal medium spiny neurons it seems that NO modulates spontaneously occurring plateau potentials, action potential amplitude and responsiveness to positive current injected into the cells (West & Grace 2004). In this project, the main effect observed in the various parameters during application of DEA was changes that would contribute towards a decrease in the excitability of the cells. Interestingly, this differs from the NO-mediated increase in excitability that has been reported in striatal cholinergic interneurons and medial vestibular nucleus neurons (Centonze et al. 2001; Podda et al. 2004).

There are various possible mechanisms for the interaction between these two neurotransmitters. Microdialysis experiments have shown that NO can modulate striatal 5HT concentrations in Wistar rats in a sGC/cGMP dependent manner (Trabace et al. 2004; Trabace & Kendrick 2000). Since NO is a highly reactive molecule, it has also been suggested that it can directly interact with 5HT creating non-effective chemical derivatives of 5HT in a concentration-dependent manner (Fossier et al. 1999). However, other evidence suggests that the modulation between these two neurotransmitters can occur through different interactions. In the pond snail, direct application of 5HT onto the B4 neuron in the snails' feeding system results in depolarisation and spiking activity. This response is greatly enhanced by co-application of NO donor, which modulates this serotonergic effect through the sGC/cGMP pathway (Straub et al. 2007).

In this project, the hypothesis that there is a functional interaction between 5HT and NO in modulating intrinsic excitability in cultured cortical neurons has been addressed. Some parameters observed presented modulation by both 5HT and DEA either in the same or opposite direction. There were parameters that were not significantly affected by the co-application of 5HT/DEA, even though the application of either drug alone would result in a significant difference from control levels, which could be accounted for by a summation of the effects observed for either drug. However, other types of co-modulation, such as non-linear interaction between 5HT and DEA can also happen, as was observed in situations where the application of either 5HT or DEA did not

produce significant results but the co-application would result in a major, significant difference from control levels.

The non-linear interaction between 5HT and DEA could be the result of interactions at different levels of their signalling pathways. Direct interaction, as mentioned before, could result in the formation of 4-nitroso-serotonin or 4-nitro-serotonin (Fossier et al. 1999). This would occur at the signalling molecule level, in which a high concentration of NO would interact with the 5HT molecule, transforming its configuration. Another interaction that would modulate the excitability of the cells could occur at the various ion channels levels, by phosphorylation through either protein kinase A (PKA), whose activity can be modulated via a range of 5HT receptors that are coupled to adenylyl cyclase or protein kinase G (PKG) which is activated by NO via sGC/cGMP (Gray et al. 1998; Centonze et al. 2001). A group of channels that is modulated by both NO and 5HT is the hyperpolarisation-activated channels (HCN). Its activity can be reduced in the presence of 5HT in the ventral tegmental area (Liu et al. 2003) and in the presence of NO in deep cerebellar nuclei (Wilson & Garthwaite 2010). PKG could also modulate the activity of the inositol 1,4,5-trisphosphate (IP$_3$) receptors, that are activated by 5HT$_2$ receptors, altering 5HT-induced calcium release from internal stores (Han et al. 2001).

One other possibility could be at the level of cyclic AMP or GMP concentrations, the first being modulated by 5HT through G$_{i/o}$ or G$_s$ receptors, the second by NO. The concentration of the cyclic nucleotides is controlled by the balance between production by adenylyl and guanylyl cyclases and their breakdown by various phosphodiesterases (PDE). Importantly, the activity of various PDEs is itself regulated by cyclic nucleotides. For example, cAMP concentrations can be modulated by cGMP, since an increase of cGMP levels could act on a cGMP-inhibited phosphodiesterase, such as PDE3 (Sonnenburg & Beavo 1994). The inverse can also occur, with cGMP concentrations being modulated by cAMP, as has previously been reported in olfactory sensory neurons (Moon et al. 2005).

Another possibility, albeit less discussed and probable, would be an interaction between sGC and PKC. NO can activate sGC in order to synthesize cGMP, but is not the

only gas to do this. Carbon monoxide also activates sGC, and this gas is produced by heme oxygenase. Interestingly, heme oxygenase is also activated via PKC, which is in turn activated by increase of diacylglycerol or calcium ions (Boehning et al. 2003). Thus, it is at least a theoretical possibility that activation of $5HT_2$ receptors could "collaborate" with NO in the activation of sGC and cGMP production.

The present work supports the hypothesis that in cortical neurons, cross-talk between 5HT and DEA is possible and can affect intrinsic membrane properties and neuronal excitability. This co-modulation appears to occur at various levels and via a variety of mechanisms.

# 5 Modulation of cortical neuronal properties and spontaneous activity by nitric oxide and serotonin in acute cortical slices

 The final results chapter concentrates on:

- The use of *k*-Means clustering algorithm to identify and group prefrontal cortical neurons in acute cortical slices;

- The modulation of intrinsic electrophysiological parameters by NO and 5HT within defined groups of prefrontal cortical neurons in acute cortical slices;

- The modulation of spontaneous synaptic activity by NO and 5HT in prefrontal cortical slices;

- The contribution of $5HT_1$ and $5HT_2$ receptors to the modulation of spontaneous synaptic activity in prefrontal cortical slices.

## 5.1 Introduction

The prefrontal cortex is responsible for controlling high-level executive tasks and goal directed behaviours. Its many functions also comprise learning, memory formation, categorisation and cognitive flexibility amongst others (Pasupathy & Miller 2005; Antzoulatos & Miller 2011; Warden & Miller 2010; Freedman et al. 2001; Clarke et al. 2004; Gruber et al. 2010). It is a region that receives dense serotonergic input from the dorsal and median raphe nuclei (Azmitia & Segal 1978), with a feedback control of cortical serotonin (5HT) release through back projections to the raphe nuclei (Hajós et al. 1998).

According to Brodmann's work (1909), the cerebral cortex consists of six different histological layers. Pyramidal neurons are present in all layers, but increase their size from layer I to layer VI. Layer I contains the Cajal-Retzius cells (CRC), which are important in the formation of the cytoarchitecture of the cortex during development. Layers I to III are the targets of corticocortical afferents, and layer III is also the principal source of corticocortical efferents. Layer IV is a target of thalamocortical afferent neurons, whereas layer VI sends efferent fibres to the thalamus. Layer V

contains large pyramidal neurons, which send axons to subcortical structures. Different neocortical regions are distinguished by the composition of this histological architecture. For example, the prefrontal cortex consists of layers I to VI, without the presence of layer IV. The neurons in these layers can be, by morphological classification, either principal pyramidal neurons, having a triangular shaped soma, a single axon and a large apical dendrite together with multiple basal dendrites, or interneurons, with various morphologies including stellate soma, multipolar and bitufted types (Gabbott et al. 1997; Kawaguchi 1993). All the different types of neurons are connected through a vast number of synapses between cells in the same layer or across layers. A chain of connected neurons which extends throughout the various layers and perpendicular to the pial surface can be grouped together into a cortical unit, the minicolumn (Mountcastle 1997). Thus, the transmission of information in the prefrontal cortex occurs more in a hierarchical, top-down structure than horizontally throughout the same layer.

$5HT_1$ and $5HT_2$ receptors are expressed globally in the prefrontal cortex (Pompeiano et al. 1992; Pompeiano et al. 1994; Willins et al. 1997). In pyramidal neurons, around 60% of the cells express at least one of these receptors and of those, 80% co-express both $5HT_1$ and $_2$ receptors (Amargós-Bosch et al. 2004; Santana et al. 2004). This co-expression has not been shown in the interneurons, including the fast spiking neurons. Fast spiking neurons have been reported to express either $5HT_1$ or $5HT_2$, or even $5HT_3$ receptors, in prefrontal cortical neurons from layers II/III from rats (Morales & Bloom 1997; Weber & Andrade 2010; Willins et al. 1997; Puig et al. 2010). On the other hand, slow spiking interneurons express $5HT_3$ type receptors (Vucurovic et al. 2010; Férézou et al. 2002). In general, it is understood that $5HT_1$ would inhibit the activity of the cells whereas $5HT_2$ and $5HT_3$ would excite the neurons (Araneda & Andrade 1991; Xiang & Prince 2003; Foehring et al. 2002; Goodfellow et al. 2009; Zhong & Yan 2011). However, especially for the pyramidal neurons that co-express both $5HT_1$ and $_2$ receptors, the response can be bimodal. This is due to the fact that $5HT_1$ receptors are expressed mainly on the axon initial segment, suppressing the generation of APs (Martín-Ruiz et al. 2001), whereas $5HT_2$ receptors are abundant in the apical dendrites,

increasing excitatory postsynaptic current frequency by modulating glutamatergic inputs (Jakab & Goldman-Rakic 1998; Marek & Aghajanian 1999).

Nitric oxide synthase (NOS) is generally present in the prefrontal cortex of rats (Liu et al. 2004) and it seems to be related to the increase of spike firing in the rat medial prefrontal cortex after addictive drug sensitisation (Nasif et al. 2011), even though only around 1% of γ-aminobutyric acid (GABAergic) inhibitory interneurons of the mouse visual cortex presented double labelling with NOS antibody (Gonchar et al. 2008). NOS production can also be induced by activity in layer V pyramidal neurons (Lourenço et al. 2014), and it was demonstrated that serotonergic raphe nuclei neurons projecting to the prefrontal cortex in rats also possess NOS activity (Lu et al. 2010). NOS is the principal activator of soluble guanylyl cyclase (sGC), and this component has been shown to be co-localised to dendritic marker MAP2 on parietal cortex of Sprague-Dawley rats (Ding et al. 2005). On hippocampal pyramidal cells, it has been shown that neuronal NOS is present in the postsynaptic density of axospinous synapses, and that there is a high correlation between sGC and the presynaptic terminals of the active zone (Burette et al. 2002).

This chapter firstly describes the electrophysiological properties of the various types of neurons in layers II/III of the prefrontal cortex of young adult Wistar rats (14 to 20 days old) to enable direct comparison to the data obtained from cultured neurons. This is followed by a limited analysis on how the electrophysiological properties of these neurons are changed in the presence of 5HT, DEA and the combined application of both drugs. Furthermore, in this structured and developed network, the spontaneous excitatory synaptic inputs that the cortical neurons receive from the columnar units were recorded. The frequency, amplitude and decay times of spontaneous EPSCs were analysed in the presence of 5HT, diethylamine NONOate sodium salt hydrate (DEA) and both drugs in the presence and absence of inhibitory synaptic activity. Finally, an attempt was made to identify the 5HT receptors that are responsible for the changes in spontaneous synaptic potentials.

## 5.2 Identification of types of cells using clustering algorithm

The prefrontal cortex contains many different types of neurons, which could be divided into two major groups: principal pyramidal neurons and interneurons, with the former being the majority of neurons in layers II/III. Previously the classification of these neurons was based on visual identification of excitability traces or the morphology of the cells. In this work, in order to identify the various types of cells recorded around layer III from the prefrontal cortex (Figure 5-1A), the same set of parameters obtained from current clamp recordings and the same type of algorithm, *k*-Means, as described before for cell cultures, were used to cluster the recorded cells into distinct groups. Based on the resulting scores for grouping the data into between 2 and 30 clusters, a k value of 7 was chosen, which is somewhat lower than the k = 10 for cell culture (Figure 5-1B). Outliers were identified the same way as for the cell culture data, i.e. z-scores outside the range of ± 5. Based on this criterion 5 out of 173 cells were excluded from further analysis. The resulting clusters had four major groups with n=41, 34, 32 and 27, while the other 3 groups only contained between ~5% and ~9% of the total cells (Figure 5-1C).

By comparing threshold of action potentials (APs) and number of APs elicited at various current levels, it was attempted to associate the different clusters of cells obtained from recordings in acute cortical slices to the ones from cultured cortical neurons (Figure 5-1D). The seven cell clusters identified in acute slices can be correlated tentatively to cell types 1, 3, 5, 7, 8 and 10 identified in cell culture.

The association between the types of cells from cultured cortical neurons to the ones obtained from slices allowed similar excitability behaviours to be compared (Figure 5-2). The first type shows a low spiking threshold and relatively high numbers of APs for any current step. Two different groups observed in slices could be compared to cultured cell type 5. Cell types 5 obtained from cultured cortical neurons could be just a supergroup of the two ones from slices, or conversely, the cells in type 5 on slices could have been forced into a split by the clustering algorithm. The groups related to types 3 and 5, although very similar, can be divided by the average number of APs elicited at the last current step, with type 3 generating the highest, and type 5 the
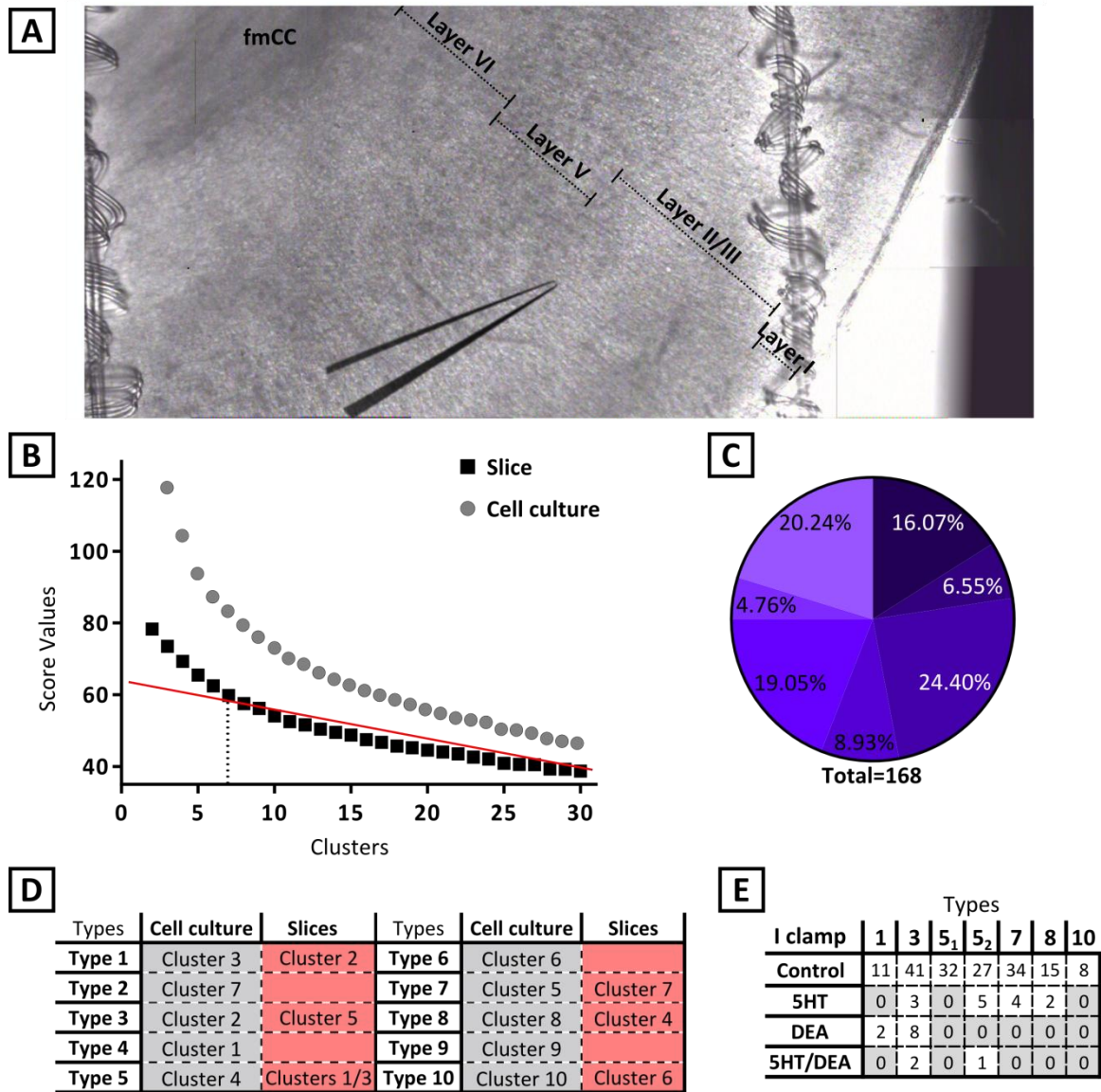
Figure 5-1: (A) Position in the layers of the prefrontal cortex that neurons were recorded (fmCC = forceps minor corpus callosum). The cells were recorded from layer II/III of the prefrontal cortex. (B) Plot of score values against k values (clusters) obtained from *k*-Means clustering using parameters obtained from current clamp recordings from prefrontal cortical neurons in acute brain slices. (C) Percentage of cells allocated to each clusters for a k value of 7. (D) Proposed correlation between the various clusters obtained from cultured cortical neurons and clusters based on data from acute brain slices. (E) Number of cells recorded per experiment for the various different types of cells in cortical slices.

fewest number of APs. In contrast to type 1, these two types show a rather gradual and very linear increase in number of APs elicited by progressively larger current steps.

Of the remaining three groups, cells of the type 7 produce a low, steady linear number of APs with the increase of current, whereas type 8 cells don't produce more than a few APs, although their average rheobase is comparable to cell types 5 and 7. In comparison to type 8, type 10 cells have a higher firing threshold, and they don't generate more than one AP at any current step.

These behaviours are in general quite similar to the ones observed in cultured cortical neurons. However, it is notable that in slices spike-height adaptation, spike frequency accommodation and the firing-rate saturation are less prominent. The behaviour seen in cell types 6 and 9 in cell culture, in which the number of APs reduces after reaching a peak, wasn't observed in any cells in acute slices.

The similarity of the excitability plots for some of the types allowed them to be combined into major clusters. Type 1 cells are, henceforth, grouped as fast spiking (FS) interneurons, whereas types 7 and 10 are, due to their low spike frequency and higher threshold, considered as slow spiking (SS) interneurons. The remaining groups are combined into a bigger group, and are assumed to represent pyramidal cells.

As seen for the excitability plots from the cultured cortical neurons, these plots presented very small error bars, even for the groups with small n numbers, indicating that the clustering algorithm successfully combined cells with very similar activity patterns. An example of the recorded traces for each type is shown in Figure 5-3.

When overlapping the current-voltage (IV) relationships for cell types recorded in cell culture and in cortical slices, it was possible to see that the IV relationship is very similar between the preparations, especially for the negative current steps. Type 10 cells were the only group that in slice presented a markedly less steep correlation for both negative and positive steps, whereas type 7 neurons from intact tissue presented a less linear, more sigmoidal curve (Figure 5-4).
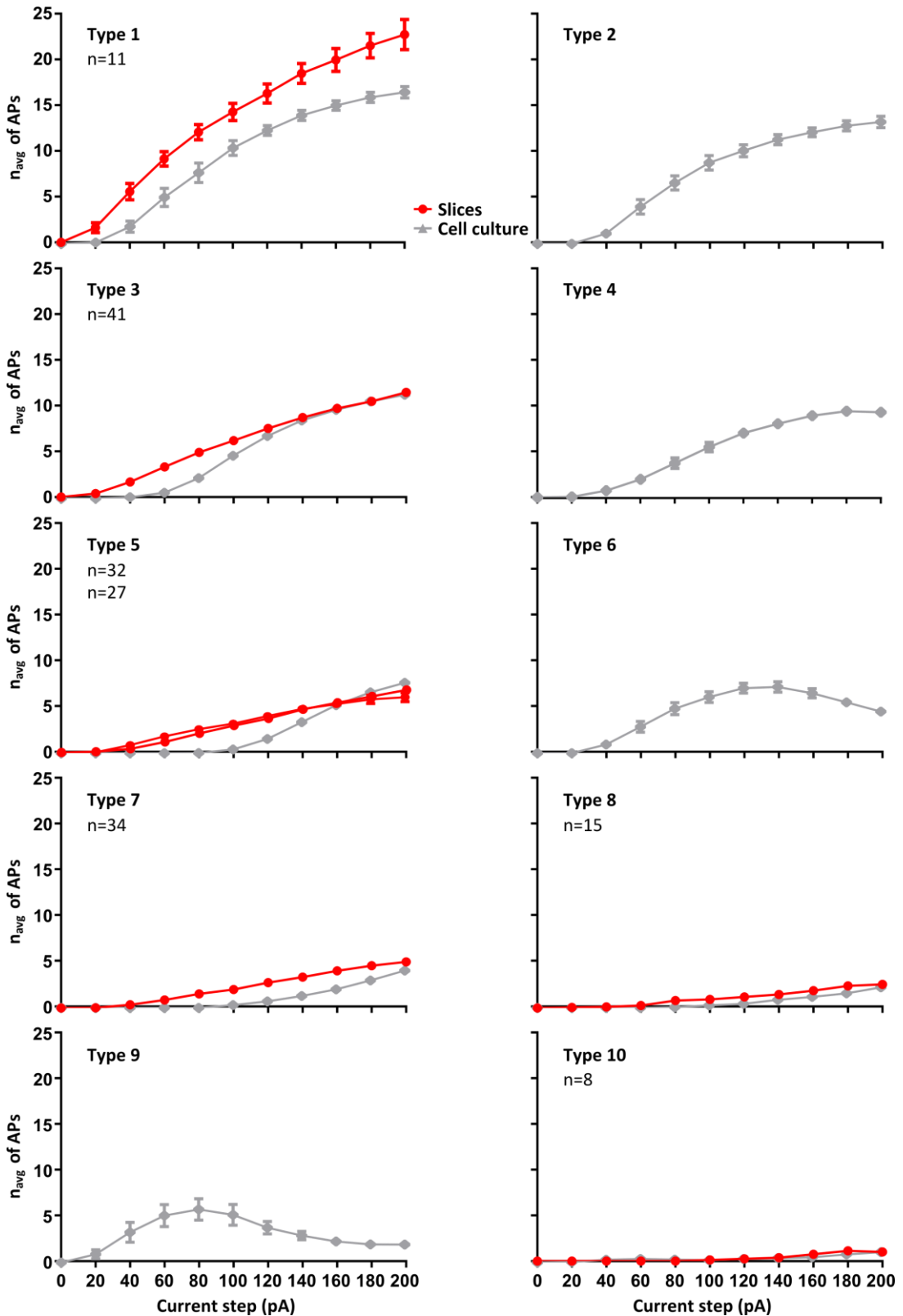
Figure 5-2: Excitability plots showing the number of APs elicited by current steps between 20 and 200 pA in cell types in cortical slices defined by *k*-Means clustering based on $PS_{10}$ (red). The plots are ordered according to maximum number of APs produced at 200 pA. For comparison, the excitability plots for individual clusters are superimposed onto the ones obtained from cultured neurons (gray).

## 5.3 Modulation of intrinsic electrophysiological parameters by nitric oxide and serotonin

In order to test if previous findings of modulation on physiological parameters from cultured cells by 5HT and NO are consistent with effects in acute cortical slices, the effects of 5HT, NO and 5HT/NO on 20 different parameters was analysed in a limited number of cells (Figure 5-1E). Table 5-1 and Table 5-2 list the percentage of change that each parameter showed when compared to the control average for individual cell types. Due to the strong similarity in the properties for cell types 3 and 5 (cell clusters 1, 3, and 5), data from these cells were combined and considered together. These cells are referred to as pyramidal neurons. Of note is that application of DEA reduced the average number of APs at 120 pA and 200 pA in all groups tested. DEA also increases the rheobase, minimum inter-spike interval (ISI) and the proportion of minimum over maximum ISI at 200 pA for the tested cells. The increase in voltage amplitude at 200 pA caused by DEA appears to be more specific to FS type 1 cells, but it is not really present in pyramidal neurons. In contrast, $I_r$ is decreased for both FS and pyramidal cells in the presence of DEA, while the minimum of the AP trough was generally shifted towards more negative values in the presence of DEA.

5HT effects appeared to be somewhat more cell type specific, decreasing the number of APs at 120 pA for pyramidal neurons, but causing an increase in SS interneurons. 5HT also increased the number of APs at 200 pA for SS interneurons. These changes are probably the result of an increase in rheobase in pyramidal cells and a decrease in the same parameter in SS interneurons. Furthermore, the amplitude of the change in membrane potential at 200 pA was decreased for the SS interneurons when 5HT was applied. The ratio of minimum to maximum ISI was increased for all cells tested, whereas the spike burst pattern was only increased in type 7 neurons. 5HT increased $I_h$ expression, but decreased the input resistance of pyramidal cells. For SS interneurons, 5HT decreased the trough amplitude of the first and last AP at 200 pA, while also increasing the width of last AP at 200 pA.

Only a very small number of pyramidal neurons (n=3) received the co-application of 5HT/DEA. The data is included in the tables for completeness, but the small n number
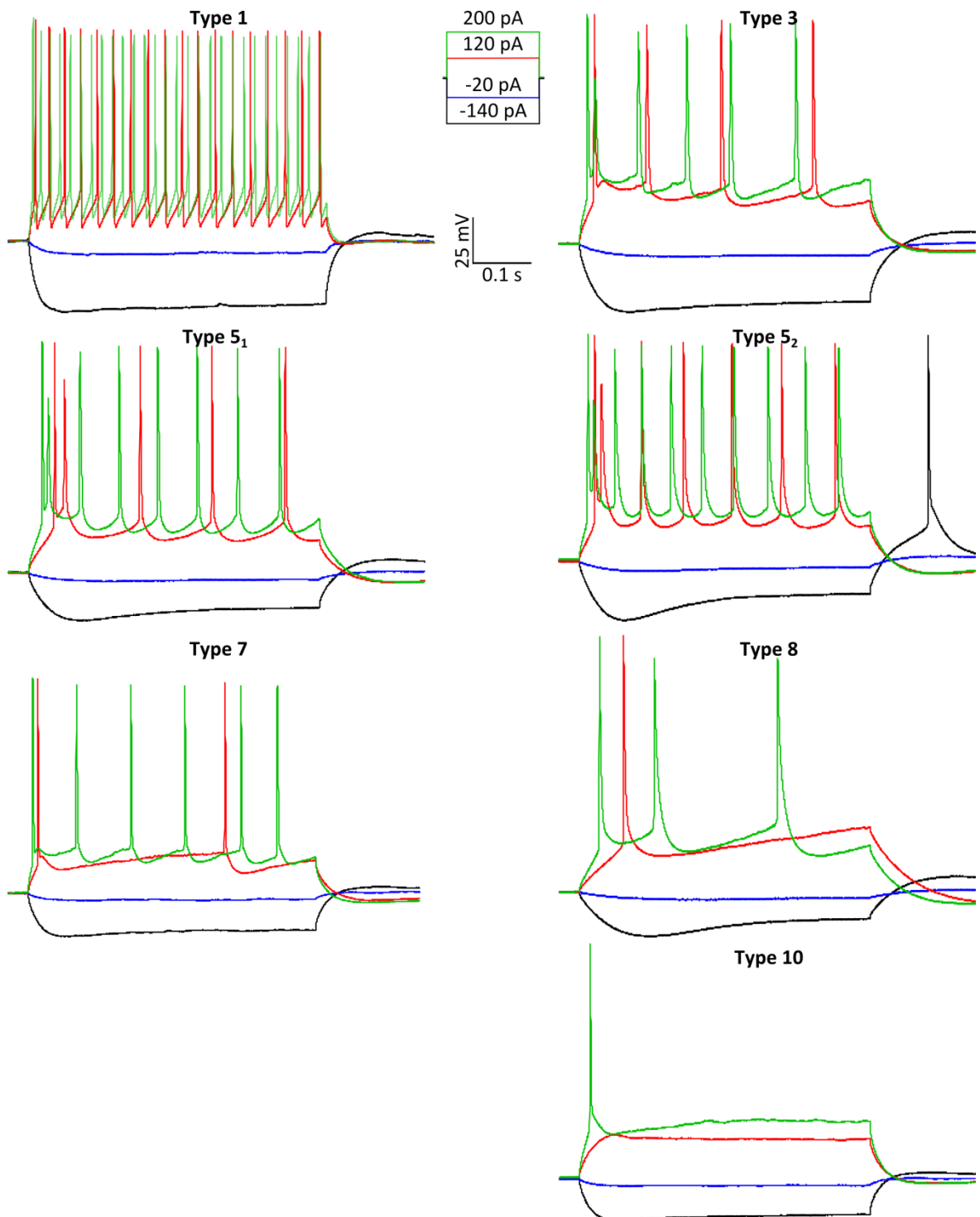
Figure 5-3: Example recordings for the seven different types of cells defined by *k*-Means clustering with $PS_{10}$ obtained from cortical slices. Traces are the responses to four different current steps, -140 pA (black), -20 pA (blue), 120 pA (red) and 200 pA (green).
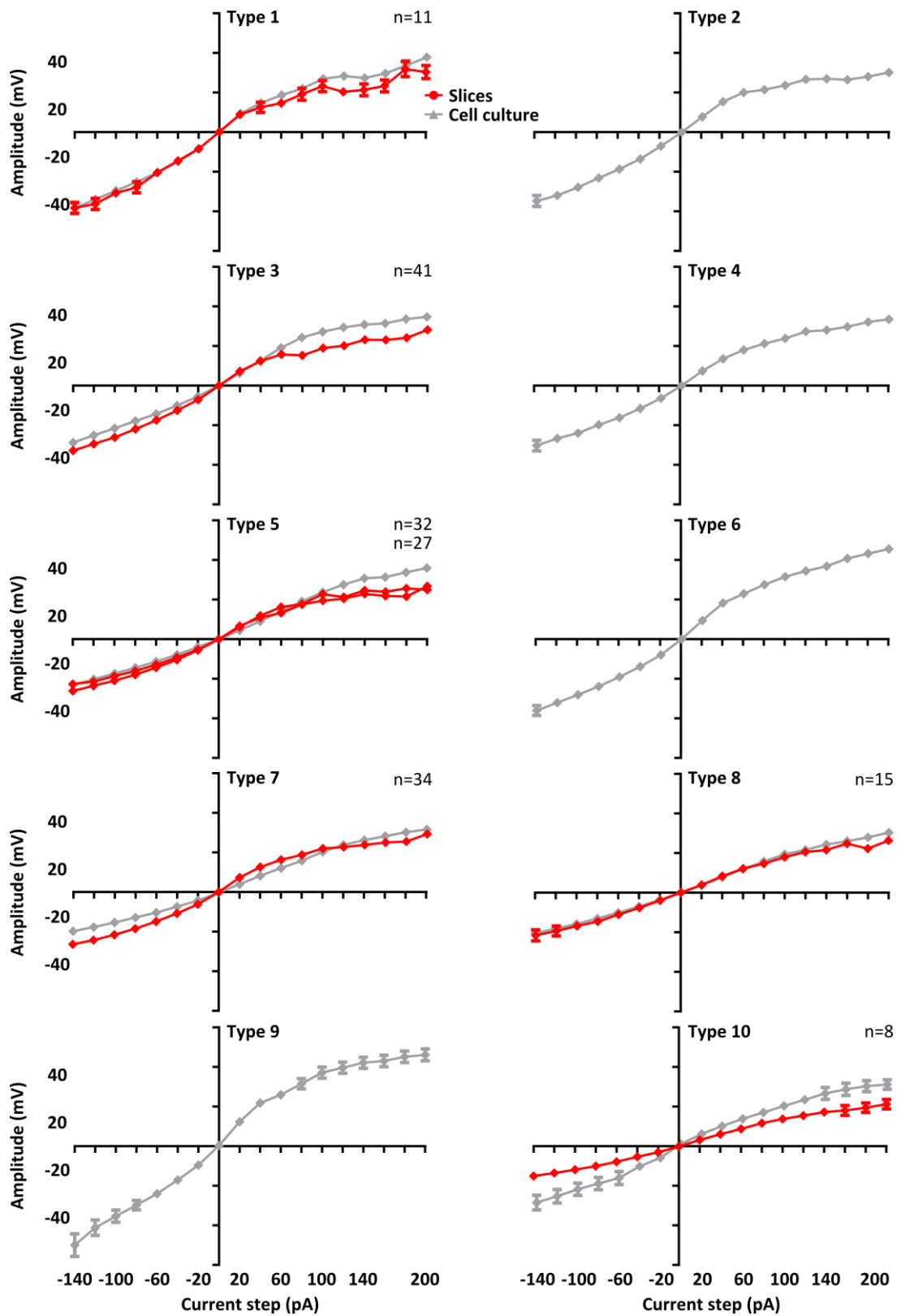
Figure 5-4: IV plots for the seven types of cells defined by *k*-Means clustering with PS$_{10}$ obtained from cortical slices (red). For comparison, IV plots obtained from cultured neurons are shown in gray. The steady state change in membrane potential from a resting membrane potential of approximately -70 mV is plotted against the amplitude of the current pulse.

made it impossible to draw any firm conclusion whether effects of 5HT/DEA are the result of linear summation of the individual effects of 5HT and DEA or suggest non-linear interactions between the two signalling pathways as observed in cell culture.

As in Chapter 4, a multi-level modelling (MLM) approach was used to test whether the effects observed in the various parameters during drug treatments were significantly different from control and between different drug treatments. As described previously, this model was developed using the various parameters as outcome, the treatments as fixed effects and the different cells in the experiments as random effects. Simultaneous inference was obtained by using general linear hypothesis for this model, and the $p$ values obtained were stored in a matrix and presented as a heat map.

As shown in Chapter 4, pyramidal cells in cortical slices demonstrated significant differences compared to control levels in the values of many of the parameters as the result of bath perfusion of 5HT and DEA (Figure 5-5). However, rheobase and $I_r$ are the only two pyramidal cell parameters that were significantly affected by both 5HT and DEA (Figure 5-5).

On the other hand, some parameters are solely affected by either 5HT or DEA. A total of twelve out of forty parameters tested in pyramidal neurons and SS interneurons were significantly affected by 5HT. These include ISI slope at 200 pA and the height of the first AP at 200 pA, where both types of cells showed significant difference from control levels.

Similarly, sixteen out of forty parameters tested in pyramidal neurons and FS interneurons were significantly affected by DEA. However, further analysis shows that there were only four parameters that were affected significantly differently by 5HT and DEA, with a small number of additional parameters where this comparison reaches near significance. This suggests that there are more than two parameters that can be modulated by both 5HT and DEA.

The IV relationships for the 3 groups of cells, similar to what was seen in cultured cortical neurons, also show non-linear behaviour in response to negative current

| | Treatment | Type 1 C2 | Pyramidal C1, C3, C7 | Type 7 C4 |
|---|---|---|---|---|
| N of APs at 120 pA | Control | 13.5 ± 0.4 | 6.1 ± 0.3 | 1.1 ± 0.2 |
| | Δ5HT | | -1.1 ± 0.9 | 1.2 ± 1.6 |
| | ΔDEA | -3.0 ± 1.8 | -1.0 ± 0.4 | |
| | Δ5HT/DEA | | -1.1 ± 0.8 | |
| N of APs at 200 pA | Control | 18.5 ± 0.3 | 9.4 ± 0.4 | 2.9 ± 0.1 |
| | Δ5HT | | 0.0 ± 0.5 | 0.3 ± 1.7 |
| | ΔDEA | -2.0 ± 2.3 | -1.2 ± 0.9 | |
| | Δ5HT/DEA | | -2.1 ± 1.8 | |
| Rheobase (x10 pA) | Control | 3.5 ± 0.3 | 5.1 ± 0.2 | 9.1 ± 0.8 |
| | Δ5HT | | 1.1 ± 0.6 | -0.6 ± 3.4 |
| | ΔDEA | 3.5 ± 0.5 | 0.6 ± 0.5 | |
| | Δ5HT/DEA | | 2.2 ± 1.3 | |
| Vm Amplitude at 200 pA (x10 mV) | Control | 2.3 ± 0.2 | 2.9 ± 0.1 | 2.7 ± 0.3 |
| | Δ5HT | | -0.2 ± 0.1 | -0.4 ± 0.3 |
| | ΔDEA | 1.5 ± 1.0 | 0.1 ± 0.2 | |
| | Δ5HT/DEA | | -0.2 ± 0.4 | |
| ISI Slope at 200 pA | Control | 0.0 ± 0.1 | 4.2 ± 1.1 | 65.9 ± 18.1 |
| | Δ5HT | | 0.0 ± 0.7 | -0.1 ± 3.1 |
| | ΔDEA | 0.0 ± 0.0 | 0.0 ± 0.4 | |
| | Δ5HT/DEA | | 0.0 ± 0.2 | |
| Minimum ISI at 200 pA (x10 ms) | Control | 1.5 ± 0.0 | 2.9 ± 0.3 | 9.8 ± 0.8 |
| | Δ5HT | | -0.1 ± 0.7 | 0.0 ± 2.1 |
| | ΔDEA | 0.7 ± 1.0 | 1.4 ± 1.4 | |
| | Δ5HT/DEA | | 0.4 ± 0.6 | |
| Min/Max ISI at 200 pA ($10^{-1}$) | Control | 4.6 ± 0.1 | 3.6 ± 0.3 | 6.4 ± 0.7 |
| | Δ5HT | | 1.0 ± 1.0 | 1.8 ± 0.4 |
| | ΔDEA | 0.9 ± 2.0 | 0.7 ± 1.2 | |
| | Δ5HT/DEA | | 0.6 ± 0.3 | |
| Spike Burst Pattern (x10 %) | Control | 9.2 ± 0.0 | 7.3 ± 0.2 | 1.6 ± 0.2 |
| | Δ5HT | | -0.4 ± 0.7 | 1.3 ± 3.1 |
| | ΔDEA | -0.2 ± 0.4 | -0.6 ± 0.9 | |
| | Δ5HT/DEA | | 0.3 ± 0.4 | |
| Spike Height Adaptation (x10 %) | Control | 8.4 ± 0.3 | 8.1 ± 0.2 | 7.7 ± 0.3 |
| | Δ5HT | | 0.1 ± 0.3 | 0.2 ± 0.9 |
| | ΔDEA | -0.2 ± 0.6 | 0.0 ± 0.1 | |
| | Δ5HT/DEA | | 0.2 ± 0.2 | |
| $I_h$ (x10 %) | Control | 8.8 ± 0.1 | 8.3 ± 0.1 | 6.7 ± 0.2 |
| | Δ5HT | | -1.2 ± 1.3 | 0.1 ± 0.6 |
| | ΔDEA | -0.1 ± 0.3 | 0.1 ± 0.1 | |
| | Δ5HT/DEA | | 0.8 ± 0.5 | |

>500% | >100% | >50% | >10% | ≤10% and ≥-10% | <-10% | <-50% | <-100% | <-500%

Table 5-1: Mean ± standard error of the means (SEM) for control values (in darker grey) and difference between treatment and control for 10 parameters in cell type 1 (FS interneurons), pyramidal neurons (cell clusters 1, 3 and 7) and cell type 7 (SS interneurons). The colour-coded column to the right of each group represents the percentage of increase (red) or decrease (blue) of the values when compared to control.

| | Treatment | Type 1 — C2 | Pyramidal — C1, C3, C7 | Type 7 — C4 |
|---|---|---|---|---|
| $I_r$ (x10² MΩ) | Control | 3.8 ± 0.3 | 3.4 ± 0.1 | 1.6 ± 0.2 |
| | Δ5HT | | -0.4 ± 0.1 | 0.1 ± 0.7 |
| | ΔDEA | -0.7 ± 0.2 | -0.6 ± 0.2 | |
| | Δ5HT/DEA | | -0.9 ± 0.5 | |
| AP Height 1st AP at Threshold (x10 mV) | Control | 10.0 ± 0.1 | 9.1 ± 0.1 | 8.8 ± 0.2 |
| | Δ5HT | | -0.1 ± 0.1 | 0.1 ± 0.4 |
| | ΔDEA | -0.2 ± 0.2 | -0.1 ± 0.1 | |
| | Δ5HT/DEA | | -0.5 ± 0.2 | |
| AP Trough 1st AP at Threshold (x10 mV) | Control | -0.1 ± 0.2 | -0.4 ± 0.1 | -0.6 ± 0.1 |
| | Δ5HT | | 0.0 ± 0.1 | 0.0 ± 0.0 |
| | ΔDEA | -0.1 ± 0.1 | -0.1 ± 0.1 | |
| | Δ5HT/DEA | | -0.3 ± 0.1 | |
| AP Width 1st AP at Threshold (ms) | Control | 2.2 ± 0.1 | 2.5 ± 0.1 | 2.8 ± 0.1 |
| | Δ5HT | | -0.1 ± 0.1 | -0.1 ± 0.0 |
| | ΔDEA | 0.0 ± 0.0 | 0.1 ± 0.1 | |
| | Δ5HT/DEA | | 0.2 ± 0.1 | |
| AP Height 1st AP at 200 pA (x10 mV) | Control | 9.6 ± 0.1 | 9.0 ± 0.1 | 9.3 ± 0.2 |
| | Δ5HT | | -0.1 ± 0.1 | -0.2 ± 0.6 |
| | ΔDEA | 0.1 ± 0.1 | 0.0 ± 0.0 | |
| | Δ5HT/DEA | | -0.4 ± 0.1 | |
| AP Trough 1st AP at 200 pA (x10 mV) | Control | 0.8 ± 0.1 | 0.5 ± 0.0 | 0.4 ± 0.2 |
| | Δ5HT | | 0.0 ± 0.1 | -0.3 ± 0.2 |
| | ΔDEA | -0.2 ± 0.0 | -0.1 ± 0.1 | |
| | Δ5HT/DEA | | -0.4 ± 0.1 | |
| AP Width 1st AP at 200 pA (ms) | Control | 2.4 ± 0.1 | 2.6 ± 0.1 | 2.7 ± 0.1 |
| | Δ5HT | | 0.0 ± 0.1 | 0.1 ± 0.1 |
| | ΔDEA | 0.0 ± 0.0 | 0.1 ± 0.1 | |
| | Δ5HT/DEA | | 0.1 ± 0.1 | |
| AP Height Last AP at 200 pA (x10 mV) | Control | 8.1 ± 0.3 | 7.3 ± 0.2 | 7.3 ± 0.4 |
| | Δ5HT | | 0.0 ± 0.3 | 0.0 ± 1.2 |
| | ΔDEA | -0.1 ± 0.7 | 0.0 ± 0.1 | |
| | Δ5HT/DEA | | -0.1 ± 0.2 | |
| AP Trough Last AP at 200 pA (x10 mV) | Control | -0.1 ± 0.0 | -0.7 ± 0.1 | -0.9 ± 0.1 |
| | Δ5HT | | 0.0 ± 0.1 | 0.5 ± 0.0 |
| | ΔDEA | 0.0 ± 0.1 | -0.2 ± 0.1 | |
| | Δ5HT/DEA | | -0.2 ± 0.1 | |
| AP Width Last AP at 200 pA (ms) | Control | 3.4 ± 0.3 | 3.8 ± 0.2 | 3.7 ± 0.2 |
| | Δ5HT | | 0.2 ± 0.2 | 0.6 ± 1.3 |
| | ΔDEA | 0.0 ± 0.1 | -0.1 ± 0.1 | |
| | Δ5HT/DEA | | 0.2 ± 0.3 | |

Legend: >500% | >100% | >50% | >10% | ≤10% and ≥-10% | <-10% | <-50% | <-100% | <-500%

Table 5-2: Mean ± SEM for control values (in darker grey) and difference between treatment and control for 10 parameters in cell type 1 (FS interneurons), pyramidal neurons (cell clusters 1, 3 and 7) and cell type 7 (SS interneurons). The colour-coded column to the right of each group represents the percentage of increase (red) or decrease (blue) of the values when compared to control.

pulses, suggesting the presence of hyperpolarising-activated currents (Figure 5-6). However, different from the observation in cultured cortical neurons, the treatments resulted in an increase of this non-linearity. This is observed with the application of DEA in type 1 cells and DEA, 5HT and 5HT/DEA in pyramidal neurons.

For type 1 cells, in the presence of DEA the change in the amplitude of the membrane potential at -140 pA compared to control is significantly different from 0 (one-way $t$ test, $p<0.01$, n=2). For pyramidal cells the difference of the IV relationship is also significant for all treatments (one-way $t$ test, $p<0.01$, n=12 for 5HT, 8 for DEA and 3 for 5HT/DEA).

In contrast, 5HT has no apparent effect on the IV relationship in cell type 7 in cortical slices (one-way $t$ test: $p>0.05$, n=2).

Finally, the difference of excitability in the presence of 5HT, DEA or both drugs was analysed in comparison to control values (Figure 5-7). For type 1 cells, DEA considerably decreased the number of APs at the various injected currents, with significant $p$ values at 40, 80 and 100 pA. In contrast, excitability in pyramidal cells was not significantly affected by DEA. Similarly, 5HT and 5HT/DEA applications had no significant effects on pyramidal cell excitability.

The same was also the case for type 7 that showed no significant change in response to 5HT application.

## 5.4 Modulation of spontaneous synaptic activity by nitric oxide and serotonin in cortical slices

Another aspect of complex brain tissue is the connectivity between the various neurons. Even in acute slices, many of the connections between the various cortical neuron types are retained and there is a certain level of spontaneous activity as indicated by frequent spontaneous synaptic inputs and action potentials. Thus the network in slices can be used to study how various neurotransmitters affect cortical network activity. In order to analyse the effects of 5HT and NO on the activity of
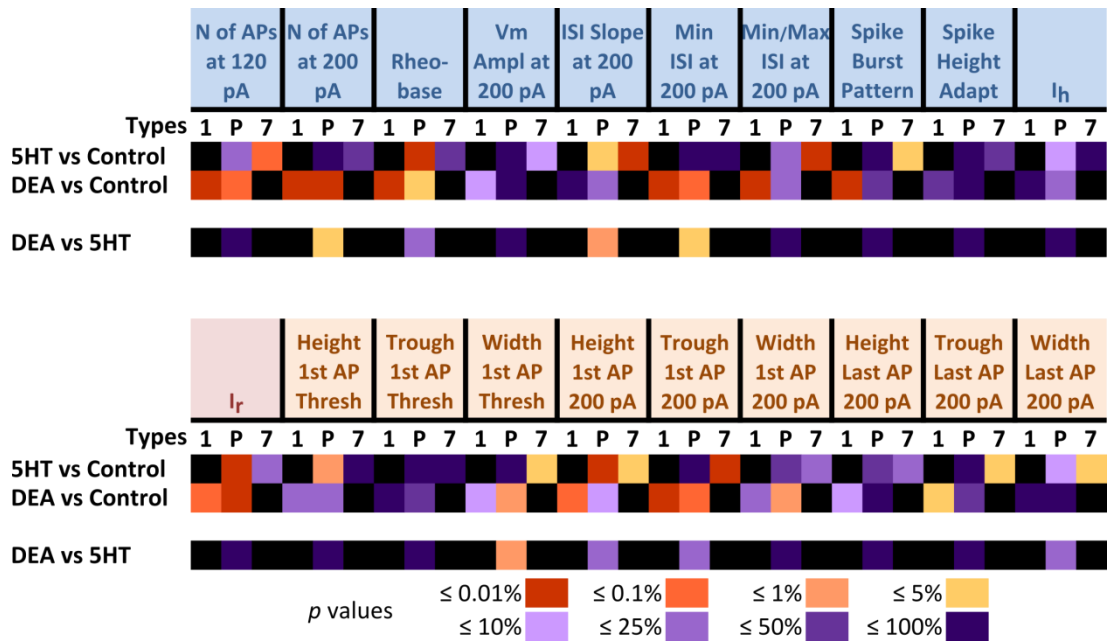
Figure 5-5: Heat map of *p* values obtained from MLM. The three types of cells are in sub columns for each parameter (type 1 = fast spiking interneurons; P = pyramidal cells; type 7 = slow spiking interneurons). Each row represents a specific pairwise comparison between two conditions as indicated on the left of the figure. Darker orange colour indicates a significant difference between treatments, darker purple colour shows less significance.
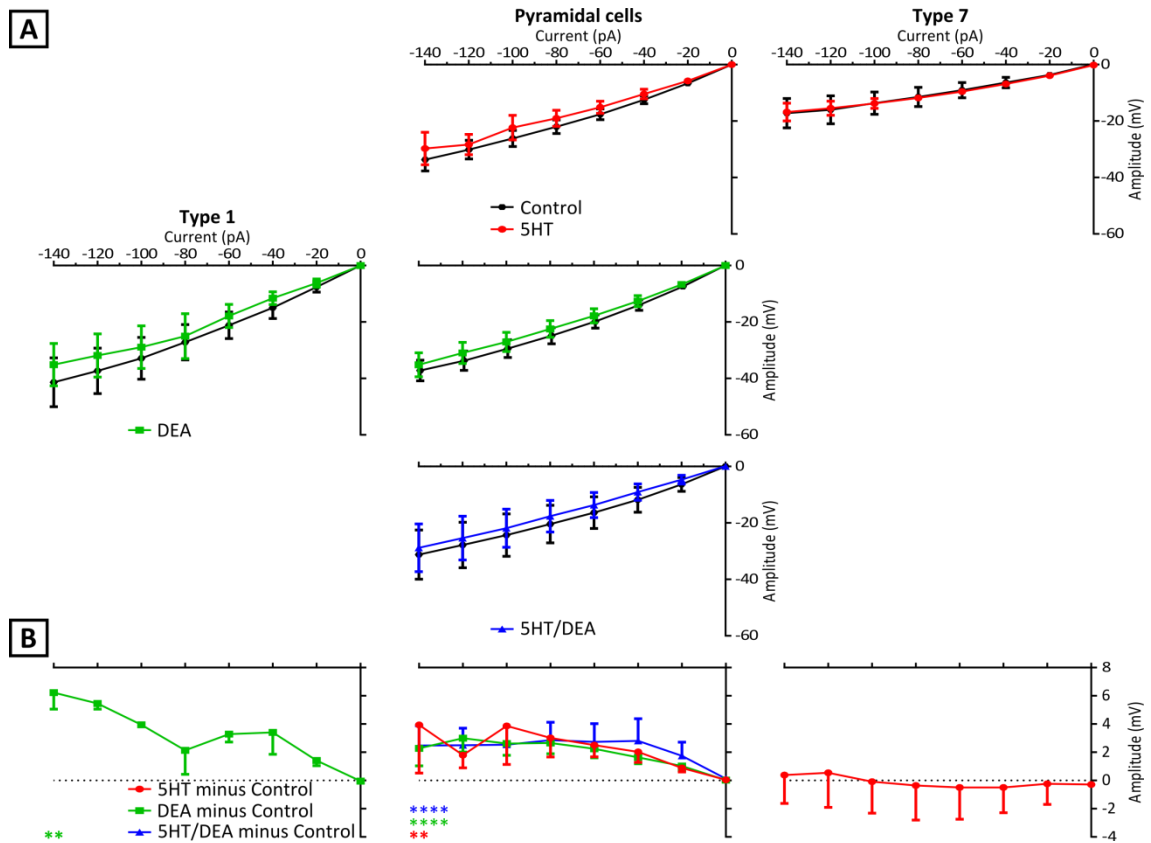
Figure 5-6: Effects of 5HT, DEA and 5HT/DEA on IV relationship for cell type 1, pyramidal cells and cell type 7. (A) The IV plots are shown for current steps from -140 to 0 pA under control conditions (black) and in the presence of 5HT (red), DEA (green) and 5HT/DEA (blue). (B) Plots of differences in amplitudes of voltage-responses during drug treatment minus control for each current step. One-way $t$ test were used to test whether differences at -140 pA were significantly different from 0 (** $p<0.01$, **** $p<0.0001$).

cortical slices, voltage clamp recordings were obtained from cells in the same region as described before, i.e. the deeper regions of prefrontal cortex layer II/III. Some of the records were conducted in the presence of picrotoxin or ODQ/picrotoxin. As mentioned in chapter 2, during the recordings the cells were clamped at -70 mV, and spontaneous excitatory post-synaptic currents (EPSCs) with amplitude higher than 5 pA were counted, and for each EPSC, the amplitude and decay time constant were analysed. It was decided to look at EPSCs rather than mini-EPSCs in order to gain an understanding of the network activity, reflecting the changes in cellular excitability at the network level. Although recording mini-EPSCs with pharmacological tools like tetrodotoxin would show potential effects of 5HT and NO on vesicle release, it is not part of the scope of this research.

As described in the previous sections the recorded cells were divided into pyramidal cells, fast spiking and slow spiking interneurons. Sample records for all the treatments on pyramidal neurons can be seen in Figure 5-8. The experiments consisted of the bath application of 5HT, DEA and 5HT/DEA. The recorded cells showed spontaneous EPSCs at an average frequency of 0.82 ± 0.09 Hz, with slow spiking interneurons having the highest frequency of 1.56 ± 0.31 Hz (n=15), followed by pyramidal neurons with a frequency of 0.73 ± 0.09 Hz (n=70) and the fast spiking interneurons with a frequency of 0.25 ± 0.09 Hz (n=8). The frequency observed on pyramidal neurons (DMC: $p$ = 0.0334), as well as fast spiking interneurons (DMC: $p$ = 0.0026) are significantly different to slow spiking interneurons.

Initially the number of EPSCs per 60 seconds, shown as frequency, was analysed for the control period (baseline) and in the presence of the various drugs. The four cell groups showed average baseline EPSC frequencies of no more than 2 Hz, with slow spiking interneurons showing the fastest EPSC rate, followed by pyramidal cells and the fast spiking interneurons (Figure 5-9A).

The cortical network is composed of both excitatory and inhibitory connections. Some experiments were carried out to analyse the effects of 5HT and NO solely on cortical excitatory connections. Picrotoxin, a non-competitive $GABA_A$ receptor blocker, was applied during these experiments to block all fast inhibitory interactions. In the
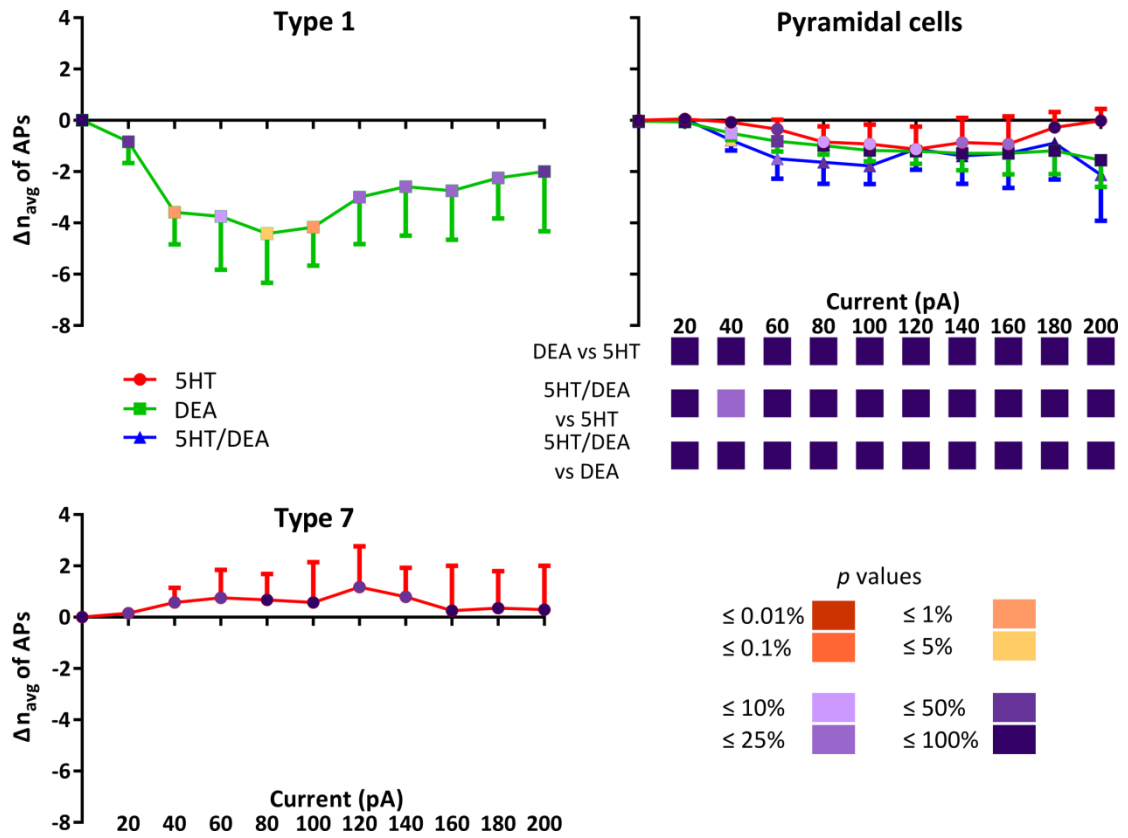
Figure 5-7: Plots of the change in excitability for the three types of cells recorded in current clamp mode. The plots show the difference of the average numbers of APs between treatments and control, to highlight changes in the presence of 5HT (red), DEA (green) and 5HT/DEA (blue). For each current step, data points were colour-coded according to the $p$ values obtained from one-way $t$ test to test whether value is significantly different from 0. Below pyramidal cells plot is a heat map of the $p$ values for pairwise comparison between individual treatments based on MLM.
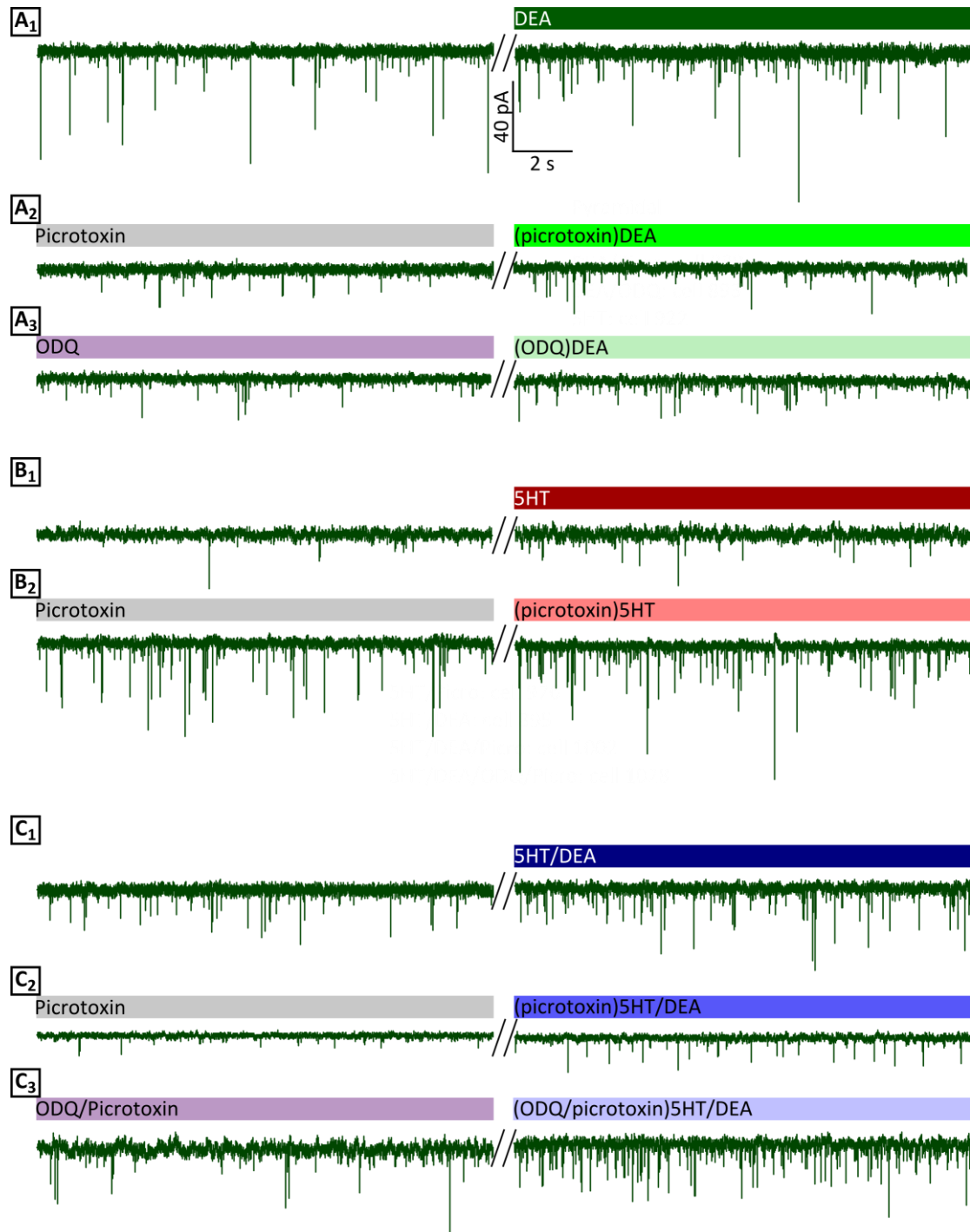
Figure 5-8: Example of traces from pyramidal neurons and the effects of drugs on the frequency of EPSCs. (A1-A3) Sample traces for frequency of EPSCs, comparing control, picrotoxin and ODQ to DEA, with or without the previous drugs. (B1-B2) Sample traces as previously described but for control, picrotoxin and 5HT. (C1-C3) Sample traces for control, picrotoxin, ODQ/picrotoxin and 5HT/DEA.

presence of picrotoxin the spontaneous frequency of EPSCs doesn't vary much from control levels (Figure 5-9B), with the values for pyramidal and slow spiking interneurons in the presence of picrotoxin being similar to control levels. When the prefrontal cortical slices were bathed with 50 µM 5HT, the average frequency of EPSCs increased by 2-3 times for all groups but fast spiking interneurons (Figure 5-9C). For pyramidal neurons the difference was 0.86 ± 0.96 Hz (one-way $t$ test: $p$ = 0.0101, n=12), and for slow spiking interneurons the difference was 1.99 ± 2.09 Hz (one-way $t$ test: $p$ = 0.4080, n=2). Fast spiking interneurons presented a difference of EPSC frequency of only 0.06 ± 0.05 Hz (one-way $t$ test: $p$ = 0.1189, n=4). 5HT in the presence of picrotoxin increased the frequency of EPSCs in a similar way to 5HT alone, with pyramidal neurons showing an increase of EPSCs frequency of 1.13 ± 1.05 Hz (one-way $t$ test: $p$ = 0.0287, n=7) and slow spiking interneurons to 3.20 Hz (one-way $t$ test: $p$ = 0.1939, n=3). The average effects of 5HT on EPSC frequency in the absence and presence of picrotoxin were comparable.

In contrast, the difference in EPSC frequency between 100 µM DEA application and the control period is quite small for all groups, showing that in the presence of DEA there is no increase or decrease in spontaneous network activity in either the pyramidal, fast or slow spiking interneurons (Figure 5-9; one-way t-tests for change in EPSC frequency: $p$ between 0.08 and 0.47). Similarly DEA in the presence of picrotoxin also had no effect on EPSC frequency in pyramidal neurons (one-way $t$ tests: $p$ = 0.2148, n=10; only one record was obtained for a slow spiking interneuron under these conditions that also showed no change. No records were obtained for fast spiking interneurons).The EPSC frequency was increased in the presence of 5HT/DEA for all groups when compared to control levels. Pyramidal neurons showed a difference of 0.76 ± 0.39 Hz (one-way $t$ test: $p$ = 0.0836, n=9), which is a slightly weaker effect than 5HT on its own. However, in the presence of picrotoxin, 5HT/DEA, unlike the increase caused by 5HT alone, failed to increase the EPSC frequency (one-way $t$ test: $p$ = 0.3499, n=12). A direct comparison between the effects of 5HT and 5HT/DEA in the presence of picrotoxin revealed a significant difference (unpaired $t$ test: $p$ = 0.0171).

Perhaps there is some indication of a reduction in the effects of 5HT on EPSC frequency by DEA in slow spiking interneurons as the average change in EPSC
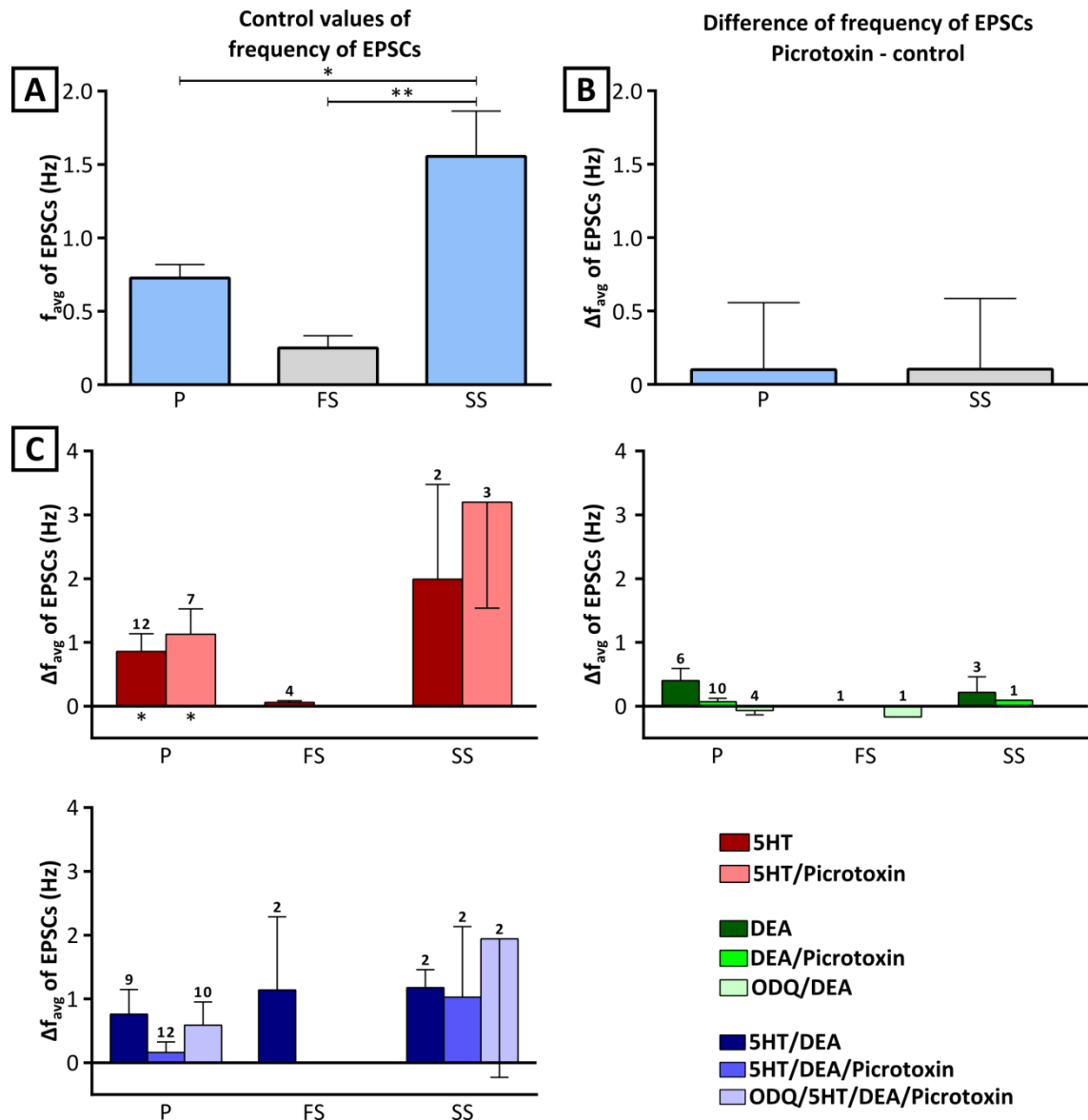
Figure 5-9: Difference of frequency of EPSCs events in the presence of different treatments divided by groups (P = pyramidal cells; FS = fast spiking interneurons; SS = slow spiking interneurons; n numbers showing on top of each column; DMC: * $p$ = 0.0334, ** $p$ = 0.0026). (A) Bar plot showing the average of the baseline frequency of EPSCs. (B) Bar plot showing the difference of frequency of EPSCs when bath perfusion of picrotoxin. (C) Bar plot showing the difference of frequency of EPSCs when bath perfusion of 5HT and (picrotoxin)5HT (red), DEA in the presence of picrotoxin or ODQ (green) and 5HT/DEA in the presence of picrotoxin or (ODQ/picrotoxin) (blue) (one-way $t$ test: * $p<0.05$).

frequency appears to be somewhat lower following 5HT/DEA application compared to 5HT alone. However, the small n number precludes any definite conclusions. In contrast, there is some indication that co-application of 5HT and DEA produces a more pronounced increase in EPSC frequency in fast spiking interneurons, but again the n number is too small to draw any firm conclusions.

The apparent lack of an effect of DEA only on EPSC frequency with or without picrotoxin, when compared to control levels, could be due to opposing effects of the two main NO-activated intracellular signalling pathways (sGC/cGMP dependent and independent). To dissect these effects, the experiments that involved DEA were also repeated in the presence of ODQ. In the presence of (ODQ)DEA, the EPSC frequency showed no change in pyramidal neurons (-0.07 ± 0.13 Hz; one-way $t$ test: $p$ = 0.3851, n=4). However, the observation that ODQ appears to actually block the small increase in EPSC frequency caused by DEA, without revealing a significant sGC/cGMP-independent effect on EPSC frequency in pyramidal neurons argues against the hypothesis that the lack of an effect was due to different signalling pathways having opposing effects of EPSC frequency.

Similar tests were done for 5HT/DEA in the presence of picrotoxin and ODQ. Interestingly, ODQ seemed to abolish, at least partially, the reduction that (picrotoxin)5HT/DEA caused in the EPSC frequency in pyramidal neurons. In the presence of ODQ and picrotoxin, 5HT/DEA caused a more pronounced increase in EPSC frequency in pyramidal neurons (0.59 ± 0.36 Hz; one-way $t$ test: $p$ = 0.139) compared to (picrotoxin)5HT/DEA suggesting the involvement of sGC/cGMP-mediated signalling. Consistent with the previous data that provided no evidence for any effect of DEA on the EPSC frequency in slow spiking interneurons, 5HT/DEA application in the presence of ODQ and picrotoxin had a tendency to increase the EPSC frequency (1.94 ± 3.07 Hz, one-way $t$ test:  $p$ = 0.5352) comparable to 5HT/DEA in the presence of picrotoxin or 5HT alone.

In order to study whether 5HT and/or NO not only affect EPSC frequency, but also EPSC shape, the amplitude and time course of EPSCs was analysed. For this purpose, EPSCs occurring during the last 3 minutes of control were pooled together and

compared to the pooled data during 3 minutes of drug treatments. Distribution and cumulative histogram plots were used for visual comparison of EPSC amplitudes (Figure 5-10) and tau values (Figure 5-11). For the distribution histograms, bins of 10 pA were plotted, starting centering at 5 pA; Kolmogorov-Smirnov (KS) test was used for statistical comparison between the control and drug treated distributions. The data is described in detail for pyramidal neurons and slow spiking interneurons. Data for fast spiking interneurons is also shown, but not described due to the relative low n numbers that made it difficult to draw any firm conclusion from this data.

The analysis showed that DEA shifted the cumulative frequency curve of the amplitudes to the left for pyramidal as well as fast and slow spiking interneurons. This shift was significant for pyramidal cells (KS test: $p<0.0001$) and slow spiking interneurons (KS test: $p<0.0001$), but not for the fast spiking interneurons (KS test: $p = 0.086$; possibly due to the much smaller n number). The average amplitude of the control values was 28.13 ± 0.6 pA for pyramidal neurons, whereas in the presence of DEA it was reduced to 25.93 ± 0.6 pA. For slow spiking interneurons, control values were 32.03 ± 0.9 pA and in the presence of DEA they were 27.9 ± 0.9 pA. Fast spiking interneurons presented a control value of 34.95 ± 2.1 pA, and in the presence of DEA it was 27.69 ± 1.3 pA. The results indicate that while DEA has no apparent effect on the EPSC frequency, it causes a small but significant decrease in the average EPSC amplitude.

Unlike DEA, 5HT caused a subtle but statistically significant (KS test: $p = 0.0016$) right shift in the cumulative EPSC frequency distribution of amplitudes for pyramidal neurons, with the average values of control being 27.2 ± 0.4 pA and following 5HT treatment 28.14 ± 0.2 pA. In contrast, 5HT decreased the average EPSC amplitude in slow spiking interneurons (KS test: $p<0.0001$), while it had no effect on fast spiking interneurons. The average values of slow spiking neurons were 38.35 ± 1.0 pA for control and 31.64 ± 0.6 pA after 5HT, whereas for fast spiking neurons control values were 25.25 ± 1.2 pA and 25.39 ± 0.9 pA in the presence of 5HT.

Interestingly, co-application of 5HT/DEA had no significant effect on EPSC amplitudes in pyramidal neurons, possibly due to the opposing effects of 5HT and DEA on their
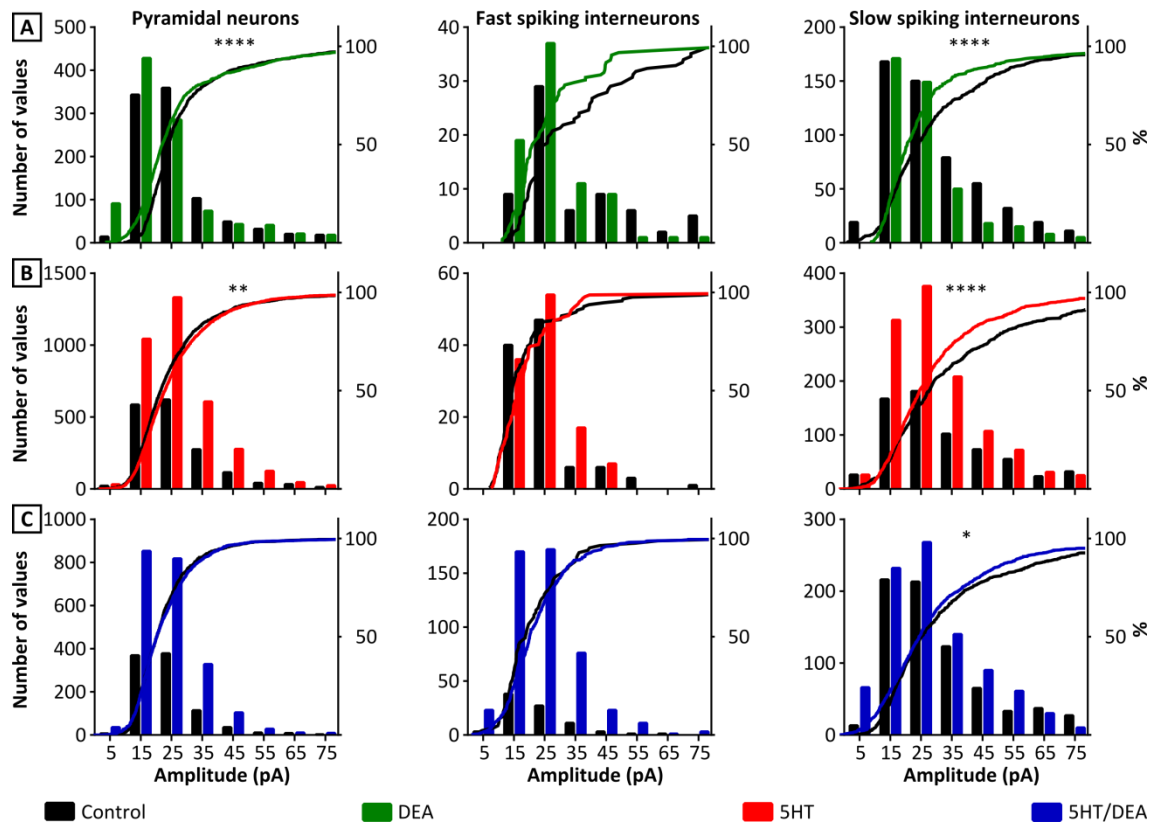
Figure 5-10: Effects of drugs on EPSC amplitude, shown as distribution histograms (bar graph, left y axis) and cumulative frequency plots (lines, right y axis). The events in frequency distribution histograms were binned by 10 pA, centred initially at 5 pA. (A) Modulation of DEA (green), (B) 5HT (red) and (C) 5HT/DEA (blue) on pyramidal neurons, fast spiking and slow spiking-interneurons.

own that might have cancelled each other. In contrast, it caused a weak left shift in the cumulative frequency distribution in slow spiking interneurons. However, this effect appears to be smaller than the effect of either 5HT or DEA alone.

The decay time constant (tau) values of the EPSCs were also analysed in a similar way to the EPSCs amplitude (Figure 5-11). For the distribution histograms, the values were binned by 2 ms and the first bin centred at 1 ms. In the presence of DEA, the curve for cumulative frequency of tau had a significant right shift for pyramidal cells (KS test: $p$ = 0.0094), whereas for slow spiking interneurons this shift was left-wise (KS test: $p$<0.0001). The average tau values for pyramidal neurons were 4.34 ± 0.1 ms under control conditions and 4.72 ± 0.2 ms after DEA application, whereas for slow spiking interneurons the tau values were 10.67 ± 0.3 ms and 7.15 ± 0.3 ms, respectively.

5HT again decreased tau values, which was shown as a left shift of the cumulative frequency. The change appears more pronounced for slow spiking interneurons (KS test: $p$<0.0001) than for pyramidal cells (KS test: $p$ = 0.0009). The averages of tau values for pyramidal neurons were 5.90 ± 0.1 ms under control conditions and 5.68 ± 0.1 ms in the presence of 5HT, whereas for slow spiking neurons they were 7.82 ± 0.2 ms and 6.10 ± 0.2 ms, respectively.

In the presence of 5HT/DEA there was a left shift of the cumulative frequency distribution of tau values for the pyramidal neurons (KS test: $p$ <0.0001) and slow spiking interneurons (KS test: $p$ = 0.0017). The averages of tau values for pyramidal neurons were 6.24 ± 0.1 ms before 5HT/DEA and 5.99 ± 0.1 ms in the presence of 5HT/DEA, whereas for slow spiking interneurons they were 8.85 ± 0.2 ms and 7.67 ± 0.2 ms, respectively.

The effects of DEA and 5HT on tau values appear to be opposite to the effects observed on EPSCs amplitudes in pyramidal neurons, i.e. DEA reduces amplitude but increases tau values, while 5HT causes a small increase in amplitude, but reduces tau values. However, in slow spiking interneurons, both 5HT and DEA cause a decrease in tau and EPSCs amplitude, in a more pronounced way.
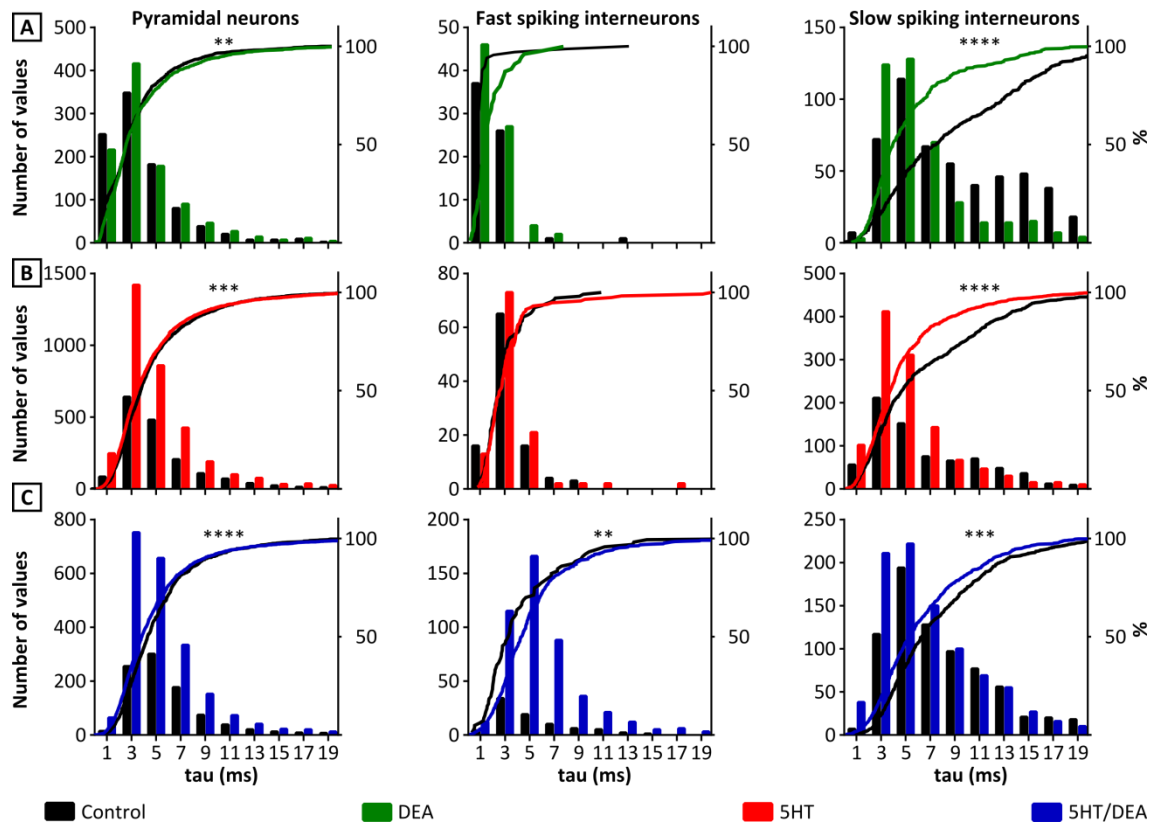
Figure 5-11: Effects of drugs on decay time constant of EPSCs, shown as distribution histograms (bar graph, left y axis) and cumulative frequency plots (lines, right y axis). The events in frequency distribution histograms were binned by 2 ms, centred initially at 1 ms. (A) Modulation of DEA (green), (B) 5HT (red) and (C) 5HT/DEA (blue) on pyramidal neurons and interneurons.

Picrotoxin on its own doesn't affect EPSC amplitude in either pyramidal neurons or slow spiking interneurons (Figure 5-12A). However, picrotoxin appears to abolish the slight left shift in the EPSC amplitude distribution caused by DEA in pyramidal cells (Figure 5-12B). This suggests that the DEA effect on EPSC amplitude is caused indirectly by effects on inhibitory post-synaptic potentials (IPSCs). It is difficult to say whether picrotoxin affects the DEA-induced change in EPSC amplitude in slow spiking interneurons due to the very low number of EPSCs recorded in these cells in the presence of DEA plus picrotoxin (Figure 5-12B).

The effect of 5HT on EPSC amplitude was not really changed by picrotoxin in pyramidal neurons and slow spiking interneurons, but is perhaps a bit more pronounced in slow spiking interneurons (Figure 5-12C). Interestingly, co-application of 5HT/DEA in the presence of picrotoxin caused a marked right-shift in the EPSC amplitude distribution that was not observed in the absence of picrotoxin in pyramidal cells. Picrotoxin also abolished the left-shift in EPSC amplitude (Figure 5-12D) that was observed in slow spiking interneurons after 5HT/DEA application. This suggests that 5HT and DEA can interact to enhance EPSC amplitudes, and that this effect might be counteracted by a simultaneous enhancement of IPSC amplitudes in the absence of picrotoxin.

Picrotoxin on its own appears to have some very subtle but significant effects on EPSC decay time constants (KS test: $p<0.01$; Figure 5-13A). This is consistent with the idea that EPSCs and IPSCs are highly co-ordinated - so removing one should affect the time course of the other. Interestingly, the effects of DEA on the time course of both pyramidal and especially slow spiking interneurons are abolished in the presence of picrotoxin, which suggests that DEA on its own affects predominantly IPSCs, and that the effect of DEA on EPSC tau values was indirect (Figure 5-13B). In contrast, 5HT in the presence of picrotoxin produces a considerably larger left shift in tau values compared to the effect of 5HT without picrotoxin, while the 5HT effect on EPSC tau values in slow spiking interneurons is less pronounced in the presence of 5HT (Figure 5-13C).

The effect of 5HT on the tau distribution in pyramidal neurons appears to be markedly altered by co-application of DEA in the presence of picrotoxin, which suggests that DEA can modulate the effects of 5HT on the EPSC decay time constant. In slow spiking
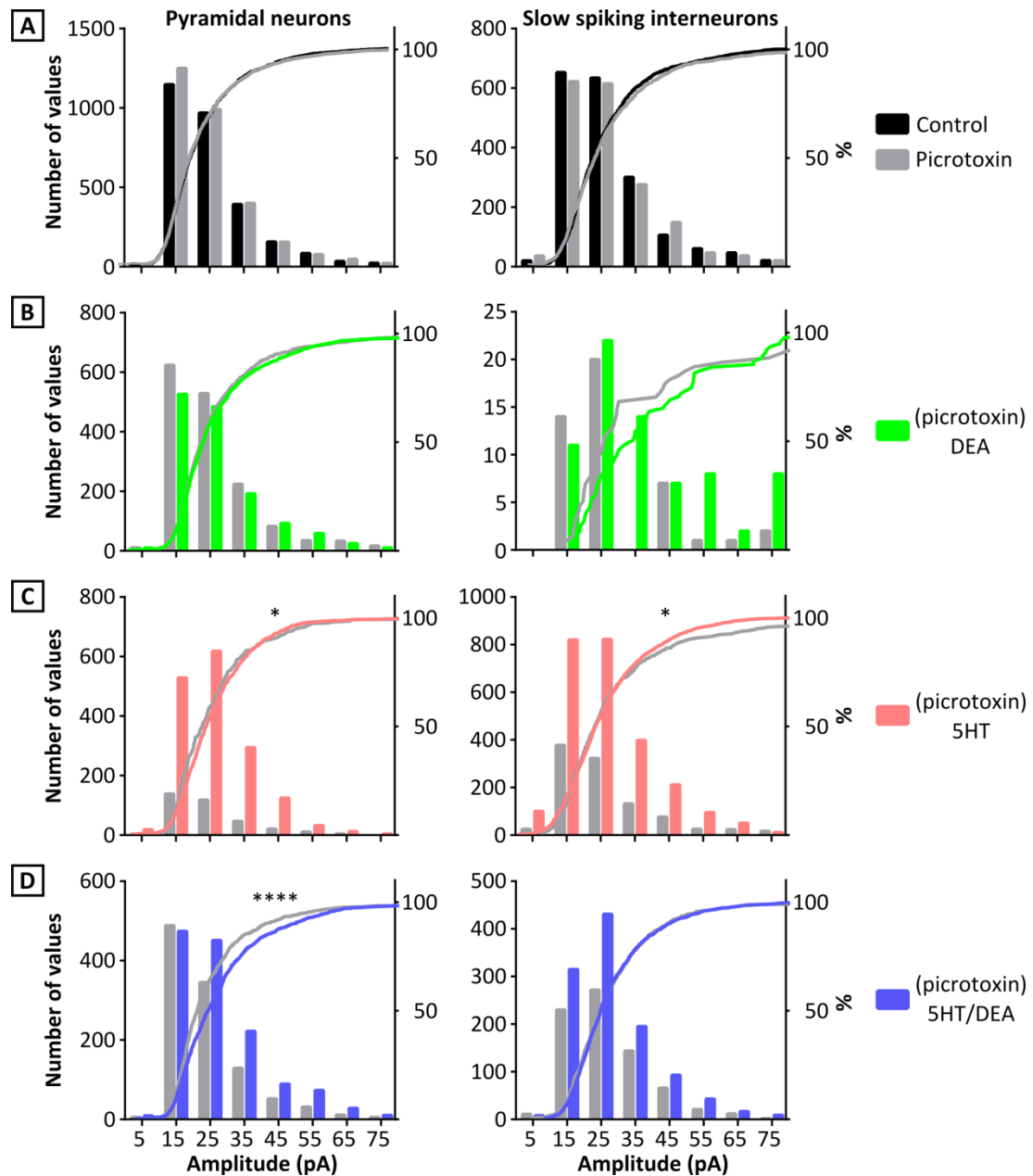
Figure 5-12: Effects of picrotoxin on amplitude of EPSCs, shown as distribution (bar graph, right y axis) and cumulative histograms (lines, left y axis). (A) Comparison of modulation of picrotoxin (gray) against control (black) for pyramidal neurons and slow spiking interneurons. (B) Comparison of picrotoxin (gray) against (picrotoxin)DEA (green). (C) Comparison of picrotoxin against (picrotoxin)5HT (red). (D) Comparison of picrotoxin against (picrotoxin)5HT/DEA (blue). KS test was done on the cumulative frequency distribution (* $p$ = 0.05, **** $p$<0.0001).
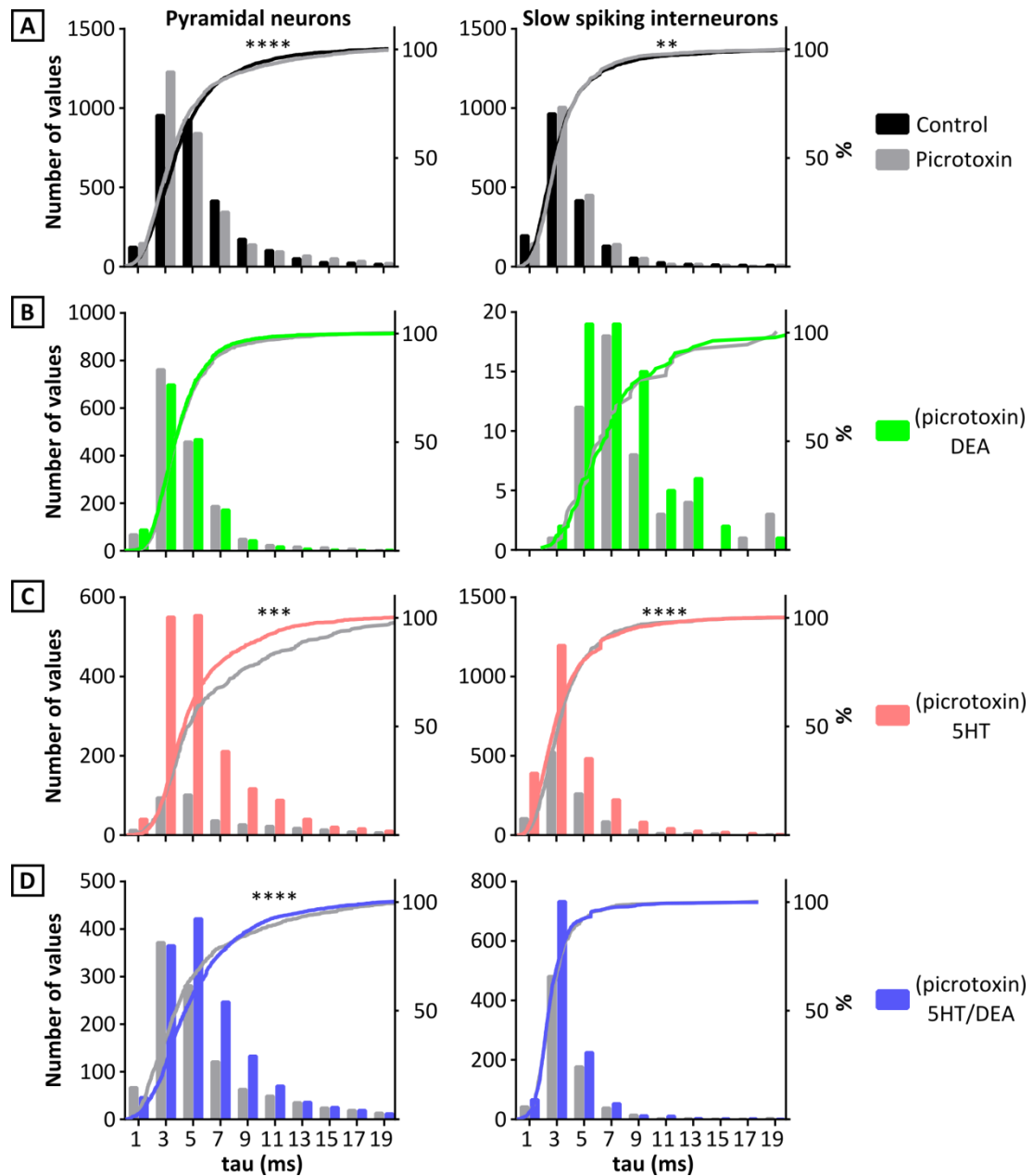
Figure 5-13: Effects of picrotoxin on tau values of EPSCs, shown as distribution (bar graph, right y axis) and cumulative histograms (lines, left y axis). (A) Comparison of modulation of picrotoxin (gray) against control (black) for pyramidal neurons and slow spiking interneurons. (B) Comparison of picrotoxin (gray) against (picrotoxin)DEA (green). (C) Comparison of picrotoxin against (picrotoxin)5HT (red). (D) Comparison of picrotoxin against (picrotoxin)5HT/DEA (blue). KS test was done on the cumulative frequency distribution (* $p = 0.05$, **** $p<0.0001$).

interneurons the less pronounced effect of 5HT on the EPSCs tau values is reduced even further in the presence of DEA, which suggests that DEA would be acting on the 5HT effect on slow spiking interneurons EPSCs tau values (Figure 5-13D).

Like picrotoxin on its own, ODQ (plus picrotoxin) does not appear to affect EPSC amplitude distribution (Figure 5-14A) in pyramidal and slow spiking interneurons compared to control, but it appears to affect EPSC decay time constants (Figure 5-15A). The effects look different to the effects of picrotoxin on its own suggesting that they are not due to blocking inhibitory interactions, but direct effects of ODQ on EPSC time constants.

In pyramidal neurons ODQ (plus picrotoxin) alters the effect of 5HT/DEA on the EPSC amplitude (Figure 5-14B) and decay time constant (Figure 5-15B) distribution observed in presence of picrotoxin. Generally, the effects of 5HT/DEA in the presence of ODQ are less pronounced suggesting that the interaction between 5HT and DEA is mediated by the sGC/cGMP pathway. In contrast, 5HT/DEA co-application in slow spiking interneurons in the presence of ODQ and picrotoxin has stronger effects on the EPSC amplitude and tau distribution compared to just in the presence of picrotoxin. This indicates that both sGC/cGMP-dependent and –independent signalling pathways mediate interactions between 5HT and NO in modulating EPSCs in slow spiking interneurons. Furthermore, it suggests that cGMP-dependent and independent pathways have opposing effects on EPSCs.

## 5.5 Serotonin acts through $5HT_2$ receptor type in the network

The results described above suggest that NO suppresses the 5HT induced increase in spontaneous EPSC activity in the prefrontal cortical network through sGC/cGMP mediated signalling. A more detailed picture of the serotonergic signalling pathways would help in understanding the actions of 5HT and potential mechanisms of interaction in the prefrontal cortex. As previously described, it has been reported that many serotonergic receptors are present in the cortical neurons. Two of these receptors that are abundantly expressed are $5HT_1$ and $5HT_2$. In order to assess the
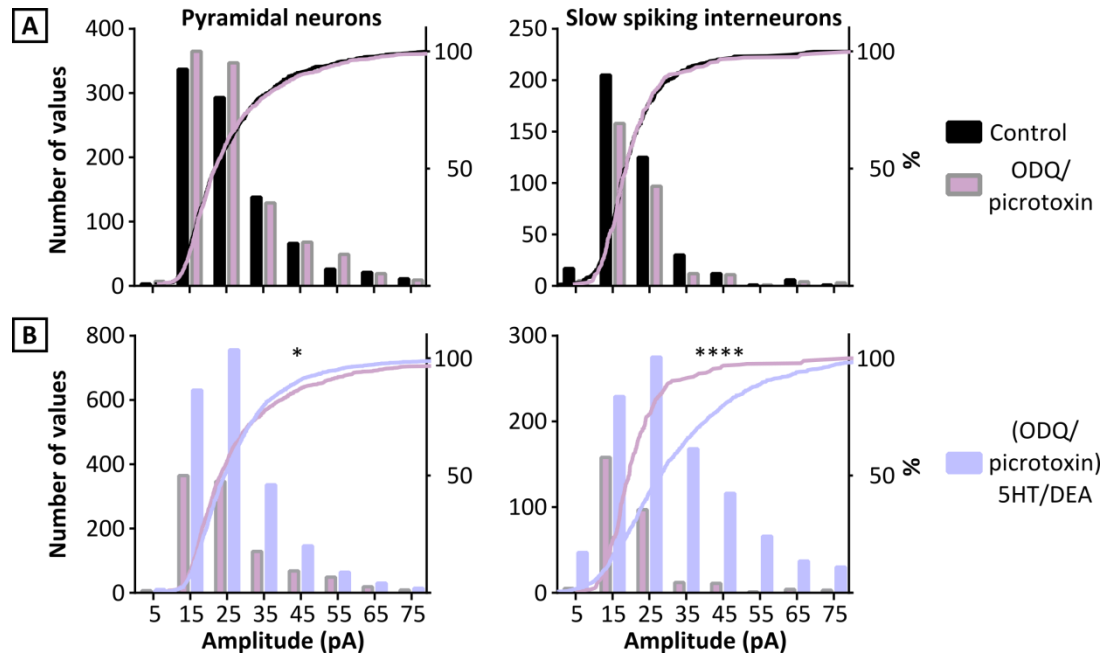
Figure 5-14: Effects of ODQ/picrotoxin on amplitude of EPSCs, shown as distribution (bar graph, right y axis) and cumulative histograms (lines, left y axis). (A) Comparison of modulation of ODQ/picrotoxin (gray box with purple filling) against control (black) for pyramidal neurons and slow spiking interneurons. (B) Comparison of ODQ/picrotoxin (gray box with purple filling) against (ODQ/picrotoxin)5HT/DEA (blue). KS test was done on the cumulative frequency distribution (* $p$ = 0.05, **** $p<0.0001$).
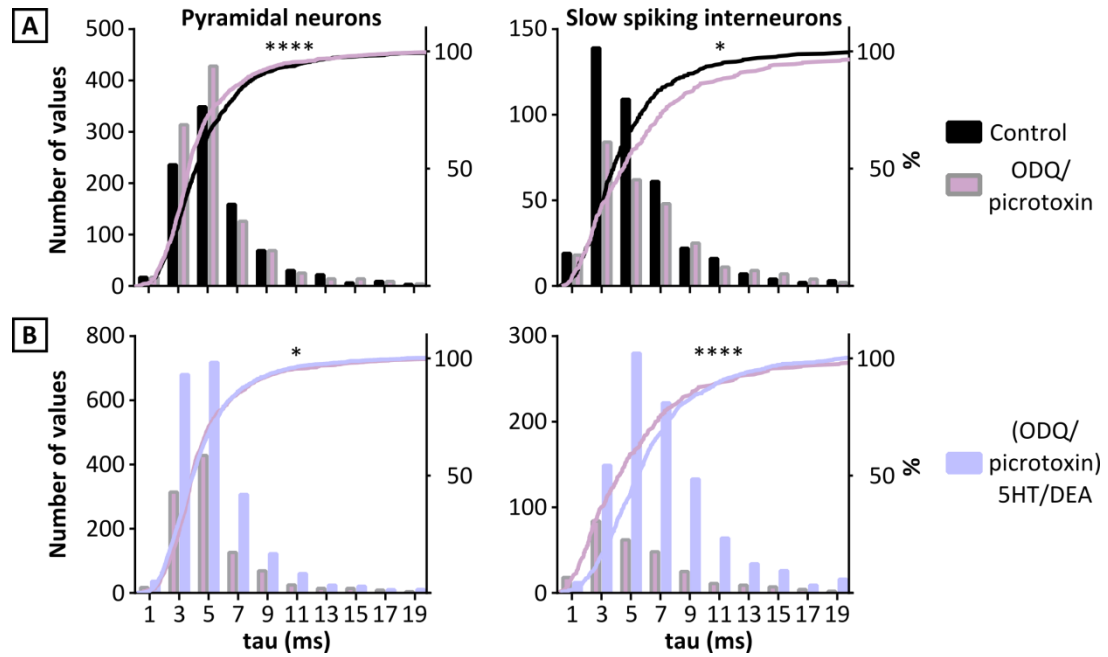
Figure 5-15: Effects of ODQ/picrotoxin on tau values of EPSCs, shown as distribution (bar graph, right y axis) and cumulative histograms (lines, left y axis). (A) Comparison of modulation of ODQ/picrotoxin (gray box with purple filling) against control (black) for pyramidal neurons and slow spiking interneurons. (B) Comparison of ODQ/picrotoxin (gray box with purple filling) against (ODQ/picrotoxin)5HT/DEA (blue). KS test was done on the cumulative frequency distribution (* $p$ = 0.05, **** $p$<0.0001).

potential roles of these receptor types, the $5HT_1$ agonist (R)-(+)-8-Hydroxy-DPAT hydrobromide (8-OH-DPAT) and the $5HT_2$ agonist α-methyl-5-hydroxytryptamine (αMe5HT) alone or in combination were applied by bath perfusion onto the intact tissue slice. These experiments were conducted in the presence of picrotoxin. Sample records of the experiments demonstrating the changes in the frequency of EPSCs in pyramidal neurons are shown in Figure 5-16. In these sample records, the application of αMe5HT produced a marked increase in the number of EPSCs (Figure $5-17A_1$), whereas together with 8-OH-DPAT the number of EPSCs increased only slightly (Figure $5-17A_2$). Similarly, αMe5HT co-applied with DEA alone (Figure $5-17B_1$) or in combination with 8-OH-DPAT (Figure $5-17B_2$) resulted in only modest increases in the number of EPSCs.

When αMe5HT was applied together with picrotoxin, there was an average increase in the frequency of EPSCs for both pyramidal by $1.40 \pm 3.0$ Hz (n=5), and slow spiking neurons by $3.48 \pm 2.2$ Hz (n=2). Co-application of 5HT with DEA, however, reduced the increase in EPSC frequency in pyramidal neurons to $0.77 \pm 1.3$ Hz (n=7; Figure 5-17A). Co-application of αMe5HT and 8-OH-DPAT also resulted, for both pyramidal and slow spiking interneurons in a marked reduction in the αMe5HT-induced increase in EPSC frequency. The average increase in pyramidal neurons was only $0.31 \pm 0.2$ Hz (n=2) and 0.5 Hz (n=1) for slow spiking interneurons. This increase was similar when both $5HT_1$ and $5HT_2$ agonists were co-applied with DEA in pyramidal neurons ($0.27 \pm 0.3$ Hz, n=2). None of the changes in EPSC frequency observed in the presence of the various drugs were significantly different from zero (one-sample t test, p>0.17). This is probably due to the relatively small n number and considerable variability between individual cells.

The amplitude and time course of the EPSCs in these experiments was also analysed as described previously (Figure 5-17B). In the presence of αMe5HT, the distribution of EPSC amplitudes in pyramidal cells was shifted to the right (i.e. increased) for all treatments tested. Similarly, EPSC amplitudes were significantly increased in slow spiking interneurons by αMe5HT or αMe5HT plus 8-OH-DPAT application.

In contrast to the EPSC amplitude, in pyramidal neurons the decay time constant of the EPSCs was only significantly increased by the application of αMe5HT in the presence of
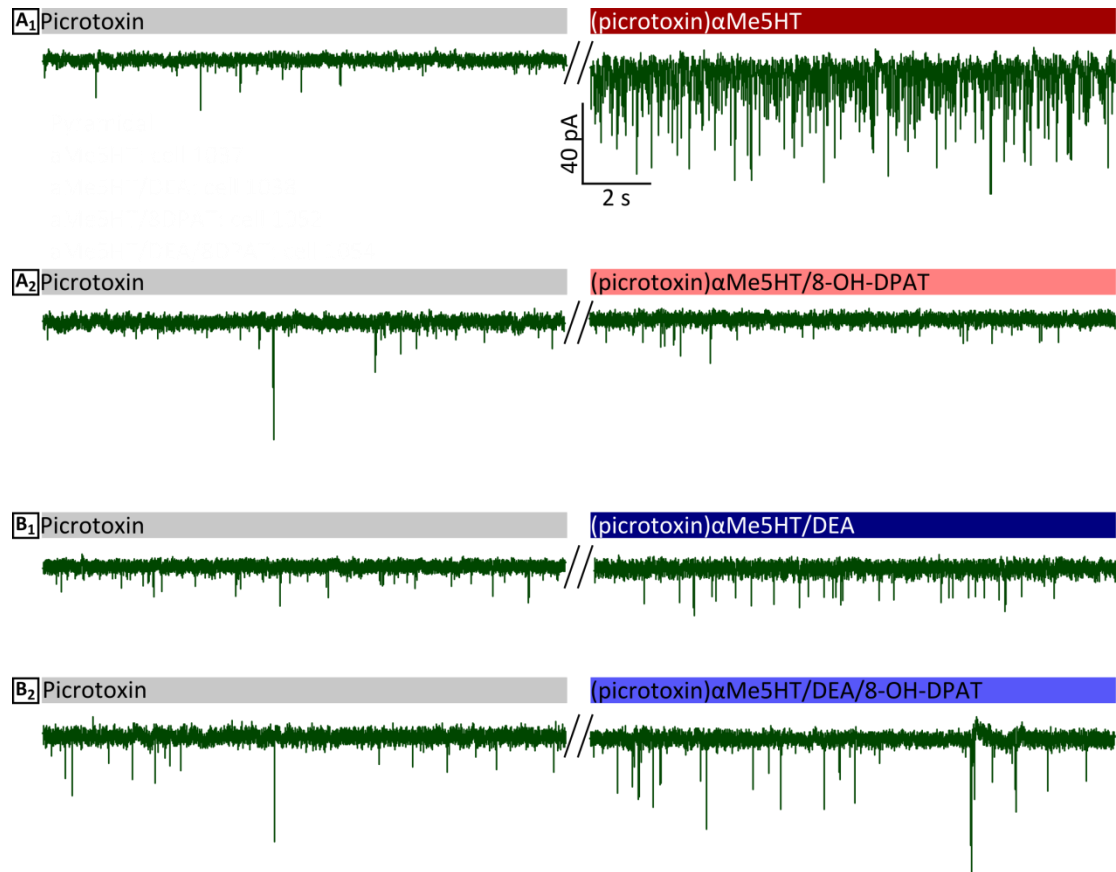
Figure 5-16: Example records from pyramidal neurons and the effects of drugs on the frequency and shape of EPSCs. (A1-A2) Sample traces of voltage clamp recordings, comparing EPSCs in the presence of picrotoxin to the ones in the presence of αMe5HT or αMe5HT/8-OH-DPAT. (B1-B2) Sample traces comparing EPSCs in the presence of picrotoxin to the ones in the presence of αMe5HT/DEA or αMe5HT/8-OH-DPAT/DEA.
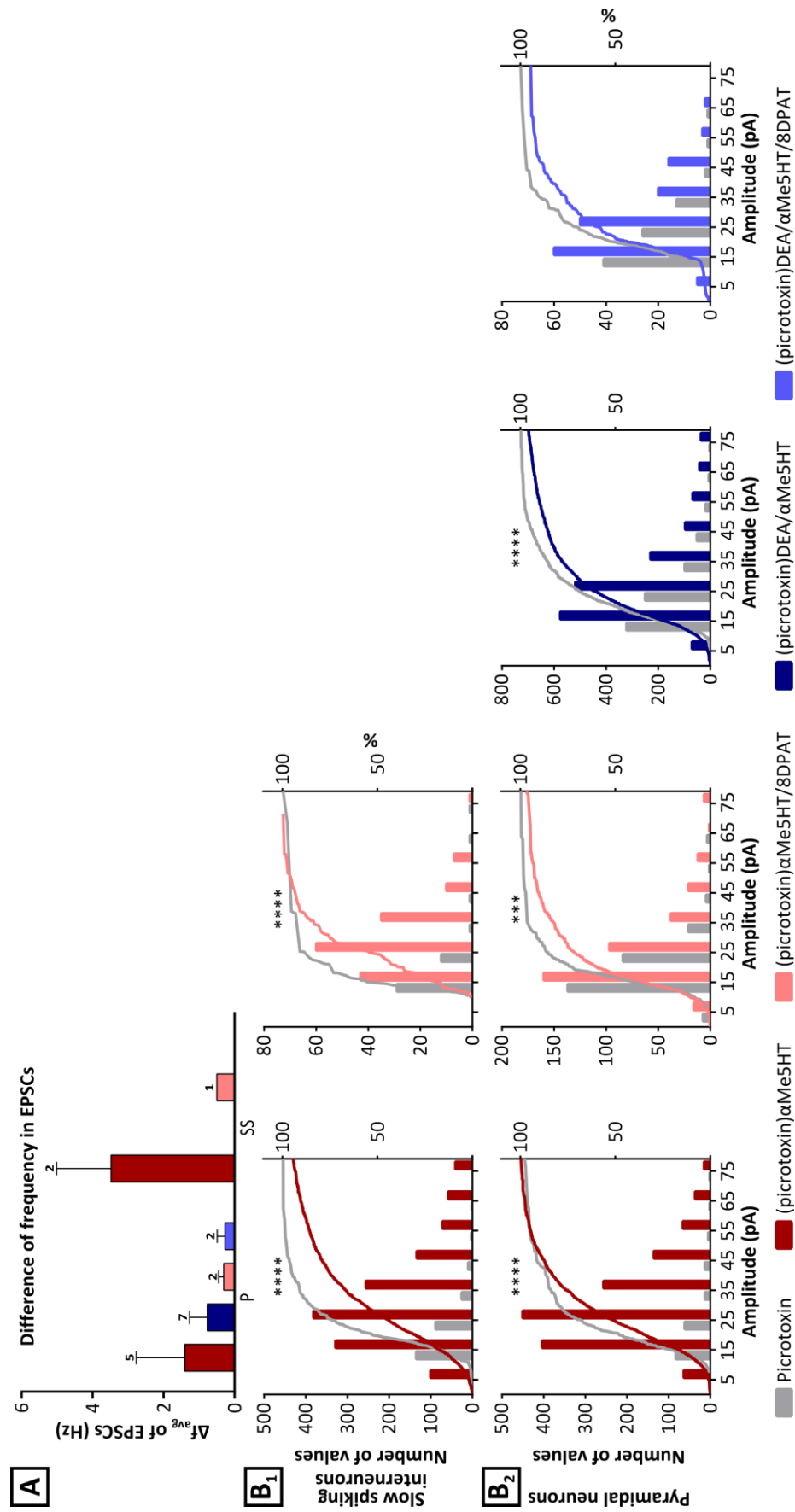
Figure 5-17: Effects of αMe5HT and 8-OH-DPAT on difference of frequency of EPSCs and on amplitude of EPSCs, shown as distribution (bar graph, right y axis) and cumulative histograms (lines, left y axis), all in the presence of picrotoxin (grey). (A) Modulation of αMe5HT (dark red) and αMe5HT/8-OH-DPAT (light red), with or without co-application of DEA (dark and light blues), on the frequency of EPSCs. (B1) Modulation of the response by the agonists with or without DEA, on slow spiking interneurons and pyramidal neurons (B2).
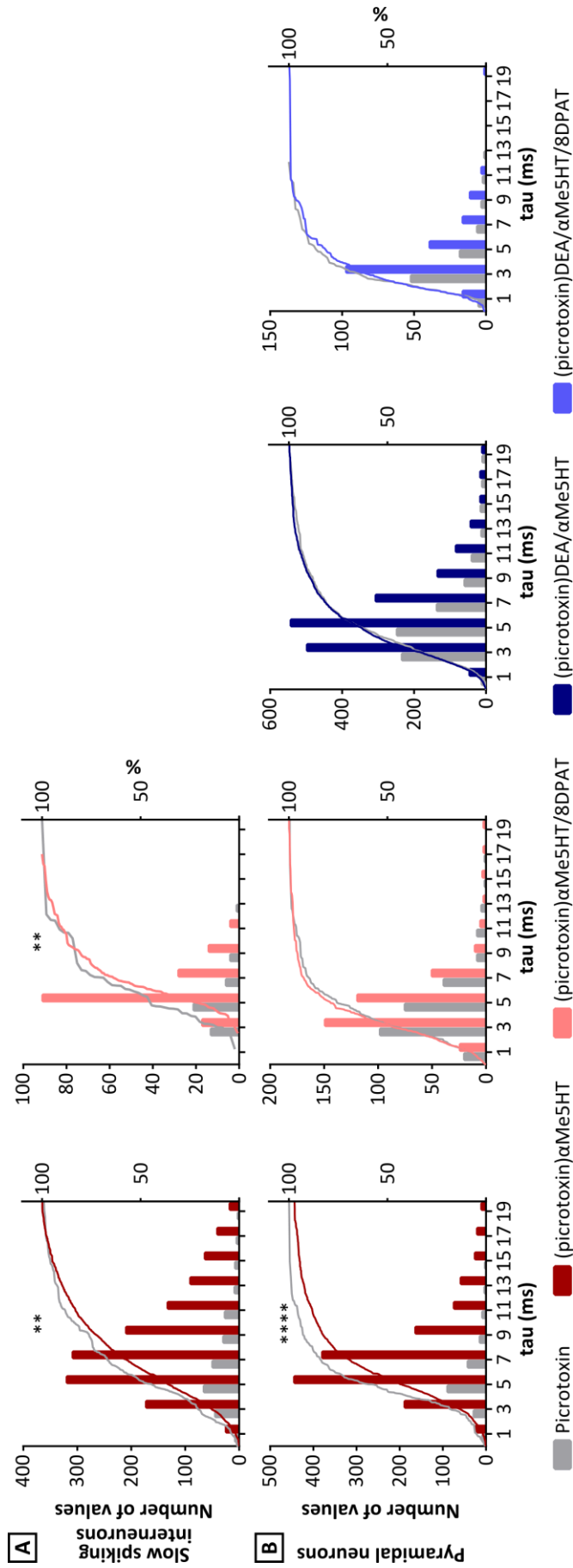
Figure 5-18: Effects of αMe5HT and 8-OH-DPAT on tau values of EPSCs, shown as distribution (bar graph, right y axis) and cumulative histograms (lines, left y axis), in the presence of picrotoxin (grey). (A) Modulation of the response by αMe5HT (dark red) and αMe5HT/8-OH-DPAT (light red), with or without DEA (dark and light blues), on slow spiking interneurons and pyramidal neurons (B).

picrotoxin, but not when αMe5HT was co-applied with either 8-OH-DPAT, DEA or both (Figure 5-18A, B). A slightly less prominent increase in the EPSC decay time constant was observed in slow spiking interneurons in the presence of αMe5HT (KS test: $p$ = 0.0044). This increase persisted when αMe5HT and 8-OH-DPAT were co-applied.

## 5.6 Discussion

It is possible to divide the prefrontal cortical neurons into two main groups: the principal, pyramidal neurons, and the interneurons, on the basis of their firing characteristics. These neurons can also be classified into fast spiking interneurons or regular spiking principal neurons on the basis of global gene expression (Subkhankulova et al. 2010). Their work, using data obtained from previously identified fast or regular spiking neurons, lead to the clustering of two major groups with the use of unsupervised hierarchical clustering algorithms.

Based on morphology alone, pyramidal neurons from layers II/III could be classified in one single group (Larkman & Mason 1990). However, in the medial prefrontal cortex from Wistar rats, it has been shown that, after using unsupervised clustering analysis based on various morphological and electrophysiological parameters, layer II has one type of pyramidal neuron whereas layer III pyramidal neurons can be subdivided into four different classes (Aerde & Feldmeyer 2013). Similarly, *in vivo* electrophysiology enabled the classification of pyramidal neurons into two groups in Sprague-Dawley rats, either regular spiking or burst spiking neurons (Dégenètais et al. 2002). In monkey pyramidal neurons from the same layer, however, it appears that they can be classified into three different groups, regular spiking, low threshold spiking and an intermediate firing pattern (Zaitsev et al. 2012).

It was previously reported that in young Wistar rats there are many electrophysiologically different interneurons located in layers II/III (Kawaguchi 1995). From the sets mentioned in that work, there are similarities to groups obtained from the clustering algorithm used in this project. The so-called fast spiking interneurons are similar to the types 1 and 2 recorded, with constant-rate repetitive firing throughout

higher positive injected current steps. However, their work was based on rate and times of APs firing, plus morphological properties such as branching of dendrites and axons.

In this current work, using *k*-Means unsupervised clustering algorithm with parameters obtained from whole-cell patch clamp recordings in current clamp mode, seven different groups of cells were identified in the prefrontal cortex layers II/III from Wistar rats aged 14-20 days old. From the seven groups, two groups showed quite similar behaviours and were assigned to fast spiking interneurons due to their high number of APs elicited in response to positive current steps. Three other groups were believed to be pyramidal neurons, whereas the last two groups were similar to slow spiking interneurons. The pyramidal neurons in this work presented regular spiking, with the number of APs elicited at the higher current steps, the ISI and input resistance quite similar to the ones observed in previous studies (Kawaguchi 1993; Moyer et al. 2002; Zaitsev et al. 2012).

The identification of more than one group for fast spiking interneurons and more than one group for pyramidal neurons could be explained due to the use of multiple parameters, including hyperpolarizing sag, amplitude of membrane potential at 200 pA, and spike height adaptation, a few examples of parameters that were not used in any prefrontal cortical neuron classification before. The previously described studies that used electrophysiology for classifying neuron types used mostly the frequency of APs and the ISI of specific pairs of APs. This could lead to a masking of the neuronal behaviour in the presence of any drug, since grouping different classes of neurons might reduce the real effects on each cluster. However, in this study there was an appearance of two groups of pyramidal neurons that shared similar IV relationships and excitability plots. This could be due to the choice of k numbers. If it were one too many, than the clustering algorithm could have artificially split a larger cluster into two subtypes.

The clustering algorithm used in this work resulted in seven different groups that when compared to the clusters observed in cell culture showed some similarities in their excitability and IV plots. The similarities and differences between the cell types in cell

culture and acute cortical slices will be discussed in detail in the overall discussion at the end of the thesis.

The changes in intrinsic properties of the neurons in the prefrontal cortex when 5HT or DEA were applied could lead to a modulation of excitatory synaptic inputs to PFC neurons and the overall PFC network activity. It's been previously shown that application of 5HT increases the frequency and amplitude of EPSCs in layer V (Aghajanian & Marek 1997) and the deeper parts of the layers II/III (Lambe et al. 2000) in the prefrontal cortex. Here we demonstrated that 5HT increased the frequency of EPSCs in almost all types of prefrontal cortical neurons identified with the clustering algorithm.

This 5HT increase of frequency of EPSCs was not modulated by the application of DEA. It has been reported previously that NO can potentiate the inhibitory frequency, but not amplitude, of postsynaptic potentials in the thalamus (Yang & Cox 2007). Glucocorticoid enhancement of IPSCs in the hippocampus and in the prefrontal cortex is also mediated by retrograde NO signalling (Hu et al. 2010; Teng et al. 2013). On the other hand, NO can also enhance the N-methyl-D-aspartate (NMDA) component of the corticogeniculate EPSCs (Alexander et al. 2006). In this project, the co-application of DEA with 5HT appeared to reduce the increase in EPSC frequency compared to the application of 5HT alone. However, this effect of DEA was most pronounced in the presence of picrotoxin, which makes it unlikely that the effect is mediated by DEA actions on IPSCs. Instead, it suggests that DEA can directly reduce the excitatory effect of 5HT. Blocking NO sGC/cGMP signalling with ODQ (in the presence of picrotoxin), appears to be able to restore the ability of 5HT/DEA application to increase the EPSC frequency. This strongly suggests a modulatory interaction between 5HT and NO. The fact that the interaction between the two neuromodulators can only be observed when the inhibitory part of the network is blocked suggests that 5HT and DEA may also interact in the modulation of IPSCs that counteract the effects on EPSPs. This could be part of the cortical mechanism that maintains the relationship between inhibitory and excitatory network inputs in pyramidal neurons (Haider & McCormick 2009; Xue et al. 2014). DEA also increases the amplitude of EPSCs while in the presence of 5HT and picrotoxin. Therefore, DEA, in the presence of 5HT and picrotoxin would reduce the

5HT-induced increase in EPSC frequency, but at the same time increase the amplitude of the remaining EPSCs. This is also reflected by the fact that the decay times of these events were also increased. This DEA modulation of the effects of 5HT on EPSCs is mainly through sGC/cGMP pathway.

With the mechanisms that DEA modulates the effects of 5HT on the network partially resolved, there remains the question of which serotonergic receptors are responsible for the modulation of 5HT in the synaptic inputs. The prefrontal cortex is enriched with $5HT_1$ and $5HT_2$ receptors (Pompeiano et al. 1992; Pompeiano et al. 1994). The fact that application of a $5HT_2$ agonist can mimic the enhancement in EPSC frequency and amplitude produced by 5HT in pyramidal neurons and slow spiking interneurons strongly suggests that this effect is predominantly mediated by $5HT_2$ receptors. This is consistent with a wide-range of studies that have demonstrated excitatory effects of $5HT_2$ receptors (Aghajanian & Marek 1997; Zhang & Arsenault 2005; Araneda & Andrade 1991; Béïque et al. 2007; Béïque et al. 2004; Zhong & Yan 2011). In the presence of the $5HT_2$ agonist and DEA, the increase in EPSC frequencies in pyramidal neurons appears somewhat reduced, suggesting that NO can modulate $5HT_2$ mediate responses. On the other hand, co-application of $5HT_1$ and $5HT_2$ receptors agonists dramatically decreased the changes in the EPSCs frequencies. This observation is generally consistent with the inhibitory role associated with $5HT_1$ receptor activation (Araneda & Andrade 1991; Béïque et al. 2004; Zhong & Yan 2011). Interestingly, application of the $5HT_1$ agonist together with DEA and the $5HT_2$ agonist completely masks any effects of DEA on the $5HT_2$ receptor mediated increase in EPSC frequency. This could be due to NO acting by modulating $5HT_1$ receptor function. However, it has been reported that 8-OH-DPAT has a slightly higher affinity to $5HT_{1A}$ receptors than 5HT (Noël et al. 2014), which could result in more efficient activation with less possibility for modulation by NO. $5HT_1$ receptors have also been reported to exist in either a low or high affinity state (Clawges et al. 1997; Watson et al. 2000), which could be a target for NO modulation. Alternatively, NO and $5HT_1$ receptor signalling could both independently reduce cAMP concentrations; $5HT_1$ receptors via their inhibition of adenylate cyclase activity and NO via the activation of a cGMP-stimulated phosphodiesterase (e.g. PDE2).

In this chapter it is demonstrated that results obtained from cultured cortical neurons show similarities to records obtained from intact prefrontal cortical tissue. The clustering algorithm previously used to group cultured cortical neurons also demonstrated seven different types of neurons from the prefrontal cortex. Similar to cortical cultures, 5HT and NO can modulate various intrinsic parameters in these cell types that affect their excitability and firing properties. At the network level, 5HT increases the frequency of spontaneous synaptic inputs in the prefrontal cortex, whereas NO doesn't. However, after blocking the inhibitory synaptic connections within the prefrontal cortex, NO modulates the 5HT-induced increase of synaptic events through a sGC/cGMP pathway.

## 6 General discussion

In the current study, interactions between the neuromodulators serotonin (5HT) and nitric oxide (NO) in the modulation of various intrinsic membrane properties of cortical neurons were investigated in dissociated cell cultures and the neocortical layered network in acute brain slices. The two complementary approaches enabled direct comparisons between cellular properties and modulatory effects in cell culture and slices. The identification of specific effects was aided by the classification of the recorded cortical cells into specific groups with similar electrophysiological parameters using clustering analysis.

The data obtained in this work provides evidence for some conservation of cellular properties in cell culture. It also shows that 5HT and NO exerted specific effects on individual cellular properties, and the results indicated interactions between 5HT and NO in the modulation of some specific individual parameters. These interactions could be characterised in several ways: application of one neuromodulatory reducing the effects observed in the presence of the other; both 5HT and NO could have similar independent effects; summation of the effects observed with either 5HT or NO; or the interaction between 5HT and NO were required to cause an effect. Interaction between the two neuromodulators also alters how 5HT affects cortical network activity, reducing the increase in excitatory post-synaptic current (EPSC) frequency caused by 5HT in the presence of picrotoxin.

In short, this study presented:

- An overview of the variability of cultured cortical neurons by:
  - Comparing the spontaneous activity of cultured cortical neurons and its diverse modulation by 5HT and NO;
  - Demonstrating the variability in the NO and 5HT modulation of glutamate-elicited responses (e.g. number of APs);
- Various clustering algorithms methods for the grouping of cortical neurons into distinct cell types based on electrophysiological and morphological parameters; following careful evaluation, *k*-Means clustering using a set of ten parameters was judged to provide the best clustering technique;

- Data showing the specific modulation of various electrophysiological parameters including excitability and IV relationships by NO and 5HT in distinct cortical cell types based on their classification using *k*-Means clustering;

- Pharmacological data aimed at identifying the NO signalling pathways that mediate the modulatory effects on the electrophysiological properties of the different groups of cultured cortical neurons;

- Evidence that 5HT causes a depolarisation in a subset of cultured cortical neurons due to the action of $5HT_3$ receptors;

- Data to shows that various cell types present in layer II/III of the prefrontal cortex present similar electrophysiological characteristics to specific groups of cultured cortical neutrons;

- Data to show the modulation by NO and 5HT of various electrophysiological parameters (including excitability and IV relationships) in defined pyramidal neurons located in layer II/III of the prefrontal cortex;

- Evidence for the modulation of spontaneous synaptic activity recorded in neurons in layer II/III by NO and 5HT in prefrontal cortical slices:
  - NO alone had no effect on spontaneous EPSC frequency, whereas 5HT, through $5HT_2$ receptors, increased the activity;
  - NO application in the presence of picrotoxin suppressed the increase in EPSC frequency produced by 5HT;
  - The NO-induced reduction in EPSC frequency was accompanied by an increase in the amplitude and longer tau values of EPSCs.

## 6.1 How do the electrical properties of cultured cortical neurons compare to neurons recorded in cortical slices?

Use of the unsupervised *k*-Means clustering algorithm based on a set of ten electrophysiological parameters resulted in the classification of neurons recorded in the deeper regions of layers II/III of the prefrontal cortex into seven different types. The *k*-Means algorithm performed better than other clustering algorithms in the current work, especially when considering the intrinsic excitability of the cells. It does

not follow that this algorithm would be the best option for all applications, and it is recommended to evaluate various algorithms for a specific application as discussed in more detail in chapter 3. One of the disadvantages of *k*-Means clustering is the necessity of choosing the k number for clusters. While certain principles can be used to guide this decision, it is a somewhat arbitrary decision. An alternative approach is the affinity propagation method, which is based on the concept of 'passing messages' between data points. This algorithm has the advantage that it does not require a predetermined number of clusters. It also produces exemplars, representatives of each cluster that are part of the data points, which are similar to the centroids found in *k*-Means clustering (Frey & Dueck 2007). When used on a database of cortical interneurons, affinity propagation performed better than Ward's method (Santana et al. 2013) in separating four different types of interneurons. However, Santana et al. compared their results to a previous classification of these neurons, and used this comparison as a measure of accuracy for the clustering algorithms. Without *a priori* knowledge of the types of cells, the number of clusters would have been higher than expected. Thus, affinity propagation appears to provide overestimates for the number of distinct cell types. Regardless, it seems that depending on the parameters used and the specific task, some clustering algorithms can work better than others (Vlasblom & Wodak 2009).

Based on results of the clustering, it was possible to compare the excitability and general firing behaviour of the seven clusters identified in cortical slices to the ten distinct clusters observed in cultured cortical neurons. With some notable exceptions, the majority of excitability plots and current-voltage (IV) relationships recorded in cell culture for specific types of cells could be matched to similar cell types recorded in acute slices. The exceptions are the two cell types identified in cortical cultures that show a progressive reduction in the number of action potentials (APs) elicited with increasing current pulses due to AP failure. The lack of cells with equivalent behaviours suggests that this behaviour is a culture artefact and could be either a sign of immaturity (Zhang 2004) or compromised cell health. Two groups of cells identified in slices showed similar properties to a single group in cell culture. Conversely, putative fast spiking interneurons in cell culture were divided into two distinct types, while

there was only a single equivalent cell type in acute slices. This could be due to the apparently slightly higher variability of the neurons recorded in cell culture, which may have led to splitting of certain clusters, while other clusters were fused together into a major cluster.

Nevertheless, type 1 and 2 cells in cultured cortical neurons possess similar characteristics to fast spiking interneurons according to the Petilla terminology (Ascoli et al. 2008). Besides the high number of APs elicited in response to positive current steps, they have the briefest APs and large after-hyperpolarisations when compared to other types of cells (Ascoli et al. 2008). The fast firing rates and the brevity of APs are also features shared with the neurons from type 1 in slices, which have also been labelled as fast spiking interneurons.

The number of APs elicited at the various positive current steps observed in slices is higher than that observed in cell culture for fast spiking interneurons. In both models input resistance ($I_r$) is quite similar although the rheobase is higher in cell cultures than in slices, as is the membrane potential amplitude at 200 pA. Interestingly, fast spiking interneurons in slices present a more pronounced sag ($I_h$) at -140 pA and a less pronounced spike height adaptation when compared to equivalent cultured cortical neurons. The values for minimum inter-spike interval (ISI), proportion of minimum over maximum ISI at 200 pA, and spike burst pattern are similar in the two preparations, along with the IV relationships, especially for negative current steps.

In this work, cell types 7, 8 and 10 in cell culture and their counterparts in slices have been labelled as 'slow spiking interneurons'. Their relationship to previous descriptions in the literature of cortical cell types is less well defined (Ascoli et al. 2008), however, there are some hints that they could correspond to interneurons that have been described as 'irregular spiking' (Markram et al. 2004). The records also show some resemblance to records of Martinotti cells (Klostermann & Wahle 1999). The difficulty of directly comparing the data presented in this study to published characterisations of cortical neurons is due to the relatively narrow current range used in this work (only up to 200 pA), whilst published characterisations of neuron types report current injections of up to 2 nA (Helm et al. 2013; Karagiannis et al. 2009; Oswald et al. 2013;

Chen et al. 1996; Dégenètais et al. 2002). The limited current range was chosen based on results in cell culture that showed the firing rate of some neurons appeared to saturate at the current levels used, and that higher levels of current injections could be detrimental to the health of the cells. For consistency, the same range of current injections was also used for the experiments conducted in slices.

For recordings in both slices and cortical cultures, the $I_r$ of 'slow spiking interneurons' is similar as is the membrane potential amplitude at 200 pA. Cells recorded from slices again present a slightly higher excitability, showing a higher number of APs at the various current steps, which is also reflected in having a somewhat lower rheobase than the cultured cortical neurons. The slope of ISI in slices is more pronounced than in cultured neurons, along with the proportion of minimum over maximum ISI, the spike height adaptation and $I_h$. Spike burst pattern and minimum ISI have higher values in cultured cortical neurons than in slices. Cell type 7 in slices presents a less linear IV relationship, with the membrane amplitude as a response to negative currents being larger than in cell cultures. By contrast, the IV relationship for cell type 10 is shallower in slices than in cell cultures.

Based on differences in electrophysiological properties, four types of pyramidal neurons have been reported in the medial prefrontal cortex of rats (Aerde & Feldmeyer 2013), i.e. regular, bursting, and low- and high-resistance adapting spiking neurons. In this project the clustering algorithm identified three neuron types with properties suggesting that they are pyramidal neurons (cell types 3, 4 and 5 in cell culture). Again, the limited range of current injection in the current study hinders a direct comparison to the cell types described in the literature. However, it was possible to compare excitability and IV plots of equivalent groups recorded in slices and cell culture. As described previously, the excitability plot for one of the pyramidal types identified in slices was most similar to cell type 3 in cell culture, while the other two pyramidal types in slices were very similar to each other and both corresponded most to cell type 5 in cell culture (chapter 5: Figure 5-2). Grouping cell types 3 and 5 from neurons in slices into a super-group labelled pyramidal neurons gives a higher input resistance than cell types 3 and 5 recorded in cell culture. Consequently, the rheobase of the cells in slices was lower and the excitability was slightly higher than in cultured

cortical neurons. However, the steady-state amplitude of the membrane potential change in response to a 200 pA current step was lower in slices than in cell cultures. The remaining parameters (slope of ISI at 200 pA, minimum ISI, proportion of minimum over maximum ISI, spike burst pattern and spike height adaptation) did not differ greatly between the two models. Of these parameters, the firing rate, input resistance and maximum over minimum ratio of ISI were similar to pyramidal neurons from described neurons in layer II/III of the medial prefrontal cortex (Aerde & Feldmeyer 2013). The shape of the IV relationship between the two preparations was similar, with only the positive current steps in slices having lower amplitude than in cell cultures, as mentioned above.

## 6.2 Do serotonin and nitric oxide have similar effects on cortical neuronal properties in cell culture and acute brain slices?

The discussion above clearly illustrates that there are similarities in the electrophysiological properties of cortical neurons recorded in acute slices and dissociated cell cultures. However, it also highlights several marked differences. This raises the question of whether the effects of 5HT and NO on intrinsic cellular properties are comparable in slices and cultured cortical neurons.

It was possible to make a comparison between pyramidal neurons from slices and types 3 or 5 from cultured cortical neurons. Interestingly, only two parameters (height of $1^{st}$ AP at threshold and at 200 pA) are significantly reduced by 5HT in both pyramidal neurons in slices and in cell type 3 in cortical cultures (Figure 6-1; note that 5HT has no significant effect on any of the parameters recorded in cell type 5 in cell culture). Furthermore, seven parameters are not significantly affected by 5HT in either cell cultures or slices (number of APs at 120 pA, minimum ISI at 200 pA, minimum to maximum ISI ratio, $I_h$, $I_r$, width of $1^{st}$ AP at 200 pA and the AP trough of $1^{st}$ and last AP at 200 pA). However, there are eleven parameters that are either significantly affected by 5HT in pyramidal cells in slices or in cell type 3 in cultures, but not in both. In eight of these eleven parameters, the net effects of 5HT actually go in opposite directions.

The effects of NO on pyramidal neurons appear more consistent across slices and cultures than those of 5HT. There are at least four parameters that show qualitatively similar, significant changes in pyramidal neurons in slices and in cell types 3 and 5 in cultures (number of APs at 200 pA, minimum ISI at 200 pA, 1st AP width at threshold and at 200 pA). An additional eight parameters show qualitatively similar changes in response to NO application across pyramidal neurons recorded in slices and in culture that differ only in their magnitude (i.e. consistent increases or decreases in the parameter values; Figure 6-1). Furthermore, three parameters are not significantly affected by NO in any of the pyramidal cell types (spike height adaptation, $I_h$ and trough of last AP at 200 pA). This leaves five parameters that show qualitative and quantitative differences between the effects of NO on pyramidal neurons in slices and cell types 3 and 5 in cultures. Three of these show at least qualitative similarities between pyramidal neurons in slices and cell type 3 in cultures (number of APs at 120 pA, rheobase and $I_r$), while the remaining two (trough of 1st AP at threshold, width of last AP at 200 pA) are affected similarly in cell types 3 and 5 in culture, but not in slices.

The effects of NO on cellular properties appear to be somewhat more robust and conserved in cultures and slices compared to the effects of 5HT. This could be due to the relative simplicity of NO signalling compared to 5HT signalling. As discussed previously, NO mainly acts either via direct S-nitrosylation of proteins or via the soluble guanylyl cyclase/cyclic guanosine monophosphate (sGC/cGMP) signalling pathway. In contrast, 5HT acts via a more diverse set of receptors, some of which have opposing effects on downstream signalling pathways (e.g. stimulation versus suppression of adenylate cyclase activity) and neuronal properties (e.g. $5HT_1$ receptor mediated decrease in excitability versus $5HT_2$ mediated increase in excitability; e.g. Zhong et al. 2008). Therefore, shifts in the balance of expression of the various components of the signalling pathways and their targets could dramatically alter the effects of 5HT. Comparison of the electrophysiological parameters of pyramidal neurons in slices and in cell culture certainly suggests that the balance of the different voltage-gated ion channels differs between the two models, leading to differences in the response to series of current steps.
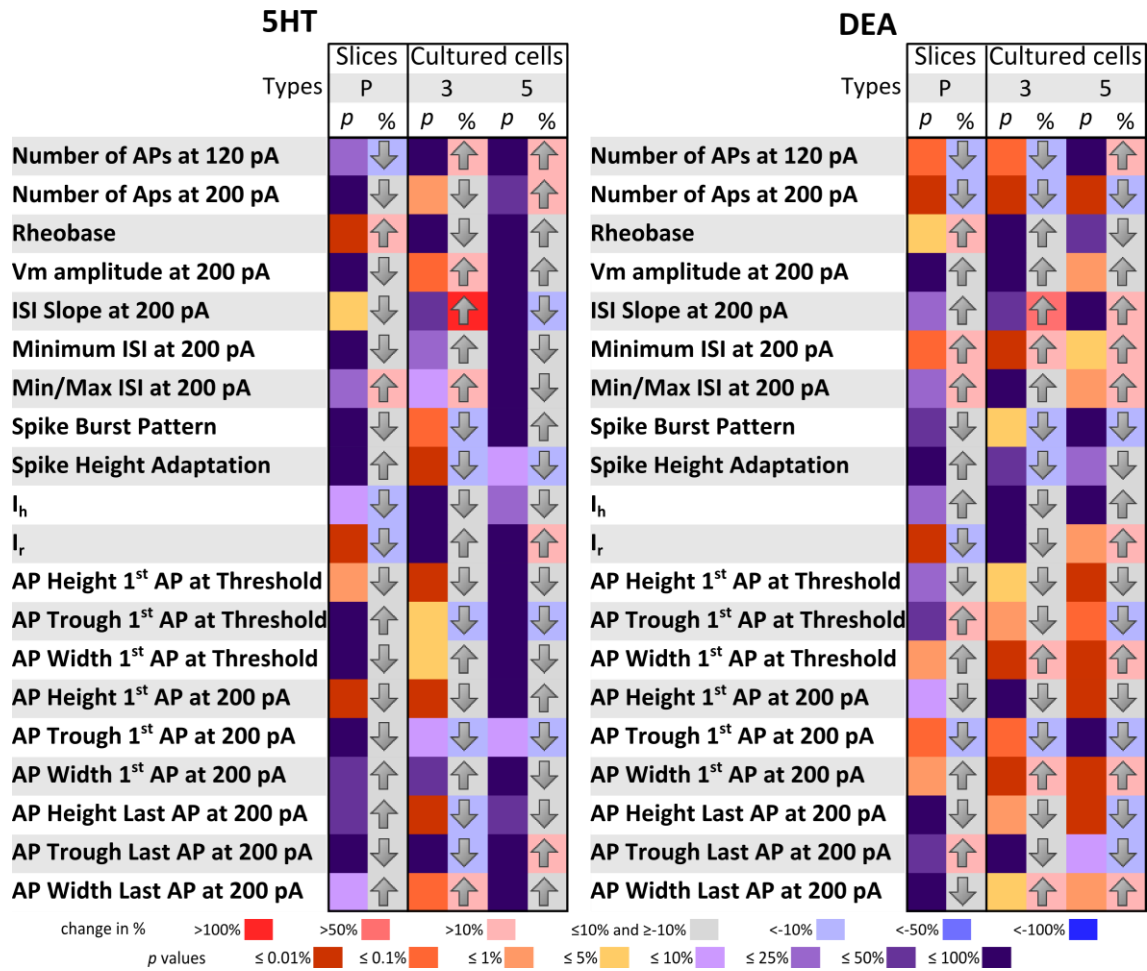
Figure 6-1: Comparison of the modulation on the various parameters between cultured cortical cell types 3 and 5, and pyramidal (P) neurons obtained from slices.

Individual aspects of the observed effects on specific parameters correspond to previous reports of NO effects.  For example, the decrease in the excitability of pyramidal cells could be linked to the direct activation of calcium-dependent potassium channels by NO as described for smooth muscle cells (Bolotina et al. 1994). NO can also modulate the strength and intrinsic excitability of the cells by inhibiting Kv3 channels and enhancing Kv2 currents in the auditory brain stem and the hippocampus (Steinert et al. 2011), possibly through a sGC/cGMP pathway (Steinert et al. 2008). In the current work, through the application of 1H-[1,2,4]oxadiazolo[4,3-a]quinoxalin-1-one (ODQ) in cultured cortical neurons, it was possible to infer that the excitability of pyramidal cells was modulated by NO through both sGC/cGMP and S-nitrosylation pathways, which suggests that this effect is not solely due to S-nitrosylation events.

The NO-induced increase in the width of the APs could be explained by an increase of transient endogenous $Ca^{2+}$ similar to the effect of NO on calcium-spikes in astrocytes (Schipke et al. 2008). This increase may be due to the activation of calcium channels, as reported in olfactory receptor cells and retinal ganglion cells trough sGC/cGMP (Kawai & Miyachi 2001; Hirooka et al. 2000). In hippocampal neurons, cGMP seems to indirectly depress the activity of calcium channels by reducing intracellular 3',5'-cyclic adenosine monophosphate (cAMP) through phosphodiesterases (PDE, Doerner & Alger 1988). In this work, for these cell types S-nitrosylation is likely responsible for the increase in width of the APs. S-nitrosylation has been shown to increase the channel activity of the ryanodine receptors present in the sarcoplasmic reticulum. This increased endogenous $Ca^{2+}$ from intracellular stores has been previously reported in smooth and cardiac muscle cells (Stoyanovsky et al. 1997). It is also possible that, through S-nitrosylation, NO enhances the activity of L-type calcium ($Ca_v1$) channels, similar to observations in neurons from mouse medial nucleus of the trapezoid body (Tozer et al. 2012). In Tozer's work, NO also enhanced the P/Q-type currents ($Ca_v2.1$) through the activation of sGC. However, this project provided no evidence for a role of sGC/cGMP signalling in causing the increase in AP width.

One parameter had a significant reduction of its values in the presence of 5HT in pyramidal cells in slices, which was the height of first AP at threshold and at 200 pA,

similar to what was observed in cell type 3 in cell culture. It has been previously reported that 5HT can modulate G protein-activated inwardly rectifying potassium currents (Takigawa & Alzheimer 1999) responsible for maintaining the membrane potential and excitability of the neurons (Mark & Herlitze 2000).

## 6.3 What are the potential mechanisms that underlie the effects of serotonin and nitric oxide on spontaneous EPSC frequency in cortical slices?

The increase in spontaneous EPSC frequency caused by 5HT in pyramidal cells recorded in cortical slices cannot easily be explained by the effect of 5HT on the excitability of the cells. In slices, 5HT slightly increased the excitability of 'slow spiking' interneurons, but not of pyramidal cells. There is some evidence for a small increase in the number of APs elicited by low amplitude positive current steps in putative pyramidal cell types 3 and 4 in cell culture, but overall it is difficult to explain the increases in spontaneous EPSC frequency in cortical slices on the basis of the effects of 5HT on neuronal excitability. However, the effects of 5HT on neuronal excitability were studied in the presence of kynurenic acid and picrotoxin in order to block synaptic inputs. It has been reported that 5HT modulation of the excitability of prefrontal cortex pyramidal neurons via either $5HT_{1A}$ or $5HT_{2A/C}$ receptors requires N-methyl-D-aspartate (NMDA) receptor activation (Zhong et al. 2008). Furthermore, $5HT_{1A}$ and $5HT_{2A/C}$ are reported to have opposing effects on excitability. Thus, the apparent lack of 5HT effects on excitability could either be a consequence of the lack of NMDA receptor activity, or due to the opposing effects of $5HT_{1A}$ and $5HT_{2A/C}$ receptor activity cancelling each other out.

Alternatively, it may be that the increase in EPSC frequency was due to the activation of $5HT_3$ receptors, distributed throughout the cerebral cortex layers (Tecott et al. 1993). Depolarisation of a subset of neurons due to activation of $5HT_3$ receptors has been observed in cultured cortical neurons; therefore this option could also be viable in slices. $5HT_3$ receptors in the cortex are predominantly expressed in inhibitory interneurons (Morales & Bloom 1997; Puig et al. 2004), however the 5HT-induced increase in EPSC frequency persisted even after blocking inhibitory synaptic

interactions with picrotoxin. $5HT_3$ receptors are also expressed in Cajal-Retzius (CR) cells during post-natal development (Chameau et al. 2009; Lee et al. 2010), which are excitatory and could at least partially account for the increase in EPSC frequency.

Another possible explanation is the excitation of layer V pyramidal neurons through $5HT_2$ receptors (Stephens et al. 2014; Béïque et al. 2007) providing an excitatory drive to the slices increasing the overall EPSC frequency.

In the present work, the application of diethylamine NONOate sodium salt hydrate (DEA) reduced the excitability of cortical neurons in both cultures and slices. In slices, this decrease was especially pronounced in fast spiking interneurons. It has also been reported that γ-aminobutyric acid (GABAergic) neurons in the various layers of the cortex can express nitric oxide synthase (NOS, Karagiannis et al. 2009; Kubota et al. 2011), helping to maintain the balance of excitatory and inhibitory inputs (Le Roux et al. 2009). However, the frequency of EPSCs observed in this work increased only slightly in the presence of DEA, which could be due to the inhibition of GABAergic interneurons enhancing the activity of the pyramidal neurons. This limited effect of DEA application on EPSC frequency could also be due to a corresponding reduction in excitability of pyramidal neurons. However, picrotoxin application had barely any effect on spontaneous EPSC frequency, suggesting that the balance between fast excitatory and inhibitory synaptic transmission is not very important in setting the level of spontaneous EPSC frequency in layer III pyramidal neurons.

Although it was not possible to infer the effects of 5HT/DEA co-application on the excitability of cortical neurons in slices due to a low n number for these experiments, the comparison to cultured cortical neurons suggests that most pyramidal neurons would present an effect on excitability similar to summation of the individual effects of 5HT and DEA. This view is supported by the limited number of experiments carried out on 5HT/DEA co-application in slices (see chapter 5, Figure 5-7). Again, the data provided little evidence for an increase in excitability. However, when 5HT/DEA was applied, the frequency of EPSCs increased similar to the increase observed in the presence of 5HT alone. Interestingly, when fast excitatory and inhibitory synaptic interactions were uncoupled by the application of picrotoxin, the increase in EPSC

frequency caused by 5HT alone was almost completely abolished. This suggests that NO can modulate the effects of 5HT on the frequency of spontaneous synaptic EPSCs, but that this effect is counterbalanced by an NO effect on spontaneous IPSCs.

This co-modulation of 5HT/DEA is far from the enhancement of serotonergic postsynaptic effects by NO in *Lymnaea stagnalis* (Straub et al. 2007). It also suggests that the mammalian excitatory-inhibitory balance found in the cerebral cortex is robust to changes in NO signalling, possibly because the NO modulation of the 5HT effect on EPSC frequency is counterbalanced by NO effects on IPSCs. This is similar to the observation that the functional balance between excitation and inhibition in the auditory cortex of mice remains stable during *in vivo* transitions from quiescence to active behaviour (Zhou et al. 2014). However, it differs from a recent report that NO is involved in the unlocking of the excitatory-inhibitory balance in layer V pyramidal neurons (Lourenço et al. 2014).

The reduction of the 5HT-induced increase in spontaneous EPSC frequency by DEA when only the excitatory pathways of the neocortex are active could be due to an enhancement of the inhibitory effects of $5HT_1$ receptors by NO, or the modulation of the $5HT_2$ pathway by NO.

## 6.4 How could the questions raised by this project be addressed in the future?

The current work uses electrophysiological properties of cortical neurons in two models, cultured cells and slices, and endeavours to compare how consistent cellular behaviour is across the two model systems. However, due to the uncertainty of the relationship between the cell types in the two models, this question has not been addressed completely. It would be possible to overcome this problem in the future by utilising increasingly available transgenic animals that express fluorescent markers in defined subpopulations of neurons (Lima et al. 2009; Kay & Brunjes 2014; Jin et al. 2014). Also, the use of electrophysiology together with genetic and immunocytochemical characterisation of neurons has the potential to lead to a less ambiguous identification of the various cell types.

The apparent differences between slices and cell cultures in the effects of 5HT and NO on various parameters at the cellular level of individual neuron types could be due to changes in the balance of voltage-gated ion channels and elements of the different signalling pathways in cell culture compared to slices. For example, 5HT could affect two different voltage-gated ion channels, hypothetically A and B, in one cell that both have opposing influences on one cellular parameter. If the balance of A and B is different in slices and in cell culture, this could result in quantitative and even qualitative differences in the effects on this parameter. This problem could be partially overcome by studying the effects of 5HT and NO on pharmacologically isolated currents. This would reduce the chances of masking the effects of 5HT and NO by other currents that would contribute to the overall cell behaviour.

Understanding how the modulation of NO on the serotonergic activity is mediated (whether it is through sGC/cGMP signalling or S-nitrosylation), and in which part of the receptors' pathways the interaction occurs, is also important for fully comprehend the effects of both neuromodulators. Some attempts to characterise the signalling pathways mediating NO effects have been made by trying to differentiate between sGC/cGMP-dependent and –independent effects. However, due to time limitations, it was not possible to carry out a detailed pharmacological characterisation of the signalling pathways that mediate 5HT effects. Furthermore, it will be important to characterise whether 5HT and NO modulate each other's receptor function, whether there is crosstalk between the secondary messenger cascades, or whether they independently act on a common target protein (e.g. a voltage-gated ion channel). Thus, further pharmacological studies on the mechanisms of interaction between serotonergic receptors and NO in the cortical network and the various intrinsic membrane properties of the cortical neurons would help understanding the interaction between 5HT and NO in the neocortical neurons. This might also open up the possibility for new therapeutic strategies to target specific aspects of serotonergic signalling by targeting NO signalling that modulates serotonergic functions. It has already been reported that the effects of SSRI's can be modulated by altering NO signalling (Harkin et al. 2003; Harkin et al. 2004; Gigliucci et al. 2010; Inan et al. 2004) and combination drugs targeting both serotonin and nitric oxide signalling have been

considered for the treatment of depression (Abdul-Hay et al. 2011). A better understanding of the mechanisms of interaction between 5HT and NO at the cellular level will clearly benefit these developments.

It is also important to further study the effects observed on network activity by 5HT and NO. In particular, it would be of interest to study whether 5HT and NO modulate the integrative properties of cortical neurons by affecting the propagation of EPSCs from the synapse to the cell soma. If 5HT and NO, alone or in combination, affect the integration of synaptic inputs, this could potentially explain the effects of 5HT and NO on spontaneous synaptic activity in the absence of significant changes in neuronal excitability. This could be studied by selectively stimulating specific input pathways (e.g. local field stimulation of thalamocortical pathways or stimulation in layer V to mimic excitatory drive from layer V pyramidal neurons), while recording postsynaptic activity in layer III pyramidal neurons. Alternatively, flash-photolysis of caged glutamate on selected dendritic positions could be used to mimic EPSCs, which would show whether 5HT and/or NO has site-specific effects on the somatic response of these glutamate-evoked events.

# 7 References

Abdul-Hay, S. et al., 2011. NO-SSRIs: nitric oxide chimera drugs incorporating a selective serotonin reuptake inhibitor. *ACS medicinal chemistry letters*, 2(9), pp.656–661.

Adesnik, H. et al., 2012. A neural circuit for spatial summation in visual cortex. *Nature*, 490(7419), pp.226–231.

Aerde, K.I. van & Feldmeyer, D., 2013. Morphological and physiological characterization of pyramidal neuron subtypes in rat medial prefrontal cortex. *Cerebral Cortex*, pp.2279–2295.

Aghajanian, G.K. & Marek, G.J., 1997. Serotonin induces excitatory postsynaptic potentials in apical dendrites of neocortical pyramidal cells. *Neuropharmacology*, 36(4-5), pp.589–599.

Alexander, G.M. et al., 2006. Cortical feedback to the thalamus is selectively enhanced by nitric oxide. *Neuroscience*, 142(1), pp.223–234.

Amargós-Bosch, M. et al., 2004. Co-expression and in vivo interaction of serotonin1A and serotonin2A receptors in pyramidal neurons of prefrontal cortex. *Cerebral Cortex*, 14(3), pp.281–299.

Andjelic, S. et al., 2009. Glutamatergic nonpyramidal neurons from neocortical layer VI and their comparison with pyramidal and spiny stellate neurons. *Journal of Neurophysiology*, 101(2), pp.641–654.

Andrade, R. & Weber, E.T., 2010. Htr2a gene and 5-HT2A receptor expression in the cerebral cortex studied using genetically modified mice. *Neuropharmacology*, 4, pp.36–48.

Angoa-Pérez, M. et al., 2014. Mice genetically depleted of brain serotonin do not display a depression-like behavioral phenotype. *ACS chemical neuroscience*, (Article ASAP).

Antzoulatos, E.G. & Miller, E.K., 2011. Differences between neural activity in prefrontal cortex and striatum during learning of novel abstract categories. *Neuron*, 71(2), pp.243–249.

Aoki, C. et al., 1998. The subcellular distribution of nitric oxide synthase relative to the NR1 subunit of NMDA receptors in the cerebral cortex. *Progress in Brain Research*, 118, pp.83–97.

Araneda, R. & Andrade, R., 1991. 5-Hydroxytryptamine2 and 5-hydroxytryptamine 1A receptors mediate opposing responses on membrane excitability in rat association cortex. *Neuroscience*, 40(2), pp.399–412.

Arlotta, P. et al., 2005. Neuronal subtype-specific genes that control corticospinal motor neuron development in vivo. *Neuron*, 45(2), pp.207–221.

Ascoli, G.A. et al., 2008. Petilla terminology: nomenclature of features of GABAergic interneurons of the cerebral cortex. *Nature Reviews Neuroscience*, 9(7), pp.557–568.

Azmitia, E.C. & Segal, M., 1978. An autoradiographic analysis of the differential ascending projections of the dorsal and median raphe nuclei in the rat. *The Journal of Comparative Neurology*, 179(3), pp.641–667.

Barnes-Davies, M. & Forsythe, I.D., 1995. Pre- and postsynaptic glutamate receptors at a giant excitatory synapse in rat auditory brainstem slices. *The Journal of physiology*, 488 (Pt 2), pp.387–406.

Béïque, J.-C. et al., 2007. Mechanism of the 5-hydroxytryptamine 2A receptor-mediated facilitation of synaptic activity in prefrontal cortex. *Proceedings of the National Academy of Sciences*, 104(23), pp.9870–9875.

Béïque, J.-C. et al., 2004. Serotonergic regulation of membrane potential in developing rat prefrontal cortex: coordinated expression of 5-hydroxytryptamine (5-HT)1A, 5-HT2A, and 5-HT7 receptors. *The Journal of Neuroscience*, 24(20), pp.4807 – 4817.

Belgard, T.G. et al., 2011. A transcriptomic atlas of mouse neocortical layers. *Neuron*, 71(4), pp.605–616.

Bellamy, T.C. & Garthwaite, J., 2001. Sub-second kinetics of the nitric oxide receptor, soluble guanylyl cyclase, in intact cerebellar cells. *The Journal of Biological Chemistry*, 276(6), pp.4287–4292.

Bender, A.T. & Beavo, J.A., 2006. Cyclic nucleotide phosphodiesterases: molecular regulation to clinical use. *Pharmacological Reviews*, 58(3), pp.488 –520.

Benhar, M., Forrester, M.T. & Stamler, J.S., 2009. Protein denitrosylation: enzymatic mechanisms and cellular functions. *Nature Reviews Molecular Cell Biology*, 10(10), pp.721–732.

Berridge, M.J., 1993. Inositol trisphosphate and calcium signalling. *Nature*, 361(6410), pp.315–325.

Bers, D.M., 2002. Cardiac excitation–contraction coupling. *Nature*, 415(6868), pp.198–205.

Bianchi, C. et al., 2007. Serotonin modulation of cell excitability and of [3H]GABA and [3H]d-aspartate efflux in primary cultures of rat cortical neurons. *Neuropharmacology*, 52(3), pp.995–1002.

Biemann, C., 2007. *Unsupervised and knowledge-free natural language processing in the structure discovery paradigm*, p. 162.

Boehning, D. et al., 2003. Carbon monoxide neurotransmission activated by CK2 phosphorylation of heme oxygenase-2. *Neuron*, 40(1), pp.129–137.

Bolotina, V.M. et al., 1994. Nitric oxide directly activates calcium-dependent potassium channels in vascular smooth muscle. *Nature*, 368(6474), pp.850–853.

Bonaventure, P. et al., 2004. Radioligand binding analysis of knockout mice reveals 5-hydroxytryptamine7 receptor distribution and uncovers 8-hydroxy-2-(di-n-propylamino)tetralin interaction with α2 adrenergic receptors. *Neuroscience*, 124(4), pp.901–911.

Bonsi, P. et al., 2007. Endogenous serotonin excites striatal cholinergic interneurons via the activation of 5-HT2C, 5-HT6, and 5-HT7 serotonin receptors: implications for extrapyramidal side effects of serotonin reuptake inhibitors. *Neuropsychopharmacology*, 32(8), pp.1840–1854.

Bredt, D.S. et al., 1991. Nitric oxide synthase protein and mRNA are discretely localized in neuronal populations of the mammalian CNS together with NADPH diaphorase. *Neuron*, 7(4), pp.615–624.

Brodmann, K., 1909. *Vergleichende Lokalisationslehre der Grosshirnrinde in ihren Prinzipien dargestellt auf Grund des Zellenbaues*, Johann Ambrosius Barth Verlag.

Brown, S.P. & Hestrin, S., 2009. Intracortical circuits of pyramidal neurons reflect their long-range axonal targets. *Nature*, 457(7233), pp.1133–1136.

Bryan-Lluka, L.J. et al., 2004. Nitric oxide donors inhibit 5-hydroxytryptamine (5-HT) uptake by the human 5-HT transporter (SERT). *British Journal of Pharmacology*, 143(1), pp.63–70.

Bunin, M.A. & Wightman, R.M., 1998. Quantitative evaluation of 5-hydroxytryptamine (serotonin) neuronal release and uptake: an investigation of extrasynaptic transmission. *The Journal of Neuroscience*, 18(13), pp.4854–4860.

Burette, A. et al., 2002. Synaptic localization of nitric oxide synthase and soluble guanylyl cyclase in the hippocampus. *The Journal of Neuroscience*, 22(20), pp.8961–8970.

Calvin, W.H. & Sypert, G.W., 1976. Fast and slow pyramidal tract neurons: an intracellular analysis of their contrasting repetitive firing properties in the cat. *Journal of neurophysiology*, 39(2), pp.420–434.

Carr, D.B. et al., 2002. Serotonin receptor activation inhibits sodium current and dendritic excitability in prefrontal cortex via a protein kinase C-dependent mechanism. *The Journal of Neuroscience*, 22(16), pp.6846–6855.

Cauli, B. et al., 2000. Classification of fusiform neocortical interneurons based on unsupervised clustering. *Proceedings of the National Academy of Sciences*, 97(11), pp.6144–6149.

Cauli, B. et al., 1997. Molecular and physiological diversity of cortical nonpyramidal cells. *The Journal of Neuroscience*, 17(10), pp.3894–3906.

Centonze, D. et al., 2001. Stimulation of nitric oxide-cGMP pathway excites striatal cholinergic interneurons via protein kinase G activation. *The Journal of Neuroscience*, 21(4), pp.1393–1400.

Cha, C.I. et al., 1998. Immunocytochemical study on the distribution of NOS-immunoreactive neurons in the cerebral cortex of aged rats. *Neuroreport*, 9(10), pp.2171–2174.

Chameau, P. et al., 2009. The N-terminal region of reelin regulates postnatal dendritic maturation of cortical pyramidal neurons. *Proceedings of the National Academy of Sciences*, 106(17), pp.7227–7232.

Chanrion, B. et al., 2007. Physical interaction between the serotonin transporter and neuronal nitric oxide synthase underlies reciprocal modulation of their activity. *Proceedings of the National Academy of Sciences*, 104(19), pp.8119 –8124.

Chen, L. et al., 2008. 5-HT excites globus pallidus neurons by multiple receptor mechanisms. *Neuroscience*, 151(2), pp.439–451.

Chen, W. et al., 1996. Electrophysiological and morphological properties of pyramidal and nonpyramidal neurons in the cat motor cortex in vitro. *Neuroscience*, 73(1), pp.39–55.

Chiavegatto, S. et al., 2001. Brain serotonin dysfunction accounts for aggression in male mice lacking neuronal nitric oxide synthase. *Proceedings of the National Academy of Sciences*, 98(3), pp.1277 –1281.

Chung, Y.H., Kim, Y.S. & Lee, W.B., 2004. Distribution of neuronal nitric oxide synthase-immunoreactive neurons in the cerebral cortex and hippocampus during postnatal development. *Journal of Molecular Histology*, 35(8-9), pp.765–770.

Clarke, H.F. et al., 2004. Cognitive inflexibility after prefrontal serotonin depletion. *Science*, 304(5672), pp.878–880.

Clawges, H.M. et al., 1997. Human 5-HT1 receptor subtypes exhibit distinct G protein coupling behaviors in membranes from Sf9 cells. *Biochemistry*, 36(42), pp.12930–12938.

Clemett, Delyth A et al., 2000. Immunohistochemical localisation of the 5-HT2C receptor protein in the rat CNS. *Neuropharmacology*, 39(1), pp.123–132.

Cook, E.H. & Leventhal, B.L., 1996. The serotonin system in autism. *Current Opinion in Pediatrics*, 8(4), pp.348–354.

Cruikshank, S.J., Lewis, T.J. & Connors, B.W., 2007. Synaptic basis for intense thalamocortical activation of feedforward inhibitory cells in neocortex. *Nature Neuroscience*, 10(4), pp.462–468.

Cudeiro, J. et al., 1997. Actions of compounds manipulating the nitric oxide system in the cat primary visual cortex. *The Journal of Physiology*, 504(Pt 2), pp.467–478.

Davies, M.F. et al., 1987. Two distinct effects of 5-hydroxytryptamine on single cortical neurons. *Brain Research*, 423(1-2), pp.347–352.

DeFelipe, J., 1997. Types of neurons, synaptic connections and chemical characteristics of cells immunoreactive for calbindin-D28K, parvalbumin and calretinin in the neocortex. *Journal of Chemical Neuroanatomy*, 14(1), pp.1–19.

Dégenètais, E. et al., 2002. Electrophysiological properties of pyramidal neurons in the rat prefrontal cortex: an in vivo intracellular recording study. *Cerebral Cortex*, 12(1), pp.1–16.

Dempster, A.P., Laird, N.M. & Rubin, D.B., 1977. Maximum likelihood from incomplete data via the EM algorithm. *Journal of the Royal Statistical Society. Series B (Methodological)*, 39(1), pp.1–38.

Demšar, J. et al., 2013. Orange: data mining toolbox in python. *Journal of Machine Learning Research*, 14, pp.2349–2353.

Derkach, V., Surprenant, A. & North, R.A., 1989. 5-HT3 receptors are membrane ion channels. *Nature*, 339(6227), pp.706–709.

Dichter, M.A., 1978. Rat cortical neurons in cell culture: culture methods, cell morphology, electrophysiology, and synapse formation. *Brain research*, 149(2), pp.279–293.

Ding, J., Burette, A. & Weinberg, R.J., 2005. Expression of soluble guanylyl cyclase in rat cerebral cortex during postnatal development. *The Journal of Comparative Neurology*, 485(3), pp.255–265.

Dittrich, L. et al., 2014. Homeostatic sleep pressure is the primary factor for activation of cortical nNOS/NK1 neurons. *Neuropsychopharmacology*, (Article ASAP).

Do, C.B. & Batzoglou, S., 2008. What is the expectation maximization algorithm? *Nature Biotechnology*, 26(8), pp.897–899.

Doerner, D. & Alger, B.E., 1988. Cyclic GMP depresses hippocampal Ca2+ current through a mechanism independent of cGMP-dependent protein kinase. *Neuron*, 1(8), pp.693–699.

Van Donkelaar, E.L. et al., 2008. Phosphodiesterase 2 and 5 inhibition attenuates the object memory deficit induced by acute tryptophan depletion. *European Journal of Pharmacology*, 600(1-3), pp.98–104.

Dunn, J.C., 1973. A fuzzy relative of the ISODATA process and its use in detecting compact well-separated clusters. *Journal of Cybernetics*, 3(3), pp.32–57.

Van Eden, C.G. & Uylings, H.B., 1985. Cytoarchitectonic development of the prefrontal cortex in the rat. *The Journal of Comparative Neurology*, 241(3), pp.253–267.

Erisir, A. et al., 1999. Function of specific K+ channels in sustained high-frequency firing of fast-spiking neocortical interneurons. *Journal of Neurophysiology*, 82(5), pp.2476–2489.

Fame, R.M., MacDonald, J.L. & Macklis, J.D., 2011. Development, specification, and diversity of callosal projection neurons. *Trends in Neurosciences*, 34(1), pp.41–50.

Feng, G. et al., 2000. Imaging neuronal subsets in transgenic mice expressing multiple spectral variants of GFP. *Neuron*, 28(1), pp.41–51.

Férézou, I. et al., 2002. 5-HT3 receptors mediate serotonergic fast synaptic excitation of neocortical vasoactive intestinal peptide/cholecystokinin interneurons. *The Journal of Neuroscience*, 22(17), pp.7389–7397.

Fesenko, E.E., Kolesnikov, S.S. & Lyubarsky, A.L., 1985. Induction by cyclic GMP of cationic conductance in plasma membrane of retinal rod outer segment. *Nature*, 313(6000), pp.310–313.

Field, A.P., 2009. *Discovering statistics using SPSS*, London: SAGE. pp. 638-642.

Fishbein, I. & Segal, M., 2011. Active cortical innervation protects striatal neurons from slow degeneration in culture. *Journal of Neural Transmission*, 118(3), pp.445–451.

Fitzpatrick, P.F., 1999. Tetrahydropterin-dependent amino acid hydroxylases. *Annual Review of Biochemistry*, 68(1), pp.355–381.

Foehring, R.C. et al., 2002. Serotonergic modulation of supragranular neurons in rat sensorimotor cortex. *The Journal of Neuroscience*, 22(18), pp.8238–8250.

Fossier, P. et al., 1999. Nitric oxide transforms serotonin into an inactive form and this affects neuromodulation. *Neuroscience*, 93(2), pp.597–603.

Fraley, C. & Raftery, A.E., 2007. Bayesian regularization for normal mixture estimation and model-based clustering. *Journal of Classification*, 24(2), pp.155–181.

Freedman, D.J. et al., 2001. Categorical representation of visual stimuli in the primate prefrontal cortex. *Science*, 291(5502), pp.312–316.

Frey, B.J. & Dueck, D., 2007. Clustering by passing messages between data points. *Science*, 315(5814), pp.972–976.

Gabbott, P.L.A. et al., 1997. Local-circuit neurones in the medial prefrontal cortex (areas 25, 32 and 24b) in the rat: Morphology and quantitative distribution. *The Journal of Comparative Neurology*, 377(4), pp.465–499.

Garthwaite, G. et al., 2006. Signaling from blood vessels to CNS axons through nitric oxide. *The Journal of Neuroscience*, 26(29), pp.7730–7740.

Garthwaite, J. & Garthwaite, G., 1987. Cellular origins of cyclic GMP responses to excitatory amino acid receptor agonists in rat cerebellum in vitro. *Journal of Neurochemistry*, 48(1), pp.29–39.

Gigliucci, V. et al., 2010. A role for serotonin in the antidepressant activity of NG-Nitro-L-arginine, in the rat forced swimming test. *Pharmacology Biochemistry and Behavior*, 94(4), pp.524–533.

Gilbert, C.D. & Wiesel, T.N., 1979. Morphology and intracortical projections of functionally characterised neurones in the cat visual cortex. *Nature*, 280(5718), pp.120–125.

Goaillard, J.-M. & Vincent, P., 2002. Serotonin suppresses the slow afterhyperpolarization in rat intralaminar and midline thalamic neurones by activating 5-HT7 receptors. *The Journal of Physiology*, 541(2), pp.453–465.

Gonchar, Y. et al., 2008. Multiple distinct subtypes of GABAergic neurons in mouse visual cortex identified by triple immunostaining. *Frontiers in Neuroanatomy*, 1, p.3.

Gonchar, Y. & Burkhalter, A., 1997. Three distinct families of GABAergic neurons in rat visual cortex. *Cerebral Cortex*, 7(4), pp.347–358.

Goodfellow, N.M. et al., 2009. Layer II/III of the prefrontal cortex: inhibition by the serotonin 5-HT1a receptor in development and stress. *The Journal of Neuroscience*, 29(32), pp.10094–10103.

Le Grand, S.M. et al., 2011. Serotonin depletion leads to cortical hyperexcitability and trigeminal nociceptive facilitation via the nitric oxide pathway. *Headache: The Journal of Head and Face Pain*, 51(7), pp.1152–1160.

Grau, C.M. & Greene, L.A., 2012. Use of PC12 cells and rat superior cervical ganglion sympathetic neurons as models for neuroprotective assays relevant to Parkinson's disease. In S. D. Skaper, ed. *Neurotrophic Factors*. Methods in Molecular Biology. Humana Press, pp. 201–211.

Gray, P.C., Scott, J.D. & Catterall, W.A., 1998. Regulation of ion channels by cAMP-dependent protein kinase and A-kinase anchoring proteins. *Current Opinion in Neurobiology*, 8(3), pp.330–334.

Gruber, A.J. et al., 2010. More is less: a disinhibited prefrontal cortex impairs cognitive flexibility. *The Journal of Neuroscience*, 30(50), pp.17102–17110.

Guerra, L. et al., 2011. Comparison between supervised and unsupervised classifications of neuronal cell types: A case study. *Developmental Neurobiology*, 71(1), pp.71–82.

Guevara-Guzman, R., Emson, P.C. & Kendrick, K.M., 1994. Modulation of in vivo striatal transmitter release by nitric oxide and cyclic GMP. *Journal of Neurochemistry*, 62(2), pp.807–810.

Haider, B. & McCormick, D.A., 2009. Rapid neocortical dynamics: cellular and network mechanisms. *Neuron*, 62(2), pp.171–189.

Hajós, M. et al., 1998. An electrophysiological and neuroanatomical study of the medial prefrontal cortical projection to the midbrain raphe nuclei in the rat. *Neuroscience*, 87(1), pp.95–108.

Halabisky, B. et al., 2006. Electrophysiological classification of somatostatin-positive interneurons in mouse sensorimotor cortex. *Journal of Neurophysiology*, 96(2), pp.834–845.

Handl, J., Knowles, J. & Kell, D.B., 2005. Computational cluster validation in post-genomic data analysis. *Bioinformatics*, 21(15), pp.3201–3212.

Han, M.H. et al., 2001. Miniature postsynaptic currents depend on Ca2+ released from internal stores via PLC/IP3 pathway. *Neuroreport*, 12(10), pp.2203–2207.

Harkin, A. et al., 2004. Nitric oxide synthase inhibitors augment the effects of serotonin re-uptake inhibitors in the forced swimming test. *European Neuropsychopharmacology*, 14(4), pp.274–281.

Harkin, A. et al., 2003. Serotonergic mediation of the antidepressant-like effects of nitric oxide synthase inhibitors. *Neuropharmacology*, 44(5), pp.616–623.

Hartigan, J.A. & Wong, M.A., 1979. Algorithm AS 136: a k-means clustering algorithm. *Applied Statistics*, 28(1), p.100.

Haul, S. et al., 1999. Impairment of neocortical long-term potentiation in mice deficient of endothelial nitric oxide synthase. *Journal of Neurophysiology*, 81(2), pp.494–497.

Heddini, U. et al., 2014. Serotonin receptor gene (5HT-2a) polymorphism is associated with provoked vestibulodynia and comorbid symptoms of pain. *The Journal of Sexual Medicine*.

Helm, J., Akgul, G. & Wollmuth, L.P., 2013. Subgroups of parvalbumin-expressing interneurons in layers 2/3 of the visual cortex. *Journal of Neurophysiology*, 109(6), pp.1600–1613.

Hendry, S.H. et al., 1987. Numbers and proportions of GABA-immunoreactive neurons in different areas of monkey cerebral cortex. *The Journal of Neuroscience*, 7(5), pp.1503–1519.

Hirooka, K., Kourennyi, D.E. & Barnes, S., 2000. Calcium channel activation facilitated by nitric oxide in retinal ganglion cells. *Journal of Neurophysiology*, 83(1), pp.198 –206.

Hoover, W.B. & Vertes, R.P., 2007. Anatomical analysis of afferent projections to the medial prefrontal cortex in the rat. *Brain Structure and Function*, 212(2), pp.149–179.

Hoyer, D. et al., 1994. International union of pharmacology classification of receptors for 5-hydroxytryptamine (serotonin). *Pharmacological Reviews*, 46(2), pp.157–203.

Huettner, J.E. & Baughman, R.W., 1986. Primary culture of identified neurons from the visual cortex of postnatal rats. *The Journal of Neuroscience*, 6(10), pp.3044–3060.

Hu, W. et al., 2010. Stress impairs GABAergic network function in the hippocampus by activating nongenomic glucocorticoid receptors and affecting the integrity of the parvalbumin-expressing neuronal network. *Neuropsychopharmacology*.

Inan, S.Y., Yalcin, I. & Aksu, F., 2004. Dual effects of nitric oxide in the mouse forced swimming test: possible contribution of nitric oxide-mediated serotonin release and potassium channel modulation. *Pharmacology, Biochemistry, and Behavior*, 77(3), pp.457–464.

Jakab, R.L. & Goldman-Rakic, P.S., 1998. 5-Hydroxytryptamine2A serotonin receptors in the primate cerebral cortex: possible site of action of hallucinogenic and antipsychotic drugs in pyramidal cell apical dendrites. *Proceedings of the National Academy of Sciences*, 95(2), pp.735–740.

Jiménez-Trejo, F. et al., 2007. Serotonin concentration, synthesis, cell origin, and targets in the rat caput epididymis during sexual maturation and variations associated with adult mating status: morphological and biochemical studies. *Journal of Andrology*, 28(1), pp.136–149.

Jin, X., Jiang, K. & Prince, D.A., 2014. Excitatory and inhibitory synaptic connectivity to layer V fast-spiking interneurons in the freeze lesion model of cortical microgyria. *Journal of Neurophysiology*, (Article ASAP).

Johnson, M.D. & Ma, P.M., 1993. Localization of NADPH diaphorase activity in monoaminergic neurons of the rat brain. *The Journal of Comparative Neurology*, 332(4), pp.391–406.

Karagiannis, A. et al., 2009. Classification of NPY-expressing neocortical interneurons. *The Journal of Neuroscience*, 29(11), pp.3642–3659.

Kara, P. & Friedlander, M.J., 1999. Arginine analogs modify signal detection by neurons in the visual cortex. *The Journal of neuroscience*, 19(13), pp.5528–5548.

Kawaguchi, Y., 1993. Groupings of nonpyramidal and pyramidal cells with specific physiological and morphological characteristics in rat frontal cortex. *Journal of Neurophysiology*, 69(2), pp.416–431.

Kawaguchi, Y., 1995. Physiological subgroups of nonpyramidal cells with specific morphological characteristics in layer II/III of rat frontal cortex. *The Journal of Neuroscience*, 15(4), pp.2638–2655.

Kawai, F. & Miyachi, E., 2001. Modulation by cGMP of the voltage-gated currents in newt olfactory receptor cells. *Neuroscience Research*, 39(3), pp.327–337.

Kay, R.B. & Brunjes, P.C., 2014. Diversity among principal and GABAergic neurons of the anterior olfactory nucleus. *Frontiers in Cellular Neuroscience*, 8, p.111.

Kell, D.B. & Oliver, S.G., 2004. Here is the evidence, now what is the hypothesis? The complementary roles of inductive and hypothesis-driven science in the post-genomic era. *BioEssays*, 26(1), pp.99–105.

Kentish, S.J. et al., 2014. Diet-dependent modulation of gastro-oesphageal vagal afferent mechanosensitivity by endogenous nitric oxide. *The Journal of Physiology*, 592(Pt 15), pp.3287–3301.

Kilpatrick, G.J., Jones, B.J. & Tyers, M.B., 1987. Identification and distribution of 5-HT3 receptors in rat brain using radioligand binding. *Nature*, 330(6150), pp.746–748.

Kimura, H., Mittal, C.K. & Murad, F., 1975. Activation of guanylate cyclase from rat liver and other tissues by sodium azide. *Journal of Biological Chemistry*, 250(20), pp.8016–8022.

Kinsey, A.M. et al., 2001. Distribution of 5-HT5A, 5-HT5B, 5-HT6 and 5-HT7 receptor mRNAs in the rat brain. *Molecular Brain Research*, 88(1–2), pp.194–198.

Klostermann, O. & Wahle, P., 1999. Patterns of spontaneous activity and morphology of interneuron types in organotypic cortex and thalamus–cortex cultures. *Neuroscience*, 92(4), pp.1243–1259.

Kobayashi, M. et al., 2012. A primary neuron culture system for the study of Herpes simplex virus latency and reactivation. *Journal of visualized experiments : JoVE*, (62).

Kriegstein, A.R. & Dichter, M.A., 1983. Morphological classification of rat cortical neurons in cell culture. *The Journal of Neuroscience*, 3(8), pp.1634–1647.

Kronenberg, S. et al., 2008. Pharmacogenetics of selective serotonin reuptake inhibitors in pediatric depression and anxiety. *Pharmacogenomics*, 9(11), pp.1725–1736.

Kubota, Y. et al., 2011. Selective coexpression of multiple chemical markers defines discrete populations of neocortical GABAergic neurons. *Cerebral Cortex*, 21(8), pp.1803–1817.

Kumar, A.M. et al., 2014. Marked reduction in serotonergic activity in a sexually aggressive adolescent male. *The Journal of Neuropsychiatry and Clinical Neurosciences*, 26(3), pp.262–270.

Lambe, E.K., Goldman-Rakic, P.S. & Aghajanian, G.K., 2000. Serotonin induces EPSCs preferentially in layer V pyramidal neurons of the frontal cortex in the rat. *Cerebral Cortex*, 10(10), pp.974–980.

Larkman, A. & Mason, A., 1990. Correlations between morphology and electrophysiology of pyramidal neurons in slices of rat visual cortex. I. Establishment of cell classes. *The Journal of Neuroscience*, 10(5), pp.1407–1414.

Larson, S.D. & Martone, M.E., 2013. NeuroLex.org: an online framework for neuroscience knowledge. *Frontiers in Neuroinformatics*, 7.

Lee, C.C. & Sherman, S.M., 2009. Glutamatergic inhibition in sensory neocortex. *Cerebral Cortex*, 19(10), pp.2281–2289.

Leech, K.A., Kinnaird, C.R. & Hornby, T.G., 2014. Effects of serotonergic medications on locomotor performance in humans with incomplete spinal cord injury. *Journal of Neurotrauma*, 31(15), pp.1334–1342.

Lee, S. et al., 2013. A disinhibitory circuit mediates motor integration in the somatosensory cortex. *Nature Neuroscience*, 16(11), pp.1662–1670.

Lee, S. et al., 2010. The largest group of superficial neocortical GABAergic interneurons expresses ionotropic serotonin receptors. *The Journal of Neuroscience*, 30(50), pp.16796–16808.

Lefort, S. et al., 2009. The excitatory neuronal network of the C2 barrel column in mouse primary somatosensory cortex. *Neuron*, 61(2), pp.301–316.

Lima, S.Q. et al., 2009. PINP: a new method of tagging neuronal populations for identification during in vivo electrophysiological recording. *PloS One*, 4(7), p.6099.

Lin, Y.-F. et al., 2004. NO stimulation of ATP-sensitive potassium channels: Involvement of Ras/mitogen-activated protein kinase pathway and contribution to neuroprotection. *Proceedings of the National Academy of Sciences*, 101(20), pp.7799–7804.

Liu, H. et al., 2013. Acute tryptophan depletion reduces nitric oxide synthase in the rat hippocampus. *Neurochemical Research*, 38(12), pp.2595–2603.

Liu, P. et al., 2004. Age-related changes in nitric oxide synthase and arginase in the rat prefrontal cortex. *Neurobiology of Aging*, 25(4), pp.547–552.

Liu, Z. et al., 2003. Serotonin reduces the hyperpolarization-activated current (Ih) in ventral tegmental area dopamine neurons: involvement of 5-HT2 receptors and protein kinase C. *Journal of Neurophysiology*, 90(5), pp.3201–3212.

López-Vázquez, M.Á. et al., 2014. Septal serotonin depletion in rats facilitates working memory in the radial arm maze and increases hippocampal high-frequency theta activity. *European Journal of Pharmacology*, 734, pp.105–113.

Lorrain, D.S. & Hull, E.M., 1993. Nitric oxide increases dopamine and serotonin release in the medial preoptic area. *NeuroReport*, 5(1), pp.87–89.

Lourenço, J. et al., 2014. Non-associative potentiation of perisomatic inhibition alters the temporal coding of neocortical layer 5 pyramidal neurons. *PLoS biology*, 12(7), p.e1001903.

Lui, J.H., Hansen, D.V. & Kriegstein, A.R., 2011. Development and evolution of the human neocortex. *Cell*, 146(1), pp.18–36.

Lu, Y. et al., 2010. Coexpression of serotonin and nitric oxide in the raphe complex: cortical versus subcortical circuit. *The Anatomical Record: Advances in Integrative Anatomy and Evolutionary Biology*, 293(11), pp.1954–1965.

Macara, I.G. et al., 1996. The Ras superfamily of GTPases. *FASEB journal*, 10(5), pp.625–630.

Marek, G.J. & Aghajanian, G.K., 1999. 5-HT2A receptor or alpha1-adrenoceptor activation induces excitatory postsynaptic currents in layer V pyramidal cells of the medial prefrontal cortex. *European Journal of Pharmacology*, 367(2-3), pp.197–206.

Mark, M.D. & Herlitze, S., 2000. G-protein mediated gating of inward-rectifier K+ channels. *European Journal of Biochemistry*, 267(19), pp.5830–5836.

Markram, H. et al., 2004. Interneurons of the neocortical inhibitory system. *Nature Reviews Neuroscience*, 5(10), pp.793–807.

Martin, E. et al., 2006. Ligand selectivity of soluble guanylyl cyclase: effect of the hydrogen-bonding tyrosine in the distal heme pocket on binding of oxygen, nitric oxide, and carbon monoxide. *The Journal of Biological Chemistry*, 281(38), pp.27836–27845.

Martín-Ruiz, R. et al., 2001. Control of serotonergic function in medial prefrontal cortex by serotonin-2A receptors through a glutamate-dependent mechanism. *The Journal of Neuroscience*, 21(24), pp.9856–9866.

McCormick, D.A. et al., 1985. Comparative electrophysiology of pyramidal and sparsely spiny stellate neurons of the neocortex. *Journal of Neurophysiology*, 54(4), pp.782–806.

McGarry, L.M. et al., 2010. Quantitative classification of somatostatin-positive neocortical interneurons identifies three interneuron subtypes. *Frontiers in Neural Circuits*, 4, p.12.

Mengod, G. et al., 2006. Chemical neuroanatomy of 5-HT receptor subtypes in the mammalian brain. In B. L. R. MD, ed. *The Serotonin Receptors*. The Receptors. Humana Press, pp. 319–364.

Meyer, G., Goffinet, A.M. & Fairén, A., 1999. What is a Cajal-Retzius cell? A reassessment of a classical cell type based on recent observations in the developing neocortex. *Cerebral Cortex*, 9(8), pp.765–775.

Mo, E. et al., 2004. Kinetics of a cellular nitric oxide/cGMP/phosphodiesterase-5 pathway. *The Journal of Biological Chemistry*, 279(25), pp.26149–26158.

Molyneaux, B.J. et al., 2009. Novel subtype-specific genes identify distinct subpopulations of callosal projection neurons. *The Journal of Neuroscience*, 29(39), pp.12343–12354.

Moon, C. et al., 2005. Regulation of intracellular cyclic GMP levels in olfactory sensory neurons. *Journal of Neurochemistry*, 95(1), pp.200–209.

Moosmang, S. et al., 2001. Cellular expression and functional characterization of four hyperpolarization-activated pacemaker channels in cardiac and neuronal tissues. *European Journal of Biochemistry*, 268(6), pp.1646–1652.

Morales, M. & Bloom, F.E., 1997. The 5-HT3 receptor is present in different subpopulations of GABAergic neurons in the rat telencephalon. *The Journal of Neuroscience*, 17(9), pp.3157–3167.

Mountcastle, V.B., 1997. The columnar organization of the neocortex. *Brain*, 120(4), pp.701–722.

Moyer, J.R., McNay, E.C. & Brown, T.H., 2002. Three classes of pyramidal neurons in layer V of rat perirhinal cortex. *Hippocampus*, 12(2), pp.218–234.

Nasif, F.J. et al., 2011. Inhibition of neuronal nitric oxide synthase prevents alterations in medial prefrontal cortex excitability induced by repeated cocaine administration. *Psychopharmacology*, 218(2), pp.323–330.

Nishizuka, Y., 1988. The molecular heterogeneity of protein kinase C and its implications for cellular regulation. *Nature*, 334(6184), pp.661–665.

Noctor, S.C. et al., 2001. Neurons derived from radial glial cells establish radial units in neocortex. *Nature*, 409(6821), pp.714–720.

Noël, F., Pompeu, T.E.T. & Moura, B.C., 2014. Functional binding assays for estimation of the intrinsic efficacy of ligands at the 5-HT1A receptor: application for screening drug candidates. *Journal of Pharmacological and Toxicological Methods*, 70(1), pp.12–18.

Nogueira-Campos, A.A. et al., 2012. Distribution and morphology of nitrergic neurons across functional domains of the rat primary somatosensory cortex. *Frontiers in Neural Circuits*, 6, p.57.

Nozik-Grayck, E. et al., 2002. Pulmonary vasoconstriction by serotonin is inhibited by S-nitrosoglutathione. *American Journal of Physiology. Lung Cellular and Molecular Physiology*, 282(5), pp.1057–1065.

Nutsch, V.L. et al., 2014. Sexual experience influences mating-induced activity in nitric oxide synthase-containing neurons in the medial preoptic area. *Neuroscience Letters*, 579, pp.92–96.

Ogawa, S.K. et al., 2014. Organization of monosynaptic inputs to the serotonin and dopamine neuromodulatory systems. *Cell Reports*, 8(4), pp.1105–1118.

Oláh, S. et al., 2009. Regulation of cortical microcircuits by unitary GABA-mediated volume transmission. *Nature*, 461(7268), pp.1278–1281.

O'Leary, D.D. & Sahara, S., 2008. Genetic regulation of arealization of the neocortex. *Current Opinion in Neurobiology*, 18(1), pp.90–100.

Oswald, M.J. et al., 2013. Diversity of layer 5 projection neurons in the mouse motor cortex. *Frontiers in Cellular Neuroscience*, 7, p.174.

Otlivanchik, O., Le Foll, C. & Levin, B.E., 2014. Perifornical hypothalamic orexin and serotonin modulate the counterregulatory response to hypoglycemic and glucoprivic stimuli. *Diabetes*, (Article ASAP).

Pakhira, M.K., Bandyopadhyay, S. & Maulik, U., 2005. A study of some fuzzy cluster validity indices, genetic clustering and application to pixel classification. *Fuzzy Sets and Systems*, 155(2), pp.191–214.

Park, J.-H., Straub, V.A. & O'Shea, M., 1998. Anterograde signaling by nitric oxide: characterization and in vitro reconstitution of an identified nitrergic synapse. *The Journal of Neuroscience*, 18(14), pp.5463–5476.

Pasupathy, A. & Miller, E.K., 2005. Different time courses of learning-related activity in the prefrontal cortex and striatum. *Nature*, 433(7028), pp.873–876.

Paxinos, G. & Watson, C., 2007. *The rat brain in stereotaxic coordinates: hard cover edition*, Academic Press.

Perrenoud, Q. et al., 2012. Diversity of GABAergic interneurons in layer VIa and VIb of mouse barrel cortex. *Cerebral Cortex*.

Peters, A. & Kara, D.A., 1987. The neuronal composition of area 17 of rat visual cortex. IV. The organization of pyramidal cells. *The Journal of Comparative Neurology*, 260(4), pp.573–590.

Petreanu, L. et al., 2009. The subcellular organization of neocortical excitatory connections. *Nature*, 457(7233), pp.1142–1145.

Pfeffer, C.K. et al., 2013. Inhibition of inhibition in visual cortex: the logic of connections between molecularly distinct interneurons. *Nature Neuroscience*, 16(8), pp.1068–1076.

Pham, D.T., Dimov, S.S. & Nguyen, C.D., 2005. Selection of K in K-means clustering. *Proceedings of the Institution of Mechanical Engineers, Part C: Journal of Mechanical Engineering Science*, 219(1), pp.103–119.

Pinheiro, J. et al., 2012. Nlme: linear and nonlinear mixed effects models. R package version 3.1-103.

Pitsikas, N., 2014. The role of nitric oxide in the object recognition memory. *Behavioural Brain Research*, (Article ASAP).

Podda, M.V. et al., 2004. Nitric oxide increases the spontaneous firing rate of rat medial vestibular nucleus neurons in vitro via a cyclic GMP-mediated PKG-independent mechanism. *The European Journal of Neuroscience*, 20(8), pp.2124–2132.

Pollak Dorocic, I. et al., 2014. A whole-brain atlas of inputs to serotonergic neurons of the dorsal and median raphe nuclei. *Neuron*, 83(3), pp.663–678.

Pompeiano, M., Palacios, J.M. & Mengod, G., 1992. Distribution and cellular localization of mRNA coding for 5-HT1A receptor in the rat brain: correlation with receptor binding. *The Journal of Neuroscience*, 12(2), pp.440–453.

Pompeiano, M., Palacios, J.M. & Mengod, G., 1994. Distribution of the serotonin 5-HT2 receptor family mRNAs: comparison between 5-HT2A and 5-HT2C receptors. *Brain Research. Molecular Brain Research*, 23(1-2), pp.163–178.

Potter, S.M. & DeMarse, T.B., 2001. A new approach to neural cell culture for long-term studies. *Journal of Neuroscience Methods*, 110(1–2), pp.17–24.

Povysheva, N.V. et al., 2013. Electrophysiological heterogeneity of fast-spiking interneurons: chandelier versus basket cells. *PLoS ONE*, 8(8), p.e70553.

Puig, M.V. et al., 2004. In vivo excitation of GABA interneurons in the medial prefrontal cortex through 5-HT3 receptors. *Cerebral Cortex*, 14(12), pp.1365–1375.

Puig, M.V. et al., 2010. Serotonin modulates fast-spiking interneuron and synchronous activity in the rat prefrontal cortex through 5-HT1A and 5-HT2A receptors. *The Journal of Neuroscience*, 30(6), pp.2211–2222.

Quirk, M.C., 2009. A defined network of fast-spiking interneurons in orbitofrontal cortex: responses to behavioral contingencies and ketamine administration. *Frontiers in Systems Neuroscience*, 3.

Ramos, A.J. et al., 2002. Neuronal and inducible nitric oxide synthase immunoreactivity following serotonin depletion. *Brain Research*, 958(1), pp.112–121.

Rapport, M.M., 1949. Serum vasoconstrictor (serotonin) V. the presence of creatinine in the complex. A proposed structure of the vasoconstrictor principle. *Journal of Biological Chemistry*, 180(3), pp.961–969.

Rapport, M.M., Green, A.A. & Page, I.H., 1948. Serum vasoconstrictor (serotonin) IV. isolation and characterization. *Journal of Biological Chemistry*, 176(3), pp.1243–1251.

Del Río, J.A. et al., 1995. Glutamate-like immunoreactivity and fate of Cajal-Retzius cells in the murine cortex as identified with calretinin antibody. *Cerebral Cortex*, 5(1), pp.13–21.

Rodriguez-Gomez, A. et al., 2014. Perinatal exposure to genistein affects the normal development of anxiety and aggressive behaviors and nitric oxide system in CD1 male mice. *Physiology & Behavior*, 133, pp.107–114.

Rousseeuw, P.J., 1987. Silhouettes: a graphical aid to the interpretation and validation of cluster analysis. *Journal of Computational and Applied Mathematics*, 20, pp.53–65.

Le Roux, N. et al., 2009. Roles of nitric oxide in the homeostatic control of the excitation–inhibition balance in rat visual cortical networks. *Neuroscience*, 163(3), pp.942–951.

Saleh, L.A. et al., 2014. Ibuprofen suppresses depressive like behavior induced by BCG inoculation in mice: role of nitric oxide and prostaglandin. *Pharmacology, Biochemistry, and Behavior*, (Article ASAP).

Santana, N. et al., 2004. Expression of serotonin1a and serotonin2a receptors in pyramidal and GABAergic neurons of the rat prefrontal cortex. *Cerebral Cortex*, 14(10), pp.1100–1109.

Santana, R. et al., 2013. Classification of neocortical interneurons using affinity propagation. *Frontiers in Neural Circuits*, 7, p.185.

Schild, L. et al., 2006. Neuronal nitric oxide synthase controls enzyme activity pattern of mitochondria and lipid metabolism. *FASEB journal*, 20(1), pp.145–147.

Schipke, C.G. et al., 2008. Temperature and nitric oxide control spontaneous calcium transients in astrocytes. *Cell Calcium*, 43(3), pp.285–295.

Schlossmann, J. et al., 2000. Regulation of intracellular calcium by a signalling complex of IRAG, IP3 receptor and cGMP kinase Ibeta. *Nature*, 404(6774), pp.197–201.

Schwarz, G., 1978. Estimating the dimension of a model. *The Annals of Statistics*, 6(2), pp.461–464.

Selvaraj, S. et al., 2014. Alterations in the serotonin system in schizophrenia: A systematic review and meta-analysis of postmortem and molecular imaging studies. *Neuroscience and Biobehavioral Reviews*, 45C, pp.233–245.

Shipp, S., 2007. Structure and function of the cerebral cortex. *Current Biology*, 17(12), pp.R443–R449.

Simpson, K.L., Waterhouse, B.D. & Lin, R.C.S., 2003. Differential expression of nitric oxide in serotonergic projection neurons: Neurochemical identification of dorsal raphe inputs to rodent trigeminal somatosensory targets. *The Journal of Comparative Neurology*, 466(4), pp.495–512.

Smiley, J.F. & Goldman-Rakic, P.S., 1996. Serotonergic axons in monkey prefrontal cerebral cortex synapse predominantly on interneurons as demonstrated by serial section electron microscopy. *The Journal of comparative neurology*, 367(3), pp.431–443.

Soda, T. et al., 2003. Segregation and coactivation of developing neocortical layer 1 neurons. *The Journal of Neuroscience*, 23(15), pp.6272–6279.

Somogyi, P. et al., 1998. Salient features of synaptic organisation in the cerebral cortex. *Brain Research Reviews*, 26(2–3), pp.113–135.

Sonnenburg, W.K. & Beavo, J.A., 1994. Cyclic GMP and regulation of cyclic nucleotide hydrolysis. In Ferid Murad, ed. *Advances in Pharmacology*. Academic Press, pp. 87–114.

Soomro, G.M. et al., 2008. Selective serotonin re-uptake inhibitors (SSRIs) versus placebo for obsessive compulsive disorder (OCD). *The Cochrane Database of Systematic Reviews*, (1), p.CD001765.

Staiger, J.F. et al., 2004. Functional diversity of layer IV spiny neurons in rat somatosensory cortex: quantitative morphology of electrophysiologically characterized and biocytin labeled cells. *Cerebral Cortex*, 14(6), pp.690–701.

Steinert, J.R. et al., 2011. Nitric oxide is an activity-dependent regulator of target neuron intrinsic excitability. *Neuron*, 71(2), pp.291–305.

Steinert, J.R. et al., 2008. Nitric oxide is a volume transmitter regulating postsynaptic excitability at a glutamatergic synapse. *Neuron*, 60(4), pp.642–656.

Stephens, E.K., Avesar, D. & Gulledge, A.T., 2014. Activity-dependent serotonergic excitation of callosal projection neurons in the mouse prefrontal cortex. *Frontiers in Neural Circuits*, 8, p.97.

Stolyarova, A. et al., 2014. Positive and negative feedback learning and associated dopamine and serotonin transporter binding after methamphetamine. *Behavioural Brain Research*, 271, pp.195–202.

Stoyanovsky, D. et al., 1997. Nitric oxide activates skeletal and cardiac ryanodine receptors. *Cell Calcium*, 21(1), pp.19–29.

Straub, V.A. et al., 2007. Modulation of serotonergic neurotransmission by nitric oxide. *Journal of Neurophysiology*, 97(2), pp.1088 –1099.

Subkhankulova, T. et al., 2010. Grouping and classifying electrophysiologically-defined classes of neocortical neurons by single cell, whole-genome expression profiling. *Frontiers in Molecular Neuroscience*, 3, p.10.

Sugino, K. et al., 2006. Molecular taxonomy of major neuronal classes in the adult mouse forebrain. *Nature Neuroscience*, 9(1), pp.99–107.

Sunahara, R.K., Dessauer, C.W. & Gilman, A.G., 1996. Complexity and diversity of mammalian adenylyl cyclases. *Annual Review of Pharmacology and Toxicology*, 36(1), pp.461–480.

Supornsilpchai, W. et al., 2006. Serotonin depletion, cortical spreading depression, and trigeminal nociception. *Headache: The Journal of Head and Face Pain*, 46(1), pp.34–39.

Suwa, B. et al., 2014. Distribution of serotonin 4(a) receptors in the juvenile rat brain and spinal cord. *Journal of Chemical Neuroanatomy*, 55, pp.67–77.

Szczepanski, S.M. & Knight, R.T., 2014. Insights into human behavior from lesions to the prefrontal cortex. *Neuron*, 83(5), pp.1002–1018.

Tabuchi, S. et al., 2013. Influence of inhibitory serotonergic inputs to orexin/hypocretin neurons on the diurnal rhythm of sleep and wakefulness. *Sleep*, 36(9), pp.1391–1404.

Tagliaferro, P. et al., 2003. Changes in the postnatal development on nitric oxide system induced by serotonin depletion. *Brain Research. Developmental Brain Research*, 146(1-2), pp.39–49.

Takahashi, K., 1965. Slow and fast groups of pyramidal tract cells and their respective membrane properties. *Journal of neurophysiology*, 28(5), pp.908–924.

Takigawa, T. & Alzheimer, C., 1999. G protein-activated inwardly rectifying K+ (GIRK) currents in dendrites of rat neocortical pyramidal cells. *The Journal of Physiology*, 517(2), pp.385–390.

Tanaka, J. et al., 2000. Gq protein α subunits Gαq and Gα11 are localized at postsynaptic extra-junctional membrane of cerebellar Purkinje cells and hippocampal pyramidal cells. *European Journal of Neuroscience*, 12(3), pp.781–792.

Tecott, L.H., Maricq, A.V. & Julius, D., 1993. Nervous system distribution of the serotonin 5-HT3 receptor mRNA. *Proceedings of the National Academy of Sciences*, 90(4), pp.1430–1434.

Teng, Z. et al., 2013. Glucocorticoid exerts its non-genomic effect on IPSC by activation of a phospholipase C-dependent pathway in prefrontal cortex of rats. *The Journal of Physiology*, 591(13), pp.3341–3353.

Thomas D.R. & Hagan J.J., 2004. 5-HT7 Receptors. *Current Drug Targets - CNS & Neurological Disorders*, 3, pp.81–90.

Thomson, A.M., 2010. Neocortical layer 6, a review. *Frontiers in Neuroanatomy*, 4, p.13.

Thomson, A.M. & Lamy, C., 2007. Functional maps of neocortical local circuitry. *Frontiers in Neuroscience*, p.1.

Tomioka, R. et al., 2005. Demonstration of long-range GABAergic connections distributed throughout the mouse neocortex. *The European Journal of Neuroscience*, 21(6), pp.1587–1600.

Torres, G.E., Gainetdinov, R.R. & Caron, M.G., 2003. Plasma membrane monoamine transporters: structure, regulation and function. *Nature Reviews Neuroscience*, 4(1), pp.13–25.

Tozer, A.J.B., Forsythe, I.D. & Steinert, J.R., 2012. Nitric oxide signalling augments neuronal voltage-gated L-type (Cav1) and P/Q-type (Cav2.1) channels in the mouse medial nucleus of the trapezoid body. *PLoS ONE*, 7(2), p.e32256.

Trabace, L. et al., 2004. The effects of nitric oxide on striatal serotoninergic transmission involve multiple targets: an in vivo microdialysis study in the awake rat. *Brain research*, 1008(2), pp.293–298.

Trabace, L. & Kendrick, K.M., 2000. Nitric oxide can differentially modulate striatal neurotransmitter concentrations via soluble guanylate cyclase and peroxynitrite formation. *Journal of Neurochemistry*, 75(4), pp.1664–1674.

Trinchese, F. et al., 2004. Cell cultures from animal models of Alzheimer's disease as a tool for faster screening and testing of drug efficacy. *Journal of Molecular Neuroscience*, 24(1), pp.15–21.

Valtschanoff, J.G. et al., 1993. Neurons in rat cerebral cortex that synthesize nitric oxide: NADPH diaphorase histochemistry, NOS immunocytochemistry, and colocalization with GABA. *Neuroscience letters*, 157(2), pp.157–161.

Vialli, P.M. & Erspamer, D.V., 1937. Ricerche sul secreto delle cellule enterocromaffini. *Zeitschrift für Zellforschung und Mikroskopische Anatomie*, 27(1), pp.81–99.

Vincent, S.R. & Kimura, H., 1992. Histochemical mapping of nitric oxide synthase in the rat brain. *Neuroscience*, 46(4), pp.755–784.

Vlasblom, J. & Wodak, S.J., 2009. Markov clustering versus affinity propagation for the partitioning of protein interaction graphs. *BMC Bioinformatics*, 10(1), p.99.

Vucurovic, K. et al., 2010. Serotonin 3A receptor subtype as an early and protracted marker of cortical interneuron subpopulations. *Cerebral cortex*, 20(10), pp.2333–2347.

Waeber, C. et al., 1998. Putative 5-HT5 receptors: localization in the mouse CNS and lack of effect in the inhibition of dural protein extravasation. *Annals of the New York Academy of Sciences*, 861(1), pp.85–90.

Wallen, P. et al., 1989. Effects of 5-hydroxytryptamine on the afterhyperpolarization, spike frequency regulation, and oscillatory membrane properties in lamprey spinal cord neurons. *Journal of Neurophysiology*, 61(4), pp.759–768.

Walther, D.J. et al., 2003. Synthesis of serotonin by a second tryptophan hydroxylase isoform. *Science*, 299(5603), pp.76–76.

Wang, F., Kessels, H.W. & Hu, H., 2014. The mouse that roared: neural mechanisms of social hierarchy. *Trends in Neurosciences*, (Article ASAP).

Wang, H.-G. et al., 2005. Presynaptic and postsynaptic roles of NO, cGK, and RhoA in long-lasting potentiation and aggregation of synaptic proteins. *Neuron*, 45(3), pp.389–403.

Wang, Q.P., Guan, J.L. & Nakai, Y., 1995. Distribution and synaptic relations of NOS neurons in the dorsal raphe nucleus: a comparison to 5-HT neurons. *Brain Research Bulletin*, 37(2), pp.177–187.

Wang, S. et al., 2014. Nitric oxide facilitates active avoidance learning via enhancement of glutamate levels in the hippocampal dentate gyrus. *Behavioural Brain Research*, 271, pp.177–183.

Warden, M.R. & Miller, E.K., 2010. Task-dependent changes in short-term memory in the prefrontal cortex. *The Journal of Neuroscience*, 30(47), pp.15801–15810.

Ward, J.H., 1963. Hierarchical grouping to optimize an objective function. *Journal of the American Statistical Association*, 58(301), pp.236–244.

Ward, R.P. et al., 1995. Localization of serotonin subtype 6 receptor messenger RNA in the rat brain by in situ hybridization histochemistry. *Neuroscience*, 64(4), pp.1105–1111.

Watson, J. et al., 2000. 5-HT(1A) receptor agonist-antagonist binding affinity difference as a measure of intrinsic activity in recombinant and native tissue systems. *British Journal of Pharmacology*, 130(5), pp.1108–1114.

Weber, E.T. & Andrade, R., 2010. Htr2a gene and 5-HT(2a) receptor expression in the cerebral cortex studied using genetically modified mice. *Frontiers in Neuroscience*, 4, p.36.

Weissbourd, B. et al., 2014. Presynaptic partners of dorsal raphe serotonergic and GABAergic neurons. *Neuron*, 83(3), pp.645–662.

West, A.R. & Grace, A.A., 2004. The Nitric Oxide-Guanylyl Cyclase Signaling Pathway Modulates Membrane Activity States and Electrophysiological Properties of Striatal Medium Spiny Neurons Recorded In Vivo. *The Journal of Neuroscience*, 24(8), pp.1924 –1935.

Willins, D.L., Deutch, A.Y. & Roth, B.L., 1997. Serotonin 5-HT2A receptors are expressed on pyramidal cells and interneurons in the rat cortex. *Synapse*, 27(1), pp.79–82.

Wilson, G.W. & Garthwaite, J., 2010. Hyperpolarization-activated ion channels as targets for nitric oxide signalling in deep cerebellar nuclei. *European Journal of Neuroscience*, 31(11), pp.1935–1945.

Wilson, M.A. & Molliver, M.E., 1991a. The organization of serotonergic projections to cerebral cortex in primates: Regional distribution of axon terminals. *Neuroscience*, 44(3), pp.537–553.

Wilson, M.A. & Molliver, M.E., 1991b. The organization of serotonergic projections to cerebral cortex in primates: Retrograde transport studies. *Neuroscience*, 44(3), pp.555–570.

Wong, A. et al., 2012. Cyclic GMP-dependent Stimulation of Serotonin Transport Does Not Involve Direct Transporter Phosphorylation by cGMP-dependent Protein Kinase. *Journal of Biological Chemistry*, 287(43), pp.36051–36058.

Wu, C.F.J., 1983. On the convergence properties of the EM algorithm. *The Annals of Statistics*, 11(1), pp.95–103.

Xiang, Z. & Prince, D.A., 2003. Heterogeneous actions of serotonin on interneurons in rat visual cortex. *Journal of Neurophysiology*, 89(3), pp.1278–1287.

Xue, M., Atallah, B.V. & Scanziani, M., 2014. Equalizing excitation-inhibition ratios across visual cortical neurons. *Nature*, 511(7511), pp.596–600.

Xu, H. et al., 2013. Neocortical somatostatin-expressing gabaergic interneurons disinhibit the thalamorecipient layer 4. *Neuron*, 77(1), pp.155–167.

Yang, S. & Cox, C.L., 2007. Modulation of inhibitory activity by nitric oxide in the thalamus. *Journal of Neurophysiology*, 97(5), pp.3386–3395.

Young, K.W. et al., 2005. Muscarinic acetylcholine receptor activation enhances hippocampal neuron excitability and potentiates synaptically evoked Ca2+ signals via phosphatidylinositol 4,5-bisphosphate depletion. *Molecular and Cellular Neuroscience*, 30(1), pp.48–57.

Yun, H.Y. et al., 1998. Nitric oxide mediates N-methyl-D-aspartate receptor-induced activation of p21ras. *Proceedings of the National Academy of Sciences*, 95(10), pp.5773–5778.

Zaitsev, A.V. et al., 2012. Electrophysiological classes of layers 2-3 pyramidal cells in monkey prefrontal cortex. *Journal of Neurophysiology*.

Zhang, Z., 2004. Maturation of layer V pyramidal neurons in the rat prefrontal cortex: intrinsic properties and synaptic function. *Journal of Neurophysiology*, 91(3), pp.1171–1182.

Zhang, Z. & Arsenault, D., 2005. Gain modulation by serotonin in pyramidal neurones of the rat prefrontal cortex. *The Journal of Physiology*, 566(2), pp.379–394.

Zhang, Z.W. & Deschênes, M., 1998. Projections to layer VI of the posteromedial barrel field in the rat: a reappraisal of the role of corticothalamic pathways. *Cerebral Cortex*, 8(5), pp.428–436.

Zhong, P. & Yan, Z., 2011. Differential Regulation of the Excitability of Prefrontal Cortical Fast-Spiking Interneurons and Pyramidal Neurons by Serotonin and Fluoxetine H. Mansvelder, ed. *PLoS ONE*, 6(2), p.e16970.

Zhong, P., Yuen, E.Y. & Yan, Z., 2008. Modulation of neuronal excitability by serotonin-NMDA interactions in prefrontal cortex. *Molecular and Cellular Neuroscience*, 38(2), pp.290–299.

Zhou, M. et al., 2014. Scaling down of balanced excitation and inhibition by active behavioral states in auditory cortex. *Nature Neuroscience*, 17(6), pp.841–850.